SYNTHESIS AND CHARACTERIZATION OF NUCLEOBASE FUNCTIONALIZED LOCKED NUCLEIC ACIDS (LNAs): CHEMICAL MODIFICATIONS FOR THERAPEUTICS AND DIAGNOSTIC PURPOSES

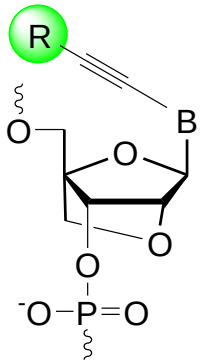

A Dissertation

Presented in Partial Fulfillment of the Requirements for the

Degree of Doctorate of Philosophy

with a

Major in Chemistry

in the

College of Graduate Studies

University of Idaho

by

Mamta Kaura

November 2014

Major Professor: Patrick J. Hrdlicka, Ph.D.

AUTHORIZATION TO SUBMIT DISSERTATION

This dissertation of Mamta Kaura, submitted for the degree of Doctorate of Philosophy with a major in Chemistry and titled, "Synthesis and Characterization of Nucleobase Functionalized Locked Nucleic Acids (LNAs): Chemical Modifications for Therapeutics and Diagnostic Purposes," has been reviewed in final form. Permission, as indicated by the signatures and dates below, is now granted to submit final copies to the College of Graduate Studies for approval.

Major Professor: _____ Date: _____
Patrick J. Hrdlicka, Ph.D.

Committee Members: _____ Date: _____
Richard V. Williams, Ph.D.

_____ Date: _____
W. Daniel Edwards, Ph.D.

_____ Date: _____
David N. McIlroy, Ph.D.

Department Administrator: _____ Date: _____
Ray von Wandruszka, Ph.D.

Discipline's College Dean: _____ Date: _____
Paul Joyce, Ph.D.

Final Approval and Acceptance

Dean of the College of Graduate Studies: _____ Date: _____
Jie Chen, Ph.D.

ABSTRACT

DNA is the genetic code of life, containing vital information required for the existence of life. An understanding of the structure of DNA, its function and Watson-Crick hybridization led to the conceptualization of the antisense strategy. The concept suggested that it is possible to design drugs that target disease-related mRNA (messenger RNA) antisense oligonucleotides (ASO) that bind to the target based on Watson-Crick hybridization rules and prevent its translation into proteins. Since, copy of target RNA present in a cell is much smaller in comparison to proteins, i.e., the most common drug target for small molecue drugs, theoretically allows for low concentrations of the antisense drug to be used as compared to conventional drugs. The simplicity of this concept has led to the use of ASO drugs as therapeutic agents. The use of conformationally restricted nucleotides as antisense modifications has led to an impressive progress in the field of oligonucleotide therapeutics. In particular, Locked Nucleic Acids (LNAs) have been outlined as a very promising antisense modification due to their unparalleled hybridization properties. Thus, LNA has become the focus of multiple research groups and pharmaceutical companies, leading to the development of LNA modified ON candidates.

During my Ph.D. work, I developed numerous chemically modified LNA building blocks by using nucleobase functionalization strategy to modulate the biophysical properties of respective building block. We conducted studies on different nucleobases (cytosine and adenosine) where we have shown that LNA building blocks, which are modified at the C5 position of cytosine pyrimidines and C8 position of adenine purines. We also studied the properties of C5 LNA (U) monomers conjugated to bulky hydrophilic carbohydrates substituents. The goal of the study was to develop nucleotides that confer stability towards exonuclease enzymes without

disrupting the duplex stability as hydrophobic substituents.

Chemically modified oligonucleotides are finding an increasing use in diagnostics as fluorescent hybridization probes to detect DNA mutations and to study DNA-protein interactions. We have developed DNA probes centrally modified with 5-[3-(1-pyrenecarboxamido) propynyl] DNA monomer, which are flanked with conventional LNAs as diagnostic probes for detection of single nucleotide polymorphism in DNA. These neighbouring LNAs influence the position of the fluorophore in a similar manner as for the C5-fluorophore functionalized LNA probes. These probes are relatively easier to synthesize and results in greater fluorescence based discrimination of matched vs mismatched duplexes than just C5-LNA or C5-DNA fluorophore functionalized probes.

These studies conducted on Locked Nucleic Acids (LNAs) suggested, that, i) nucleobase functionalization improves the therapeutic properties of LNA; ii) introduction of canonical LNAs in an ON sequence can be used to develop diagnostic probes with improved photophysical properties.

ACKNOWLEDGEMENTS

I would like to take this opportunity to express my deep gratitude to the invaluable help and support of the numerous people, without whom this work would not have the spirit that it has.

First of all, I would like to express my sincere thanks to my erudite supervisor, Dr. Patrick J. Hrdlicka, Associate Professor at U of I, for accepting me as a student in his laboratory and giving me an opportunity to work on multiple projects. His luminous guidance, stimulating criticism and constructive suggestions helped me in making this project a success. His focused and persistent attitude with strong passion for research, always motivated me to strive for excellence. I would like to thank him from the core of my heart for illuminating my vision towards research.

I am thankful to all my laboratory colleagues (Dale Guenther, Saswata Karmakar and Sujay P. Sau) for their support and cooperation. My special thanks to Dr. Pawan Kumar and Brooke Anderson for their constant help and suggestions, whenever I needed.

I owe my special thanks to all the staff members of chemistry department for lending their gentle support from time to time throughout the tenure of my research work. I am thankful to my committee members for their valuable suggestions on my dissertation writing. My sincere thanks are also due to my friends in Moscow, for making my stay comfortable. I will always cherish the lovely moments spent together.

My deepest gratitude is for my parents and my brother, for their love, support and constant encouragement. I shall always be indebted to you for what you have done for me. My Ph.D. is the result of your immense efforts and strong motivation. Last, but not the least, I am thankful to my husband and his family for their love, support and patience.

☺ *Doing what you like is passion, liking what you do is life* ☺

Mamta Kaura

TABLE OF CONTENTS

List of Figures

List of Tables

List of Schemes

ABBREVIATIONS

2’,4’-BNA	2’-O, 4’-C bridged nucleic acid
A	Adenin-9-yl
2-AP	2-Aminopurine
6-AP	6-Aminopurine
a.u.	Atomic unit
Aq	Aqueous
ASO	Antisense Oligonucleotide
Aza-ENA	2’-N,4’-C-Ethylene bridged nucleic acid
BDF	Base discriminating fluorescent
C	Cytosin-*1*-yl
CuAAC	Copper (I) catalyzed azide alkyne Huisgen 1,3-dipolar cycloaddition
COSY	^{1}H-^{1}H correlation spectroscopy
DCI	4, 5-Dicyanoimidazole
DMAP	4-Dimethylaminopyridine
DMF	Dimethylformamide
DMSO	Dimethylsulfoxide
DMTrCl	4, 4’-Dimethoxytrityl chloride
DNA	2’-Deoxyribonucleic Acid
dsDNA	Double stranded DNA
ssDNA	Single stranded DNA
ENA	2’-*O*,4’-*C* Ethylene bridged nucleic acid
FANA	2’-Fluoro arabino nucleic acid

FDA	Food and drug administration
FH	Familial hypercholesterolemia
FNA	Fluorescent nucleobase analogs
FRET	Fluorescence resonance energy transfer
G	Guanosine
h	Hour
HPLC	High performance liquid chromatography
IR	Infrared
J	Coupling constant
LNA	Locked Nucleic Acid
m	multiplet
MALDI-TOF MS	Matrix assisted laser desorption ionization time of flight mass spectrometry
MB	Molecular beacon
MOE	O2’-methoxyethyl RNA
mRNA	Messenger RNA
miRNA	Micro RNA
NMP	N-methyl pyrrolidone
NMR	Nuclear magmetic resonance
NPs	N-3’,P-5’phosphoramidates
ON	Olilgonucleotide
PCR	Polymerase chain reaction
PEG	Polyethylene glycol
PNA	Peptide nucleic acid

PPh_3	Triphenylphosphine
ppm	Parts per million
PS-DNA	Phosphorothioate DNA
Py	Pyren-1-yl
R_f	Relative to front
RISC	RNA induced silencing complex
RNA	Ribonucleic acid
RNAi	RNA interference
RNaseH	Ribonuclease H
ROESY	Rotating-frame nuclear Overhauser effect correlation spectroscopy
RP-HPLC	Reverse phase high performance liquid chromatography
s	Singlet
siRNA	Small interfering RNA
SNP	Single nucleotide polymorphism
SSO	Splice switching oligonucleotide
SSP	Single stranded probe
SVPDE	Snake venom phosphodiesterase
t	Triplet
T	Thymin-1-yl
TBAF	Tetrabutylammonium fluoride
TFO	Triplex forming oligonucleotide
THF	Tetrahydrofuran
TLC	Thin layer chromatography

T_m	Thermal denaturation temperature
TMS	Trimethylsilyl chloride
U	Uracil-1-yl
UV	Ultraviolet

Chapter 1: Conformationally Restricted Oligonucleotides

1.1. RNA targeting strategies

Single stranded oligonucleotides (ONs) targeting certain messenger RNA (mRNA), have been explored as an alternative to conventional small molecule drugs which target proteins.[1] Targeting of mRNA is conceptually more straightforward compared to protein targeting due to the availability of base pairs available for binding.[2] In 1978, it was shown for the first time that chemically modified ON, can be used to modulate gene expression through binding to mRNA.[3a] Since then, such ONs have been used to down-regulate many genes of interest via antisense,[4] ribozyme,[5] DNAzyme[6] or RNA interference (RNAi)[7] or miRNA approaches[8] (Figure 1 displays different ON-based RNA targeting strategies).

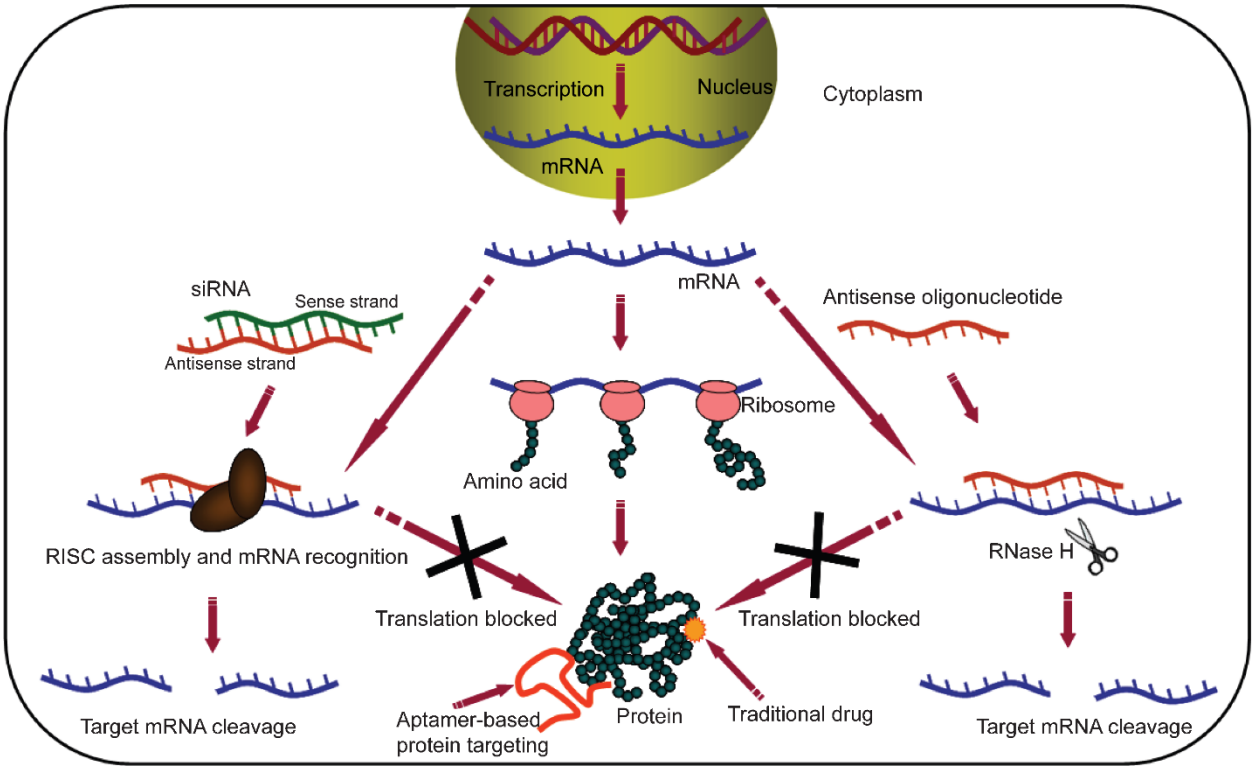

Figure 1. Oligonucleotide based RNA-targeting strategies. (Adapted with permission from ref. 3b).

Two antisense oligonucleotide (ASO) drugs have been approved by the FDA for commercial use. Vitravene,[9] also known as formivirsen, was the first drug approved and is used for the treatment of cytomegalovirus retinitis in HIV patients. The second drug is the recently approved Mipomersen, which is used to control high levels of cholesterol in patients suffering from familial hypercholesterolemia (FH), i.e., a genetic disorder, characterized by high cholesterol levels. There are over twenty AONs in clinical trials[10], including Affinitak and Alicaforsen in Phase 3 of the trials for treatment of non-small lung cancer and Crohn's disease respectively. These numbers highlight the steady progress done in the field of antisense over the past couple of years.

In this review chapter, I will provide a detailed discussion of antisense ONs, their mechanism of action and the various chemical modifications employed to improve the biophysical properties of antisense ONs. Other RNA targeting approaches viz, DNAzyme or ribozyme etc. will not be discussed here because these strategies were not a part of my study.

1.2. Antisense ONs and their mechanism of action

Antisense ONs (ASO) are short synthetic oligonucleotides usually 12-25 nucleotides (nt) in length, which are designed to bind to mRNA via Watson-Crick base pairing and thereby modulate protein expression.[11,12] These ONs interfere with protein formation (translation) in multiple ways depending on the composition of the ASO. The best categorized mechanism is RNaseH mediated mRNA degaradation i.e., induction of RNA degradation through recruitment of RNaseH[13,14], an enzyme that hydrolyses the RNA strand of an RNA/DNA heteroduplex (Figure 2a).[15a] However, there are other mechanisms as well where ONs, act by blocking targeted RNA instead, without inducing RNA degradation. Either, they act as i) steric blockers, obstructing the formation of the translation complex (multi-protein complex responsible for

protein synthesis) i.e, preventing the ribosome from reading through the sequence (Figure 2b)[15a] or, ii) they modulate splicing of pre-mRNA to mature mRNA using splice switching ONs (SSO) (Figure 3).

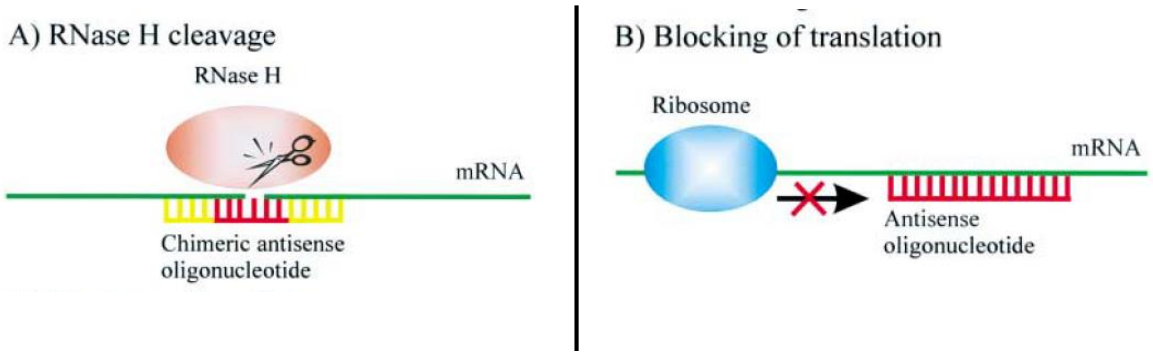

Figure 2. Mechanism of actions for AONs; a) RNase H mediated cleavage of mRNA b) Blocking of translation. (Adapted with permission from ref 1a).

Splicing of pre-mRNA is used by cells to form different isoforms of mature mRNA from pre-mRNA[15b] (Figure 3a). During the process, several fragments of pre-mRNA (called introns) are excised and the coding regions (called exons) are joined together to form mature mRNA. Introns are the regions in pre-mRNA which do not code for translation. Hence, for translation to occur, exons needs to be ligated together. Each exon codes for a specific portion of protein, hence generating different proteins. This process of splicing is regulated by a complex of proteins and RNAs called spliceosome, which is assembled at every splicing event. Splice switching ONs (SSO) can modulate pre-mRNA splicing by preventing splicesome from recognizing specific RNA sequences at the intron-exon junction. These SSOs mask these splice sites and redirect the splicesome to an alternative site, resulting in alternative splicing leading to either exon inclusion or exon skipping and production of alternative proteins (Figure 3b).

Of the above mentioned mechanisms, RNaseH mediated cleavage of mRNA is considered to be particularly desirable due to its catalytic mechanism; the mRNA is degraded, releasing the

ASO to bind another mRNA. In contrast, translational arrest follows a stoichiometric mechanism and requires higher doses of ASOs to have the same efficacy.

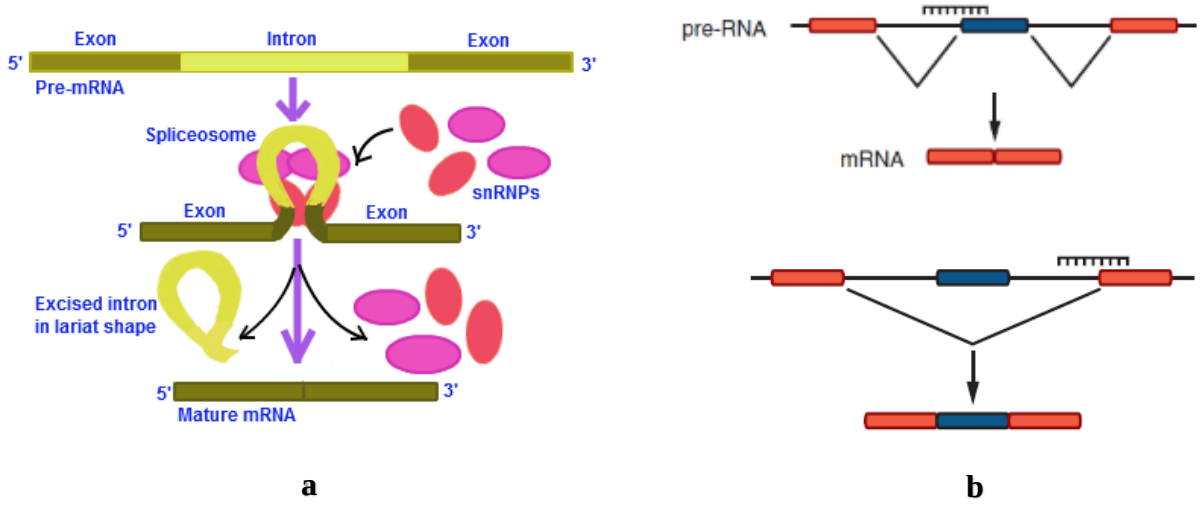

Figure 3. **a**) Pre-mRNA processing (Splicing); **b**) SSO masking the splice site, i) exon exclusion, ii) exon inclusion. (Adapted with permission from ref. 15c).

Although there has been some success with the use of antisense based drugs for the treatment of diseases, development of ASOs has proven difficult due to insufficient oligonucleotide stability towards nucleases, poor target specificity, low binding affinity towards RNA and insufficient delivery inside cells. For an ASO to inhibit gene expression, it must be taken up efficiently within cells (i.e., efficient cellular uptake). At present, for the cellular uptake of ONs, membrane bound receptors are being used; such as liposomes and cationic polymers etc.[16] These limitations have prevented this technology from becoming a big commercial success, resulting in an urgent call for the development of chemically modified constructs for the treatment of infectious diseases and complex genetic disorders. ASOs need to be chemically modified to improve on the low enzymatic stability of unmodified ONs under normal physiological conditions.[17-18]

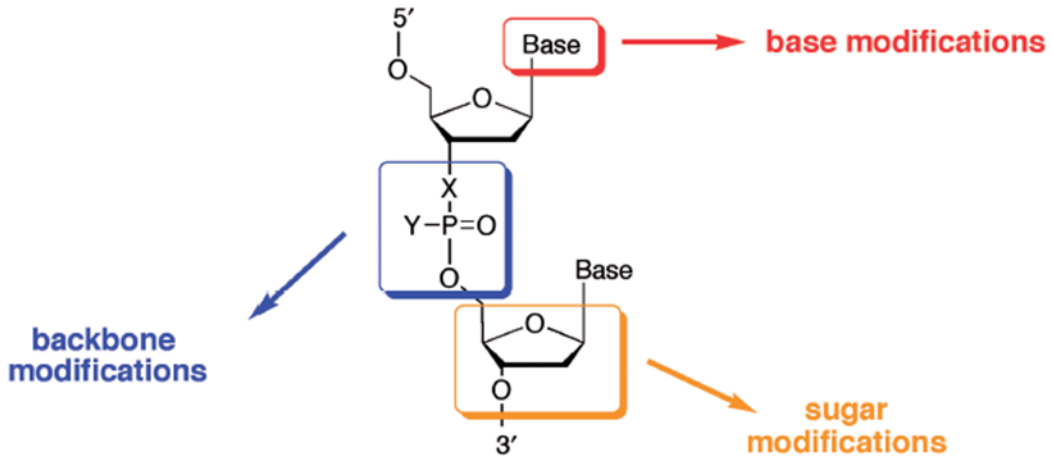

Figure 4. Sites for chemical modifications of nucleotides. (Adapted with permission from ref 19a).

Chemical modifications can be introduced on the nucleobase, sugar skeleton and/or phosphodiester backbone[19a,b,c] (Figure 4). Early studies have shown that the efficacy of AONs is strongly linked to the chemical modification used for the study, since each modification has its own impact on pharmacodynamic and pharmacokinetic characteristics of AONs.

Table 1. Chemically modified antisense nucleic acid analogs and their types.

Antisense	Chemical Modification	Type
1st Generation	Phosphorothioate	Backbone
2nd Generation	2'-O Methyl RNA (OMe) 2'-O methoxyethyl RNA(MOE)	Sugar skeleton
3rd Generation	PNA (Peptide nucleic acid) FANA (2'-floro arabino nucleic acid) LNA (Locked Nucleic Acid)	Backbone Sugar skeleton Conformationally restricted sugar skeleton

1.3. Backbone Modified Antisense Oligonucleotides.

Nucleotides in natural oligonucleotides are connected via the phosphodiester backbone. Backbone modifications were introduced to improve the stability of AONs towards endogeneous nucleases. The most common modifications include methylphosphonates, phosphorothioate (PS-DNA), N3'-P5' linked phosphoramidate DNA and peptide nucleic acid (PNA) (Figure 5).

Methylphosphonates were one of the first backbone modifications. They result in uncharged oligomers, as one nonbridging oxygen atom at each phosphorus in the oligonucleotide chain is replaced by a methyl group. Although, this backbone modification is enzymatically stable in biological systems,[20] it does not allow for recruitment of RNaseH, which is undesirable from a therapeutic perspective.

Replacement of one of the non-bridging oxygen atoms of the phosphodiester backbone group, with a sulfur atom generates phosphorothioates (PS-DNA).[21] In addition to providing resistance to nucleases, this modification still allows for recruitment of RNaseH, resulting in catalytic degradation of mRNA. The FDA approved antisense drug 'Vitravene' is an example of a phosphorothioate ASO.[9] One of the major limitations of PS-DNA are their non-sequence dependent off target effects, caused by binding to serum proteins which may result in cellular toxicity,[22] i.e., binding to certain proteins, such as heparin-binding proteins. ONs can directly bind to proteins and effect their function. This is also referred to as off-target effects.

Another example of a backbone modification is N3'- P5' DNA, where the 3'- oxygen is replaced by a nitrogen atom, (Figure 5). N3'- P5' DNA exhibit high affinity[23] towards cRNA and nuclease resistance.[24] In addition, they display high specificity (mismatch discrimination). They are less toxic than PS-DNA but do not allow recruitment of RNase H.

Peptide nucleic acids (PNAs) were introduced by Nielsen and coworkers in 1991. They consist of repeating units of nucleobases conjugated to *N*-(2-aminoethyl) glycine units that are linked via amide bonds (Figure 5).[25] Unlike DNA, they do not contain a sugar moiety and the phosphate backbone is replaced by amide backbone which is acyclic, achiral and neutral.[26] The neutral character of this backbone results in the formation of PNA: DNA duplexes that are considerably more stable than DNA: DNA duplex,[27] due to the lack of charge repulsion between PNA and DNA backbone. However, due to their neutral character, they suffer from poor aqueous solubility and limited cellular uptake. In order to overcome these limitations and for practical usage of PNAs as antisense agents, they have been coupled to lipids or peptides that are efficiently internalized by cells.[28,29] A minimum of four lysine units are required in order to achieve antisens activity of PNAs in vivo.

Morpholinos are another backbone modification in which the 2'-deoxyribose is replaced by a morpholino ring and a neutral phosphoramidate intersubunit linkage replaces the phosphodiester backbone.[30] Advantages include high RNA affinity and enzymatic resistance,[31] while poor cellular uptake and inability to recruit RNase H are some of the limitations of this type of chemistry. Since MFs do not recruit RNase H, they have been evaluated as splice switching antisense agents (SSO, for definition of SSO, please refer section 1.2) targeting pre-mRNA[32] and as steric blockers for knocking down gene expression in zebra fish embroys.[33]

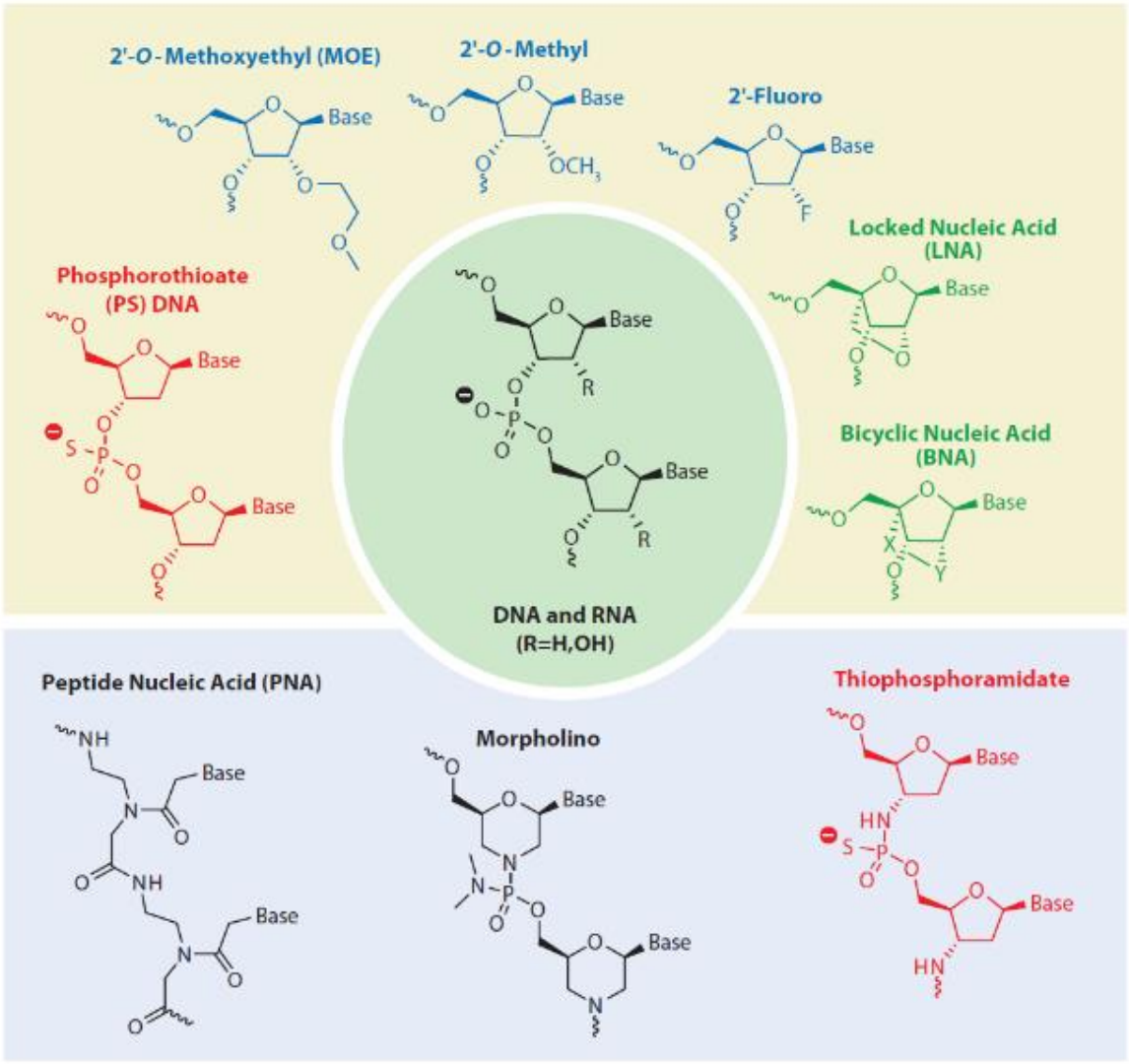

Figure 5. Chemical modifications used for antisense approaches or in the antisense technology. (Adapted with permission from ref 19c).

1.4. Sugar Modified Antisense Oligonucleotides.

The problems associated with backbone modifications have to some degree been solved through the use of sugar modified nucleotides. Although a great number of sugar modified nucleotides have been synthesized, ONs containing nucleotides with alkyl modifications at the 2' position of the ribose, i.e., 2'-*O*-methyl and 2'-*O*-methoxyethyl RNA (MOE) (Figure 5) have generally produced the most promising results. They impart increased binding affinity towards

cDNA/RNA and nuclease resistance, [34] but do not allow recruitment of RNase H since in order to have efficient RNase H cleavage, the duplexes with RNA must adopt A/B-type helix geometries, to support RNaseH cleavage. AONs in which these modifications are interspersed will inhibit protein formation via the steric block mechanism (Figure 2b). However, RNase H mediated cleavage of mRNA can be induced if conformationally restriced nucleotides are used in the so called gapmer design[35] (discussed in section 1.5, Figure 7).

2'-FANA, also known as 2'-fluoro arabino nucleic acid are one of the few sugar modified nucleotides that allows for RNase H mediated cleavage of RNA strands.[36] Their duplexes with RNA mimic DNA:RNA duplex geometry (A/B type).

An important advance with sugar modified oligonucleotides is the invention of locked nucleic acids (LNA),[37] also known by their more general name bridged nucleic acids (BNAs).[38] BNAs are bicyclic nucleotides in which the 2' and 4' positions are connected by an oxymethylene bridge. Examples include LNAs and α-L-LNA (Figure 6).[39] The LNA family will be discussed in greater detail in the subsequent section.

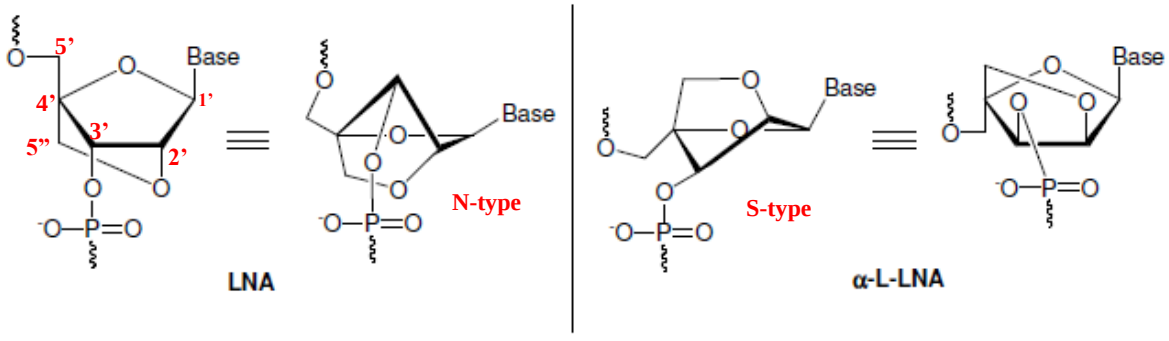

Figure 6. Structure and backbone conformation of LNA and α-L-LNA.

1.5. Conformationally restricted antisense nucleic acid analogs

Conformationally constrained nucleos(t)ides are obtained by covalently linking two atoms of the nucleoside by an alkyl chain to lock the nucleos(t)ide in a specific conformation. The first sugar locked nucleoside, 2′, 3′-exo-methylene nucleoside, was synthesized by Okabe[40a] in 1989. Later, with the development of antisense technology, the importance of sugar pucker nucleotides was highlighted in therapeutics. Soon after, Locked Nucleic Acid (LNA) was invented. The synthesis was realized independently by Iminashi (1997)[40b] and Wengel (1998).[41] In LNA, the oxymethylene bridge between 2'-OH and 4'-C restricts the conformation in the so called *N*-type conformation, (Figure 6) which is the conformation that ribonucleotides adopt in highly thermostable RNA duplexes. The advantage of incorporating a nucleotide that is conformationally restricted in a *N*-type conformation was highlighted by the reported increase in the thermal denaturation temperatures of duplexes up to ~9.6 °C per LNA modification.[42] It is known that RNA:RNA duplexes have so-called A-type helix geometry which is thermodynamically more stable than DNA:DNA duplexes having B-type geometry.[43] AON containing LNA modifications are preorganized as A-type geometry and hence exhibit very high RNA-binding affinity due to reduced entropy cost during binding. The studies have since shown that both enthalpic and entropic factors contribute towards high binding affinity. Fixed *N*-type, 3'-endo conformation (Figure 6) of LNA nucleoside[42a] and enhanced base stacking of nucleobase also results in enhanced mismatch specificity and improved nuclease stability towards exonucleases for LNA modified ONs. This renders LNA nucleotides as attractive candidates for therapeutic and diagnostic applications. Complete stability against 3'-exonuclease enzyme has been reported for fully modified LNA strands (Figure 7a).[41]

Although LNAs have proven to be potent ASOs, they are not compatible with RNase-H mediated RNA cleavage, if used in a mixmer design (Figure 7c). Thus, to elicit RNase-H activity, LNAs have also been employed as ASO modifications in gapmer design (Figure 7b). A gapmer is a chimeric antisense oligonucleotide that contains a central block of RNase H tolerant nucleotides flanked by affinity-enhancing and typically non-RNaseH tolerant nucleotides such as LNAs. The central gap allows for RNaseH recruitment.

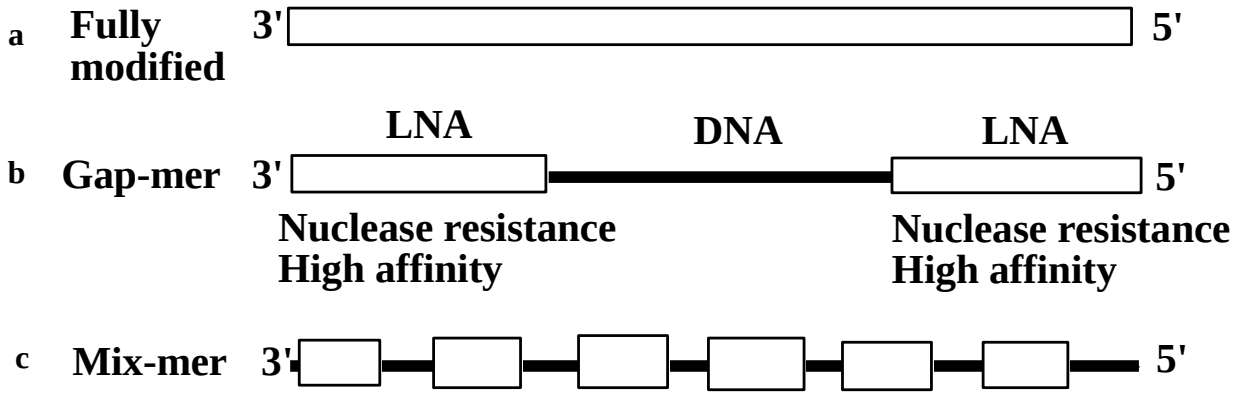

Figure 7. Design of ASO, depicted as a) fully modified, b) gapmer and c) mix-mer. The white boxes in AONs symbolize non-RNase H tolerant LNA building blocks.

LNA-DNA-LNA designed gapmers (Figure 7c) have been shown to be more potent activators of RNase H-mediated RNA degradation than the corresponding 2′-*O*-methyl-RNA gapmers.[33,44] The affinity of the gapmers toward target RNA correlates with RNase H-mediated degradation, that is, LNA>2'-O-methyl>RNA>DNA>PS-DNA.[45] Further, in vivo antisense experiments with LNA designed gapmers targeting mRNA in the central nervous system of rats has been successfully reported without causing any toxic effects.[46] In a study it has been demonstrated that LNA/DNA mix-mers enhance the inhibition of HIV-1 genome dimerization relative to DNA oligonucleotides.[47] Hence, it is clear that LNA-antisense, either

LNA/DNA/LNA gapmers for RNaseH activation or LNA mixmers for RNaseH independent activity, represents a favorable approach for gene silencing both in vitro and in vivo.

The therapeutic potential of LNA has been further explored for targeting micro RNA[48] and as modifications for siRNA.[49] Micro RNAs (miRNA) are a class of small non-coding RNAs usually 22 nt in length acting as post-transcriptional regulators of gene expression. These non-coding RNAs are found to be misregulated in cancer cells, which renders them as prime candidates for diagnostic and therapeutic applications. However, being short (~22 nt) and existing as a broad family with members often differing by only one nucleotide, emphasizes the need for RNA-targeting ONs with high binding specificity. LNA modified ON probes have been reported to be highly sensitive for efficient detection of miRNAs via northern blotting analysis.[50] In a similar context, LNAs have also been demonstrated to have a promising therapeutic value as siRNA modifications.[49] siRNAs, which are also known as small interfering RNAs, are double stranded RNAs about ~22nt long result in the degradation of mRNA upon loading into RNA-induced silencing complex via the so called RNA interference (RNAi) mechanism[51,52] (*RNAi is a biological process where RNA inhibits the expression of a protein by destroying the specific mRNA*).

α-L-LNA and other bridged nucleic acid analogs

Due to the immense therapeutic potential of locked nucleic acids, many other chemically modified locked nucleic acids have been synthesized and evaluated as antisense modifications. The synthesis of the first two diastereoisomers of LNA i.e., xylo-LNA and α-L-LNA (Figure 6)[53] was published by Wengel and coworkers. Later the properties of all eight LNA stereoisomers[54] were investigated. α-L-LNA[53] is a diasteromer of LNA with an inverted stereochemical configuration at the C2', C3'and C4' positions. The inverted stereochemistry

locks the conformation of this molecule in C2'-endo pucker, i.e, *S*-type conformation (shown in Figure 6), hence, making it more DNA like. The binding affinity of ONs modified with α-L-LNA nucleotides was studied and found to result in an increase between +1 to +5 °C against DNA and +4 to +6 °C against RNA.[55] Since, the geometry of duplexes between α-L-LNA modified ONs and cDNA gradually resemble that of unmodified DNA duplexes, these analogs have been used to successfully induce RNase-H mediated RNA cleavage in gapmer designs (Figure 7). In addition, these analogs confer improved nuclease resistance as compared to the parent LNA analog.[55]

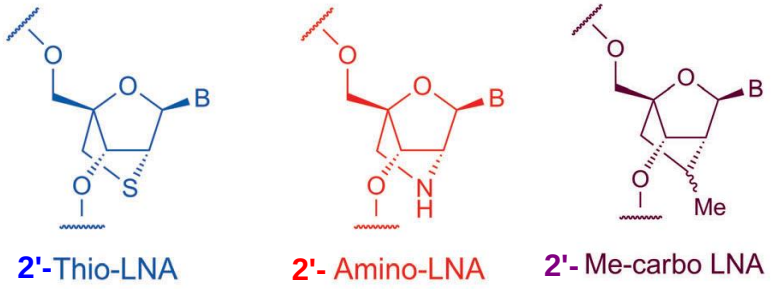

Figure 8. Chemically modified LNA analogs. (Adapted with permission from ref. 56).

Replacement of the 2'-O atom on oxymethylene bridge with other hetero/nonhetero atoms such as nitrogen, sulfur or carbon yields new classes of LNA nucleotides (Figure 8). They were the first LNA modified analogs[61] and displayed similar binding affinity towards complimentary DNA/RNA as the parent LNA analog.

Amino LNAs have been shown to display strong binding affinity toward complimentary DNA/RNA.[57a,b] The advantage of having this modification is that the N-atom acts as an additional handle to which different functional groups can be attached. Various bulky and aromatic substituents were attached to the 2'-position. The substituents will generally point into the minor groove upon duplex formation unless, the substituents are intercalators. For example,

substitution of aromatic groups such as benzene and pyrene result in the formation of stable duplexes with cDNA/RNA. Linker chemistry also plays a major role in modulating the hybridization properties, as substituents attached to the carbonyl group form more stable duplexes as compared to the methyl group. For example, in benzoyl vs benzyl and pyrene-1-ylcarbonyl vs pyrene-1-methyl, the moieties attached via carbonyl group are more stable.[57c] Recently Wengel and coworkers attached amino acids to 2'-amino LNA with the objective of increasing cellular uptake of ONs.[58] The resulting duplexes with DNA/RNA complements, display increases in T_m of +12 °C in thermal stability relative to unmodified duplexes. The increase in thermal stability is believed to be caused by decreased electrostatic repulsion between the negatively charged phosphate backbones due to positively charged amino acid residues.

The corresponding α-L-LNA diastereomer of 2'- amino LNA i.e., 2'-α-L-amino LNA have been synthesized by various coworkers, who also reported on the properties of ONs modified with these building blocks carrying aliphatic or aromatic moieties.[59] The pyrene modified ONs were found to be of particular interest since incorporation of these pyrene sustituted analogs results in the formation of very stable duplexes with complimentary DNA (ΔT_m/modification up to +19.5 °C).[60] Absorbance and fluorescence studies revealed that the duplex stabilization was a result of increased stacking interactions between the pyrene moieties and neighboring nucleobases due to intercalation.

With the goal of further improving their therapeutic potential, the complexity of LNA derivatives has continuously increased, albeit without major improvements in the hybridization properties. Chattopadhyaya and coworkers introduced the so-called carbo LNAs[62] and carbo

ENAs[63], where the 2' and 4'-positions are linked by ethylene and propylene bridges, respectively (Figure 9).

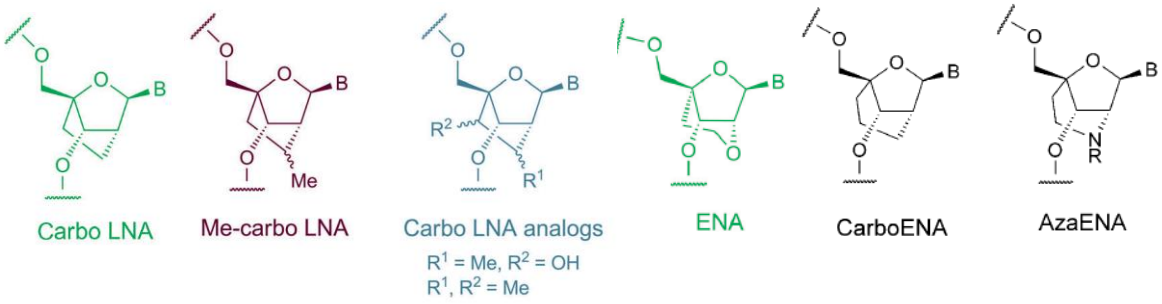

Figure 9. Carbocyclic (carbo) LNA and (carbo) ENA analogs. (Adapted with permission from ref 56).

ONs modified with these more hydrophobic locked nucleosides generally display similar affinity towards RNA as compared to ONs modified with the canonical parent LNA monomers and do show improved nuclease resistance (Figure 8).[63,64] Carbo LNA modified AONs display similar affinity towards target RNA as LNAs.[64] Motivated by their findings, the Chattopadhyaya group elaborated on the carbo LNA skeleton, by synthesizing modified carbo LNAs. The modifications were conducted on the carbocyclic bridge between C2'- and C4'-position (Figure 9). On comparison with the regular carbo LNA it was found that AONs carrying these modified carbo LNA derivatives exhibit lower affinity toward RNA targets.[65] Further, they showed that the nature of the modification (-OH versus - CH_3) (Figure 9) and their respective stereochemical orientations at C6′ and C7′ in the carbocylic moiety of carba-LNA play a significant role in modulating the AONs affinity towards target RNA. For example, when the C7'-methyl group is pointed towards the vicinal 3'-phosphate group, it destabilizes the DNA:RNA duplex by -1.5 °C to -2.0 °C. In contrast, the stereochemical orientation of C6'-OH does not have a marked effect on the duplex stability. However, the additional modification on

the carbocyclic moiety provides enhanced nuclease stability. In a similar vein, the properties of carba-ENAs were also studied. Introducing a N-atom on the bridge results in the formation of a derivative of ENA i.e., AzaENA (Figure 9). ENAs (both carba ENA and Aza ENA) have been reported to result in reduced thermal affinity towards RNA targets relative to ENA. Modifying the oxymethylene bridge with an additional methylene or N-atom does not improve the properties of these analogs.

Many more bridged nucleic acid analogs have been synthesized and their properties studied in regard to antisense. For a detail study on carba LNAs or ENAs, the reader is encouraged to read the review article of Zhou et al.[65]

1.6. Base Modifications. DNA duplexes between two complimentary strands are formed due to hydrogen bonding and efficient π-π stacking interactions between the nucleobases. Another approach for increasing duplex stability that has been pursued is modification of the nucleobase of DNA or RNA.[66] Either strengthening the hydrogen bonds by using the surrogates of natural nucleobases or by increasing the π-π stacking area.

Alteration of H-bonding: According to the Watson-Crick base pairing rules, G pairs with C forming three H-bonds whereas A pairs with T with two H-bonds. However, the H-bonding ability of adenine to thymine can be altered by substituting A with 2,6 diaminopurine. The T_m of oligonucleotides containing 2-amino-2'-deoxyadenosine residues increases by 1 °C per 2,6-diaminopurine residue.[67] Such nucleobases are also called isomorphic nucleobases. These analogs is discussed in detail in chapter 2, section 2.5.

Improvement of base stacking: Chemical modifications on the nucleobase are generally placed in one of the duplex grooves. For example, small entities such as ethynyl and propargyl amine when attached to the C5-position of pyrimidines, are well tolerated in major groove and form

stable duplexes. Also, stacking of aromatic substituted nucleotides in an ON results in the formation of stable DNA/RNA duplex due to enhanced π-π stacking interactions.[68,69] In Dr. Hrdlicka's laboratory, we have explored nucleobase-functionalization of LNA as an alternative strategy to improve the biophysical properties of LNA.[9] We have shown that LNA building blocks, which are modified with ethynyl and propargyl amine at the C5 position of pyrimidines display very high affinity toward RNA targets, excellent binding specificity and remarkable stability against exonucleases. In contrast, the corresponding C8-functionalized purine building blocks display much lower affinity toward DNA/RNA targets, most likely due to an increased preference of the nucleobases to adopt *syn* conformations about the glycosidic torsion angle which does not permit Watson-Crick base pairing. The corresponding results are discussed in detail in section B, chapter 3 and chapter 4.

1.7. Summary

In conclusion, a series of conformationally restricted analogs have been synthesized and the hybridization properties of ONs modified with such building blocks are typically superior relative to that of unmodified ONs. However, none of the modifications meet all of the desired requirements of perfect antisense modification, i.e., excellent binding affinity, specificity and enhanced enzymatic stability. As a result, there is an urgent need for analogs which can overcome these limitations.

1.8. References

1. a) Kurreck, J. *Eur. J. Biochem*. **2003**, *270*, 1628-1644; b) Watts, J. K.; Deleavey, G. F.; Damha, M. J. *Drug Discovery Today*. **2008**, *13*, 842-855; c) Duca, M.; Vekhoff, P.; Oussedik, K.; Halby, L.; Arimondo, P. B. *Nucleic Acids Res*. **2008**, *36*, 5123-5138 d) Simon, P.; Cannata, F.; Concordet, J. P.; Giovannangeli, C. *Biochimie* **2008**, *90*, 1109-1116.

2. Corey, D. R. *J. Clin. Invest*. **2007**, *117*, 3615-3622.

3. a) Stephenson, Z. *Proc. Natl. Acad. Sci*, USA. **1978**, *75*, 280-284; b) Veedu, R. N.; Wengel, J. *Chem. Biodivers*. **2010**, *7*, 536-542.

4. a) Uhlmann, E.; Peyman, A. *Chem. Rev*. **1990**, *90*, 543-584; b) Crooke, S. T. *Annu. Rev. Med*. **2004**, *55*, 61-95.

5. Schubert, S.; Kurreck, J. *Curr. Drug Targets*. **2004**, *5*, 667-681.

6. Khachigian, L. M. *Curr. Opin. Mol. Ther*. **2002**, *4*, 119-121.

7. De Fougerolles, A.; Vornlocher, H. P.; Maraganore, J.; Lieberman, J. *Nature Rev. Drug Discov*. **2007**, *6*, 443-453.

8. a) Bartel, D. P. *Cell*. **2004**, *116*, 281-297; b) He, L.; Hannon, G. J. *Nat. Rev. Genet.* **2004**, *5*, 522-531; c) Bushati, N.; Cohen, S. M. *Annu. Rev. Cell Dev. Biol*. **2007**, *23*, 175-205.

9. Jabs, D. A.; Griffiths, P. D. *Am. J. Ophthalmol*. **2002**, *133*, 552-556.

10. Pan, W. H.; Clawson, G. A. J. *Cell. Biochem*. **2006**, *98*, 14-35.

11. Millgan, J. F.; Matteucci, M. D.; Martin, J. C. *J. Med. Chem*. **1993**, *36*, 1923-1937.

12. Helene, C.; Toulme, J. *Biochim. Biophys. Acta*. **1990**, *1049*, 99-125.

13. Crooke, S. T. *Biochim. Biophys. Acta*. **1999**, *1489*, 31-44.

14. Verma, S. et al. *Annu. Rev. Biochem*. **1998**, *67*, 99-134.

15. a) Weintraub, H. M. *Sci. Am*. **1990**, *262*, 40-46; b) Bauman, J.; Jearawiriyapaisarn, N.; Kole, R. *Oligonucleotides*. **2009**, *19*, 1-14; c) Järver, P.; Coursindel, T.; Andaloussi, S. E. L.; Godfrey, C.; Wood, M. J. A.; Gait, M. J. *Mol. Ther. Nucleic Acids.* **2012**, *1*, e27, 1-17.

16. a) Stewart, A. J.; Pichon, C.; Meunier, L.; Midoux, P.; Monsigny, M.; Roche, A. C. *Mol. Pharmacol*. **1996**, *50*, 1487-1494; b) Clarenc, J. P.; Degols, G.; Leonetti, J. P.; Milhaud, P.; Lebleu, B. *Anticancer Drug Des*. **1993**, *8*, 81-94.

17. a) Carruthers, M. H.; Barone, A. D.; Beaucage, S. L.; Dodds, D. R.; Fisher, E. F.; McBride, L. J.; Matteucci, M.; Stabinsky, Z.; Tang, J. Y. *Methods Enzymol*. **1987**, *154*, 287-313; b) Crooke, S. T. *Biochim. Biophys. Acta*. **1999**, *1489*, 31-44.

18. Verma, S.; Eckstein, F. *Annu. Rev. Biochem*. **1998**, *67*, 99-134.

19. a) Duca, M.; Vekhoff, P.; Oussedik, K.; Halby, L.; Arimondo, B. P. *Nucleic Acid Res.* **2008**, *36*, 5123-5138; b) Cook, P. D. *Nucleos Nucleot Nucl*. **1999**, *18*, 1141-1162; c) Bennett, C. F.; Swayze, E. E. *Annu. Rev. Pharmacol. Toxicol*. **2010**, *50*, 259-293.

20. Miller, P. S.; Yano, J.; Yano, E.; Carroll, C.; Jayaraman, K.; Ts'o, P. O. *Biochemistry*. **1979**, *18*, 5134-5143.

21. Stein, C. A.; Subasinghe, C.; Shinozuka, K.; Cohen, J. *Nucleic Acids Res*. **1988**, *16*, 3209-3221.

22. Crooke, S. T. *Methods Enzymol*. **2000**, *313*, 3-45.

23. Egli, M.; Gryaznov, S. M. *Cell. Mol. Life Sci*. **2000**, *57*, 1440-1456.

24. Gryaznov, S. M.; Lloyd, D. H.; Chen, J. K.; Schultz, R. G.; DeDionisio, L. A.; Ratmeyer, L.; Wilson W. D. *Proc. Nat. Acad. Sci. USA.* **1995**, *92*, 5798-5802.

25. Nielsen, P. E.; Egholm, M.; Berg, R. H.; Buchardt, O. *Science* **1991**, *254*, 1497-1500.

26. Larson, H. J.; Bentin, T.; Nielsen, P. E. *Biochim. Biophys. Acta*. **1999**, *1489*, 159-166.

27. Tomac, S.; Sarkar, M.; Ratilainen, T.; Wittung, P.; Nielsen, P. E.; Norden, B.; Graslund, A. *J. Am. Chem. Soc*. **1996**, *118*, 5544-5552.

28. a) Elayadi, A. N.; Corey, D. R. *Curr. Opin. Invest. Drugs*. **2001**, *2*, 558-561; b) Braasch, D. A.; Corey, D. R. *Biochemistry* **2002**, *41*, 4503-4509.

29. Nielsen, P. E. *Methods Enzymol*. **1999**, *313*, 156-164.

30. Heasman, J. *Dev. Biol*. **2002**, *243*, 209-214.

31.a) Hudziak, R. M.; Barofsky, E.; Barofsky, D. F.; Weller, D. L.; Huang, S. B.; Weller, D. D. *Nucleic Acid Drug Dev*. **1997**, *7*, 187-195; b) Summerton, J. *Biochim. Biophys. Acta*. **1999**, *1489*, 141-158.

32. Flores-Aguilar, M. *J. Infect. Dis*. **1997**. *175*, 1308.

33. Kim, R.; Emi, M.; Matsuura, K.; Tanabe, K. *Cancer Gene Ther*. **2007**, *14*, 1-11.

34. a) Kurreck, J.; Wyszko, E.; Gillen, C.; Erdmann, V. A. *Nucleic Acids Res*. **2002**, *30*, 1911-1918; b) Crooke, S. T.; Lemonidis, K. M.; Neilson, L.; Griffey, R.; Lesnik, E. A.; Monia, B. P. *Biochem. J*. **1995**, *312*, 599-608.

35. Inoue, H.; Hayase, Y.; Iwai, S.; Ohtsukal, E. *FEBS Lett*. **1987**, *215*, 327-330.

36. Lok, C. N.; Viazovkina, E.; Min, K. L.; Nagy, E.; Wilds, C. J.; Damha, M. J.; Parniak, M. A. *Biochemistry* **2002**, *41*, 3457-3467.

37. Koshkin, A. A.; Singh S. K.; Nielson, P.; Rajwanshi, V. K.; Kumar, R.; Meldgaard, M.; Olsen, C. E.; Wengel, J. *Tetrahedron* **1998**, *54*, 3607-3630.

38. Obika, S.; Nanbu, D.; Hari, Y.; Andoh, J.; Morio, K.; Doi, T.; Imanishi, T. *Tetrahedron Lett*. **1998**, *39*, 5401-5404.

39. Seth, P. P.; Siwkowski. A.; Allerson, C. R.; Vasquez, G.; Lee. S. *J. Med. Chem*. **2009**, *52*, 10-13.

40. a) Okabe, M.; Sun, R. C. *Tetrahedron Lett*. **1989**, *30*, 2203-2206; b)Obika, S.; Nanbu, D.; Hari, Y.; Andoh, J.; Morio, K.; Doi, T.; Imanishi, T. *Tetrahedron Lett*. **1998**, *39*, 5401-5404.

41. Frieden, M.; Hansen, H. F.; Koch, T. *Nucleos. Nucleot. Nucl*. **2003**, *22*, 1041-1043.

42. a) Koshkin, A.A.; Singh, S. K.; Nielsen, P.; Rajwanshi, V. K.; Kumar, R.; Meldgaard, M.; Olsen, C. E.; Wengel, J. *Tetrahedron* **1998**, *54*, 3607-3630; b) Braasch, D. A.; Corey, D. R. *Chem. Biol*. **2001**, *8*, 1-7; c) Petersen, M.; Wengel, J. *Trends Biotechnol*. **2003**, *21*, 74-81.

43. Saenger, W. *Principles of Nucleic Acid structure*. Springer-Verlag, New York, **1984**, 556.

44. Prakash, P. T.; Siwkowski, A.; Allerson, R. C.; Migawa, M. T.; Lee, S.; Gaus, H. J.; Black, C.; Seth, P. P.; Swayze, E. E.; Bhat, B. *J. Med. Chem*. **2010**, *53*, 1636-1650.

45. Kurreck, J.; Wyszko, E.; Gillen, C.; Erdmann, V. A. *Nucleic Acids Res*. **2002**, *30*, 1911-1918.

46. a) Wahlestedt, C.; Salmi, P.; Good, L.; Kela, J.; Johnsson, T.; Hokfelt, T.; Broberger, C.; Porreca, F.; Lai, J.; Ren, K.; Ossipov, M.; Koshkin, A.; Jakobsen, N.; Skouv, J.; Oerum, H.; Jacobsen, M. H.; Wengel, J. *Proc. Natl. Acad. Sci. USA*. **2000**, *97*, 5633-5638; b) Kauppinen, S.; Vester, B.; Wengel, J. *Drug Discovery Today*:*Technol*. **2005**, *2*, 287-290; c) Ørum, H.; Wengel, J. *CurrOpinMolTher*. **2001**, *3*, 239-243; d) Koch, T.; Ørum, H.; *AntisenseDrugTechnology: Principles, Strategies,and Applications,2nd edn. Ed. S. T. Crooke, CRC Press, BocaRaton*, **2008**, 519-564.

47. Elmen, J. *FEBS Lett*. **2004**, *578*, 285-290.

48. a) Ambros, V. *Cell* **2001**, *107*, 823-826.; b) Bartel, D.P. *Cell* **2004**, *116*, 281-297.

49. Elmen, J.; Thonberg, H.; Ljungberg, K.; Frieden, M.; Westergaard, M.; Xu, Y.; Wahren, B.; Liang, Z.; Ørum, H.; Koch, T.; Wahlestedt, C. *Nucleic Acids Res*. **2005**, *33*, 439-447.

50. Valoczi, A.; Hornyik, C.; Varga, N.; Burgyán, J.; Kauppinen, S.; Havelda, Z. *Nucleic Acids Res*. **2004**, *32*, e175.

51. Fire, A.; Xu, Si.; Montgomery, M. K.; Kostas, S. A.; Driver, S. E.; Mello, C. C. *Nature* **1998**, *391*, 806-811.

52. Elmen, J.; Thonberg, H.; Ljungberg, K.; Frieden, M.; Westergaard, M.; Xu, Y.; Wahren, B.; Liang, Z.; Ørum, H.; Koch, T.; Wahlestedt, C. *Nucleic Acids Res*. **2005**, *33*, 439-447.

53. a) Rajwanshi, V. K.; Håkansson, A. E.; Dahl, B. M.; Wengel, J. *Chem. Commun*. **1999**, 1395-1396.; b) Rajwanshi, V. K.; Håkansson, A. E.; Kumar, R.; Wengel, J. *Chem Comm*. **1999**, 2073-2074.

54. Rajwanshi, V. K.; Håkansson, A. E.; Sørensen, M. D.; Pitsch, S.; Singh, S. K.; Kumar R.; Nielsen, P.; Wengel, J. *Angew. Chem., Int. Ed*. **2000**, *39*, 1656-1659.

55. Sørensen, M. D.; Kværnø, L.; Bryld, T.; Håkansson, A. E.; Verbeure, B.; Gaubert, G.; Herdewijn, P.; Wengel, J. *J. Am. Chem. Soc*. **2002**, *124*, 2164-2176.

56. Prakash, T. P. *Chem Biodivers*. **2011**, *8*, 1616-1641.

57. Rosenbohm, C.; Christensen, M. S.; Sørensen, M. D.; Pedersen, S. D.; Larsen, L. E.; Wengel, J.; Koch, T. *Org. Biomol. Chem*. **2003**, *1*, 655-663; b) Singh, S. K.; Kumar, R.; Wengel, J. *J. Org. Chem*. **1998**, *63*, 10035-10039; c) Sørensen, M. D.; Petersen, M.; Wengel, J. *Chem. Commun*. **2003**, 2130-2131.

58. Johannsen, W. M.; Crispino, L.; Wamberg, M. C.; Kalra, N.; Wengel, J. *Org. Biomol. Chem*. **2011**, *9*, 243-252.

59. Andersen, N. K.; Anderson, B. A; Wengel, J.; Hrdlicka, P. J. *J. Org. Chem*. **2013**, *78*, 12690-12702.

60. Kumar, S.; Madsen, A. S.; Wengel, J.; Hrdlicka, P. J. *Nucleos Nucleot Nucl*. **2007**, *26*, 1403–1405.

61. Kumar, R; Singh, K.; Koshkin, A. A., Rajwanshi, V. K., Meldgaard, M.; Wengel, J. *Bio. Org, Med. Chem. Lett*. **1998**, *8*, 2219-2222.

62. Xu, J.; Liu, Yi.; Dupouy, C.; Chattopadhyaya, J. *J. Org. Chem*. **2009**, *74*, 6534-6554.

63. a) Liu, Yi.; Xu, J.; Karimiahmadabadi, M.; Zhou, C.; Chattopadhyaya, J. *J. Org. Chem*. **2010**, 75, 7112-7128; b) Fluiter, K.; Frieden, M.; Vreijling, J.; Rosenbohm, C.; DeWissel, M. B.; Christensen, S. M.; Koch, T.; Ørum, H.; Baas, F. *ChemBioChem* **2005**, *6*, 1104-1109.

64. a) Zhou, C.; Liu, Y.; Andaloussi, M.; Badgujar, N.; Plashkevych, O.; Chattopadhyaya, J. *J. Org. Chem.* **2009**, *74*, 118-134; b) Zhou, C.; Plashkevych, O.; Chattopadhyaya, J. *J. Org. Chem.* **2009**, *74*, 3248-3265.

65. Zhou, C.; Chattopadhyaya, J. *Curr Opin. Drug Discov. Dev*. **2009**, *12*, 876-898.

66. a) Gibson, K. J.; Benkovic, S. J. *Nucleic Acids Res*. **1987**, *15*, 6455-6467; b) Wagner, R. W. ; Matteucci, M. D.; Lewis, J. G.; Gutierrez, J.; Moulds, C.; Froehler, B. C. *Science* **1993**, *260*, 1510-1513; c) Ahmadian, M.; Zhang, P. M.; Bergstrom, D. E. *Nucleic Acids Res*. **1998**, *26*, 3127-3135; d) Graham, D.; Parkinson, J. A.; Brown, T. *J. Chem. Soc. Perk. Trans*. **1998**, *1*, 1131-1138; e) Znosko, B. M.; Barnes, T. W.; Krugh, T. R.; Turner, D. H. *J. Am. Chem. Soc*. **2003**, *125*, 6090-6097.

67. Cheong, C.; Tinoco, I. J.; Chollet, A. *Nucleic Acids Res*. **1988**, *16*, 5115-5122.

68. a) Andersen, N. A.; Chandak, N.; Brulíková, L.; Kumar, P.; Jensen, M. D.; Jensen, F.; Sharma, P. K.; Nielsen, P. *Bioorg. Med. Chem*. **2010**, *18*, 4702-4710; b) Kocalka, P.; Andersen, N. K.; Jensen, F.; Nielsen, P. *ChemBioChem* **2007**, *8*, 2106-2116.

69. Kaura, M.; Kumar, P.; Hrdlicka, P. J. *Org. Biomol. Chem*. **2012**, *10*, 8575-8578.

Chapter 2: Fluorophore Functionalized Nucleic Acids

2.1. Detection of Nucleic Acids

Detection of specific nucleic acid sequences is an important tool in modern molecular biology as it yields critical information regarding complex biomolecular systems inside cells, which has possible medical applications. Techniques for detection of nucleic acids include, i) southern blotting for detection of DNA[1a]; ii) northern blotting for detection of RNA[1b] and iii) polymerase chain reaction (PCR), for detection of DNA and RNA,[1c,1d] which entails exponential amplification of a few DNA strands, thereby, generating a sufficient number of copies of the target DNA sequence for visualization on gels or microarrays. Radioactive ^{32}P labelling of ON probes has been one of the traditional methods used for detection.[4,5] ^{32}P was used due to the intensity of signal it produces. However, due to safety concerns, short half-lives, waste disposal issues, and high costs, alternatives to these probes are desirable.

The use of fluorescence based methods[2,3] has provided greater flexibility (i.e., easiness in terms of cost and time compared to other techniques) and sensitivity for research applications. ON probes can be labelled with different fluorophores and used as biosensors for biomedical applications. Fluorophore-labelled ON probes are widely used in, e.g., fluorescent insitu hybridization (FISH),[6,7] monitoring of gene expression,[8] single nucleotide polymorphism (SNP) analysis[9,10] and DNA sequencing.[11] In this chapter, I shall discuss different constructs of fluorescent hybridization probes, their applications and give specific examples of fluorescent nucleobase analogs used to generate these probes.

2.2. Principle of Fluorescence. Fluorescence is a nonradiative phenomenon in which a fluorophore absorbs energy from light (photons), is promoted to an excited state, and relaxes back to a ground state, with which concomitant emission of lower energy (red-shifted light).[12] The advantage of this technique lies in the ability of a fluorophore to produce highly sensitive emission which is dependent on the nature of the molecular environment.[13] Fluorophores used in routine molecular biology, consist of planar, heterocyclic rings with characteristic absorption and emission profiles. Figure 10 demonstrates the general principle of fluorescence and absorption and emission spectra of a fluorophore. The choice of fluorophore depends on several factors such as the desired Stokes shift (the difference in the positions of the absorption band and the emission band), fluorescence quantum yield (ratio of number of photons emitted to the number of photons absorbed) and emission maxima. Commonly used fluorophores for labelling of ONs are organic dyes such as DABCYL, FAM, TAMRA, Cy3, Cy5 and polycyclic aromatic hydrocarbons (PAHs), like naphthalene, pyrene, perylene or coronene. PAHs are sufficiently fluorescent to produce an emission signal. These fluorophores can be attached to an ON sequence either during solid-phase synthesis or post synthetically, or via enzyme catalyzed reactions.[13] In the subsequent section the applications of fluorescent hybridization probes in nucleic acid analysis and different types of probe designs employed for it are discussed.

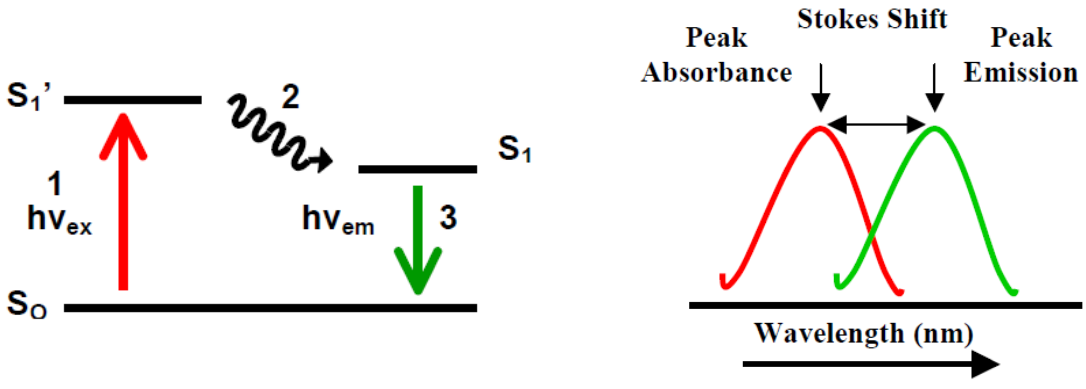

a) **b)**

Figure 10. Representation of **a**) Fluorescence phenomenon; **b**) absorption and emission spectra.[12]

2.3. Applications of fluorescent nucleic acid hybridization probes.

Fluorophore-labelled probes can be used to for detection of DNA/RNA targtes, DNA-protein interactions and single base mutations, (i.e., single nucleotide polymorphisms, SNP).[14] My focus has been on developing probes for detection of SNPs as SNPs are the most frequently occurring genetic variations in the human genome. SNPs are defined as single nucleotide variations which are in more than 1% of population.[15] Such variations are often the cause of genetic diseases and their detection enables early disease diagnosis. Hence, there is a considerable interest to develop methods for detection of these mutations. The use of fluorophore-labelled probes such as molecular beacons (MB) or binary probes are two strategies for SNP detection.[16]

2.4. Probe architectures of different fluorescent nucleic acid hybridization probes.

i) *FRET probes*. FRET, also known as Fluorescence Resonance Energy Transfer[17] is a coupling phenomenon which takes place between two chromophores acting as a donor-acceptor couple. Upon excitation, the excited state energy of the donor molecule is transferred non-radioatively to the acceptor molecule through dipole-dipole interactions. The efficiency of FRET is therefore, highly dependent on the distance and orientation between the two chromophores. The donor-acceptor pair need to be close (10-80 Å) for the energy transfer to be efficient and the emission spectrum of a donor molecule must overlap with the absorption spectra of the acceptor molecule. As a result, FRET is used as a tool for measuring the distance between two chromophores, to detect DNA hybridization and many more applications.[18a] The majority of donor-acceptor pairs used for labelling are fluorescein and rhodamine dyes. However, aromatic

hydrocarbons are also being used for labelling as they can interact with other fluorophores, giving rise to excimer or FRET signals.[18b] Given below are examples of hybridization probes (binary probes, molecular beacons, excimer-to-monomer emission probes) which utilize FRET for detection of nucleic acids.

a) *Binary probes*. Binary probes are hybridization probes consisting of two single stranded ONs which are complimentary to a target strand. Recognition results in the formation of a ternary complex (Figure 11). Typically, one ON strand is labelled with donor florophore, and the other ON is labelled with an acceptor florophore. On hybridization with the target strand, the donor-acceptor florophore pair comes in close proximity and produces a FRET based signal. Pyrene (donor) has been used to produce a FRET signal with perylene (acceptor) at much shorter distance (2/3 of Förster distance, i.e., 10-80 Å) for nucleic acid assays under homogenous solution conditions.[19]

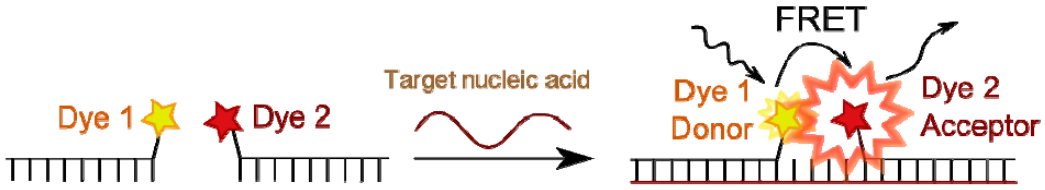

Figure 11. FRET type binary probes. (Adapted with permission from ref. 20).

b) *Molecular Beacons (MB)*. MBs are single stranded ON that are designed to fold up in a hairpin (Figure 12a), which consists of three main parts, i) a loop of 15-30 nt which hybridizes with a target strand, ii) a 5-8 base pair double stranded stem, which keeps the beacon in a closed form until target binding and iii) a fluorophore and a quencher which are connected to the termini of the hairpin probe. In the absence of a target, hairpin is closed, bringing the fluorophore-quencher pair in close proximity of each other, resulting in quenching of

fluorescence. However, duplex formation, results in separation of these two components and fluorescent dequenching.

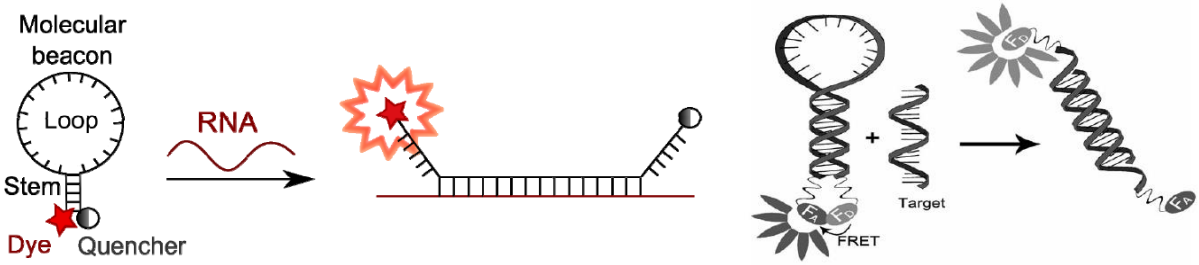

Figure 12. Molecular beacon design (Adapted with permission from ref. 20); b) Fret type MB. (Adapted with permission from ref 21a).

Replacement of the quencher with another florophore can result in FRET-based molecular beacons (Figure 12b).[21a,b] In the hairpin conformation, in the absence of a target, two florophores are in close proximity, causing FRET to take place. However, upon duplex formation with the target, the two fluorophores are separated, resulting in strong emission of the donor fluorophore.

A new class of MBs was constructed where pyrene couples were attached at the 5' and 3'end of the probe for detection of DNA and mRNA[22] (Figure 13a). The detection strategy is based on a change from excimer to monomer signal. This type of construct is different from the usual FRET type MB (shown in Figure 12b). [23,24] Both the pyrene moieties absorb energy to produce an excimer as shown in Figure 13a. Figure 13b illustrates the titration spectrum of the designed MB probe in the presence of increasing amounts of target DNA. With increasing concentration of target strand, the excimer signal decreases while the monomer emission increases due to the formation of MB probe-target duplex.

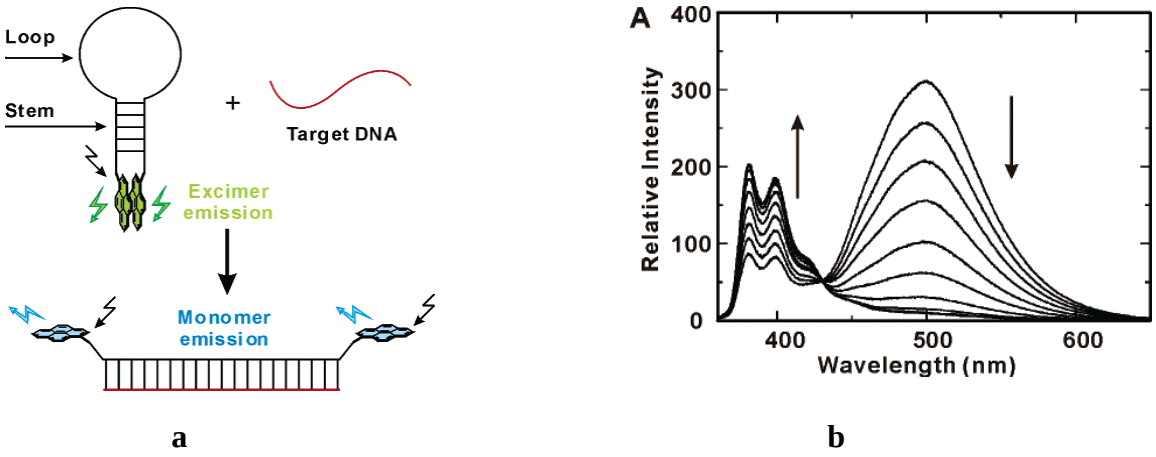

a **b**

Figure 13. a) Representation of excimer to monomer emission; b) Fluorescence titration spectra. (Adapted with permission from ref. 22).

ii) *Base discriminating fluorescent (BDF) probes*. There has been a growing interest in the detection of single nucleotide polymorphisms, (i.e., single base pair mutations), also referred to as SNP.[15] Several SNP detection methods have been developed to establish a robust and cost-effective system. However, all of these methods rely on the appropriate hybridization and washing conditions. The use of BDF probes is an alternative approach toward SNP detection.[25] The advantage of using this method is it does not require any additional washing steps and produces a clear fluorescence signal. The probes work on the principle of distinguishing the base through differences in fluorescence levels between matched and mismatched duplexes (Figure 14). Upon duplex formation with a matched target, fluorophores are typically designed to position into one of the non-quenching grooves (minor or major) of the duplex, thus, producing a strong fluorescence signal. In the presence of mismatch targets, on the other hand, the fluorophore intercalates into the duplex, resulting in nucleobases-mediated quenching of fluorescence.

Saito and coworkers have developed a series of fluorophore-labelled nucleotides for use as BDF probes.[25,26,27] For example, ONs modified with C5-pyrene carboxamide functionalized

pyrimidines display promising BDF properties, since, the fluorescence of the pyrenecarboxamide fluorophore is polarity sensitive.[28-31] When this fluorophore is attached to pyrimidines at the C5 position via a rigid propargyl linker, polarity driven differences in fluorescence are observed which are useful for discrimination of SNPs.[25]

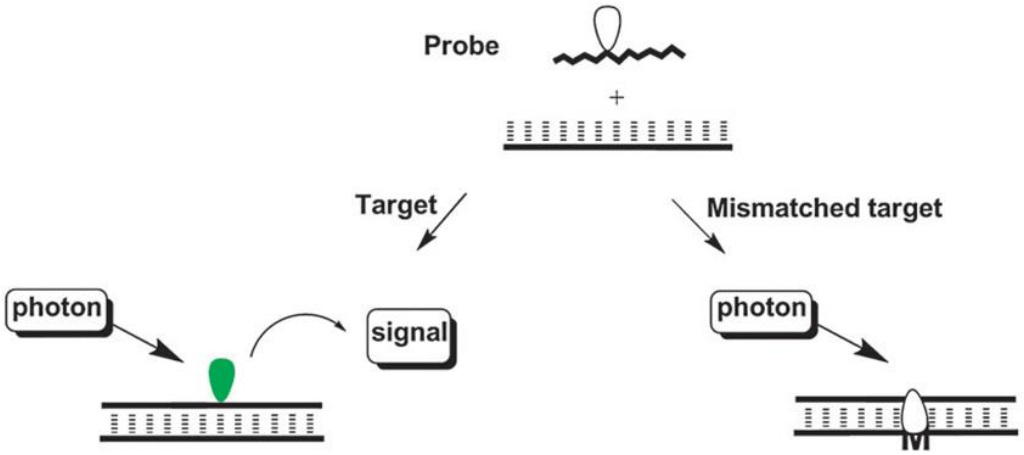

Figure 14. Principle of BDF probe. Fluorophore (droplet) labelled probe produces a signal with a matched targets, but not with mismatched targets.

iii) *Hybridization probes*. These probes are designed to produce a fluorescence change upon binding to a matched target. In the absence of a target, the fluorescence is low due to nucleobase mediated quenching of the fluoroscence[32] (Figure 15). Yamana and coworkers have developed O2'-pyrenylmethyl uridine modified ON probes (Figure 16a), which produce pronounced increases in fluorescence intensity (up to 30-fold), upon binding to target RNA[33] (discussed in section 2.5.2), while, much smaller increases are observed upon binding to DNA. This difference in fluorescence emission is attributed to the different binding modes of pyrene.[34] In case of RNA:RNA duplexes, pyrene is located in the minor groove of duplex, whereas, in case

of DNA:DNA duplexes, it intercalates inside the duplex core, thus leading to reduced fluorescence emission.

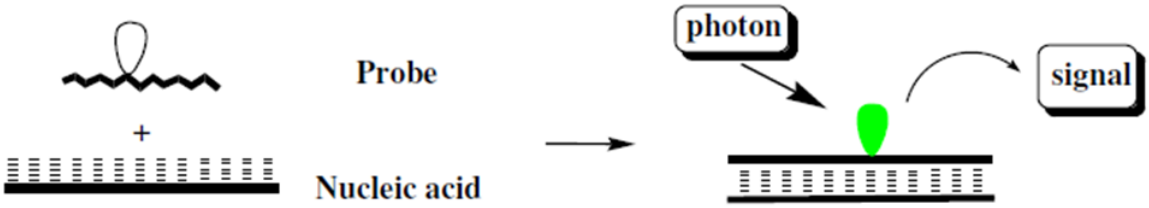

Figure 15. Principle of hybridization probe. Color of fluorophore mentioned in Figure 14. (Adapted with permission from ref. 68).

Hrdlicka and coworkers have synthesized C5 pyrenetriazole-functionalized 2'-deoxyuridine monomers 1, 2 (Figure 16b), which upon incorporation into ONs, display hybridization-induced increases in fluorescence intensity both with cDNA and cRNA.[35] In a different study, the group used pyrene-functionalized LNA as a key buiding blocks for development of hybridization probes. The results of the designed probes are discussed in greater detail in section 2.6.2.

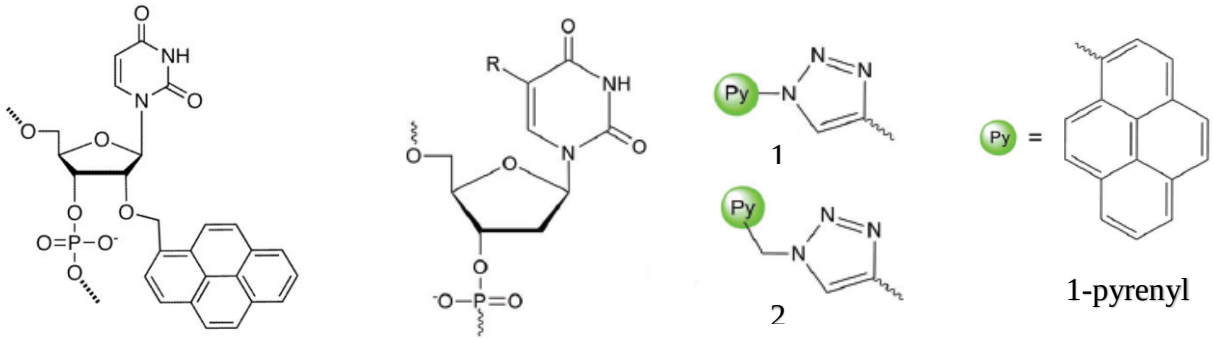

a **b**

Figure 16. Structure of 2′-O-(1-pyrenylmethyl)-uridine[46]; b) Pyrene-functionalized triazole-linked 2'-deoxyuridines. (Adapted with permission from ref. 68).

2.5. Chemistry of fluorophore substituted nucleobase analogs.

Natural nucleobases have weak fluorescence signals due to short decay times. The use of fluorophore labelled nucleobase analogs provides an alternative tool to overcome this limitation. These nucleobases can be either intrinsically fluorescent i.e, by modification of the natural nucleobases by using fluorescent nucleobase analogs or by conjugating extrinsic fluorophores to the nucleobase.

2.5.1. Intrinsically fluorescent nucleotide analogs. Intrinsically fluorescent nucleotides[36] are heterocyclic analogs that closely resemble the corresponding natural nucleobases with respect to their overall dimensions (isomorphic) and hydrogen bonding patterns. These analogs are able to base stack and form stable Watson-Crick type base-pairs to preserve the normal B-type geometry of the duplex. Some examples are discussed below.

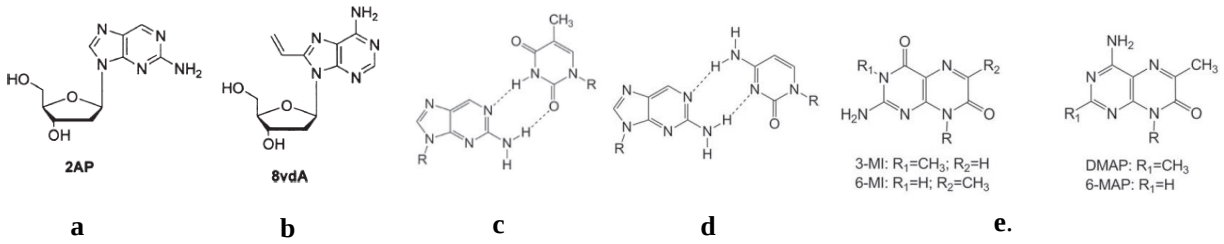

Figure 17. Structure of a) 2-amino-2'-deoxyadenosine; b) 8-vinyl, 2'-deoxyadenosine; c) 2-AP base paired with thymine; d) 2-AP base paired with cytosine; e) pteridines; R = deoxyribose. (Adapted with permission from ref. 36).

2-Amino-2'-deoxyadenosine (2-AP) (Figure 17a) was one of the first and most popular fluorescent nucleobases to be developed.[37] Like adenosine, it is able to form a stable base pair with thymine/uracil and to a lesser degree with cytosine[38,39] (Figure 17c, d). High quantum yield (Φ_F = 0.68 in H_2O), minimal pH sensitivity and improved sensitivity to environmental polarity

contribute to the utility of this analog. In addition, the absorption band of 2-AP is centered at 305nm[40], which is outside the absorption range of natural nucleosides (centered at 260 nm), which allows for selective excitation in the presence of natural nucleobases. However, upon incorporation into oligonucleotides, the fluorescence of 2-AP is quenched up to 100-fold, thus requiring a high concentration of 2-AP labelled oligonucleotide to achieve sensitive detection. Although this sensitivity of 2-AP has been exploited in studies of nucleic acid structure dynamics and nucleic acid protein interactions, there still is a need for nucleotides with more desirable florescent properties.

Replacement of the C8-hydrogen of adenosine, with a vinyl group yields 8-vinyldeoxyadenosine (8-vdA), which has improved photophysical properties (Figure 17b). Compared to 2-AP, 8-vdA exhibits an absorption maxima at 290 nm with an emission band at 382 nm and a comparable quantum yield (Φ_F = 0.66).[41] The emission of 8-vdA is sensitive to temperature and solvent but insensitive to pH. Upon incorporation into duplexes, its fluorescence is quenched, albeit to a lesser extent than 2-AP.

Pteridines

Pteridines, introduced by Hawkins and coworkers[42], are highly emissive heterocyclic purine analogs which contain two condensed six-membered rings. They are characterized by absorption bands above 300 nm and an intense emission band at ~ 435 nm. The most promising analogs in this family are the guanine analogs 3-MI (3-methyl isoxanthopterin) and 6-MI (6-methylisoxanthopterin)[3b] and the adenine analogs 6-MAP (4-amino-6-methyl-8-(2-deoxy-beta-d-ribofuranosyl)-7(8H)-pteridone) and DMAP (4-amino-2,6-dimethyl-8-(2'-deoxy-beta-d-ribofuranosyl)-7(8H)-pteridone) (Figure 17e). Their excitation maxima are located around 330 nm (for adenine analogs) and 350 nm (for guanosine analogs), well separated from the natural

absorption of natural nucleobases and hence easy to excite selectively. Φ_F of these analogs is high, ~0.4 for adenine analogs and ~0.9 for guanine analogs. However, when incorporated into ONs, the Φ_F is reduced due to nucleobases quenching. The mechanism underlying this fluorescence quenching is not well understood at present. One of the drawbacks associated with these analogs is the reduced thermostability of the resulting duplexes (6-MI is an exception). The fluorescent pteridines have been employed in numerous applications including structural studies of DNA[43] and to study base flipping as probes to evaluate hybridization specificity.[44] *DNA base flipping* is a phenomenon, in which a single nucleotide unit is completely flipped out of the duplex by specific enzymes to replace it with another base during DNA repair. The mechanism is being used for removing abnormal DNA bases. Pteridines such as 6-MAP modified probes have been used as a tool to study the dynamics of the process.[44]

2.5.2. Extrinsically fluorescent nucleosides

Nucleosides can be extrinsically labelled with fluorophores by covalent attachment. The point of attachment on the nucleoside can be either on the i) sugar residue; ii) nucleobase moiety or iii) as a nucleobase replacement. The point of attachment and the linker flexibility plays a significant role in modulating the properties of the fluorophore attached to the nucleoside. For example, C5-fluorophore modified pyrimidines directly point the coupled entity in the major groove of duplexes, whereas, sugar modified analogs often direct the moiety into the minor groove of duplexes unless long linkers are employed in which case the flurophores may intercalate into the duplex. A detail explaination with examples has been given in the subsequent section.[45]

A fluorophore conjugated to sugar skeleton. Yamana and coworkers modified the 2'-position of ribonucleotides with pyrenes to it and developed pyrene array by incorporating several

consecutive modifications into ONs.[46] Characterization by circular dichroism (CD) spectroscopy revealed that the incorporated pyrenes point outside the duplex are arranged in an array fashion along the minor groove of the duplexes. Array formation is also evidenced by a strong pyrene-pyrene excimer which can result in strong excimer fluorescence signal, observed when two pyrenes are in close proximity to each other, i.e, stacked upon each other.

Recently, Hrdlicka and coworkers utilized the same monomer to develop SNP discriminating RNA detecting probes. They constructed 2′-O-(1-pyrenylmethyl)-uridine modified ONs with LNAs as next-nearest neighbors. The hypothesis of the study was that canonical LNAs will tune the conformation of neighboring nucleoside toward N-type conformaitons and thus tune the overall duplex geometry toward an RNA-like A-type geometry.[47] This will cause the pyrene to be positioned into the minor groove of the duplex. In addition to this, the group has also used the monomer for a different application, i.e., the recognition of dsDNA via Invader approach.[48]

Fluorophore conjugated nucleobases. Fluorophores can be attached to the C5 position of pyrimidines, C7 position of deaza purines or C8 position of purines. While modifications at the first two positions do not affect the *anti-syn* equilibrium around the glycosidic torsion angle, C8 modified purines[49] tend to promote *syn* conformations and thus disrupt Watson-Crick hybridization.[50] Saito and coworkers have synthesized a substantial number of C5 pyrimidines, C7-deaza-adenosine and C8 adenosine fluorophore substituted analogs (Figure 18), and studied the photophysical properties of ONs modified with these monomers, for their use as base discriminating fluorescent (BDF) probes (principle discussed in section 2.3).[26]

A simple pyrene carboxamide fluorophore linked to the C5 position of 2’-deoxyuridine or 2’-deoxycytidine with propargyl linker has been shown to discriminate efficiently between matched and mismatched targets. These probes enabled SNP discrimination in human breast

cancer cell lines at 50 nM target concentration.[51] The same group also reported the synthesis of C7-arylethynylated 7-deaza-2'-deoxyadenosines and C8-pyrenyl substituted 2'-deoxyguanosine monomers and their use as BDF probes.[52] They also studied the effect of electron withdrawing or electron donating substituents on the solvatofluorochromic properties of C7-napthyl substituted 7-deaza-2'-deoxyadenosines (**5**, Figure 18).[27] The purpose of the study was to develop environmentally sensitive fluorescent molecules, as a tool for studying DNA-protein interactions, pH and viscosity changes, detection of genes etc. The 7-deazaadenine skeleton acts as an electron donor and results in the formation of an intramolecular donor-acceptor system with electronwithdrawing (EWG) substituted naphthalene, giving rise to large solvatofluorochromicity. In contrast, the 7-deazaadenine skeleton is unable to form such pairs when the naphthalene carries electron donating groups. Hence, an intramolecular donor-acceptor system is essential for improving solvatofluorochromic properties.

Similar studies have been conducted by Seela and coworkers where they investigated the synthesis and properties of a wide range of 7-deazapurine nucleoside derivatives.[53] They reported that C7 substituents are positioned in the major grove of the duplex.

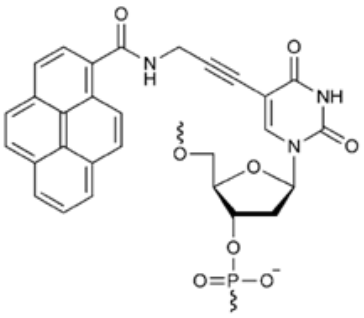

3

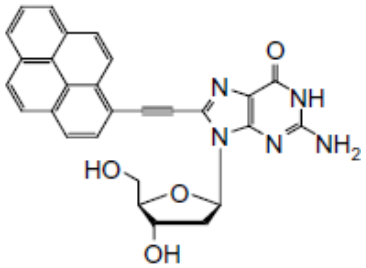

4

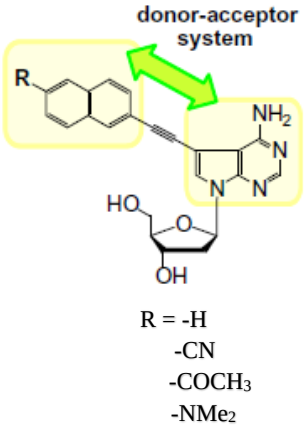

5

Figure 18. Pyrene labelled fluorescent pyrimidine and purine derivatives **3** (adapted with permission from ref. 10b) and **4** (adapted with permission from ref. 26); C7-substituted, 7-deaza-2'-deoxyadenosine **5**. (Adapted with permission from ref. 27).

Hrdlicka and coworkers have synthesized fluorophore labelled nucleobases-functionalized LNAs. Properties of these analogs will be discussed in detail in section 2.6.

iii) *Fluorophores as nucleobase replacements*. Covalent attachment of a planar fluorophore to the sugar skeleton by replacing the nucleobase altogether is an alternative strategy for generating fluorophore-conjugated compounds. The planar aromatic compounds differ in size and shape and lack the possibility to form hydrogen bonds with nucleobase at opposite positions. However, upon duplex formation, these aromatic compounds are positioned inside the duplex core and form a stable duplex via stacking interactions with the neighboring nucleobases. Much of the interest in fluorophore nucleobase replacements is centered around their ability to mimic natural nucleobases. Kool and coworkers have developed a series of such compounds by replacing the natural nucleobases with polycyclic aromatic compounds such as pyrene (**6**), perylene (**7**), oxo-perylene (**8**) and benzopyrene (**9**) (Figure 19).[54]

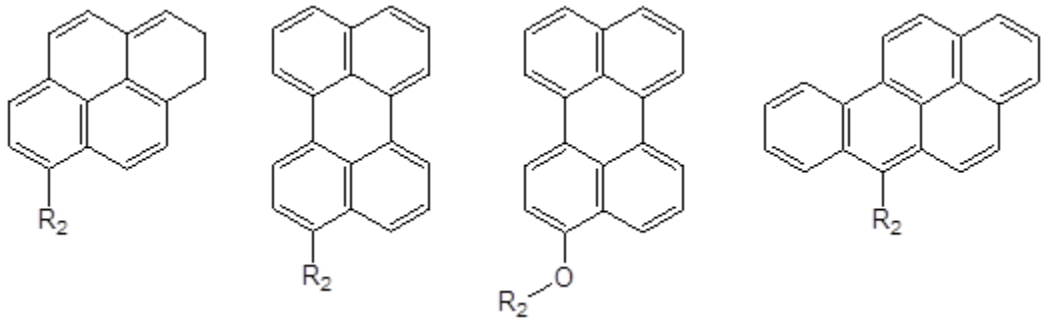

6 **7** **8** **9**

Figure 19. Structure of fluorescent hydrocarbon nucleosides 1- 4, R_2 = 2'-deoxyribose. (Adapted with permission from ref. 55).

The pyrene modified nucleoside has an excitation maximum at 375 nm, similar to the parent fluorophore with a Φ_F of 0.12. The other building blocks display blue shifted emission with high quantum yields (Φ_F = 0.88-0.98). Multiple substitution of these fluorophores result in the formation of multichromophores with enhanced emissive properties. These chromophores have been used as sensors to monitor enzyme activity or as sensors of small molecules in the vapor phase since they induce a variety of responses such as quenching or red shift or blue shift unique to each vapor analyte.[56] These multichromophore probes have also been shown to be cell permeable and have been used to label cells and zebra fish embryos.[57]

2.6. Fluorophore functionalized LNA analogs: an overview

As discussed in chapter 1, Locked nucleic acids (LNAs), are a class of conformatioanlly restricted nucleic acid (NA) analogs in which the 2' and 4'-position of the furanose ring are linked via an oxymethylene linker. The conformatioanlly restricted furanose skeleton also restricts rotation around the glycosidic bond which in turn imparts improved positional control of any fluorophores that are conjugated to the nculeobase of LNA and α-L-LNA[59,60] as compared to the corresponding deoxyribonucleotides, which modulates the properties of attached fluorophore. In light of this property, fluorophore conjugated LNA probes have been synthesized, as probes for SNP detection. Hrdlicka and coworkers have developed pyrene-functionalized LNA analogs in which pyrene moieties are conjugated to the sugar skeleton of 2'- amino LNA and 2'-amino-α-L-LNA.[58]

Because of its wide usage in diagnostic applications, emphasis was placed on the use of pyrene as a fluorophore.[61] This is due to the large aromatic surface area which allows for strong π-

stacking with neighboring nucleobase pairs through intercalation or with other pyrene moieties; (the stacking area of pyrene is ~184 Å vs. A: T base pair ~ 221 Å).[62,63,64] The position of attachment greatly influences the photophysical properties of pyrene as its fluorescence is sensitive to the microenvironment and neighboring nucleobases.[65] These features make pyrene an attractive candidate to study over other PAHs. In the subsequent section, the properties of pyrene conjugated analogs of LNA is discussed.

2.6.1. N2'-functionalized 2'-amino-LNA and 2'-amino-α-L-LNA

N2'-functionalized analogs of amino LNA and 2'-amino-α-L-LNA were synthesized by Wengel and Hrdlicka group where the fluorophores were attached via short linkers.[58] Fluorophores that are attached via acyl linkers form more stable duplexes than if connected via alkyl linkers. ONs with alternate incorporations of 2'-*N*-(pyren-1-yl)carbonyl-2'-amino-LNA monoemrs **11**, (Figure 20), have been shown to i) form highly thermostable duplexes with cDNA/RNA; ii) produce large hybridization-induced increases in fluorescence intensity and iii) exhibit intense fluorescence emission with high quantum yields (Φ_F = 0.28-0.99).[66,67]

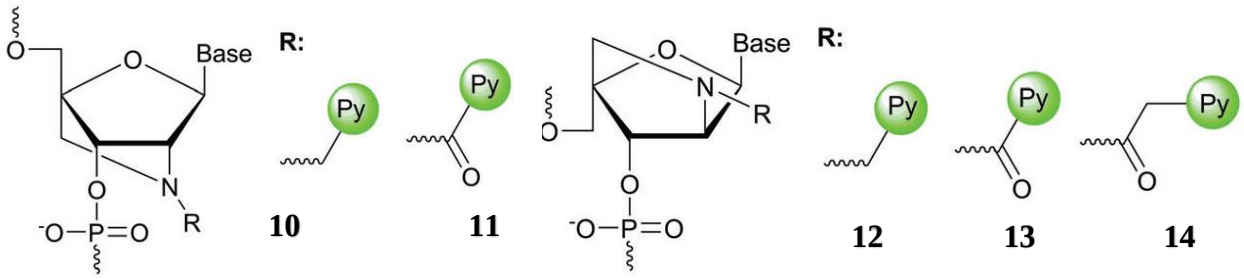

Figure 20. Pyrene-functionalized 2'- amino LNA and 2'-amino-α-L-LNA. (Adapted with permission from ref. 68).

Molecular modelling studies suggest that the locked sugar skeleton and amide linkage places the pyrene in the minor groove of duplexes, thereby, reducing nucleobases-mediated quenching

of pyrene fluorescence. Due to their large hybridization-induced increase in fluorescence intensity, these monomers were used as components of quencher free MBs, which were used for detection of cellular mRNA.[67]

ONs modified with 2'-amino-α-L-LNA[68] display reduced binding affinity towards cDNA/RNA compared to amino LNA, when substituted with small substituents. However, attachment of pyrene moieties at the N2'-position results in markedly increased affinity toward DNA targets. Monomers in which the pyrene is connected via a short alkanoyl linker induces greater thermal stabilization than monomers connected via long alkanoyl linkers or alkyl linkers (13>14>12; trend in DNA affinity). For example, ONs modified with monomer **13**, display an increase in T_m of 19.5 °C per modification (Figure 21a). Molecular modelling studies suggest that the remarkable affinity towards cDNA is due to precise positioning of the pyrene moiety inside the duplex (i.e., intercalation), which induces stacking interactions with the neighboring base pairs and thus stabilizes the duplex (Figure 21b, c). The characteristic feature has been exploited to develop probes for diagnostic applications.

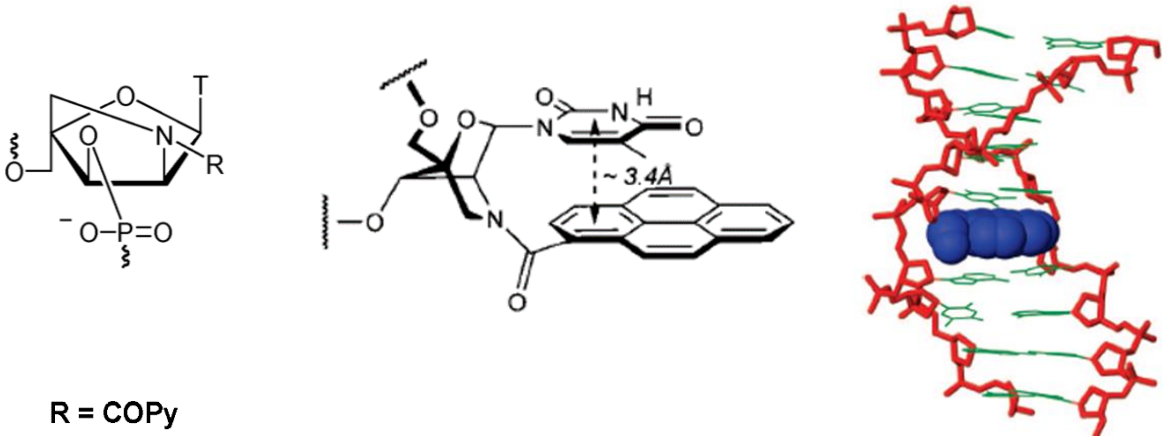

a **b** **c**

Figure 21. a) Structure of pyrene-functionalized 2'-amino-α-L-LNA; b) directed positioning of pyrene moiety in duplex core; c) Binding mode of pyrene (color scheme; nucleobases, green; sugar-phosphate backbone, red; pyrene moiety, blue). (Adapted with permission from ref. 69).

Thus, ONs with next nearest neighbor incorporations of monomer **14** (Figure 20) display an excimer signal in the presence of a DNA/RNA mismatch.[70] On the other hand, hybridization with cDNA/RNA, does not result in quenching due to intercalation of the pyrene moiety inside the duplex core (Figure 22a), a binding mode which is supported by the molecular modelling studies. Thus, the probes are promising tools for detection of SNP mismatches. Figure 22b illustrates the mechanism of detection and the fluorescence spectra of the modified ON in the presence of matched/mismatched DNA/RNA targets.

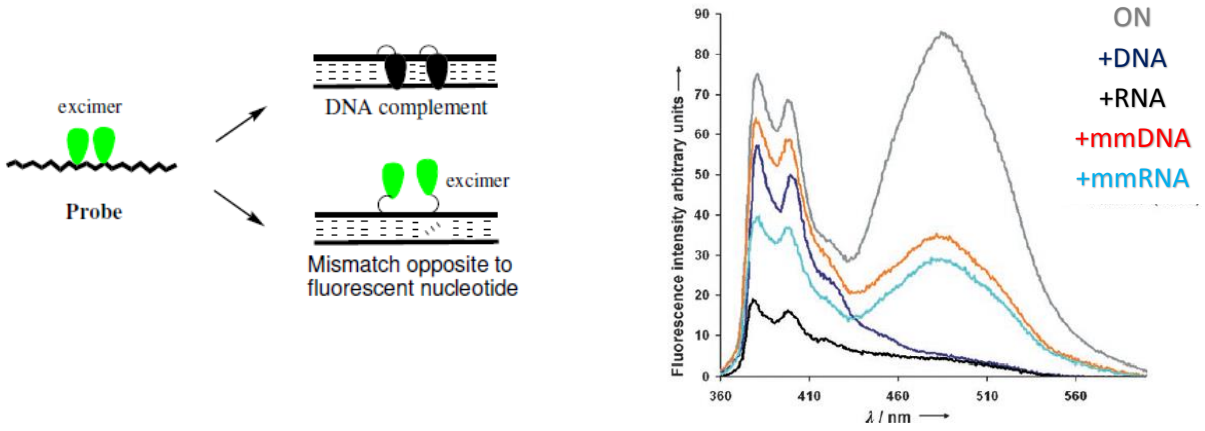

Figure 22. Illustration of mismatch detection using monomer **14**; b) Steady state fluorescence spectra of ON modified with monomer 14, and corresponding duplexes with cDNA/cRNA and mismatches. (Adapted with permission from ref. 70).

2.6.2. Nucleobase-functionalized LNA analogs. C5-pyrene-functionalized LNA U and α-L-LNA U analogs have been synthesized, in which pyrene was attached via ethynyl and triazole linkers to the C5-position of uracil nucleobases[59,60] (Figure 23). The hypothesis for the use of

these analogs is that the conformatioanlly restricted nature of LNA restricts rotation around the glycosidic bond, resulting in greater energy barriers for *anti*-to-*syn* rotation, arguably leading to even stricter SNP-discrimination. ONs of uracil that are modified with LNA monomers conjugated to pyrene moieties at the C5 position, display low cDNA/RNA affinity suggesting that the bulky aromatic substituents are not well tolerated in the major groove of duplexes.

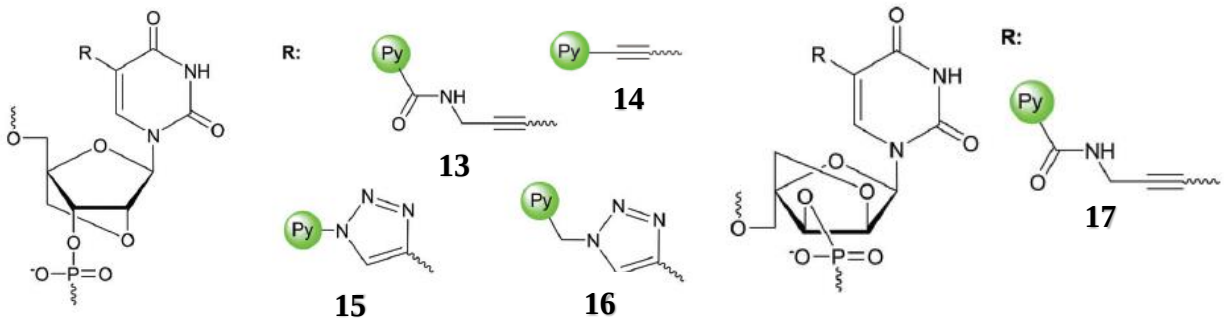

Figure 23. C5-functionalized LNA and α-L-LNA derivatives. (Adapted with permission from ref. 68).

C5 pyrene-substituted LNAs (Figure 23), display broad emission peaks at ~390/402 nm (**13**), ~381/398 nm (**15**), and ~376/396/416 nm (**16**), respectively, which are typical emission maxima for electronically isolated pyrene units.[60] However, C5-ethynyl-substituted pyrene monomer (**14**), display broad red-shifted emission (bathochromic shift) centered on ~465 nm, which is indicative of strong electronic coupling between the pyrene and nucleobase moiety. ONs modified with these analogs display between ~3 to 50-fold increases in fluorescence intensity upon duplex formation with cDNA. Much smaller increases in intensity are observed with mismatched DNA targets, indicating that these probes are BDF probes. Thus, in the case of matched duplexes, the pyrene fluorophore positions into major groove of duplex due to a preferred *anti* conformation of the nucleobase, whereas, in the case of mismatched duplex, the

nucleobase is in a *syn* conformation causing the pyrene moiety to intercalate inside the duplex, which leads to nucleobase-mediated quenching of pyrene fluorescence.

ONs modified with LNA (**13**) and α-L-LNA monomer (**17**), (Figure 23), results in larger increase in fluorescence intensity and brightness than the corresponding probes modified with 5-[3-(1-pyrenecarboxamido) propynyl]-DNA (U) monomer **3**, (Figure 18).[71] Force field calculations suggest that the extreme pucker of the LNA skeleton indeed influences the rotational freedom around the N1-C1′ glycosyl bond due to steric hindrance between H6 and H3′, leading to different positioning of florophore (Figure 24), and hence, modulation of the photophysical properties of the fluorophore relative to the analogous C5 propargyl DNA monomer.[10b]

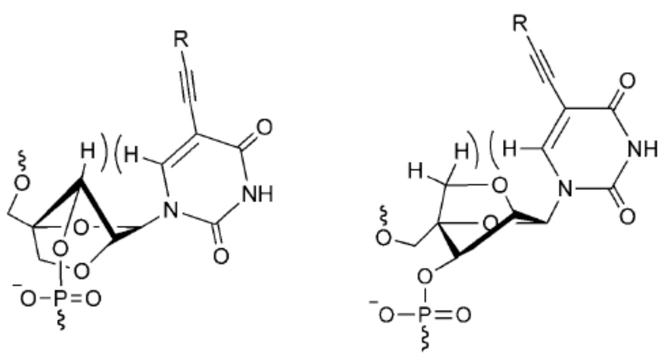

LNA **α-L-LNA**

Figure 24. Interaction between H6 and furanose hydrogens of LNA and α-L-LNA. (Adapted with permission from ref. 71).

2.7. Summary. The use of fluorophore-conjugated ONs is becoming a reliable tool for molecular biologists. The focus of this review has been on the properties of pyrene-labelled ONs and their applications in diagnostics. Pyrene can be conjugated using different linkers either to the nucleobases or the sugar skeleton and the resulting nucleotides can be utilized as diagnostic probes to study nucleic acid structure and function. Depending on the point of attachment, the pyrene moieties can either intercalate inside the duplex core or point into the major or minor groove of the duplex. The use of these fluorophores has generated an inexpensive means of designing sensitive probes for diagnostic applications. Further research on fluorophore-conjugated nucleotides will promote an in-depth understanding of their potential applications in biology and chemistry.

2.8. References.

1. a) Schlamp, K.; Weinmann, A.; Krupp, M.; Maass, T.; Galle, P. R.; Teufel, A. *Gene*. **2008**, *427*, 47-50; b) Towbin, H.; Staehelin, T; Gordon, J. *Proc. Natl. Acad. Sci.* **1979**, *76*, 4350-4354; c) Bartlett, J. M. S.; Stirling, D. *PCR Protocols*. **2003**, *226*, 3-6; d) Saiki, R.; Scharf, S.; Faloona, F.; Mullis, K.; Horn, G.; Erlich, H.; Arnheim, N. *Science* **1985**, *230*, 1350-1354.

2. a) Mayer, A.; Neuenhofer, S. *Angew. Chem. Int. Ed*. **1994**, *33*, 1044-1072; b) Wilson, J. N.; Kool, E. T. *Org. Biomol. Chem*. **2006**, *4*, 4265-4274.

3. a) Hawkins, M. E. Cell. *Biochem. Biophys*. **2001**, *34*, 257; b) Hawkins, M. E.; Pfleiderer, W.; Mazumder, A.; Pommier, Y. G.; Falls, F. M. *Nucleic Acids Res*. **1995**, *23*, 2872-2880.

4. Dahlberg, A. E.; Dingman, C. W.; Peacock, A. C. *J. Mol. Biol.* **1969**, *41*, 139-147.

5. Hellman, L. M.; Fried, M. G. *Nat. Protoc*. **2007**, *2*, 1849-1861.

6. Taurai, T.; Bernhard, A.; Martine, D.; Holger, W.; Sabine, D.; Ulrich, H.; Mario, A. *Nucleic Acids Res*. **2003**, *31*, 2636-2646.

7. Asseline, U. *Curr. Org. Chem*. **2006**, *10*, 491-518.

8. Park, Y. J.; Dyer, P. N.; Tremethick, D. J.; Luger, K. A. *J. Biol. Chem*. **2004**, *279*, 24274-24282.

9. a) Cekan, P.; Sigurdsson, S. T. *Chem. Commun*. **2008**, *29*, 3393-3395; b) Tanaka, K.; Okamoto, A. *Bioorg. Med. Chem*. **2008**, *16*, 400-404.

10. a) Okamoto, A.; Kanatani, K.; Saito, I. *J. Am. Chem. Soc*. **2004**, *126*, 4820-4827; b) Okamotoa, A.; Saito, Y.; Saito, I. *J Photoch Photobio C.* **2005**, *6*, 108-122.

11. Markiewiez, W. T. *Nucleic Acids Res*. **1997**, *25*, 3672-3680.

12. Behlke, M. A.; Huang, L.; Bogh, L.; Rose, S.; Devor, E. J. Fluorescence and Fluorescence Applications, *Integrated DNA Technologies* (*IDT*).

13. Weisbrod, S. H.; Marx, A. *Chem. Commun*. **2008**, 5675-5685.

14. Millar, D. P. *Curr. Opin. Struc. Biol*. **1996**, *6*, 322-326.

15. Kim, S.; Misra, A. *Annu. Rev. Biomed. Eng*. **2007**, *9*, 289-320.

16. Mhlanga, M. M.; Malmberg, L. *Methods*. **2001**, *25*, 463-471.

17. Yuan, L.; Lin, W.; Zheng, K.; Zhu, S. *Acc*. *Chem*. *Res*. **2013**, *46*, 1462-1473.

18. a) Didenko, V. V. *Biotechniques* **2001**, 31, 1106-1121; b) Yamana, K.; Gokota, T.; Ozaki, H.; Nakano, H.; Sangen, O.; Shimidzu, T. *Nucl*. *Nucl*. **1992**, *11*, 383-390.

19. Shimadzu, A. *Nucleic Acids Res*. **2000**, *28*, e34.

20. Boutorine, A. S.; Novopashina, D. S.; Krasheninina, O. A.; Nozeret, K.; Venyaminova, A. G. *Molecules*. **2013**, *18*, 15357-15397.

21. a) Venkatesan, N.; Seo, Y. J.; Kim, B. H. *Chem. Soc. Rev*. **2008**, *37*, 648-663; b) Juskowiak, B. *Anal Bioanal Chem*. **2011**, *399*, 3157-3176.

22. Fujimoto, K.; Shimizu, Hisao.; Inouye, Masahiko. *J. Org. Chem*. **2004**, *69*, 3271-3275.

23. Krasheninina, O. A.; Novopashina, D. S.; Venyaminova, A. G. *Russ. J. Bioorg. Chem*. **2011**, *37*, 244-248.

24. Mart, A. A.; Li, X.; Jockusch, S.; Li, Z.; Raveendra, B.; Kalachikov, S.; Russo, J. J.; Morozova, I.; Puthanveetti, S. V.; Ju, J.; Turro, N. J. *Nucleic Acids Res*. **2006**, *34*, 3161-3168.

25. Okamotoa, A.; Saito, Y.; Saito, I. *J. Photoch. Photobio. C.* **2005**, *6*, 108-122.

26. Saito, Y.; Suzuki, A.; Imai, K.; Nemoto, N.; Saito, I. *Tetrahedron. Lett*. **2010**, *51*, 2606-2609.

27. Suzuki, A.; Kimura, K.; Ishioroshi, S.; Saito, I.; Nemoto, N.; Saito, Y. *Tetrahedron. Lett*. **2013**, *54*, 2348-2352.

28. a) Kalyanasundaram, K.; Thomas, J. K. *J. Phys. Chem*. **1977**, *81*, 2176-2180; b) De Silva A. P.; Gunaratne, H. Q. N.; Gunnlaugsson, T.; Huxley, A. J. M.; McCoy, C. P.; Rademacher, J. T.; Rice, T. E. *Chem. Rev*. **1997**, *97*, 1515-1566.

29. a) Lianos, P.; Cremel, G. *Photochem. Photobiol*. **1980**, *31*, 429-434; b) Kumar, C.V.; Chattopadhyay, S. K.; Das, P. K. *Photochem. Photobiol*. **1983**, *38*, 141-152.

30. Smith, D. B.; Gilbert, A.; Cundall, R. B. *Photochemistry*. **1992**, *23*, 3-50.

31. Ahuja, R. C.; Moebius, D. *Langmuir*. **1992**, *8*, 1136-1144.

32. Manoharan, M.; Tivel, K. L.; Zhao, M.; Nafisi, K.; Netzel, T. L. *J. Phys. Chem*. **1995**, *99*, 17461-17472.

33. Yamana, K.; Zako, H.; Asazuma, K.; Iwase, R.; Nakano, H.; Murakami, A. *Angew. Chem. Int. Ed*. **2001**, *40*, 1104-1106.

34. Nakamura, M.; Fukunaga, Y.; Sasa, K.; Ohtoshi, Y.; Kanaori, K.; Hayashi, H.; Nakano, H.; Yamana, K. *Nucleic Acids Res*. **2005**, *33*, 5887-5895.

35. Østergaard, M. E.; Guenther, D. C.; Kumar, P.; Baral, B.; Deobald, L.; Paszczynski, A. J.; Sharma, P. K.; Hrdlicka, P. J. *Chem. Commun*. **2010**, 4929-4931.

36. Wilhelmsson, L. M. *Quart. Rev. Biophys.* **2010**, *43*, 159-183.

37. Ward, D. C.; Reich, E.; Stryer, L. *J. Biochem*. **1969**, *244*, 1228-1237.

38. Sowers, L. C.; Boulard, Y.; Fazakerley, G. V. *Biochemistry* **2000**, *39*, 7613-7620.

39. Sowers, L. C.; Fazakerley, G. V.; Eritja, R.; Kaplan, B. E.; Goodman, M. F. *Proc. Natl. Acad. Sci. USA*. **1986**, *83*, 5434-5438.

40. Holmén, A.; Nordén, B.; Albinsson, B. *J. Am. Chem. Soc*. **1997**, *119*, 3114-3121.

41. Gaied, B. N.; Glasser, N.; Ramalanjaona, N.; Beltz, H.; Wolff, P.; Marquet, R.; Burger, A.; Me'ly, Y. *Nucleic Acids Res*. **2005**, *33*, 1031-1039.

42. Hawkins, M. E.; Pfleiderer, W.; Jungmann, O.; Balis, F. M. *Anal. Biochem*. **2001**, *298*, 231-240.

43. Hawkins, M. E.; Balis, F. M. *Nucleic Acids Res*. **2004**, *32*, e62.

44. Yang, K. S.; Matsika, S.; Stanley, R. J. *J. Phys. Chem. B.* **2007**, *111*, 10615-10625.

45. Teo, Y. N.; Kool, E. T. *Chem. Rev*. **2012**, *112*, 4221-4245.

46. Nakamura, M.; Ohtoshi, Y.; Yamana, K. *Chem. Commun*. **2005**, *41*, 5163.

47. Karmakar, S.; Hrdlicka, P. J. *Chem Sci*. **2013**, *4*, 3447-3454.

48.a) Karmakar, S.; Anderson, B. A.; Rathje, R. L.; Andersen, S.; Jensen, T. B.; Nielsen, P.; Hrdlicka, P. J. *J. Org. Chem*. **2011**, *76*, 7119-7131; b) Karmakar, S.; Guenther, D. C.; Hrdlicka, P. J. *J. Org. Chem*. **2013**, *78*, 12040-12048; c) Didion, B. A.; Karmakar, S.; Guenther, D. C.; Sau, S.; Verstegen, J. P.; Hrdlicka, P. J. *ChemBioChem* **2013**, *14*, 1534-1538; d) Denn, B.; Karmakar, S.; Guenther, D. C.; Hrdlicka, P. J. *ChemCommun*. **2013**, *49*, 9851-9853.

49. a) Zilbershtein, L.; Silberman, A.; Fischer, B. *Org. Biomol. Chem*. **2011**, *9*, 7763-7773; b) Kaura, M.; Kumar, P.; Hrdlicka, P. J. *J. Org. Chem*. **2014**, *79*, 6256-6268.

50. Seela, F.; Zulauf, M. *Helv. Chim. Acta*. **1999**, 82, 1878-1898; b) Wagenknecht, H. A. *Angew. Chem. Int. Ed*. **2009**, 48, 2838-2841; c) Taniguchi, Y.; Kool, E. T. *J. Am. Chem. Soc*. **2007**, *129*, 8836-8844; d) Valis, L.; Mayer, E. E.; Wagenknecht, H. A. *Bioorg. Med. Chem*. **2006**, *16*, 3184-3187.

51. Okamoto, A.; Tainaka, K.; Ochi, Y.; Kanatani, K.; Saito, I. *Mol. Bio. Syst*. **2006**, *2*, 122-126.

52. Okamoto, A.; Ochi, Y.; Saito, I. *Chem. Commun*. **2005**, 1128-1130.

53. Seela, F.; Budow, S.; Peng, X. *Curr. Org. Chem*. **2012**, *16*, 161-223; b) Seela, F.; Thomas, H. *Helv. Chim. Acta*. **1995**, *78*, 94-108; c) Seela, F.; Zulauf, M. *Synthesis* **1996**, 726-732; d)

Seela, F.; Zulauf, M. *Chem. Eur. J*. **1998**, *4*, 1781-1790; e) Seela, F.; Zulauf, M. *Helv. Chim. Acta*, **1999**, 82, 1878-1898; f) Seela, F.; Zulauf, M.; Sauer, M.; Deimel, K. *Helv. Chim. Acta*, **2000**, 83, 910-927.

54. a) Ren, R. X. F.; Chaudhuri, N. C.; Paris, P. L.; Rumney, S.; Kool, E. T. *J. Am. Chem. Soc*. **1996**, *118*, 7671-7678; b) Gao, J.; Str¨assler, C.; Tahmassebi, D.; Kool, E. T. *J. Am. Chem. Soc*. **2002**, *124*, 11590-11591; c) Gao, J.; Watanabe, S.; Kool, E. T. *J. Am. Chem. Soc*. **2004**, *126*, 12748-12749; d) Teo, Y. N.; Kool, E. T. *Chem Rev*. **2012**. 112, 4221-4245.

55. Chiba, J.; Takeshima, S.; Mishima, K.; Maeda, H.; Nanai, Y.; Mizuno, K.; Inouye, M. *Chem. Eur. J*. **2007**, *13*, 8124-8130.

56. a) Samain, F.; Ghosh, S.; Teo, Y. N.; Kool, E. T. *Angew. Chem. Int. Ed*. **2010**, *49*, 7025-7029; b) Samain, F.; Dai, N.; Kool, E. T. *Chem. Eur. J*. **2011**, *17*, 174-183.

57. Teo, Y. N.; Wilson, J. N.; Kool, E. T. *J. Am. Chem. Soc*. **2009**, 131, 3923-3933.

58. Andersen, Nicolai K.; Anderson, B. A.; Wengel, J.; Hrdlicka, P. J. *J. Org. Chem*. **2013**, *78*, 12690-12702.

59. Kumar, P.; Baral, B.; Anderson, B. A.; Guenther, D. C.; Østergaard, M. E.; Sharma, P. K.; Hrdlicka, P. J. *J. Org. Chem*. **2014**, *79*, 5062-5073.

60. Kumar, P.; Østergaard, M. E.; Baral, B.; Anderson, B. A.; Guenther, D. C.; Kaura, M.; Raible, D. J.; Sharma, P. K.; Hrdlicka, P. J.; *J. Org. Chem*. **2014**, *79*, 5047-5061.

61. a) Yamana, K.; Iwai, T.; Ohtani, Y.; Sato, S.; Namakura, M.; Nakano, H. *Bioconjugate Chem*. **2002**, *13*, 1266-1273; b) Martin, R. B.; Qu, L.; Harruff, B. A.; Bunker, C. E.; Gord, J. R.; Allard, L. F. Sun, Y. P. *J. Phys. Chem. B*, **2004**, *108*, 11447-11453; c) Strauss, J.; Daub, J. *Org. Lett*. **2002**, *4*, 683-686; c) Benniston, A. C.; Harriman, A.; Lawrie, D. J.; Mayeux, A.;

Rafferty, K.; Russel, O. D. *Dalton Trans*. **2003**, 4762-4769; d) Barboiu, M.; Prodi, L.; Montalti, M.; Zaccheroni, N.; Kyritsakas, N. Lehn, J. M. *Chem. Eur. J*. **2004**, *10*, 2953-2959.

62. Guckian, K. M.; Schweitzer, B. A.; Ren, R. X. F.; Sheils, C. J.; Tahmassebi, D. C.; Kool, E. T. *J. Am. Chem. Soc*. **2000**, *122*, 2213-2222.

63. Enthart, E. M.; Wagenknecht, H. A. *Angew. Chem. Int. Ed*. **2006**, *45*, 3372-3375.

64. Barbaric, J.; Wagenknecht, H. A. *Org. Biomol. Chem*. **2006**, *4*, 2088-2090.

65. Dougherty, G.; Pilbrow, J. R. *Int. J. Biochem*. **1984**, *16*, 1179-1192.

66. Hrdlicka, P. J.; Babu, B. R.; Sørensen, M. D.; Harrit, N.; Wengel, J. *J. Am. Chem. Soc*. **2005**, *127*, 13293-13299.

67. Østergaard, M. E.; Cheguru, P.; Papasani, M. R.; Hill, R. A.; Hrdlicka, P. J. *J. Am. Chem. Soc*. **2010**, *132*, 14221-14228.

68. Østergaard, M. E.; Hrdlicka, P. J. *Chem. Soc. Rev*. **2011**, *40*, 5771-5788.

69. Kumar, T. S.; Madsen, A. S.; Østergaard, M. E.; Sau, S. P.; Wengel, J.; Hrdlika, P. J. *J. Org. Chem*. **2009**, *74*, 1070-1081.

70. Kumar, T. S.; Wengel, J.; Hrdlicka, P. J. *ChemBioChem*. **2007**, 8, 1122-1125.

71. Østergaard, M. E.; Kumar, P.; Baral, B.; Guenther, D. C.; Anderson, B. A.; Ytreberg, F. M.; Deobald, L.; Paszczynski, A. J.; Sharma P. K.; Hrdlicka, P. J. *Chem. Eur. J*. **2011**, *17*, 3157-3165.

Chapter 3: Synthesis and Characterization of C5-Carbohydrate functionalized Locked Nucleic Acids

The following paper by **Kaura**, **M**.; Guenther, D. C. and Hrdlicka, P. J. was published in *Org. Lett*. **2014**, *16* (12), 3308-3311.

Abstract. C5-carbohydrate-functionalized locked nucleic acid (LNA) uridine phosphoramidites were synthesized and incorporated into DNA strands using an automated nucleic acid synthesizer. C5-carbohydrate-functionalized LNA display higher affinity toward complementary DNA/RNA targets (ΔT_m/modification up to +11.0 °C), more stringent mismatch discrimination and superior resistance against 3'-exonucleases compared to conventional LNA. These properties render C5-carbohydrate-functionalized LNAs as promising modifications for use in the antisense technology and other nucleic acid targeting applications.

3.1. Introduction.

Chemically modified oligonucleotides are widely used in molecular biology, biotechnology and biomedical sciences for modulation of gene expression and detection of specific nucleic acid targets.[1] Incorporation of conformationally restricted nucleotide monomers is a particularly popular strategy for increasing the affinity of oligonucleotides toward their targets.[2,3] LNA[4,5] (Locked Nucleic Acid, Figure 25) - also known as Bridged Nucleic Acid (BNA)[6] - is one of the most promising members of this compound class, as it produces some of the largest increases in thermal denaturation temperatures (T_m's) of duplexes reported thus far. Moreover, LNA-modified oligonucleotides display improved target specificity and enzymatic stability,[7] and they have accordingly been used extensively in RNA-targeting applications.[8] The promising

characteristics of LNA fuelled substantial efforts to develop next-generation LNA monomers with even more desirable biophysical characteristics.[2,3,9]

As part of our ongoing interest in LNA chemistry, [10] we recently set out to synthesize and study oligodeoxyribonucleotides (ONs) modified with various C5-alkynyl-functionalized LNA uridine monomers.[11] The thermostabilities of the corresponding duplexes with complementary DNA/RNA depend strongly on the nature of the C5-alkynyl group. Thus, ONs that are modified with C5-aminopropynyl-functionalized LNA-U monomer N (Figure 25) display moderately greater resistance against degradation by snake venom phosphordiesterase (SVPDE – a 3'-exonuclease) and significantly higher affinity toward DNA/RNA targets than unmodified ONs or conventional LNA (duplex T_m's are 6.5-13.0 °C and 2.5-3.5 °C per modification higher than with unmodified ONs or conventional LNA, respectively).[11] In contrast, ONs that are modified with C5-cholesterol-functionalized LNA-U monomer S (figure 25) display much lower affinity toward DNA/RNA targets but are essentially inert toward SVPDE-mediated degradation.[11]

Clearly, it would be desirable to develop antisense building blocks that display very high target affinity and confer very high levels of protection against nucleases. At the onset of the current study, we hypothesized that conjugation of bulky yet polar groups such as mono- or disaccharides to the C5-position of LNA-U monomers would yield building blocks with such characteristics. Our hypothesis is based on the assumption that the bulk of the carbohydrates confers protection against nucleases, while their polar nature allows them to be positioned in the hydrated major groove without exhibiting the same detrimental effects on duplex stability as large hydrophobic C5-substituents. Moreover, conjugation of carbohydrate moieties on LNA nucleotides is also interesting from a pharmacokinetic perspective as antisense ONs conjugated

to glycoclusters are known to display improved cellular uptake due to receptor-mediated endocytosis.[12]

Herein, we describe the synthesis and biophysical characterization of ONs modified with three different C5-carbohydrate-functionalized LNA-U monomers X-Z (Figure. 25). The monomers were selected in order to study the influence of steric bulk (monosaccharides vs disaccharides, monomers X/Y vs Z) and stereochemical configuration (glucose vs galactose configuration, monomers X vs Y). The ONs display very high affinity toward complementary DNA/RNA (ΔT_m/modification up to 11.0 °C) and extraordinary resistance against SVPDE-mediated degradation.

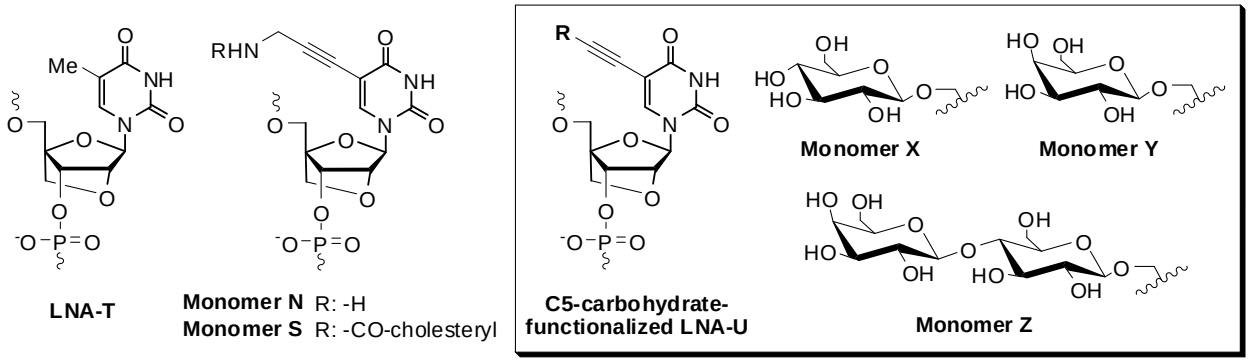

Figure 25. Chemical structures of LNA-T and C5-alkynyl-functionalized LNA-U monomers discussed herein.

3.2. Results and Discussion

Phosphoramidites 3X-3Z were synthesized in a similar manner as other C5-alkynyl-functionalized LNA-U building blocks (Scheme 1).[11] Thus, glucose/galactose/lactose-functionalized alkynes[13] were coupled to known C5-iodo LNA-U nucleotide 1[11] using Sonogashira conditions[14] to afford nucleosides 2X-2Y in 62-66% yield, which upon treatment with 2-cyanoethyl-N,N'-diisopropylchlorophosporamidite and N,N'-diisopropylethylamine provided 3X-3Z in 60-70% yield.

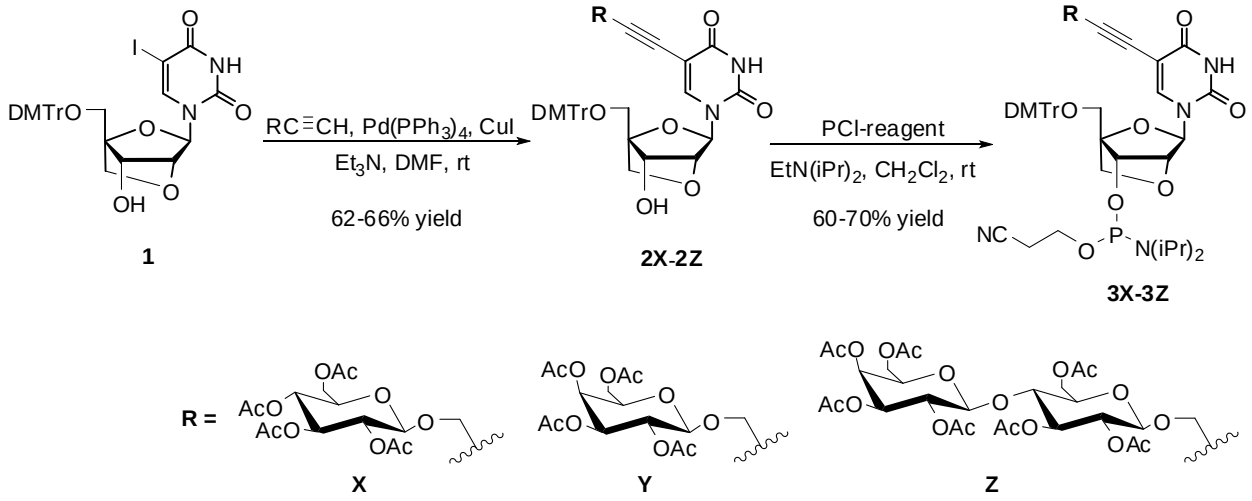

Scheme 1. Synthesis of C5-carbohydrate-functionalized LNA phosphoramidites. PCl-reagent: 2-cyanoethyl-N,N'-diisopropylchlorophosporamidite.

Phosphoramidites 3X-3Z were incorporated into ONs via machine-assisted solid-phase DNA synthesis using extended hand-coupling (20 min, 5-(ethylthio)-1H-tetrazole as activator)), which resulted in stepwise coupling yields of ~95% for monomers X-Z. ONs were purified by ion-pair reversed-phased HPLC and their composition was verified by MALDI MS analysis (Table S1). The hybridization characteristics of ONs modified with one or two X-Z monomers were studied in 9-mer mixed-sequence contexts, which we use as a model system (Table 1). The thermostabilities of duplexes between C5-carbohydrate-functionalized LNA and complementary DNA/RNA were determined by thermal denaturation experiments using medium salt buffer conditions (110 mM NaCl, pH 7). Unless otherwise stated, the thermal denaturation temperatures (T_m's) are discussed relative to unmodified reference duplexes.

Interestingly, all of the modified ONs result in the formation of duplexes that are significantly more thermostable than reference duplexes, which suggests that the bulky yet polar carbohydrate units are well-tolerated in the major groove of nucleic acid duplexes. Greater

increases in T_m's are observed with RNA targets (ΔT_m = 4.5-8.5 °C and 8.0-11.0 °C for B1-B4 series with complementary DNA and RNA, respectively, Table 2). Monosaccharide-functionalized monomers X/Y result in formation of duplexes that are up to 4.0 °C more thermostable than duplexes modified with lactose-conjugated monomer Z (compare Δ T_m's for X/Y- vs Z-series, Table 1). Galactose-conjugated monomer Y generally induces slightly greater thermostabilization than glucose-conjugated monomer X, which suggests that the stereochemical configuration at the C4-position of the carbohydrate may play a minor role in determining duplex thermostability. Incorporation of two X-Z monomers as next-nearest neighbors results in further stabilization of the duplexes although the increases in T_m per modification are slightly lower than with singly modified duplexes (compare Δ T_m's for B2/B3- vs B4-series, Table 2). As expected, C5-carbohydrate-functionalized LNA-U monomers induce similar levels of thermostabilization as conventional LNA and C5-aminopropynyl LNA monomers.[11]

Table 2. Thermal denaturation temperatures for duplexes between C5-carbohydrate-functionalized LNA and cDNA/cRNA[a]

ON	Sequence	**B** =	ΔT_m/°C				
			L[b]	**N**[b]	**X**	**Y**	**Z**
B1 **D2**	5′-GTG A**B**A TGC 3′-CAC TAT ACG		+5.0	+8.0	+6.0	+7.0	+5.5
D1 **B2**	5′-GTG ATA TGC 3′-CAC **B**AT ACG		+4.0	+6.5	+5.5	+8.5	+4.5
D1 **B3**	5′-GTG ATA TGC 3′-CAC TA**B** ACG		+6.5	+9.5	+7.0	+5.5	+4.5
D1 **B4**	5′-GTG ATA TGC 3′-CAC **B**A**B** ACG		+5.5	+8.0	+5.8	+5.8	+3.8
B1 **R2**	5′-GTG A**B**A TGC 3′-CAC UAU ACG		+9.5	+13.0	+10.0	+11.0	+8.5
R1 **B2**	5′-GUG AUA UGC 3′-CAC **B**AT ACG		+6.5	+10.0	+9.0	+11.0	+9.0
R1 **B3**	5′-GUG AUA UGC 3′-CAC TA**B** ACG		+9.5	+12.5	+9.0	+9.0	+8.0
R1 **B4**	5′-GUG AUA UGC 3′-CAC **B**A**B** ACG		+8.0	+11.0	+8.3	+8.5	+7.0

[a] ΔT_m = change in T_m's relative to unmodified reference duplexes **D1**:**D2** ($T_m \equiv 29.5$ °C), **D1**:**R2** ($T_m \equiv 27.0$ °C) and **D2**:**R1** ($T_m \equiv 27.0$ °C); T_m's determined as the first derivative maximum of denaturation curves (A_{260} vs T) recorded in medium salt buffer ($[Na^+] = 110$ mM, $[Cl^-] = 100$ mM, pH 7.0 (NaH_2PO_4/Na_2HPO_4)), using 1.0 µM of each strand. T_m values are averages of at least two measurements within 1.0 °C; See Figure 1 for structures of monomers. [b] Data from reference 11.

The binding specificities of centrally modified C5-carbohydrate-functionalized LNAs were determined using DNA/RNA targets with mismatched nucleotides opposite of the modification (Table 3). Importantly, **X1**/**Y1**/**Z1** display significantly improved mismatch discrimination relative to both unmodified reference strands **D1 and R1** and similar binding fidelity as the corresponding ON modified with C5-aminopropynyl LNA monomer **N** (see reference 11).

Table 3. Discrimination of singly mismatched DNA/RNA targets by C5-carbohydrate-functionalized LNAs and reference strands.

		DNA: 3′-CAC T**B**T ACG				RNA: 3′-CAC U**B**U ACG			
		T_m/°C	ΔT_m/°C			T_m/°C	ΔT_m/°C		
ON	**B** =	A	C	G	T	A	C	G	U
D1		**29.5**	-16.5	-8.0	-15.5	**27.0**	<-17.0	-4.5	<-17.0
L1[b]		**34.5**	-18.0	-11.0	-16.0	**36.5**	-19.0	-8.0	-18.5
N1[b]		**37.5**	-19.0	-12.0	-17.5	**40.0**	-18.5	-11.5	-22.5
X1		**35.5**	-19.5	-13.0	-20.0	**37.0**	-19.0	-12.5	-21.5
Y1		**36.5**	-20.5	-15.0	-20.0	**38.0**	-20.0	-11.0	-22.0
Z1		**35.0**	-20.5	<-25.0	<-25.0	**35.5**	<-25.5	<-25.5	<-25.5

[a] For conditions of thermal denaturation experiments, see Table 1. T_m's of fully matched duplexes are shown in bold. ΔT_m = change in T_m relative to fully matched DNA:RNA duplex (B=A). [b] Data from reference 11.

Finally, we studied the enzymatic stability of D2/X2/Y2/Z2 in the presence of snake venom phosphordiesterase by recording the change in absorbance at 260 nm as a function of time (Figure 26). As expected, unmodified reference strand D2 is quickly degraded (~90% degradation within ~10 min, Figure 26). Gratifyingly, C5-carbohydrate-functionalized LNA X2/Y2/Z2 are essentially inert against SVPDE-mediated degradation, once a ~5 min period of cleavage - corresponding to degradation of the 3'-terminal deoxyribonucleotides - has elapsed (see degradation profiles for X2/Y2/Z2, Figure. 26). Pseudo-first order rate constants - determined for the first ~5 min of SVPDE-mediated degradation of ONs - are ~10-fold lower for X2/Y2/Z2 than for D2 (Figure 29 and Table 5). This strongly suggests that the bulky carbohydrate moieties also confer significant protection against nucleases for 3'-flanking deoxyribonucleotides.

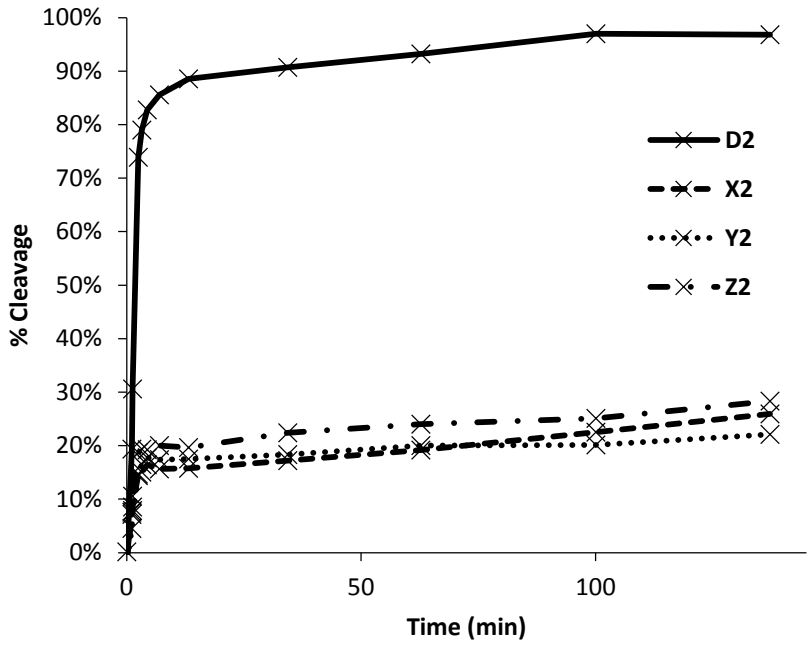

Figure 26. 3'-Exonuclease degradation of singly modified C5-carbohydrate-functionalized LNA and reference strands (B2 series). Nuclease degradation studies were performed in magnesium buffer (50 mM Tris-HCl, 10 mM $Mg^{2+,}$ pH 9.0) by using 3.3 µM ONs and 0.03 U of snake venom phosphodiestaerase.

3.3. Conclusion. In conclusion, a series of C5-carbohydrate-functionalized LNA-U phosphoramidites have been synthesized and incorporated into ONs. The modified ONs display exceptional affinity toward complementary DNA/RNA targets, excellent binding specificity and outstanding resistance against 3'-exonucleases. This study demonstrates that it is possible to augment the beneficial properties of LNA monomers through functionalization of the nucleobase moiety. These properties render C5-carbohydrate-functionalized LNAs as promising modifications for use in the antisense technology and other nucleic acid targeting applications.

3.4. Supporting Information

3.4.1 General experimental section. Unless otherwise noted, reagents and solvents were commercially available, of analytical grade and used without further purification. Petroleum ether of the distillation range 60-80 °C was used. Anhydrous DMF was used as obtained from commercial suppliers. Dicholoromethane, 1,2-dichloroethane, triethylamine and N,N′-diisopropylethylamine were dried over activated molecular sieves (4Å). Reactions were monitored by TLC using silica gel coated plates with a fluorescence indicator (SiO_2-60, F-254) which were visualized under UV light and by dipping in 5% conc. H_2SO_4 in absolute ethanol (v/v) followed by heating. Silica gel column chromatography was performed with silica gel 60 (particle size 0.040-0.063 mm) using moderate pressure (pressure ball). Columns were built in the listed starting eluent containing 0.5% v/v pyridine. Evaporation of solvents was carried out under reduced pressure at temperatures below 45 °C. Following column chromatography, appropriate fractions were pooled, evaporated and dried at high vacuum for at least 12h to give the obtained products in high purity (>95%) as ascertained by 1D NMR techniques. Chemical shifts are reported relative to deuterated solvent or other internal standards (80% phosphoric acid for ^{31}P NMR). Exchangeable (ex) protons were detected by disappearance of signals upon D_2O addition. Assignments of NMR spectra are based on 2D spectra (HSQC, COSY) and DEPT spectra. Quaternary carbons are not assigned but their presence is verified via HSQC and DEPT spectra (absence of signals). MALDI-HRMS spectra of compounds were recorded on a Q-TOF mass spectrometer using 2,5-dihydroxybenzoic acid as a matrix and mixture of polyethylene glycol (PEG 600) and (PEG 1000) as internal calibration standards.

3.4.2 Experimental section; *Representative protocol for Sonogashira couplings*.

Nucleoside 1[S1], $Pd(PPh_3)_4$, CuI and the alkyne were added to anhydrous DMF (quantities and volumes specified below) and the reaction chamber was degassed and placed under an argon atmosphere. To this was added anhydrous Et_3N and the reaction mixture was stirred at rt for ~12 h at which point analytical TLC indicated full conversion of the starting material. Solvents were evaporated off and the resulting residue was taken up in EtOAc (100 mL) and washed with brine (2×50 mL) and sat. aq. $NaHCO_3$ (50 mL). The combined aqueous layer was then back-extracted with EtOAc (100 mL). The combined organic layer was dried (Na_2SO_4), evaporated to dryness and the resulting residue purified by silica gel column chromatography (0-5% MeOH in CH_2Cl_2 (v/v) to afford the desired product.

*(1R,3R,4R,7S)-1-(4,4'-Dimethoxytrityloxymethyl)-7-hydroxy-3-[5-(3-(2,3,4,6-tetra-O-acetyl-β-D-glucopyranosyloxy)-prop-1-ynyl)uracil-1-yl]-2,5-dioxabicyclo[2.2.1]heptane (**2X**).*

Nucleoside **1** (250 mg, 0.36 mmol), $Pd(PPh_3)_4$ (45 mg, 0.035 mmol), CuI (15 mg, 0.07 mmol), 3-(2,3,4,6-tetra-*O*-acetyl-*β*-D-glucopyranosyloxy)-prop-1-yn[S2] (0.30 g, 0.80 mmol), anhydrous Et3N (0.20 mL, 1.45 mmol) and anhydrous DMF (5 mL) were mixed, reacted and purified as described above to obtain **2X** (220 mg, 64%) as a pale yellow solid material. R_f = 0.4 (5% MeOH in CH_2Cl_2, v/v); ESI-HRMS *m/z* 965.2990 ($[M+Na]^+$, $C_{48}H_{50}N_2O_{18}{\cdot}Na^+$, calc. 965.2951); ^{1}H NMR (DMSO-d_6) δ 11.73 (s, 1H, ex, NH), 7.83 (s, 1H, H6), 7.41-7.45 (m, 2H, Ar), 7.22-7.35 (m, 7H, Ar), 6.90 (dd, 4H, J = 9.0 Hz, 2.0 Hz, Ar), 5.73 (d, 1H, ex, J = 5.0 Hz, 3′-OH), 5.44 (s, 1H, H1′), 5.28 (ap t, 1H, J = 9.8 Hz, $H3_{glu}$), 4.89-4.95 (t+d, 2H, J = 9.8 Hz + 8.2 Hz, $H4_{glu}$, $H1_{glu}$), 4.76-4.81 (dd, 1H, J = 8.2 Hz, 9.8 Hz, $H2_{glu}$), 4.35-4.38 (d, 1H, J = 16.0 Hz, $CH_2C{\equiv}C$), 4.27-4.30 (d, 1H, J = 16.0 Hz, $CH_2C{\equiv}C$), 4.24 (s, 1H, H2′), 4.16-4.19 (dd, 1H, J = 12.3 Hz, 4.8 Hz, $H6_{glu}$), 4.04 (d, 1H, J = 5.0 Hz, H3′), 3.97-4.02 (m, 2H, $H6_{glu}$, $H5_{glu}$), 3.77-

3.82 (2d, 2H, J = 8.0 Hz, H5″), 3.75 (br s, 6H, CH_3O), 3.53-3.56 (d, 1H, J = 11.0 Hz, H5′), 3.26-3.30 (d, 1H, J = 11.0 Hz, H5′ – partial overlap with H_2O), 2.00 (s, 3H, CH_3CO), 1.99 (s, 3H, CH_3CO), 1.94 (s, 6H, CH_3CO); ^{13}C NMR (DMSO-d_6) δ 170.0, 169.5, 169.2, 169.0, 161.7, 158.10, 158.08, 149.0, 144.8, 142.2 (C6), 135.3, 134.9, 129.8 (Ar), 129.6 (Ar), 127.9 (Ar), 127.5 (Ar), 126.6 (Ar), 113.24 (Ar), 113.22 (Ar), 97.9 (C1glu), 97.1, 87.6, 87.5, 86.9 (C1′), 85.6, 79.1, 78.8 (C2′), 72.1 ($C3_{glu}$), 71.3 (C5″), 70.7 ($C2_{glu}$), 70.6 ($C5_{glu}$), 69.5 (C3′), 68.0 ($C4_{glu}$), 61.5 ($C6_{glu}$), 59.0 (C5′), 56.6 ($CH_2C{\equiv}C$), 55.0 (CH_3O), 20.4/20.31/20.27/20.2 (CH_3CO).

*(1R,3R,4R,7S)-1-(4,4'-Dimethoxytrityloxymethyl)-7-hydroxy-3-[5-(3-(2,3,4,6-tetra-O-acetyl-β-D-galactopyranosyloxy)-prop-1-ynyl)uracil-1-yl]-2,5-dioxabicyclo[2.2.1]heptane (**2Y**).*

Nucleoside **1** (0.50 g, 0.72 mmol), $Pd(PPh_3)_4$ (90 mg, 0.07 mmol), CuI (30 mg, 0.14 mmol), 3-(2,3,4,6-tetra-*O*-acetyl-*β*-D-galactopyranosyloxy)-prop-1-yn[S2] (0.46 g, 1.60 mmol), anhydrous Et_3N (0.40 mL, 3.00 mmol) and anhydrous DMF (10 mL) were mixed, reacted and purified as described above to obtain **2Y** (0.42 g, 61%) as a pale yellow solid material. R_f = 0.5 (5% MeOH in CH_2Cl_2, v/v); ESI-HRMS *m/z* 965.2948 ($[M+Na]^+$, $C_{48}H_{50}N_2O_{18}.Na^+$, calc. 965.2951); ^1H NMR (DMSO-d_6) δ 11.72 (s, 1H, ex, NH), 7.83 (s, 1H, H6), 7.41-7.45 (m, 2H, Ar), 7.22-7.35 (m, 7H, Ar), 6.91 (dd, 4H, J = 9.0 Hz, 2.0 Hz, Ar), 5.73 (d, 1H, ex, J = 4.5 Hz, 3′-OH), 5.44 (s, 1H, H1′), 5.26-5.27 (d, 1H, J = 3.5 Hz, $H4_{gal}$), 5.17-5.20 (dd, 1H, J = 10.0 Hz, 3.5 Hz, $H3_{gal}$), 4.92-4.97 (dd, 1H, J = 10.0 Hz, 8.0 Hz, $H2_{gal}$), 4.79-4.81 (d, 1H, J = 8.0 Hz, $H1_{gal}$), 4.34-4.38 (d, 1H, J = 16.0 Hz, $CH_2C{\equiv}C$), 4.25-4.30 (d, 1H, J = 16.0 Hz, $CH_2C{\equiv}CH$), 4.24 (s, 1H, H2′), 4.21 (t, 1H, J = 6.5 Hz, $H5_{gal}$), 4.03-4.08 (m, 3H, $H6_{gal}$, H3′), 3.78-3.82 (2d, 2H, J = 8.5 Hz, H5″), 3.75 (br s, 6H, CH_3O), 3.52-3.57 (d, 1H, J = 11.5 Hz, H5′), 3.28-3.32 (d, 1H, J = 11.5 Hz, H5′, partial overlap with H_2O), 2.11 (s, 3H, CH_3CO), 1.99 (s, 3H, CH_3CO), 1.95 (s, 3H,

CH_3CO), 1.92 (s, 3H, CH_3CO); ^{13}C NMR (DMSO-d_6) δ 169.9, 169.8, 169.4, 169.1, 161.6, 158.11, 158.09, 149.0, 144.8, 142.2 (C6), 135.3, 134.9, 129.8 (Ar), 129.6 (Ar), 127.9 (Ar), 127.5 (Ar), 126.6 (Ar), 113.2 (Ar), 98.4 ($C1_{gal}$), 97.1, 87.6, 86.9 (C1′), 85.6, 78.9, 78.8 (C2′), 71.3 (C5″), 70.2 ($C3_{gal}$), 69.9 ($C5_{gal}$), 69.6 (C3′), 68.4 ($C2_{gal}$), 67.2 ($C4_{gal}$), 61.1 ($C6_{gal}$), 58.9 (C5′), 56.5 ($CH_2C{\equiv}C$), 55.0 (CH_3O), 20.4/20.29/20.26 (CH_3CO).

*(1R,3R,4R,7S)-1-(4,4′-Dimethoxytrityloxymethyl)-7-hydroxy-3-[5-(3-(2,3,4,6-tetra-O-acetyl-β-D-galactopyranosyl-(1→4)-2,3,6-tri-O-acetyl-β-D-glucopyranosyloxy)-prop-1-ynyl)uracil-1-yl]-2,5-dioxabicyclo[2.2.1]heptane (**2Z**).* Nucleoside **1** (0.50 g, 0.72 mmol), $Pd(PPh_3)_4$ (90 mg, 0.07 mmol), CuI (30 mg, 0.14 mmol), 3-(2,3,4,6-tetra-*O*-acetyl-*β*-D-galactopyranosyl-(1→4)-2,3,6-tri-*O*-acetyl-*β*-D-glucopyranosyloxy)-prop-1-yn[S2] (1.00 g, 1.60 mmol), anhydrous Et_3N (0.40 mL,3.00 mmol) and anhydrous DMF (10 mL) were mixed, reacted and purified as described above to obtain **2Z** (0.550 g, 61%) as an off-white solid material. R_f = 0.5 (5% MeOH in CH_2Cl_2, v/v); ESI-HRMS *m/z* 1253.3796 ($[M+Na]^+$,$C_{60}H_{66}N_2O_{26}{\cdot}Na^+$, calc. 1253.3796); ^1H NMR (DMSO-d_6) δ 11.72 (s, 1H, NH), 7.81 (s, 1H, H6), 7.41-7.44 (m, 2H, Ar), 7.22-7.34 (m, 7H, Ar), 6.90 (dd, 4H, *J* = 9.0 Hz, 2.0 Hz, Ar), 5.72 (d, 1H, ex, *J* = 5.0 Hz, 3′-OH), 5.43 (s, 1H, H1′), 5.22-5.23 (d, 1H, *J* = 3.5 Hz, $H4_{gal}$), 5.13-5.18 (m, 2H, $H3_{gal}$, $H3_{glu}$), 4.81-4.87 (m, 2H, $H2_{gal}$, $H1_{glu}$), 4.68-4.76 (m, 2H, $H1_{gal}$, $H2_{glu}$), 4.30-4.36 (m, 2H, $CH_2C{\equiv}C$, $H6_{gal}$), 4.21-4.26 (m, 3H, H2′, $CH_2C{\equiv}C$, $H5_{gal}$), 4.00-4.08 (m, 4H, H3′, $H6_{gal}$, 2×$H6_{glu}$), 3.78-3.84 (m, 4H, 2×H5′, $H4_{glu}$, $H5_{glu}$), 3.74 (br s, 6H, CH_3O), 3.52-3.56 (d, 1H, *J* = 11.5 Hz, H5″), 3.25-3.29 (d, 1H, *J* = 11.5 Hz, H5″, partial overlap with H_2O), 2.10 (s, 3H, CH_3CO), 2.05 (s, 3H, CH_3CO), 2.00 (s, 6H, CH_3CO), 1.97 (s, 3H, CH_3CO), 1.92 (s, 3H, CH_3CO), 1.90 (s, 3H, CH_3CO); ^{13}C NMR (DMSO-d_6) δ 170.2, 169.82, 169.79, 169.4, 169.2, 169.1, 169.0, 161.7, 158.11, 158.09, 149.0, 144.8, 142.2 (C6), 135.3, 134.9, 129.8 (Ar), 129.7 (Ar), 127.9 (Ar), 127.5 (Ar), 126.6 (Ar),

113.24 (Ar), 113.22 (Ar), 99.8 ($C1_{gal}$), 97.7 ($C1_{glu}$), 97.1, 87.6, 87.5, 86.9 (C1′), 85.6, 79.0, 78.8 (C2′), 76.0 ($C4_{glu}$), 72.4 ($C3_{glu}$), 71.7 ($C5_{glu}$), 71.4 (C5′), 71.0 ($C2_{glu}$), 70.3 ($C3_{gal}$), 69.64/69.55 ($C5_{gal}$/C3′), 68.9 ($C2_{gal}$), 67.0 ($C4_{gal}$), 62.1 ($C6_{gal}$), 60.8 ($C6_{glu}$), 59.0 (C5″), 56.5 ($CH_2C{\equiv}C$), 55.0 (CH_3O), 20.5/20.38/20.36/20.32/20.29/20.24 (CH_3CO).

Representative protocol for O3'-phosphitylation. Nucleosides 2X-2Z were dried through coevaporation with anhydrous 1,2-dichloroethane (2×10 mL) and dissolved in anhydrous CH_2Cl_2. To this were added anhydrous N,N′-diisopropylethylamine (DIPEA) and 2-cyanoethyl-N,Ndiisopropylchlorophosphoramidite (PCl-reagent) (quantities and volumes specified below) and the reaction was stirred at rt until analytical TLC indicated complete conversion (3-4 h). The reaction mixture was diluted with CH_2Cl_2 (25 mL), washed with 5% aq. $NaHCO_3$ (2×10 mL) and the combined aqueous layers back-extracted with CH_2Cl_2 (2×10 mL). The combined organic layers were dried (Na_2SO_4), evaporated to dryness, and the resulting residue purified by silica gel column chromatography (0-4% MeOH/ CH_2Cl_2, v/v) and subsequent trituration from CH_2Cl_2 and petroleum ether to afford phosphoramidites 3X-3Z.

*(1R,3R,4R,7S)-7-[2-Cyanoethoxy(diisopropylamino)phosphinoxy]-1-(4,4'-dimethoxytrityloxymethyl)-3-[5-(3-(2,3,4,6-tetra-O-acetyl-β-D-glucopyranosyloxy)-prop-1-ynyl)uracil-1-yl]-2,5-dioxabicyclo[2.2.1]heptane (**3X**).*

Nucleoside **2X** (220 mg, 0.23 mmol) in anhydrous CH_2Cl_2 (5 mL), DIPEA (0.16mL, 0.93 mmol) and PCl-reagent (0.12 mL, 0.51 mmol) were mixed, reacted, worked up and purified as described above to provide phosphoramidite **3X** (160 mg, 60%) as a white foam. R_f = 0.5 (2% MeOH in CH_2Cl_2, v/v); ESI-HRMS *m/z* 1165.4034 ($[M+Na]^+$, $C_{57}H_{67}N_4O_{19}P{\cdot}Na^+$, calc. 1165.4029); ^{31}P NMR ($CDCl_3$) δ 149.1, 149.9.

*(1R,3R,4R,7S)-7-[2-Cyanoethoxy(diisopropylamino)phosphinoxy]-1-(4,4'-dimethoxytrityloxymethyl)-3-[5-(3-(2,3,4,6-tetra-O-acetyl-β-D-galactopyranosyloxy)-prop-1-ynyl)uracil-1-yl]-2,5-dioxabicyclo[2.2.1]heptane (**3Y**).*

Nucleoside **2Y** (0.50 g 0.53 mmol) in anhydrous CH_2Cl_2 (10 mL), DIPEA (0.40 mL, 2.12 mmol) and PCl-reagent (0.26 mL, 1.20 mmol) were mixed, reacted, worked up and purified as described above to provide phosphoramidite **3Y** (0.42 g, 70%) as a white foam. R_f = 0.8 (3% MeOH in CH_2Cl_2, v/v); ESI-HRMS *m/z* 1165.4005 ($[M+Na]^+$, $C_{57}H_{67}N_4O_{19}P{\cdot}Na^+$, calc. 1165.4029); ^{31}P NMR ($CDCl_3$) δ 149.8, 149.1.

*(1R,3R,4R,7S)-7-[2-Cyanoethoxy(diisopropylamino)phosphinoxy]-1-(4,4'-dimethoxytrityloxymethyl)-3-[5-(3-(2,3,4,6-tetra-O-acetyl-β-D-galactopyranosyl-(1→4)-2,3,6-tri-O-acetyl-β-D-glucopyranosyloxy)-prop-1-ynyl)uracil-1-yl]-2,5-dioxabicyclo[2.2.1]heptane (**3Z**).* Nucleoside **2Z** (0.52 g 0.42 mmol) in anhydrous CH_2Cl_2 (10 mL), DIPEA (0.30 mL, 1.70 mmol) and PCl-reagent (0.21 mL, 0.93 mmol) were mixed, reacted, worked up and purified as described above to provide phosphoramidites **3Z** (0.36 g, 60%) as a white foam. R_f = 0.6 (4% MeOH in CH_2Cl_2, v/v); ESI-HRMS *m/z* 1453.4895 ($[M+Na]^+$, $C_{69}H_{83}N_4O_{27}P{\cdot}Na^+$, calc. 1453.4875); ^{31}P NMR ($CDCl_3$) δ 149.8, 149.1.

3.4.3. Synthesis and purification of ONs. ONs were made on a DNA synthesizer (0.2 μmol scale) using succinyl linked LCAA-CPG (long chain alkyl amine controlled pore glass) columns with 500Å pore size. Standard protocols for incorporation of DNA phosphoramidites were used. A ~50-fold molar excess of modified phosphoramidites in anhydrous dichloromethane (0.05 M) was used along with extended oxidation (45s) and hand-coupling (20 min, 0.25 M 5-(ethylthio)-1*H*-tetrazole in CH_3CN as activator), which resulted in coupling yields greater than 95%. Cleavage from solid support and removal of nucleobase protecting

groups was realized using 32% aq. ammonia (55 °C, 18h). Crude 5′-DMTr-ONs were purified on HPLC (XTerra MS C18 column) using a 0.05 mM triethylammonium acetate buffer - 25% water/acetonitrile (v/v) gradient. Purified ONs were detritylated using 80% aq. AcOH (20 min) and precipitated ($NaOAc/NaClO_4$/acetone, -18 °C). The identity of the synthesized ONs was verified through MS analysis recorded in positive ion mode on a quadrupole time-of-flight tandem mass spectrometer equipped with a MALDI source using anthranilic acid as a matrix (Table 27), while purity (>75% for **X/Y**-modified ONs and ~65% for **Z**-modified ONs) was verified by ion-pair reverse phase HPLC running in analytical mode.

Table 4. MALDI-ToF MS of synthesized ONs.[a]

ON	**Sequence**	Calc. $(M+H)^+$	Exp. $(M+H)^+$
X1	5′-GTG A**X**A TGC	2983.0	2983.0
X2	5′-GCA **X**AT CAC	2912.0	2912.0
X3	5′-GCA TA**X** CAC	2912.0	2912.0
X4	5′-GCA**X**A**X**CAC	3142.0	3142.0
Y1	5′-GTG A**Y**A TGC	2983.5	2983.5
Y2	5′-GCA **Y**AT CAC	2912.0	2912.0
Y3	5′-GCA TA**Y** CAC	2912.5	2912.5
Y4	5′-GCA**Y**A**Y**CAC	3142.5	3142.5
Z1	5′-GTG A**Z**A TGC	3145.5	3145.5
Z2	5′-GCA **Z**AT CAC	3074.5	3074.5
Z3	5′-GCA TA**Z** CAC	3074.5	3074.5
Z4	5′-GCA**Z**A**Z**CAC	3466.5	3466.5

[a] For structures of monomer X ,Y and Z see Figure 25 in the main manuscript.

3.4.4. Thermal denaturation experiments. ON concentrations were estimated using the following extinction coefficients for DNA (OD/µmol): G (12.01), A (15.20), T (8.40), C (7.05); for RNA (OD/µmol): G (13.70), A (15.40), U (10.00), C (9.00). The strands comprising a given duplex (1.0 µM each strand) were mixed and annealed. Thermal denaturation temperatures of duplexes (1.0 µM final concentration of each strand) were determined using a temperature-controlled UV/VIS spectrophotometer and quartz optical cells with 1.0 cm path lengths. T_m's were determined as the first derivative maximum of thermal denaturation curves (A_{260} vs. T) recorded in medium salt phosphate buffer (100 mM NaCl, 0.1 mM EDTA, pH 7.0 adjusted with 10 mM Na_2HPO_4 and 5 mM Na_2HPO_4). The temperature of the denaturation experiments ranged from at least 15 °C below T_m to 20 °C above T_m (although not below 5 °C). A temperature ramp of 0.5 °C/min was used in all experiments. Reported T_m's are reported as averages of two experiments within ± 1.0 °C.

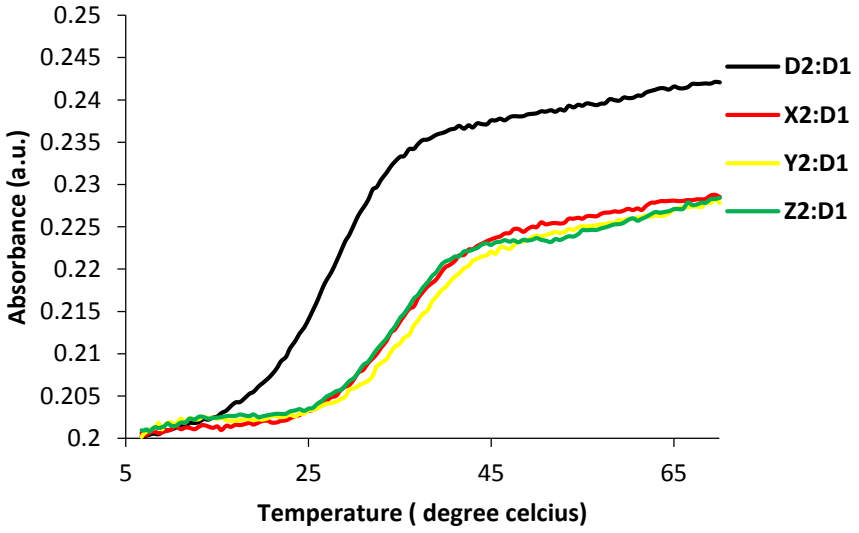

Figure 27. Representative thermal denaturation curves of duplexes between **B2** and complementary DNA.

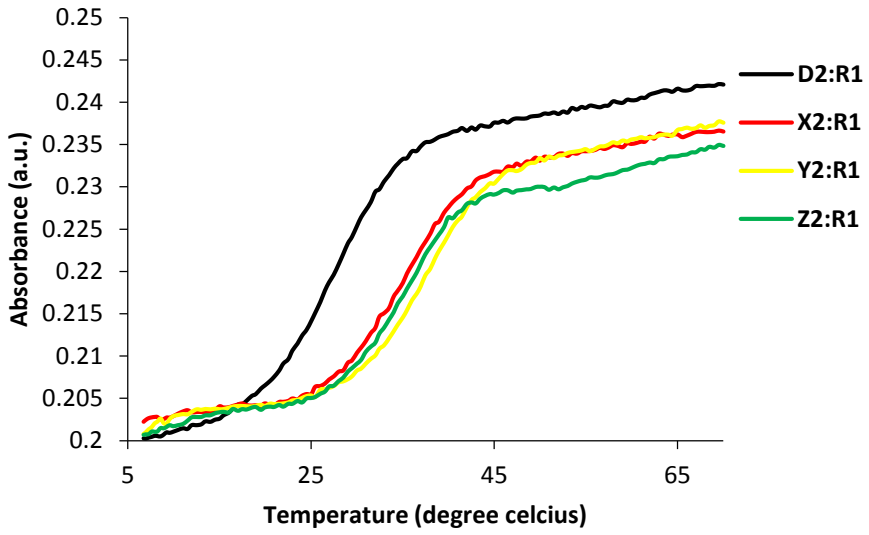

Figure 28. Representative thermal denaturation curves of duplexes between **B2** and complementary RNA.

3.4.5. Exonuclease studies. The change in absorbance at 260 nm as a function of time was monitored for a solution of ONs (3.3 μM) in magnesium buffer (600 μL, 50 mM Tris.HCl, 10 mM $MgCl_2$, pH 9.0) at 37 °C, to which snake venom phosphordiesterase (SVPDE, Worthington Biochemical Corporation) dissolved in H_2O was added (1.3 μL, 0.52 μg, 0.03 U). Rate constants were determined from -ln (1-*C*) versus time plots recorded during initial stages of degradation (Figure 29 and Table 5). *C* denotes the fraction of degraded oligonucleotide. The linear fit suggests that the reaction follows pseudo-first order kinetics.

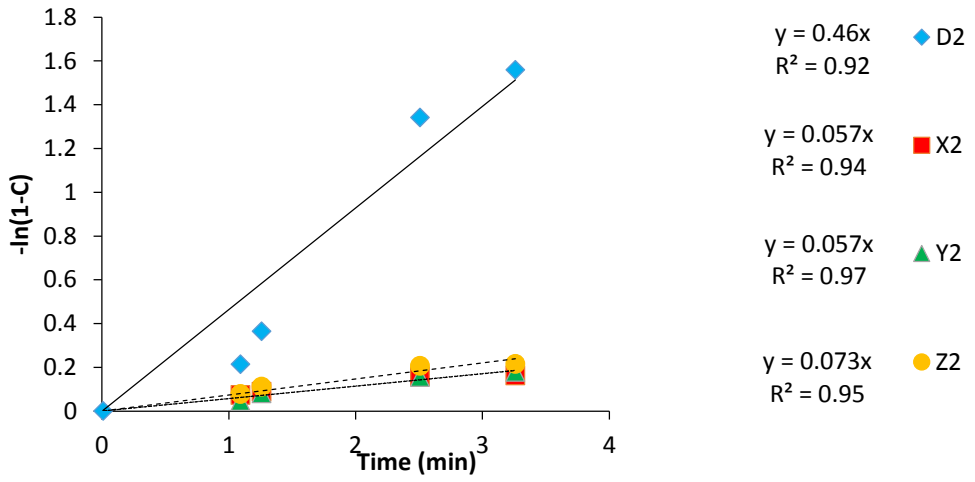

Figure 29. Plot of -ln (1-*C*) vs time (min) for SVPDE-mediated degradation of **B2** C5-carbohydrate-functionalized LNA.

Table 5. Rate constants for enzymatic degradation of **B2** ONs.[a]

ON	3′-CAC **B**AT ACG	
	k_{obs} (min^{-1})	k_{rel}
D2	4.6×10^{-1}	1.0
X2	5.7×10^{-2}	0.12
Y2	5.7×10^{-2}	0.12
Z2	7.3×10^{-2}	0.16

[a] k_{rel}'s calculated relative to k_{obs} of **D2**.

3.5. References.

1. a) Asseline, U. *Curr. Org. Chem*. **2006**, *10*, 491. b) Dodd, D. W.; Hudson, R. H. E. *Mini-Rev. Org. Chem*. **2009**, *6*, 378. c) Bennett, C. F.; Swayze, E. E. *Annu. Rev. Pharmacol. Toxicol*. **2010**, *50*, 259. d) Sinkeldam, R. W.; Greco, N. J.; Tor, Y. *Chem. Rev*. **2010**, *110*, 2579. e) Watts, J. K.; Corey, D. *R. J. Pathol*. **2012**, *226*, 365. f) Dong, H.; Lei, J.; Ding, L.; Wen, Y.; Ju, H.; Zhang, X. *Chem. Rev*. **2013**, *113*, 6207.

2. For recent reviews, see: a) Obika, S.; Abdur Rahman, S. M.; Fujisaka, A.; Kawada, Y.; Baba, T.; Imanishi, T. *Heterocycles* **2010**, *81*, 1347. b) Prakash, T. P. *Chem. Biodiv*. **2011**, *8*, 1616. c) Deleavey, G. F.; Damha, M. J. *Chem. Biol*. **2012**, *19*, 937. d) Zhou, C.; Chattopadhyaya, J. *Chem. Rev*. **2012**, *112*, 3808. e) Østergaard, M. E.; Hrdlicka, P. J. *Chem. Soc. Rev*. **2011**, *40*, 5771.

3. For recent representative examples, see: a) Haziri, A. I.; Leumann, C. J. *J. Org. Chem*. **2012**, *77*, 5861. b) Gerber, A.-B.; Leumann, C. J. *Chem.Eur. J.* **2013**, *19*, 6990. c) Hari, Y.; Osawa, T.; Kotobuki, Y.; Yahara, A.; Shrestha, A. R.; Obika, S. *Bioorg. Med. Chem.* **2013**, *21*, 4405. d) Hari, Y.; Morikawa, T.; Osawa, T.; Obika, S. *Org. Lett.* **2013**, *15*, 3702. e) Migawa, M. T.; Prakash, T. P.; Vasquez, G.; Seth, P. P.; Swayze, E. E. *Org. Lett.* **2013**, *15*, 4316. f) Hanessian, S.; Wagger, J.; Merner, B. L.; Giacometti, R. D.; Østergaard, M. E.; Swayze, E. E.; Seth, P. P. *J. Org. Chem.* **2013**, *78*, 9064. g) Shrestha, A. R.; Kotobuki, Y.; Hari, Y.; Obika, S. *Chem. Commun.* **2014**, *50*, 575.

4. Singh, S. K.; Nielsen, P.; Koshkin, A. A.; Wengel, J. *Chem. Commun.* **1998**, 455.

5. Kaur, H.; Babu, B. R.; Maiti, S. *Chem. Rev.* **2007**, *107*, 4672.

6. Obika, S.; Nanbu, D.; Hari, Y.; Andoh, J.-I.; Morio, K.-I.; Doi, T.; Imanishi, T. *Tetrahedron Lett.* **1998**, *39*, 5401.

7. a) Yong, Y.; Bernardo, G. M.; Behlke, M. A.; Owczarzy, R. *Nucleic Acids Res.* **2006**, *34*, e60. b) Wahlestedt, C.; Salmi, P.; Good, L.; Kela, J.; Johnsson, T.; Hokfelt, T.; Broberger, C.; Porreca, F.; Lai, J.; Ren, K. K.; Ossipov, M.; Koshkin, A.; Jacobsen, N.; Skouv, J.; Oerum, H.; Jacobsen, M. H.; Wengel, J. *Proc. Natl. Acad. Sci. U.S.A.* **2000**, *97*, 5633.

8. For an excellent summary, see: Watts, J. K. *Chem. Commun.* **2013**, *49*, 5618.

9. For particularly interesting earlier examples, see: a) Sørensen, M. D.; Kværnø, L.; Bryld, T.; Håkansson, A. E.; Verbeure, B.; Gaubert, G.; Herdewijn, P.; Wengel, J. *J. Am. Chem. Soc.* **2002**, *124*, 2164. b) Sørensen, M. D.; Petersen, M.; Wengel, J. *Chem. Commun.* **2003**, 2130. c) Albæk, N.; Petersen, M.; Nielsen, P. *J. Org. Chem.* **2006**, *71*, 7731. d) Varghese, O. P.; Barman, J.; Pathmasiri, W.; Plashkevych, O.; Honcharenko, D.; Chattopadhyaya, J. *J. Am. Chem. Soc.* **2006**, *128*, 15173. e) Rahman, S. M. A.; Seki, S.; Obika, S.; Yoshikawa, H.; Miyashita, K.; Imanishi, T. *J. Am. Chem. Soc.* **2008**, *130*, 4886. f) Zhou, C.; Liu, Y.; Andaloussi, M.; Badgujar, N.; Plashkevych, O.; Chattopadyaya, J. *J. Org. Chem.* **2009**, *74*, 118. g) Seth, P. P.; Vasquez, G.; Allerson, C. A.; Berdeja, A.; Gaus, H.; Kinberger, G. A.; Prakash, T. P.; Migawa, M. T.; Bhat, B.; Swayze, E. E. *J. Org. Chem.* **2010**, *75*, 1569.

10. For recent examples, see: a) Andersen, N. K.; Anderson, B. A.; Wengel, J.; Hrdlicka, P. J. *J. Org. Chem.* **2013**, *78*, 12690. b) Sau, S. P.; Madsen, A. S.; Podbevsek, P.; Andersen, N. K.; Kumar, T. S.; Andersen, S.; Rathje, R. L.; Anderson, B. A.; Guenther, D. C.; Karmakar, S.; Kumar,

P.; Plavec, J.; J. Wengel, J.; Hrdlicka, P. J. *J. Org. Chem.* **2013**, *78*, 9560. c) Karmakar, S.; Hrdlicka, P. J. *Chem. Sci.* **2013**, *4*, 3447.

11. Kumar, P.; Østergaard, M. E.; Baral, B.; Anderson, B. A.; Guenther, D. C.; Kaura, M.; Raible, D. J.; Sharma, P. K.; Hrdlicka, P. J. *J. Org. Chem.* **2014**, *79*, 5047-5061.

12. a) Manoharan, M. *Antisense Nucleic Acid Drug Rev*. **2002**, *12*, 103. b) Spinelli, N.; Defrancq, E.; Morvan, F. *Chem. Soc. Rev*. **2013**, *42*, 4557.

13. Yang, R.; Ding, H.; Song, Y.; Xiao, W.; Xiao, Q.; Wu, J. *Lett. Org. Chem*. **2008**, *5*, 518.

14. Agrofoglio, L. A.; Gillaizeau, I.; Saito, Y. *Chem. Rev.* **2003**, *103*, 1875.

15. Kumar, P.; Baral, B.; Anderson, B. A.; Guenther, D. C.; Østergaard, M. E.; Sharma, P. K.; Hrdlicka, P. J. *J. Org. Chem.* **2014**, *79*, 5062-5073.

S1. Kumar, P.; Østergaard, M. E.; Baral, B.; Anderson, B. A.; Guenther, D. C.; Kaura, M.; Raible, D. J.; Sharma, P. K.; Hrdlicka, P. J. *J. Org. Chem.* **2014**, *79*, 5047-5061

S2. Yang, R.; Ding, H.; Song, Y.; Xiao, W.; Xiao, Q. and Wu, J. *Lett. Org. Chem*. **2008**, *5*, 518-521.

Chapter 4: Synthesis and Characterization of Oligonucleotides modified with nucleobase functionalized LNAs Adenosine and Cytosine

The following paper by **Kaura**, **M**.; Kumar, P. and Hrdlicka, P. J. is published in the *J. Org. Chem.* **2014**, *79* (13), 6256-6268.

Abstract. Conformationally restricted nucleotides such as locked nucleic acids (LNAs) are very popular as affinity-, specificity- and stability-enhancing modifications in oligonucleotide chemistry to produce probes for nucleic acid targeting applications in molecular biology, biotechnology and medicinal chemistry. Considerable efforts have been devoted in recent years to optimize LNA's biophysical properties through additional modification of the sugar skeleton. We recently introduced C5-functionalization of LNA uridines as an alternative and synthetically more straightforward approach to improve LNA's biophysical properties. In the present report, we set out to test the generality of this concept by studying the characteristics of oligonucleotides modified with four different C5-functionalized LNA cytidine and C8-functionalized LNA adenosine monomers. The results strongly suggest that C5-functionalization of LNA pyrimidines indeed is a robust approach for improving the binding affinity, target specificity and enzymatic stability of LNA-modified ONs, whereas C8-functionalization of LNA adenosines is detrimental to binding affinity and specificity.

4.1. Introduction.

Conformationally restricted nucleotides[1,2] are widely used as affinity-, specificity- and stability-enhancing modifications in oligonucleotides for nucleic acid targeting applications in molecular biology, biotechnology and medicinal chemistry.[3] Locked Nucleic Acid (LNA, Figure 30),[4] which was independently developed by Wengel[5] and Imanishi,[6] is one of the most promising examples of this compound class. LNA-modified oligodeoxyribonucleotides (ONs) form

highly thermostable duplexes with complementary DNA/RNA; increases in thermal denaturation temperatures (T_m's) of up to 10 °C per modification relative to unmodified duplexes have been observed along with improved binding specificity. LNA has accordingly been used to alter gene expression through binding to mRNA, pre-mRNA or miRNA, leading to the development of LNA-based drug candidates against diseases of genetic origin.[7] Given these interesting properties, it is not surprising that a plethora of LNA analogues have been developed over the past fifteen years, which aim to improve the biophysical properties of LNA.[1,2,8] These analogues have primarily focused on modification of the oxymethylene bridge spanning the C2′/C4′-positions and/or introduction of minor-groove-oriented substituents on the bridge.

We began exploring nucleobase-functionalization of LNA as an alternative and synthetically more straightforward strategy to modulate the biophysical properties of LNA.[9] For example, we have shown that ONs modified with small C5-alkynyl-functionalized LNA uridine (U) monomers display improved affinity, specificity and enzymatic stability relative to ONs modified with conventional LNA.[10] Moreover, we have shown that ONs modified with C5-pyrene-functionalized LNA-U monomers display more desirable photophysical properties than ONs modified with the corresponding 2′-deoxyruridine monomers, most likely due to more well-defined placement of the fluorophore in the major groove.[10,11] Similar improvements have been observed for ONs modified with diastereomeric C5-functionalized α-L-LNA-U, which suggests that C5-functionalization of uridines is a general and synthetically straightforward approach for improvement of biophysical properties of conformationally restricted nucleotides building blocks.[11,12]

Intrigued by these results and keen to test the generality of this concept across LNA nucleotides with other nucleobases, we set out to study a series of representative C5-functionalized LNA cytidine (C) and C8-functionalized LNA adenosine (A) monomers (Figure 27). Unlike C5-functionalized pyrimidine monomers, which predictably position the substituent toward the major groove of nucleic acid duplexes,[13,14] the binding modes of C8-functionalized purines are more complex.[15] Bulky substituents promote adoption of *syn* conformations about the glycosyl link (N1-C1′) to minimize clashes between the C8-substituent and the sugar protons, whereas the equilibrium is not completely shifted to the *syn* conformation with medium sized substituents. The conformational ambiguity has been utilized to develop fluorophore-functionalized ON probes with interesting photophysical properties.[16] We hypothesized that the extreme pucker and conformationally restricted nature of LNA skeletons would influence the barrier between *syn* and *anti* conformations of C8-functionalized LNA-A monomers, resulting in building blocks with even stronger biases for particular conformations. Here, we report the synthesis of four C5-functionalized LNA-C and C8-functionalized LNA-A phosphoramidites, their incorporation into ONs and the characterization of the modified ONs by thermal denaturation, absorption, steady-state fluorescence and enzymatic stability experiments.

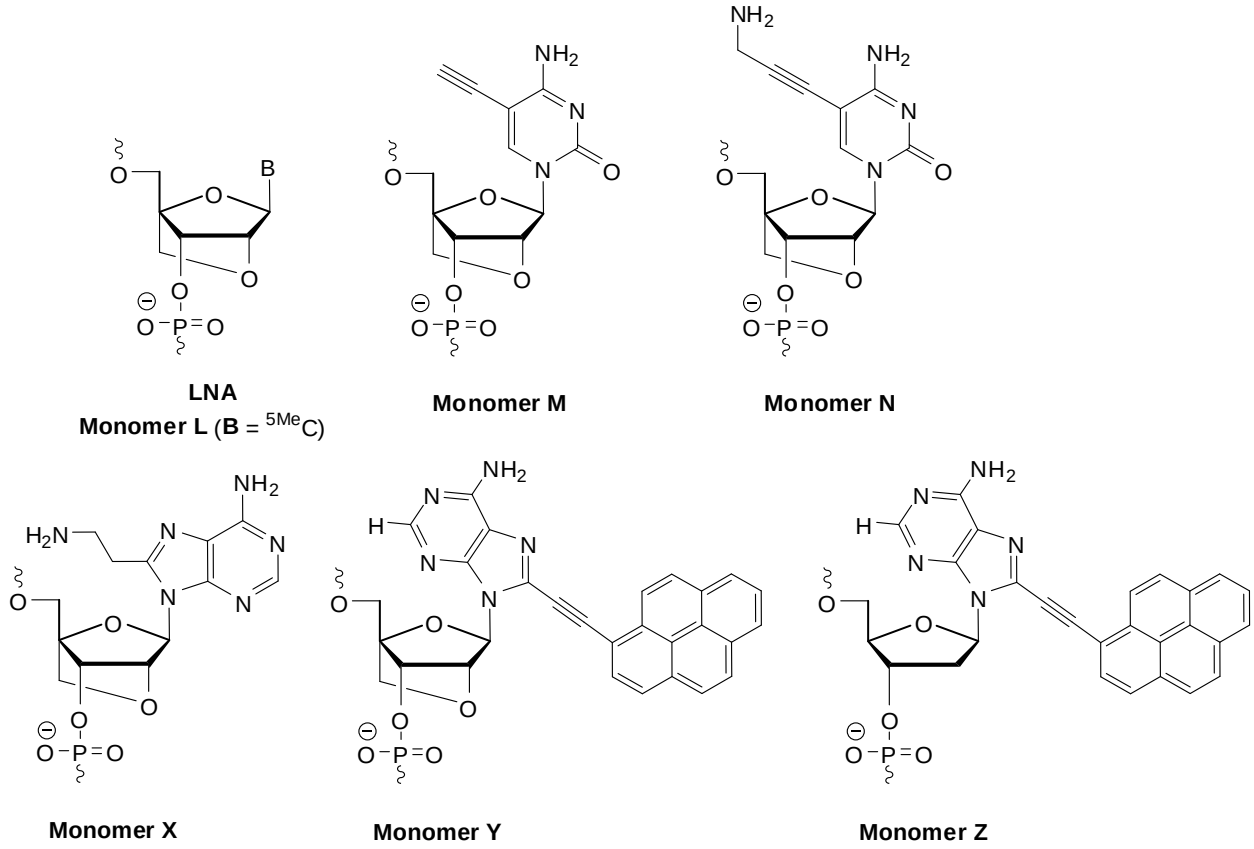

Figure 30. Structures of C5 LNA C and C8 LNA A monomers discussed herein.

4.2. Results and Discussion.

Synthesis of C5-functionalized LNA-C phosphoramidites. Our synthetic strategy toward target phosphoramidites **6a** and **6b** (Scheme 2) was prompted by: i) large-scale availability of starting material **1**, which is obtained from diacetone-α-$_D$-allose in ~38% yield),[10] ii) reports on successful uracil-to-cytosine transformations for closely related LNA analogues,[8k] and iii) a desire to introduce the C5-substitutent at the latest stage possible to reduce the total number of synthetic steps. Thus, LNA C5-iodouridine **1** was first protected at the O3′-position as a tert-butyldimethylsilyl ether in the presence of TBDMS-Cl, *N*-methylimidazole and iodine[17] to afford nucleoside **2** in excellent yield. The uracil-to-cytosine conversion was realized using the

phosphoryl chloride/1,2,4-triazole/ammonia method[18] to give nucleoside **3** in 72% yield. Subsequent coupling of trimethylsilyl-protected acetylene or trifluroacetyl-protected propargylamine to the C5-position of **3** at Sonogashira conditions[19] proceeded smoothly to afford nucleosides **4a** and **4b** in excellent yield. N4-Benzoylation of **6** was followed by O3′-desilylation to furnish alcohols **5a** and **5b** in 70% and 41% yield, respectively. The low yield of **5b** was in part due to the unexpected formation of LNA pyrrolocytosine **5c** during the desilylation step (results not shown). Attempts to change the order of reactions, i.e., conducting the Sonogashira coupling after N4-bezoylation and O3′-desilylation, also led to LNA pyrrolocytosine formation (results not shown). O3′-phosphitylation of **5a** and **5b** using 2-cyanoethyl-*N*,*N*-diisopropylchlorophosphoramidite and Hünig's base afforded targets **6a** and **6b** in moderate yields.

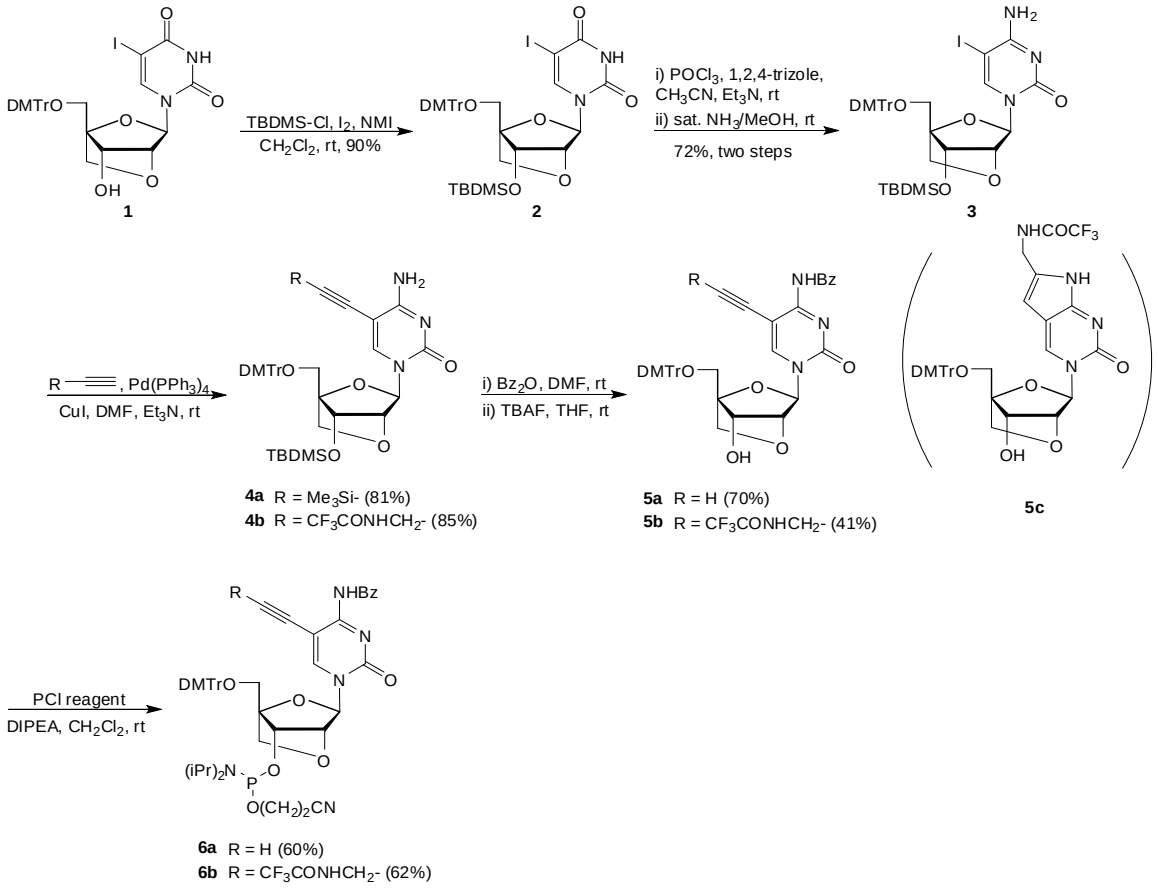

Scheme 2. Synthesis of C5-functionalized LNA cytidine phosphoramidites **6a** and **6b**. NMI = *N*-methylimidazole; PCl = 2-cyanoethyl-*N*,*N*-diisopropylchlorophosphoramidite; DIPEA = *N*,*N*′-diisopropylethylamine.

Synthesis of C8-functionalized LNA-A nucleosides. Known LNA adenosine diol **7**, which is obtained in ~25% yield from diacetone-α-D-allose,[20] was identified as a convenient starting material for the preparation of phosphoramidites **12** and **16** (Schemes 3 and 4). Treatment of **7** with molecular bromine in 1,4-dioxane and aqueous sodium acetate buffer (pH 4.5)[21] afforded nucleoside **8** in 85% yield. Subsequent O5′-dimethoxytritylation using standard conditions provided **9** in 77% yield. This was followed by protection of the exocyclic amine of the adenine moiety as a *N*,*N*-dimethyl formamidine group (90% yield).[22] We found this approach to be higher yielding and more convenient than N6-benzoylation of nucleoside **9** via the so-called transient protection protocol[23] (72% yield, over three steps, Scheme 5). A vinyl moiety, which is converted to an aminoethyl group during standard oligonucleotide deprotection,[24] was introduced at the 8-position of **10** via a Stille coupling[19] to give functionalized nucleoside **11** in 75% yield. Subsequent O3′-phosphitylation using 2-cyanoethyl-*N*,*N*-diisopropylchlorophosphoramidite afforded target phosphoramidite **12** in 64% yield.

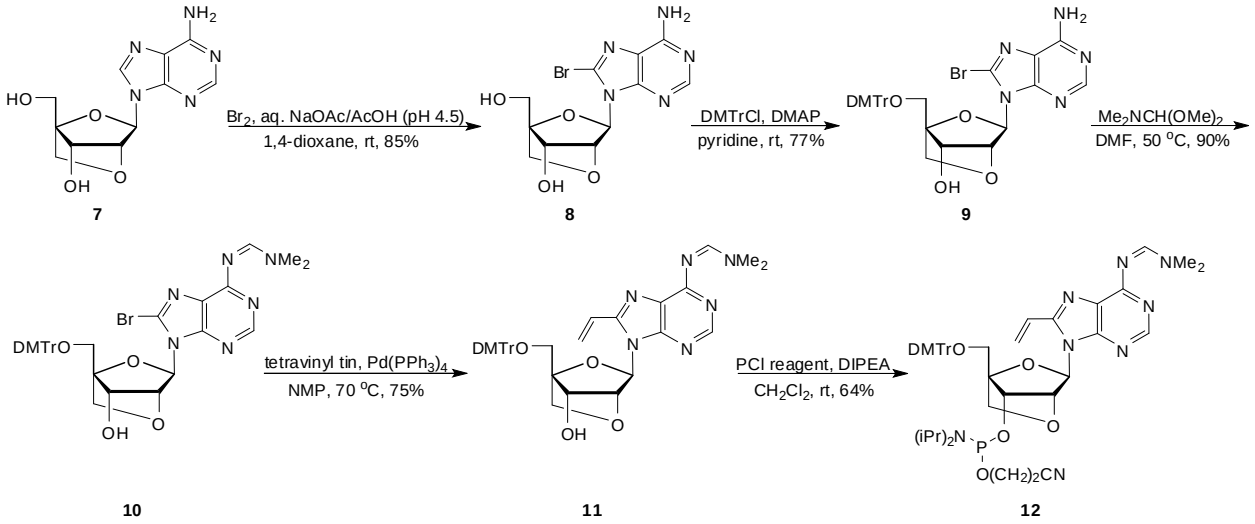

Scheme 3. Synthesis of C8-vinyl LNA adenosine phosphoramidite **12**. DMTrCl = 4,4′-dimethoxytrityl chloride; NMP = *N*-methyl pyrrolidone; PCl reagent = 2-cyanoethyl-*N*,*N*-diisopropylchlorophosphoramidite; DIPEA = *N*,*N*′-diisopropylethylamine.

The reaction sequence had to be modified for the synthesis of C8-pyrene-functionalized LNA adenosine phosphoramidite **16** (Scheme 4) as the Sonogashira reaction between C8-brominated nucleoside **10** and 1-acetylenepyrene was sluggish and did not proceed to completion, presumably due to steric interference from the O5′-DMTr group. Instead, unprotected C8-bromo LNA adenosine 8 proved to be a viable substrate for Sonogashira coupling with 1-acetylenepyrene as nucleoside 13 was obtained in 61% yield. Subsequent O5′-dimethoxytritylation (80%), N6-protection (90%) and O3′-phosphitylation (64%) finally provided phosphoramidite **16**.

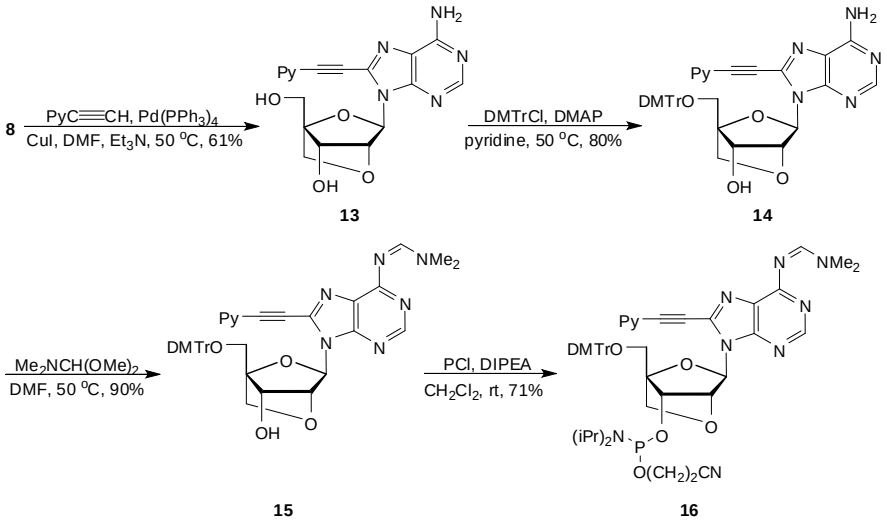

Scheme 4. Synthesis of C8-pyrene-functionalized LNA adenosine phosphoramidites **16**. DMTrCl = 4,4′-dimethoxytrityl chloride; PCl reagent = 2-cyanoethyl-*N*,*N*-diisopropylchlorophosphoramidite; DIPEA = *N*,*N*′-diisopropylethylamine.

Conformational analysis of C8-functionalized LNA-A nucleosides

ROESY (rotating-frame nuclear Overhauser effect correlation spectroscopy) spectra of selected nucleosides were recorded to examine if C8-functionalization influences the *syn-anti* equilibrium about the glycosyl link. Bulky C8-substituents are known to shift this equilibrium toward an increasing *syn* preference in 2′-deoxyribonucleosides due to steric repulsion between the C8-substituent and the sugar ring.[15] However, these shifts are accompanied by changes in the sugar pucker, which are more difficult (if not impossible) with the conformationally restricted sugar skeleton of LNA.

ROESY spectra of C8-bromo or C8-vinyl substituted LNA-A nucleosides 10 and 11 offer little evidence of significant *syn* populations (Figures 34 and 35). Most notably, there is an absence of cross peaks corresponding to through-space interactions between H2 and any of the sugar protons. In fact, the only sign that nucleoside 11 adopts *syn* conformations is a through-space coupling between H1′ and the non-terminal protons of the vinyl group. In contrast, the ROESY

spectrum of nucleoside 13 displays numerous cross peaks consistent with *syn* conformations (Figure 36), including through-space interactions between: i) H2 and H2′/H3′/5′-OH, and ii) pyrene protons and H1′/H2′/H5″/3′-OH.

ON synthesis.

Phosphoramidites **6a** and **6b** were used in machine-assisted solid-phase DNA synthesis to incorporate monomers **M** and **N** into 9-mer mixed-sequence ONs, while phosphoramidites **12** and **16** were used to incorporate monomers **X** and **Y** into 13-mer mixed-sequence ONs. To examine if the LNA skeleton has any influence on the position of C8-substituents, we also synthesized ONs modified with the DNA analogue of monomer **Y** (i.e., monomer **Z**). The following hand-coupling conditions were used (activator, coupling time, coupling yield) for monomer **M** (4,5-dicyanoimidazole, 15 min, ~95%), monomer **N** (pyridinium hydrochloride, 15 min, ~90%), monomers **X**/**Y** (5-(ethylthio)-1H-tetrazole, 20 min, ~95%) and monomer **Z** (5-[3,5-bis(trifluoromethyl)phenyl]-1*H*-tetrazole, 20 min, ~95%). The composition and purity of all modified ONs was ascertained by MALDI MS analysis (Tables 9 and 10) and ion-pair reversed-phase HPLC, respectively.

Thermal denaturation studies–experimental setup. Thermal denaturation temperatures of duplexes between modified ONs and DNA/RNA targets were evaluated by UV-Vis thermal denaturation experiments performed in a medium salt buffer ($[Na^+]$ = 110 mM). All denaturation curves displayed monophasic sigmoidal transitions (Figures 34 and 35).

Binding affinities/specificities of ONs modified with C5-functionalized LNA-C monomers. ONs modified with C5-ethynyl or C5-aminopropynyl LNA-C monomers **M** and **N** display markedly increased affinity toward complementary DNA and RNA targets relative to unmodified ONs (ΔT_m between +5.5 °C and +10.0 °C, Table 6); larger increases are observed with RNA targets.

The stabilizing effects of monomers **M** and **N** are additive as evidenced by the similar ΔT_m per modification values observed for triply modified **B4** and singly modified **B1**-**B3**. Remarkably, the duplex between **N4** and its complementary RNA has an absolute T_m of 69 °C, which is 33 °C higher than the corresponding unmodified duplex. Interestingly, **M**- and **N**-modified ONs display similar or slightly higher affinity toward DNA/RNA targets than corresponding ONs modified with conventional LNA 5-methylcytidine ($5^{Me}C$) monomer **L**, which reinforces our observations with the C5-LNA series in the preceding article.[10] Most likely, the stabilizing properties of monomer **N** are the result of favorable stacking and electrostatic interactions, in a similar manner as previously suggested for C5-aminopropynyl-modified DNA monomers.[14e,14h]

Table 6. T_m's of duplexes between **L**/**M**/**N**-modified ONs and complementary DNA or RNA.[a]

			T_m (ΔT_m/mod)/°C					
			DNA 3′-CGT AGA GTG			RNA 3′-CGU AGA GUG		
ON	Sequence	B =	L	M	N	L	M	N
B1	5′-GBA TCT CAC		40.0 (+5.0)	40.5 (+5.5)	42.5 (+7.5)	46.0 (+10.0)	45.0 (+9.0)	46.0 (+10.0)
B2	5′-GCA TBT CAC		41.0 (+6.0)	40.5 (+5.5)	43.0 (+8.0)	44.0 (+8.0)	45.0 (+9.0)	44.5 (+8.5)
B3	5′-GCA TCT BAC		42.0 (+7.0)	41.5 (+6.5)	42.0 (+7.0)	44.0 (+8.0)	45.0 (+9.0)	44.0 (+8.0)
B4	5′-GBA TBT BAC		53.0 (+6.0)	53.0 (+6.0)	60.0 (+8.3)	64.0 (+9.3)	63.5 (+9.2)	69.0 (+11.0)

[a] T_m's determined as maximum of the first derivative of denaturation curves (A_{260} vs T) recorded in T_m buffer ($[Na^+]$ = 110 mM, $[Cl^-]$ = 100 mM, pH 7.0 (NaH_2PO_4/Na_2HPO_4)) using 1.0 µM of each strand. T_m's are averages of at least two measurements within 1.0 °C. "ΔT_m/mod" = change in T_m per incorporation relative to unmodified reference duplex. T_m's of unmodified DNA:DNA and DNA:RNA duplexes are 35 °C and 36 °C, respectively.

The binding specificities of singly or triply modified **B2** and **B4** were evaluated against DNA/RNA targets with centrally mismatched nucleotides (Table 7). **M**- and **N**-modified ONs discriminate mismatched targets very efficiently as evidenced by the large drops in T_m's of

mismatched duplexes. However, comparison with ONs modified with conventional LNA-C monomers reveals that the C5-substituents of monomers **M** and **N** do not induce additional improvements in binding specificity, which contrasts our observations with the corresponding C5-functionalized LNA-U monomers.[10]

Table 7. Discrimination of mismatched DNA/RNA targets by **B2** and **B4** ONs.[a]

			DNA: 3′-CGT A**B**A GTG				RNA: 3′-CGU A**B**A GUG			
			T_m/°C	ΔT_m/°C			T_m/°C	ΔT_m/°C		
ON	**Sequence**	**B** =	**G**	**A**	**C**	**T**	**G**	**A**	**C**	**U**
D1	5′-GCA TCT CAC		**35.0**	<-25.0	<-25.0	-21.5	**36.0**	-23.5	<-26.0	<-26.0
L2	5′-GCA T**X**T CAC		**41.0**	-25.0	-28.0	-24.5	**44.0**	-25.0	-26.0	-26.0
L4	5′-G**X**A T**X**T **X**AC		**53.0**	-27.0	-29.0	-25.0	**64.0**	-24.0	-29.0	-27.0
M2	5′-GCA T**Y**T CAC		**40.5**	-24.5	-25.0	-22.0	**45.0**	-21.0	-28.0	-26.0
M4	5′-G**Y**A T**Y**T **Y**AC		**53.0**	-22.0	-25.0	-21.0	**63.5**	-18.5	-26.0	-22.0
N2	5′-GCA T**Z**T CAC		**43.0**	-24.5	-26.5	-23.5	**44.5**	-19.0	-28.0	-23.0
N4	5′-G**Z**A T**Z**T **Z**AC		**60.0**	-22.0	-29.0	-24.0	**69.0**	-19.0	-24.0	-22.0

[a] For experimental conditions, see Table 2. ΔT_m = change in T_m relative to fully matched ON:DNA or ON:RNA duplex (**B**=G).

Binding affinities/specificities of ONs modified with C8-functionalized LNA-A monomers. ONs modified with C8-functionalized LNA-A monomers **X** or **Y** generally display lower affinity toward complementary DNA than control ONs (ΔT_m for **X5**-**X8** and **Y5**-**Y8** between -6.0 and +0.5 °C, Table 8). Duplex destabilization is more pronounced when the monomers are flanked by pyrimidines, most likely due to less efficient stacking interactions (compare ΔT_m for **B5**/**B7** with **B6**/**B8**, Table 8). Interestingly, only very minor differences in T_m's are observed between **X**- and **Y**-modified DNA duplexes despite the very different nature of the C8-substituents. It is also noteworthy that DNA duplexes involving ONs modified with LNA-based monomer **Y** or

DNA-based monomer **Z** display similar T_m's, which indicates that the LNA skeleton has little influence on the position of the destabilizing structural elements.

The binding specificities of **X**/**Y**/**Z**-modified ONs were determined by performing thermal denaturation experiments using DNA targets with mismatched nucleotides opposite of the modified monomer (Table 8). As expected, unmodified duplexes with mismatched base pairs display significantly lower T_m's than fully complementary duplexes. ONs modified with C8-aminoethyl-functionalized LNA-A monomer **X** display less efficient discrimination of DNA targets with centrally mismatched dA or dC nucleotides than unmodified ONs, but improved discrimination of targets with mismatched dG nucleotides (compare ΔT_m for mismatched DNA duplexes involving **D5**-**D8** and **X5**-**X8**, Table 8). The latter observation is interesting since the dA moiety of mismatched dA:dG base pairs is known to have a preference for *syn* conformations in certain sequence contexts.[15d,25] We speculate that adoption of *syn* conformations is energetically unfavorable for C8-aminoethyl LNA-A monomer **X**, leading to more destabilized and better discriminated **X**:dG mismatches.

Conversely, **Y**-modified ONs display poor binding specificity (compare ΔT_m for mismatched DNA duplexes involving **Y5**-**Y8** and **D5**-**D8**, Table 8), which is indicative of a preference for *syn* conformations and (partial) intercalation of the pyrene moiety, as intercalating moieties are known to reduce binding specificity.[26] Only very minor differences in binding specificities are observed for **Y**- and **Z**-modified ONs.

Table 8. T_m's of duplexes between centrally modified ONs and complementary or singly mismatched DNA targets.[a]

		T_m (ΔT_m) / °C	Mismatch ΔT_m / °C		
ON	Sequence B=	**T**	**A**	**C**	**G**
D5	5′-GCGTT AAA TTGCG	48.5	-11.0	-12.0	-9.0
D6	5′-GCGTT CAC TTGCG	55.0	-9.5	-13.5	-4.5
D7	5′-GCGTT GAG TTGCG	55.5	-8.0	-10.0	-8.0
D8	5′-GCGTT TAT TTGCG	48.5	-10.0	-14.0	-5.0
X5	5′-GCGTT A**X**A TTGCG	47.0 (-1.5)	-5.0	-10.0	-11.0
X6	5′-GCGTT C**X**C TTGCG	50.0 (-5.0)	-5.0	-11.0	-8.0
X7	5′-GCGTT G**X**G TTGCG	56.0 (+0.5)	-6.0	-7.0	-12.0
X8	5′-GCGTT T**X**T TTGCG	44.0 (-4.5)	-12.0	-8.0	-7.0
Y5	5′-GCGTT A**Y**A TTGCG	47.0 (-1.5)	-1.0	+1.0	-1.0
Y6	5′-GCGTT C**Y**C TTGCG	49.0 (-6.0)	-2.0	-5.0	-1.0
Y7	5′-GCGTT G**Y**G TTGCG	52.0 (-3.5)	+0.5	+1.0	-3.5
Y8	5′-GCGTT T**Y**T TTGCG	44.5 (-4.0)	-2.0	-2.0	+2.0
Z5	5′-GCGTT A**Z**A TTGCG	46.5 (-2.0)	-0.5	+1.5	-1.0
Z6	5′-GCGTT C**Z**C TTGCG	47.0 (-8.0)	-1.0	-5.0	-0.5
Z7	5′-GCGTT G**Z**G TTGCG	53.5 (-2.0)	-2.0	±0.0	-5.5
Z8	5′-GCGTT T**Z**T TTGCG	44.5 (-2.0)	-2.5	-1.5	+0.5

[a] For experimental conditions, see Table 3. "Mismatch ΔT_m" = change in T_m relative to fully matched duplex (B = T). DNA targets: 3′-CGCAA T**B**T AACGC (for **B5**), 3′-CGCAA G**BG** AACGC (for **B6**), 3′- CGCAA C**B**C AACGC (for **B7**) and 3′-CGCAA A**B**A AACGC (for **B8**). For structures of monomers **X**-**Z** see Figure 30.

Photophysical characterization of ONs modified with C8-pyrene-functionalized LNA-A monomer Y. To gain additional insight into the binding mode of the pyrene moiety of monomer **Y**, absorption and steady state fluorescence emission spectra of **Y**-modified ONs were recorded in the absence or presence of complementary or centrally mismatched DNA targets. Single-stranded probes **Y5**-**Y8** and the corresponding duplexes with complementary/mismatched DNA targets have very similar UV-Vis absorption spectra including a well-defined absorption maximum at ~420 nm as well as shoulders at ~385 nm and ~400 nm (Figure 31). The absence of major hybridization-induced shifts in pyrene absorption maxima [27] ($\Delta\lambda$ between -2 and +1

nm, Table 11) suggests that the pyrene moiety is in a similar microenvironment in the single-stranded and double-stranded state. This is in agreement with the expected preference for syn conformations, which would place the pyrene moiety of monomer **Y** in close contact with flanking nucleobases regardless of the hybridization state. The most notable difference between **Y**- and **Z**-modified ONs/duplexes is that the pyrene absorption maxima of single-stranded **Z**-modified ONs are blue-shifted by 1-3 nm, which points toward weaker pyrene-nucleobase interactions (Table 11 and Figure 37). Accordingly, subtle hybridization-induced bathochromic shifts are generally observed for **Z**-modified ONs ($\Delta\lambda$ = -1 to +4 nm, Table 11).

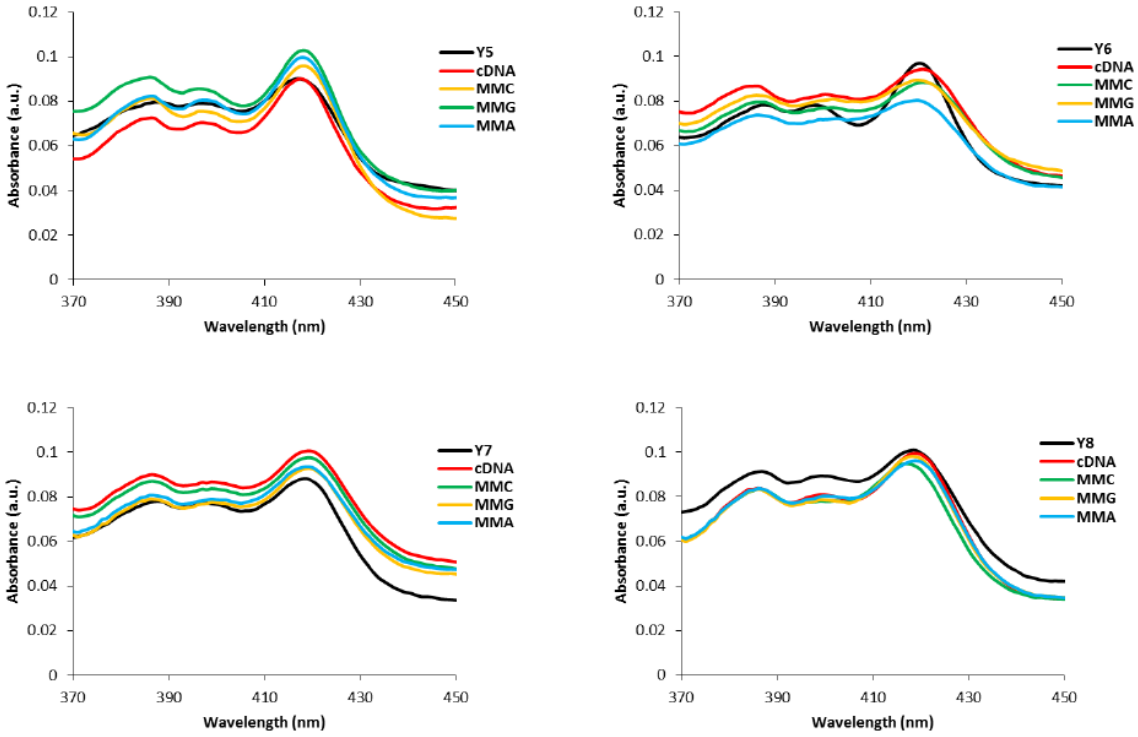

Figure 31. UV-Vis absorption spectra of single-stranded **Y5-Y8** and the corresponding duplexes with complementary (cDNA) or centrally mismatched DNA targets (MM – central

mismatched nucleotide is specified). Spectra were recorded in T_m buffer at T = 5 °C using each strand at 1.0 μM concentration.

Steady-state fluorescence emission spectra (λ_{ex} ~ 385 nm, T = 5 °C) of duplexes between **Y5**-**Y8** and complementary or centrally mismatched DNA targets exhibit a broad emission maximum centered at ~ 460 nm, which is indicative[16a] of strong electronic interactions between the pyrene and adenine moieties (Figure 32). Up to two-fold increases in fluorescence intensity are observed upon hybridization of **Y5** or **Y8** with DNA targets, whereas hybridization of **Y6** or **Y7** with DNA results in subtle decreases in fluorescence intensity. The nature of the nucleotide opposite of the modification does not appear to have a major influence on the fluorescence properties. The different trends of **Y5**/**Y8** and **Y6**/**Y7**, in which A/T and C/G base pairs flank monomer **Y**, respectively, strongly suggest that monomer **Y** predominantly adopts syn conformations leading to intercalation of pyrene and nucleobase-mediated quenching[11,16b,28] of pyrene fluorescence. Thus, in duplexes involving **Y5** or **Y8** the pyrene moiety is near weakly quenching A/T base pairs, while it is near strongly quenching C/G base pairs in duplexes involving **Y6**/**Y7**. Additional support for this hypothesis comes from the fact that the fluorescence intensity of duplexes involving **Y6** and **Y7** is very low. Similar trends are seen for **Z**-modified duplexes, again suggesting that the LNA skeleton only has a minor influence on the position of the C8-fluorophore (Figure 38).

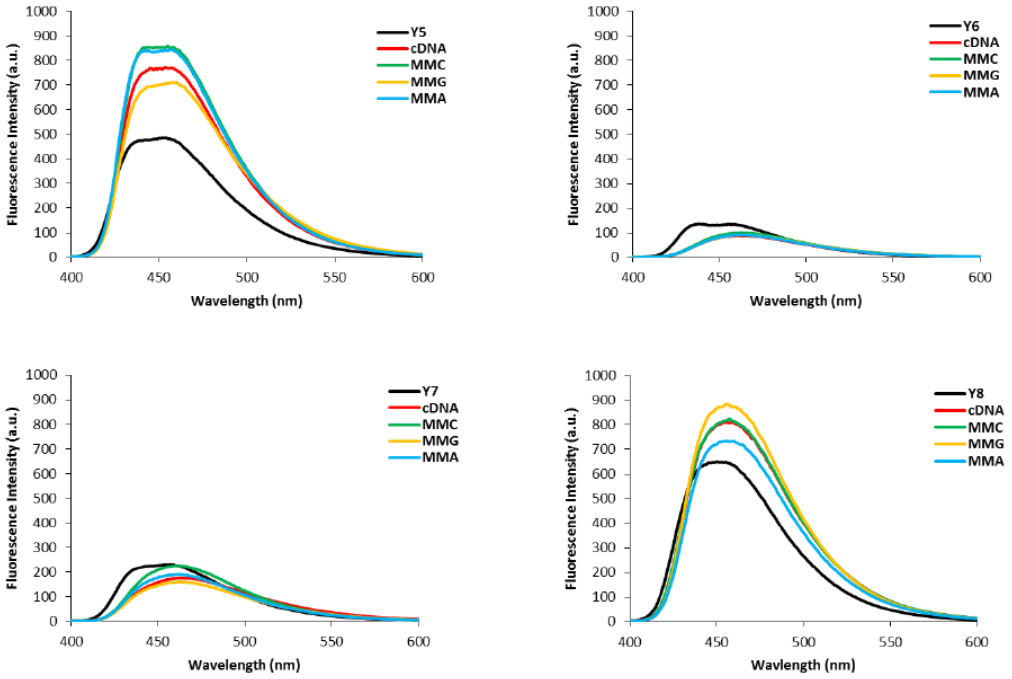

Figure 32. Steady-state fluorescence emission spectra of single-stranded **Y5-Y8** and the corresponding duplexes with complementary (cDNA) or centrally mismatched DNA targets (MM – central mismatched nucleotide is specified). Spectra were recorded in T_m buffer at T = 5 °C using each strand at 1.0 μM concentration; λ_{ex} = 385 nm. Please note that different Y-axis scales are used.

3′-Exonuclease stability of ONs modified with C5-functionalized LNA-C monomers.

Inspired by the interesting hybridization characteristics of **M**- and **N**-modified ONs, we set out to determine the stability of singly modified **M3** and **N3** against the 3′-exonuclease snake venom phosphordiesterase (SVPDE) by monitoring the change in absorbance at 260 nm of the ONs (Figure 33). As expected, unmodified DNA strand D1 is rapidly cleaved, whereas conventional LNA **L3** exhibits moderate resistance against degradation by SVPDE (~70% cleavage within ~50 min). Gratifyingly, **M3** and **N3** are considerably more resistant toward

degradation by SVPDE (~50% and ~30% cleavage within ~50 min, respectively), presumably since the C5-substituents act as steric blockers for SVPDE. These results are in agreement with our observations in the C5-alkynyl-functionalized LNA-U series,[10] which suggests that conjugation of alkynes to the C5-position of LNA pyrimidines is a general approach toward improving the enzymatic stability of LNA-modified ONs.

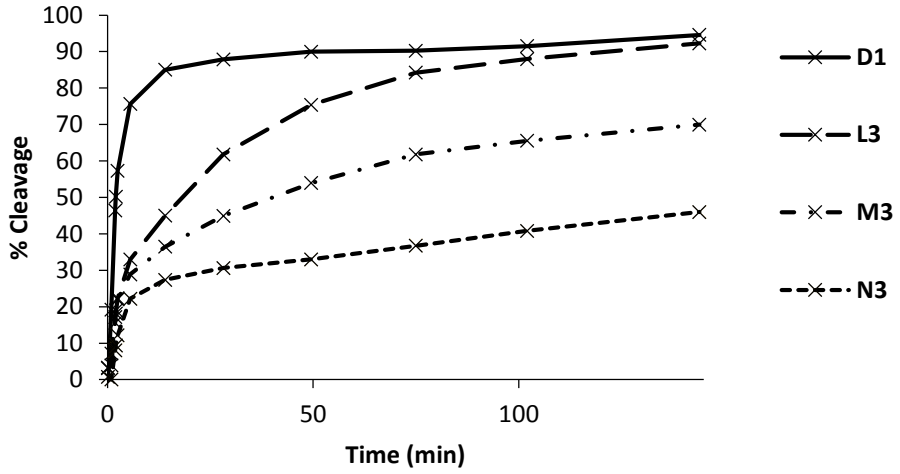

Figure 33. 3′-Exonuclease (SVPDE) degradation of singly modified **B3** and reference strands. Nuclease degradation studies were performed in magnesium buffer (50 mM Tris-HCl, 10 mM Mg^{2+}, pH 9.0) by using 3.3 μM ONs and 0.03 U of SVPDE.

4.3. Conclusion.

The current study demonstrates that attachment of alkynes to the C5-position of LNA pyrimidines is a straightforward approach for improving the binding affinity, target specificity and enzymatic stability of LNA-modified ONs. This strategy extends to α-L-LNA and presumably many other conformationally restricted pyrimidines.[12] In contrast, C8-functionalization of LNA adenosines is detrimental to binding affinity and specificity, demonstrating that the beneficial effects of the LNA skeleton do not supersede the destabilizing

effect of the C8-substituent. These properties render C5-functionalized LNA pyrimidines as interesting affinity-, specificity- and stability-enhancing modifications for use in oligonucleotide chemistry and the development of enabling tools for nucleic acid targeting applications in molecular biology, biotechnology and medicinal chemistry.

4.4 Experimental Section.

4.4.1. Experimentals of C5 and C8 LNA functionalized Cytosine and Adenosine derivatives.

(1R,3R,4R,7S)-7-(tert-Butyldimethylsilyloxy)-1-(4,4'-dimethoxytrityloxymethyl)-3-(5-iodouracil-1-yl)-2,5-dioxabicyclo[2.2.1]heptane (2). To a solution of nucleoside **1**[10] (3.20 g, 4.67 mmol), I_2 (3.50 g, 14.0 mmol) and *N*-methylimidazole (1.2 mL, 14.0 mmol) in anhydrous CH_2Cl_2 (50 mL) was added TBDMS-Cl (1M in CH_2Cl_2, 5.6 mL, 5.60 mmol). The reaction mixture was stirred at rt for 4 h whereupon it was diluted with CH_2Cl_2 (100 mL) and sat. aq. sodium thiosulfate (100 mL). The layers were separated and the organic layer was washed with sat. aq. solution of sodium thiosulfate (2 × 200 mL). The combined aqueous phase was then extracted with CH_2Cl_2 (100 mL). The combined organic layers were dried (Na_2SO_4) and evaporated to dryness to afford a residue that was purified by column chromatography (0-40% EtOAc in petroleum ether, v/v) to afford nucleoside **2** (3.30 g, 90%) as slight yellow solid material. R_f = 0.5 (40% EtOAc in petroleum ether, v/v); ESI-HRMS *m/z* 821.1731 ($[M+Na]^+$, $C_{37}H_{43}IN_2O_8Si{\cdot}Na^+$, Calc. 821.1758; ^{1}H NMR (DMSO-d_6) δ 11.74 (s, 1H, ex, NH), 8.08 (s, 1H, H6), 7.42-7.45 (m, 2H, Ar), 7.21-7.36 (m, 7H, Ar), 6.89 (d, 4H, *J* = 8.5 Hz, Ar), 5.48 (s, 1H, H1′), 4.27 (s, 2H, H2′, H3′), 3.72-3.76 (m, 7H, 2×CH_3O, H5″), 3.65-3.68 (d, 1H, *J* = 8.0 Hz, H5″), 3.33-3.36 (d, 1H, *J* = 11.0 Hz, H5′), 3.21-3.24 (d, 1H, *J* = 11.0 Hz, H5′), 0.71 (s, 9H, Me_3C), 0.04 (s, 3H, CH_3Si), -0.03 (s, 3H, CH_3Si); ^{13}C NMR (DMSO-d_6) δ 160.7, 158.11, 158.10, 149.8, 144.5, 143.0 (C6), 135.20, 135.17, 129.6 (Ar), 129.5 (Ar), 127.9 (Ar), 127.5

(Ar), 126.7 (Ar), 113.3 (Ar), 113.2 (Ar), 87.6, 87.2 (C1′), 85.6, 78.5 (C2′), 71.6 (C5″), 70.4 (C3′), 69.0, 58.5 (C5′), 55.0 (CH_3O), 25.3 (Me_3C), 17.3, -4.9 (CH_3Si), -5.4 (CH_3Si).

(1R,3R,4R,7S)-7-(tert-Butyldimethylsilyloxy)-1-(4,4'-dimethoxytrityloxymethyl)-3-(5-iodocytosin-1-yl)-2,5-dioxabicyclo[2.2.1]heptane (3). To a cold stirred suspension of 1,2,4-triazole (4.60 g, 66.3 mmol) in anhydrous acetonitrile (25 mL) was added freshly distilled $POCl_3$ (1.5 mL, 15.6 mmol). The mixture was stirred at ~0 °C for 15 min, whereupon anhydrous triethyamine (11.0 mL, 79.2 mmol) was added. After stirring for another 30 min at 0 °C, a solution of nucleoside **2** (1.60 g, 2.00 mmol) in anhydrous acetonitrile (45 mL) was added. The reaction mixture was stirred at rt for 3 h at which point solvents were removed under reduced pressure. The resulting residue was taken up in EtOAc (100 mL) and water (100 mL). The layers were separated and the organic layer was washed with sat. aq. $NaHCO_3$ (2 × 100 mL). The combined aqueous layer was then extracted with EtOAc (100 mL). The combined organic phase was dried (Na_2SO_4) and evaporated to dryness to afford a solid material that was dissolved in sat. methanolic ammonia (150 mL). The reaction mixture was stirred at rt for ~12 h at which point solvents were evaporated off and the resulting residue was purified by column chromatography (0-2% MeOH in CH_2Cl_2) to afford **3** (1.15 g 72%) as a slightly yellow solid material. R_f = 0.4 (2% MeOH in CH_2Cl_2); ESI-HRMS *m/z* 820.1895 ($[M+Na]^+$, $C_{37}H_{44}IN_3O_7Si{\cdot}Na^+$, Calc. 820.1891; ^{1}H NMR (DMSO-d_6) δ 8.06 (s, 1H, H6), 7.91 (br s, 1H, ex, NH), 7.43-7.46 (m, 2H, Ar), 7.21-7.35 (m, 7H, Ar), 6.89-6.92 (m, 4H, Ar), 6.68 (br s, 1H, ex, NH), 5.47 (s, 1H, H1′), 4.26 (s, 1H, H2′), 4.20 (s, 1H, H3′), 3.72-3.75 (m, 7H, 2×CH_3O, H5″), 3.64-3.66 (d, 1H, J = 8.0 Hz, H5″), 3.34-3.37 (d, 1H, J = 11.0 Hz, H5′), 3.18-3.21 (d, 1H, J = 11.0 Hz, H5′), 0.71 (s, 9H, Me_3C), 0.00 (s, 3H, CH_3Si), -0.06 (s, 3H, CH_3Si); ^{13}C NMR (DMSO-d_6) δ 164.0, 158.1, 153.5, 145.4 (C6), 144.5, 135.3, 135.2, 129.6 (Ar), 129.5 (Ar),

127.9 (Ar), 127.5 (Ar), 126.7 (Ar), 113.28 (Ar), 113.25 (Ar), 87.5 (C1′), 87.4, 85.6, 78.5 (C2′), 71.5 (C5″), 70.3 (C3′), 58.6 (C5′), 56.7, 55.0 (CH_3O), 25.3 (Me_3C), 17.4, -5.0 (CH_3Si), -5.3 (CH_3Si).

(1R,3R,4R,7S)-7-(tert-Butyldimethylsilyloxy)-1-(4,4'-dimethoxytrityloxymethyl)-3-[5-(trimethylsilylethynyl)cytosin-1-yl]-2,5-dioxabicyclo[2.2.1]heptane (4a). Nucleoside **3** (0.50 g, 0.63 mmol), $Pd(PPh_3)_4$ (72 mg, 0.06 mmol), CuI (24 mg, 0.13 mmol) and trimethylsilyl acetylene (0.25 mL, 1.76 mmol) were added to anhydrous DMF (10 mL) and the reaction chamber was degassed and placed under an argon atmosphere. To this was added anhydrous Et_3N (0.35 mL, 2.51 mmol) and the reaction mixture was stirred at rt for ~12 h at which point solvents were evaporated off. The resulting residue was taken up in EtOAc (100 mL) and washed with brine (2 × 50 mL) and sat. aq. $NaHCO_3$ (50 mL). The combined aqueous layer was then extracted with EtOAc (100 mL). The combined organic layer was dried (Na_2SO_4), evaporated to dryness and the resulting residue purified by column chromatography (0-5% MeOH in CH_2Cl_2 (v/v) to afford nucleoside **4a** (0.39 g, 81%) as a pale yellow solid material. R_f = 0.4 (5% MeOH in CH_2Cl_2, v/v); ESI-HRMS *m/z* 790.3310 ($[M+Na]^+$, $C_{42}H_{53}N_3O_7Si_2 \cdot Na^+$, Calc. 790.3319); ^{1}H NMR (DMSO-d_6) δ 8.00 (s, 1H, H6), 7.86 (br s, 1H, ex, NH), 7.41-7.45 (m, 2H, Ar), 7.20-7.27 (m, 7H, Ar), 6.86-6.90 (m, 4H, Ar), 6.68 (br s, 1H, ex, NH), 5.43 (s, 1H, H1′), 4.28 (s, 1H, H2′), 4.21 (s, 1H, H3′), 3.75-3.78 (d, 1H, J = 7.5 Hz, H5″), 3.72-3.73 (2s, 6H, CH_3O), 3.69-3.71 (d, 1H, J = 7.5 Hz, H5″), 3.30-3.36 (m, 2H, H5′), 0.73 (s, 9H, Me_3C), -0.01 (s, 3H, CH_3Si), -0.04 (s, 9H, Me_3Si), -0.07 (s, 3H, CH_3Si); ^{13}C NMR (DMSO-d_6) δ 164.2, 158.10, 158.07, 152.9, 144.5, 143.6 (C6), 135.3, 135.1, 129.7 (Ar), 129.4 (Ar), 127.8 (Ar), 127.5 (Ar), 126.6 (Ar), 113.18 (Ar), 113.15 (Ar), 99.7, 96.4, 89.7, 87.6 (C1′), 87.5, 85.5, 78.3

(C2′), 71.5 (C5″), 70.4 (C3′), 58.6 (C5′), 55.0 (CH_3O), 25.3 (Me_3C), 17.4, -0.6 (Me_3Si), -4.9 (CH_3Si), -5.3 (CH_3Si).

(1R,3R,4R,7S)-7-(tert-Butyldimethylsilyloxy)-1-(4,4'-dimethoxytrityloxymethyl)-3-[5-(3-trifluoroacetylaminopropyn-1-yl)cytosin-1-yl]-2,5-dioxabicyclo[2.2.1]heptane (4b). Nucleoside **3** (0.50 g, 0.63 mmol), $Pd(PPh_3)_4$ (72 mg, 0.06 mmol), CuI (24 mg, 0.13 mmol) and 2,2,2-trifluoro-*N*-(2-propynyl)acetamide[29] (0.33 mL, 1.88 mmol) were added to anhydrous DMF (10.0 mL) and the reaction chamber was degassed and placed under an argon atmosphere. To this was added anhydrous Et_3N (0.35 mL, 2.51 mmol) and the reaction mixture was stirred at rt for ~12 h at which point solvents were evaporated off. The resulting residue was taken up in EtOAc (100 mL) and washed with brine (2×50 mL) and sat. aq. $NaHCO_3$ (50 mL). The combined aqueous layer was back-extracted with EtOAc (100 mL) and the combined organic layer was dried (Na_2SO_4) and evaporated to dryness. The resulting residue was purified by column chromatography (0-7% MeOH in CH_2Cl_2 (v/v) to afford nucleoside **4b** (0.44 g, 85%) as a pale yellow solid material. R_f = 0.5 (7% MeOH in CH_2Cl_2, v/v); ESI-HRMS *m*/*z* 843.3040 ($[M+Na]^+$, $C_{42}H_{47}F_3N_4O_8Si{\cdot}Na^+$, Calc. 843.3013); ^{1}H NMR (DMSO-d_6) δ 9.84 (t, 1H, ex, J = 4.7 Hz, $NHCH_2$), 7.95 (br s, 2H, 1 ex, H2, NH_2), 7.40-7.44 (m, 2H, Ar), 7.21-7.34 (m, 7H, Ar), 6.88-6.92 (d, 4H, J = 8.5 Hz, Ar), 6.84 (br s, 1H, ex, NH_2), 5.50 (s, 1H, H1′), 4.20 (s, 1H, H2′), 4.14-4.19 (m, 2H, H3′, CH_2NH), 4.06-4.12 (dd, 1H, J = 17.8 Hz, 4.7 Hz, CH_2NH), 3.77-3.80 (d, 1H, J = 8.0 Hz, H5″), 3.74 (br s, 6H, CH_3O), 3.69-3.72 (d, 1H, J = 8.0 Hz, H5″), 3.40-3.44 (d, 1H, J = 11.0 Hz, H5′), 3.30-3.34 (d, 1H, J = 11.0 Hz, H5′), 0.70 (s, 9H, Me_3C), -0.02 (s, 3H, CH_3Si), -0.08 (s, 3H, CH_3Si); ^{13}C NMR (DMSO-d_6) δ 164.6, 158.2, 158.1, 155.9 (q, J = 36.5 Hz, $-COCF_3$), 153.0, 144.7, 142.6 (C6), 135.2, 134.7, 129.8 (Ar), 129.5 (Ar), 127.8 (Ar), 127.4 (Ar), 126.6 (Ar), 115.7 (q, J = 286 Hz, CF_3CO), 113.3 (Ar), 113.2 (Ar) , 89.7, 88.9, 87.5 (C1′),

87.3, 85.5, 78.6 (C2′), 75.6, 71.5 (C5″), 70.3 (C3′), 58.6 (C5′), 55.0 (CH_3O), 29.9 (CH_2NH), 25.3 (Me_3C), 17.4, -5.0 (CH_3Si), -5.4 (CH_3Si); ^{19}F NMR (DMSO-d_6) δ -74.8.

(1R,3R,4R,7S)-3-[4-N-Benzoyl-5-ethynylcytosin-1-yl]-1-(4,4′-dimethoxytrityloxymethyl)-7-hydroxy-2,5-dioxabicyclo[2.2.1]heptane (5a). To a solution of nucleoside **4a** (0.73 g, 0.95 mmol) in anhydrous DMF (14.0 mL) was added benzoic anhydride (0.47 g, 2.10 mmol). The reaction mixture was stirred at rt for 24 h, at which point it was concentrated to near dryness and diluted with EtOAc (100 mL) and washed with brine (2×50 mL). The aqueous layer was back-extracted with EtOAc (100 mL). The combined organic layer was dried (Na_2SO_4), evaporated to dryness and the resulting residue (~ 0.73 g) dissolved in THF (20 mL). TBAF (1M in THF, 1.45 mL, 1.45 mmol) was added to this and the reaction mixture was stirred at rt for ~3.5 h at which point EtOAc (100 mL) was added. The organic layer was washed with brine (2×50 mL) and H_2O (50 mL). The aqueous layer was back-extracted with EtOAc (100 mL). The combined organic layer was dried (Na_2SO_4), evaporated to dryness and the resulting residue purified by column chromatography (0-5% MeOH in CH_2Cl_2, v/v) to afford nucleoside **5a** (0.46 g, 70% over two steps) as a slightly yellow solid material. R_f = 0.3 (7% MeOH in CH_2Cl_2, v/v); ESI-HRMS *m*/*z* 708.2294 ($[M+Na]^+$, $C_{40}H_{35}N_3O_8 \cdot Na^+$, Calc. 708.2316); ^1H NMR[30] (DMSO-d_6) δ 12.78 (br s, 0.5H, ex, NH_A), 10.81 (br s, 0.5H, ex, NH_B), 7.9-8.3 (broad signal, 3H, Ar, H6), 7.60-7.65 (broad signal, 1H, Ar), 7.50-7.55 (m, 2H, Ar), 7.42-7.46 (m, 2H, Ar), 7.30-7.36 (m, 6H, Ar), 7.22-7.26 (m, 1H, Ar), 6.91 (d, 4H, *J* = 9.0 Hz, Ar), 5.73 (br s, 1H, ex, 3′-OH), 5.54 (br s, 1H, H1′), 4.32 (s, 1H, H2′), 4.08-4.10 (2s, 2H, H3′, HC≡C), 3.78-3.83 (m, 2H, H5″), 3.75 (br s, 6H, CH_3O), 3.48-3.52 (1H, d, *J* = 11.0 Hz, H5′), 3.30-3.33 (1H, d, *J* = 11.0 Hz, H5′, partial overlap with H_2O signal); ^{13}C NMR (DMSO-d_6) δ 158.1, 144.6, 135.3,

135.2, 132.7 (Ar), 129.7 (Ar), 129.6 (Ar), 128.4 (Ar), 127.9 (Ar), 127.6 (Ar), 126.7 (Ar), 113.3 (Ar), 87.8 (C1′), 85.7, 78.6 (C2′), 75.6, 71.4 (C5″), 69.3 (C3′), 58.9 (C5′), 55.0 (CH_3O).

(1R,3R,4R,7S)-3-[4-N-Benzoyl-5-(3-trifluoroacetylaminopropyn-1-yl)cytosin-1-yl]-1-(4,4'-dimethoxytrityloxymethyl)-7-hydroxy-2,5-dioxabicyclo[2.2.1]heptane (5b). Benzoic anhydride (0.30 g, 1.34 mmol) was added to a solution of nucleoside **4b** (0.50 g, 0.61 mmol) in anhydrous DMF (10.0 mL) and the reaction mixture was stirred at rt for 24 h, at which point it was evaporated to near dryness. The resulting residue was taken up in ethyl acetate (100 mL) and washed with brine (2×50 mL). The aqueous layer was back-extracted with EtOAc (100 mL) and the combined organic layers were dried (Na_2SO_4), evaporated to dryness and the resulting residue (0.41 g, 0.44 mmol) dissolved in THF (12 mL). To this was added TBAF (1M in THF, 0.17 mL, 0.57 mmol) and the reaction mixture was stirred at rt for ~3.5 h. At this point, EtOAc (100 mL) was added and the organic layer was washed with brine (2×50 mL) and H_2O (50 mL). The aqueous layer was back-extracted with EtOAc (100 mL). The combined organic layer was dried (Na_2SO_4), evaporated to dryness and the resulting residue purified by column chromatography (0-40% EtOAc in petroleum ether, v/v) to afford nucleoside **5b** (0.20 g, 41% yield) as a slightly yellow solid material. R_f = 0.5 (40% EtOAc in petroleum ether, v/v); ESI-HRMS *m/z* 833.2415 ($[M+Na]^+$, $C_{43}H_{37}F_3N_4O_9 \cdot Na^+$, Calc. 833.2405); ^{1}H NMR (DMSO-d_6) δ 12.86 (br s, 0.5H, ex, NH), 10.46 (br s, 0.5H, ex, NH), 9.92 (br s, 1H, ex, NH), 7.9-8.2 (broad signal, 3H, Ar, H6), 7.59-7.64 (t, 1H, J = 7.0 Hz, Ar), 7.24-7.50 (m, 11H, Ar), 6.90-6.95 (m, 4H, Ar), 6.91-6.92 (d, 2H, J = 2.5 Hz, Ar), 5.77 (br s, 1H, 3′-OH), 5.50 (s, 1H, H1′), 4.32 (s, 1H, H2′), 3.94-4.09 (m, 3H, H3′, CH_2NH), 3.84 (br s, 2H, H5″), 3.75 (s, 6H, CH_3O), 3.59-3.62 (d, 1H, J = 11.0 Hz, H5′), 3.29-3.32 (d, 1H, H5′, overlap with H_2O signal); ^{13}C NMR (DMSO-d_6) δ 158.12, 158.08, 155.9 (q, J = 35.6 Hz , $COCF_3$), 144.7, 135.4, 134.9, 132.6 (Ar), 129.8

(Ar), 129.6 (Ar), 128.3 (Ar), 127.9 (Ar), 127.5 (Ar), 126.7 (Ar), 115.7 (q, J = 286 Hz, CF_3CO), 113.3 (Ar), 113.2 (Ar), 87.8 (C1′),[31] 87.5, 85.6, 78.5 (C2′), 74.8, 71.4 (C5″), 69.5 (C3′), 59.0 (C5′), 55.0 (CH_3O), 29.4 (CH_2NH); ^{19}F NMR (DMSO-d_6) δ -74.8.

(1R,3R,4R,7S)-3-[4-N-Benzoyl-5-(trimethylsilylethynyl)cytosin-1-yl]-7-[2-cyanoethoxy(diisopropylamino)phosphinoxy]-1-(4,4'-dimethoxytrityloxymethyl)-2,5-dioxabicyclo[2.2.1]heptane (6a). Nucleoside **5a** (0.45 g, 0.65 mmol) was dried through co-evaporation with anhydrous 1,2-dichloroethane (3×25 mL) and dissolved in anhydrous CH_2Cl_2 (12 mL). To this was added anhydrous *N*,*N*′-diisopropylethylamine (0.45 mL, 2.60 mmol) and 2-cyanoethyl-*N*,*N*-diisopropylchlorophosphoramidite (0.32 mL, 1.42 mmol) and the reaction mixture was stirred at rt for ~3.5 h. The reaction mixture was diluted with CH_2Cl_2 (50 mL), washed with 5% aq. $NaHCO_3$ (2×25 mL) and the combined aqueous layers back-extracted with CH_2Cl_2 (50 mL). The combined organic layers were dried (Na_2SO_4), evaporated to dryness and the resulting residue purified by column chromatography (0-4% MeOH in CH_2Cl_2, v/v) and subsequent trituration from CH_2Cl_2 and petroleum ether to provide phosphoramidite **6a** (0.34 g, 60%) as a yellow foam. R_f = 0.7 (3% MeOH in CH_2Cl_2, v/v); ESI-HRMS *m/z* 908.3429 ($[M+Na]^+$, $C_{49}H_{52}N_5O_9P{\cdot}Na^+$, Calc. 908.3395); ^{31}P NMR ($CDCl_3$) δ 149.9, 149.5.

(1R,3R,4R,7S)-3-[4-N-Benzoyl-5-(3-trifluoroacetylaminopropyn-1-yl)cytosin-1-yl]-7-[2-cyanoethoxy(diisopropylamino)phosphinoxy]-1-(4,4'-dimethoxytrityloxymethyl)-2,5-dioxabicyclo[2.2.1]heptane (6b). Nucleoside **5b** (0.25 g, 0.33 mmol) was dried through co-evaporation with anhydrous 1,2-dichloroethane (2×10 mL) and dissolved in anhydrous CH_2Cl_2 (8 mL). To this was added anhydrous *N*,*N*′-diisopropylethylamine (0.23 mL, 1.33 mmol) and 2-cyanoethyl-*N*,*N*-diisopropylchlorophosphoramidite (0.15 mL, 0.67 mmol) and the reaction mixture was stirred at rt for ~3.5 h. The reaction mixture was diluted with CH_2Cl_2 (25 mL),

washed with 5% aq. $NaHCO_3$ (2×10 mL) and the combined aqueous layers back-extracted with CH_2Cl_2 (25 mL). The combined organic layers were dried (Na_2SO_4), evaporated to dryness and the resulting residue purified by column chromatography (0-4% MeOH in CH_2Cl_2, v/v) and subsequent trituration from CH_2Cl_2 and petroleum ether to provide phosphoramidite **5b** (210 mg, 62%) as a yellow foam. R_f = 0.7 (4% MeOH in CH_2Cl_2, v/v); ESI-HRMS *m/z* 1033.3516 ($[M+Na]^+$, $C_{52}H_{54}F_3N_6O_{10}P{\cdot}Na^+$, Calc. 1033.3483); ^{31}P NMR ($CDCl_3$) δ 150.0, 149.3.

(1S,3R,4R,7S)-3-(8-Bromoadenin-9-yl)-7-hydroxy-1-hydroxymethyl-2,5-dioxabicyclo[2.2.1]heptane (8). A solution of Br_2 (0.28 mL, 5.07 mmol) in 1,4-dioxane (20 mL) was added dropwise to a solution of known diol **7**[8a] (1.13 g, 4.05 mmol) in 1,4-dioxane (12 mL) and 0.5M aq. sodium acetate buffer (23.2 mL, pH 4.5). The reaction mixture was stirred at rt overnight, at which point a sat. aq. solution of $Na_2S_2O_3$ was added until the red color from bromine disappeared. The solution was then carefully neutralized using 0.5 M aq. NaOH. The mixture was concentrated to approximately half volume and allowed to stand at ~5 °C overnight. The resulting precipitate was filtered off and washed with a cold solution of H_2O and 1,4-dioxane (1:1, v/v) to obtain C8-brominated LNA nucleoside **8** (1.23 g, 85%) as a slightly pale yellow solid material. R_f = 0.7 (10% MeOH in CH_2Cl_2, v/v); ESI-HRMS *m/z* 379.9965 ($[M+Na]^+$, $C_{11}H_{12}BrN_5O_4{\cdot}Na^+$, calc. 379.9965); ^1H NMR (DMSO-d_6) δ 8.12 (s, 1H, H2), 7.43 (br s, 2H, ex, NH_2), 5.76 (s, 1H, H1′), 5.74 (d, 1H, ex, J = 4.3 Hz, 3′-OH), 4.95 (t, 1H, ex, J = 6.0 Hz, 5′-OH), 4.83 (s, 1H, H2′), 4.69 (d, 1H, J = 4.3 Hz H3′), 3.95-3.97 (d, 1H, J = 8.0 Hz, H5″), 3.76-3.78 (d, 1H, J = 8.0 Hz, H5″), 3.72 (d, 2H, J = 6.0 Hz, H5′); ^{13}C NMR (DMSO-d_6) δ 154.9, 152.4 (C2), 149.9, 126.4, 119.0, 88.5, 87.5 (C1′), 79.4 (C2′), 71.9 (C3′), 71.8 (C5″), 57.1 (C5′).

(1R,3R,4R,7S)-3-(8-Bromoadenin-9-yl)-1-(4,4′-dimethoxytrityloxymethyl)-7-hydroxy-2,5-dioxabicyclo[2.2.1]heptane (9). Nucleoside **8** (0.50 g, 1.40 mmol), was co-evaporated with anhydrous pyridine (10 mL) and re-dissolved in anhydrous pyridine (15 mL). DMAP (10 mg, 0.35 mmol) and 4,4′-dimethoxytrityl chloride (0.62 g, 1.82 mmol) were added to this solution and the reaction mixture was stirred at rt for 6 h. Methanol (~1.25 mL) was added and the solvents were evaporated off to furnish a crude material, which was partitioned between CH_2Cl_2 (~50 mL) and aq. $NaHCO_3$ (25 mL). The phases were separated and the organic phase was washed with aq. $NaHCO_3$ (2 × 30 mL). The aqueous layer was back-extracted with CH_2Cl_2 (30 mL) and the combined organic layers were dried ($NaSO_4$) and concentrated to dryness. The resulting residue was purified by silica gel column chromatography (0-5% MeOH in $CHCl_3$, v/v) to provide nucleoside **9** (0.71 g, 77%) as a yellow solid material. R_f = 0.4 (5% MeOH in CH_2Cl_2, v/v); MALDI-HRMS *m/z* 682.1277 ($[M+Na]^+$, $C_{32}H_{30}BrN_5O_6 \cdot Na^+$, calc. 682.1272); ^{1}H NMR (DMSO-d_6) δ 8.11 (s, 1H, H2), 7.43 (bs, 2H, ex, NH_2), 7.33-7.35 (d, 2H, Ar), 7.18-7.27 (m, 7H, Ar), 6.82-6.86 (m, 4H, Ar), 5.85 (s, 1H, H1′), 5.78 (d, 1H, ex, J = 5.0 Hz, 3′-OH), 5.05 (s, 1H, H2′), 4.64 (d, 1H, J = 5.0 Hz, H3′), 3.97-4.02 (2d, 2H, J = 8.0 Hz, H5″), 3.73 (s, 3H, CH_3O), 3.72 (s, 3H, CH_3O), 3.30-3.33 (d, 1H, J = 11.0 Hz, H5′ - partial overlap with H_2O), 3.21-3.24 (d, 1H, J = 11.0 Hz, H5′); ^{13}C NMR (DMSO-d_6) δ 158.0, 154.9, 152.5 (C2), 149.9, 144.7, 135.4, 135.3, 129.7 (Ar), 129.6 (Ar), 127.7 (Ar), 127.6 (Ar), 126.7, 126.5 (Ar), 118.9, 113.1 (Ar), 87.1 (C1′), 86.6, 85.2, 78.8 (C2′), 72.7 (C3′), 72.0 (C5″), 60.1 (C5′), 55.0 (CH_3O).

(1R,3R,4R,7S)-3-(8-Bromo-6-N-(dimethylamino)methylene-adenin-9-yl)-1-(4,4′-dimethoxytrityloxymethyl)-7-hydroxy-2,5-dioxabicyclo[2.2.1]heptane (10).

N,N-dimethylformamide dimethyl acetal (0.17 mL, 1.20 mmol) was added to a solution of nucleoside **9** (0.32 g, 0.50 mmol) in anhydrous DMF (5.0 mL) and the reaction mixture was

stirred for 5 h at 50 °C. All volatile components were removed and the resulting residue was taken up in ethyl acetate (15 mL) and subsequently washed with brine (2×25 mL) and saturated aq. $NaHCO_3$ (25 mL). The organic layer was dried (Na_2SO_4), evaporated to dryness and the resulting residue purified by silica gel column chromatography (0-5% MeOH in CH_2Cl_2, v/v) to furnish nucleoside **10** (0.31 g, 90%) as a pale yellow solid material. R_f = 0.5 (5% MeOH in CH_2Cl_2, v/v); MALDI-HRMS *m/z* 715.1848 ($[M+Na]^+$, $C_{53}H_{44}N_6O_6 \cdot Na^+$, calc. 715.1874); ^{1}H NMR (DMSO-d_6) δ 8.87 (s, 1H, $CH(NMe_2)$), 8.37 (s, 1H, H2), 7.33-7.36 (m, 2H, Ar), 7.18-7.28 (m, 7H, Ar), 6.82-6.86 (m, 4H, Ar), 5.88 (s, 1H, H1′), 5.80 (d, 1H, ex, *J* = 5.0 Hz, 3′-OH), 5.08 (s, 1H, H2′), 4.65 (d, 1H, *J* = 5.0 Hz, H3′), 3.98-4.04 (2d, *J* = 7.5 Hz, H5″), 3.72 (br s, 6H, CH_3O), 3.32-3.34 (d, 1H, *J* = 11.0 Hz, H5′), 3.21-3.24 (d, 1H, *J* = 11.0 Hz, H5′), 3.20 (s, 3H, NCH_3), 3.13 (s, 3H, NCH_3); ^{13}C NMR (DMSO-d_6) δ 158.00, 157.97, 157.7 ($CH(NMe_2)$), 151.7 (C2), 144.6, 135.4, 135.3, 129.7 (Ar), 129.6 (Ar), 129.3, 127.7 (Ar), 127.63 (Ar), 126.58 (Ar), 125.4, 113.1 (Ar), 87.1 (C1′), 86.6, 85.2, 78.9 (C2′), 72.8 (C3′), 72.0 (C5″), 60.2 (C5′), 55.0 (CH_3O), 40.7 (NCH_3), 34.6 (NCH_3).

(1R,3R,4R,7S)-1-(4,4'-Dimethoxytrityloxymethyl)-3-(6-N-(dimethylamino)methylene-8-vinyl-adenin-9-yl)-7-hydroxy-2,5-dioxabicyclo[2.2.1]heptane (11). Nucleoside **10** (0.30 g, 0.42 mmol), $Pd(PPh_3)_4$ (49 mg, 0.04 mmol) and tetravinyl tin (0.17 mL, 0.92 mmol) were added to anhydrous *N*-methyl pyrrolidone (5.0 mL) and the mixture was degassed and placed under argon. The reaction mixture was stirred at 70 °C for 5 h at which point EtOAc (15 mL) and 5% aq. sodium bicarbonate (20 mL) were added. Phases were separated and the organic phase was washed with sat. aq. $NaHCO_3$ (20 mL). The aqueous phase was back-extracted with ethyl acetate (2 × 20 mL) and the combined organic phase was dried (Na_2SO_4) and evaporated to near dryness. The resulting crude was purified by column chromatography (0-5% MeOH in

CH_2Cl_2, v/v) to afford nucleoside **11** (0.21 g, 75%) as an off white solid material. R_f = 0.5 (5% MeOH in CH_2Cl_2, v/v); MALDI-HRMS *m*/*z* 663.2930 ($[M+Na]^+$, $C_{50}H_{39}N_5O_6 \cdot Na^+$, calc. 663.2931); ^{1}H NMR (DMSO-d_6) δ 8.91 (s, 1H, $CH(NMe_2)$), 8.37 (s, 1H, H2), 7.32-7.35 (m, 2H, Ar), 7.18-7.26 (m, 7H, Ar), 7.14 (dd, 1H, *J* = 17.2 Hz, 11.0 Hz, $CH=CH_2$), 6.80-6.85 (2d, 4H, *J* = 7.0 Hz, Ar), 6.47 (dd, 1H, *J* = 17.2 Hz, 2.0 Hz, $CH_2=CH_{trans}$), 6.07 (s, 1H, H1′), 5.79 (d, 1H, ex, *J* = 5.0 Hz, 3′-OH), 5.72 (dd, 1H, *J* = 11.0 Hz, 2.0 Hz, $CH_2=CH_{cis}$), 5.25 (s, 1H, H2′), 4.35 (d, 1H, *J* = 5.0 Hz, H3′), 4.02-4.04 (d, 1H, *J* = 8.0 Hz, H5″), 3.97-3.99 (d, 1H, *J* = 8.0 Hz, H5″), 3.72 (br s, 6H, CH_3O), 3.28-3.31 (d, 1H, H5′, overlap with H_2O), 3.20-3.23 (d, 1H, *J* = 11.0 Hz, H5′), 3.20 (s, 3H, NCH_3), 3.14 (s, 3H, NCH_3); ^{13}C NMR (DMSO-d_6) δ 158.7, 158.0, 157.7 ($CH(NMe_2)$), 151.4 (C2), 151.2, 149.2, 144.6, 135.4, 135.2, 129.62 (Ar), 129.59 (Ar), 127.7 (Ar), 127.6 (Ar), 126.6 (Ar), 124.84 ($CH=CH_2$), 124.81, 122.9 ($CH_2=CH$), 113.1, 86.5, 85.9 (C1′), 85.2, 78.8 (C2′), 72.6 (C3′), 72.0 (C5″), 60.1 (C5′), 54.9 (CH_3O), 40.6 (CH_3N), 34.6 (CH_3N).

(1R,3R,4R,7S)-7-[2-Cyanoethoxy(diisopropylamino)phosphinoxy]-1-(4,4′-dimethoxytrityloxymethyl)-3-(6-N-(dimethylamino)methylene-8-vinyl-adenin-9-yl)-2,5-dioxabicyclo[2.2.1]heptane (12). Nucleoside **11** (200 mg, 0.30 mmol) was dried through co-evaporation with anhydrous 1,2-dichloroethane (2×10 mL) and re-dissolved in anhydrous CH_2Cl_2 (8 mL). To this was added anhydrous *N*,*N*′-diisopropylethylamine (0.21 mL, 1.21 mmol) and 2-cyanoethyl-*N*,*N*-diisopropylchlorophosphoramidite (0.15 mL, 0.66 mmol) and the reaction mixture was stirred at rt for 3.5 h. The reaction mixture was diluted with CH_2Cl_2 (25 mL), washed with 5% aq. $NaHCO_3$ (2×10 mL) and the combined aqueous phase back-extracted with CH_2Cl_2 (2×10 mL). The combined organic layers were dried (Na_2SO_4), evaporated to dryness, and the resulting residue purified by silica gel column chromatography

(0-4% MeOH in CH_2Cl_2, v/v) and subsequent trituration from CH_2Cl_2 and petroleum ether to provide phosphoramidite **12** (165 mg, 64%) as a white foam. R_f = 0.5 (4% MeOH in CH_2Cl_2, v/v); MALDI-HRMS *m/z* 863.4039 ($[M+Na]^+$, $C_{46}H_{55}N_8O_7P{\cdot}Na^+$, calc. 863.4010); ^{31}P NMR ($CDCl_3$) δ 150.4, 150.0.

(1S,3R,4R,7S)-7-Hydroxy-1-hydroxymethyl-3-[8-(2-(1-pyrenyl)ethynyl)adenin-9-yl]-2,5-dioxabicyclo[2.2.1]heptane (13). Nucleoside **8** (0.40 g, 1.18 mmol), $Pd(PPh_3)_4$ (130 mg, 0.11 mmol), CuI (48 mg, 0.22 mmol) and 1-ethynylpyrene[32] (0.56 g, 2.46 mmol) were added to anhydrous DMF (8.0 mL) and the resulting mixture was degassed and placed under argon. To this was added anhydrous Et_3N (0.66 mL, 4.72 mmol) and the reaction mixture was stirred at 50 °C for 6 h whereupon solvents were evaporated off. The resulting residue was taken up in EtOAc (15 mL), dried (Na_2SO_4), evaporated to dryness and purified by silica gel column chromatography (0-10% MeOH in CH_2Cl_2, v/v) to obtain nucleoside **13** (0.34 g, 61%) as a bright yellow solid material. R_f = 0.6 (10% MeOH in CH_2Cl_2, v/v); MALDI-HRMS *m/z* 526.1514 ($[M+Na]^+$, $C_{29}H_{21}N_5O_4{\cdot}Na^+$, calc. 526.1491); ^1H NMR (DMSO-d_6) δ 8.73 (d, 1H, *J* = 9.0 Hz, Ar), 8.15-8.46 (m, 9H, Ar, H2), 7.61 (br s, 2H, ex, NH_2), 6.25 (s, 1H, H1′), 5.83 (d, 1H, ex, *J* = 5.0 Hz, 3′-OH), 5.02 (t, 1H, ex, *J* = 5.5 Hz, 5′-OH), 4.97 (s, 1H, H2′), 4.85 (d, 1H, *J* = 5.0 Hz, H3′), 4.12-4.14 (d, 1H, *J* = 8.0 Hz, H5″), 4.00-4.02 (d, 1H, *J* = 8.0 Hz, H5″), 3.84 (d, 2H, *J* = 6.0 Hz, H5′); ^{13}C NMR (DMSO-d_6) δ 156.0, 153.6 (C2), 148.5, 133.2, 132.0, 131.9, 130.7, 130.4, 129.9 (Ar), 129.5 (Ar), 129.2 (Ar), 127.2 (Ar), 127.0 (Ar), 126.5 (Ar), 126.4 (Ar), 125.0 (Ar), 124.5 (Ar), 123.5, 123.1, 119.2, 114.1, 94.0, 88.6, 86.9 (C1′), 84.6, 79.6 (C2′), 72.1 (C5″), 72.0 (C3′), 57.4 (C5′).

(1S,3R,4R,7S)-1-(4,4′-Dimethoxytrityloxymethyl)-7-hydroxy-3-[8-(2-(1-pyrenyl)ethynyl)adenin-9-yl]-2,5-dioxabicyclo[2.2.1]heptane (14). Diol **13** (0.30 g, 0.59 mmol) was co-evaporated with anhydrous pyridine (2 × 10 mL) and redissolved in anhydrous pyridine (10 mL). To this was added 4,4′-dimethoxytrityl chloride (0.26 g, 0.77 mmol) and DMAP (18 mg, 0.15 mmol) and the reaction mixture was stirred at ~50 °C for 6 h, whereupon it was diluted with sat. aq. $NaHCO_3$ (20 mL) and CH_2Cl_2 (25 mL). The phases were separated and the organic phase was washed with sat. aq. $NaHCO_3$ (20 mL). The aqueous phase was back-extracted with CH_2Cl_2 (2×20 mL) and the combined organic layers were dried (Na_2SO_4), evaporated to near dryness and co-evaporated with toluene/absolute EtOH (2×30 mL, 1:2, v/v). The resulting crude was purified by silica gel column chromatography (0-5% MeOH in CH_2Cl_2, v/v) to afford nucleoside **14** (0.38 g, 80%) as a slightly yellow solid material. R_f = 0.5 (5% MeOH in CH_2Cl_2, v/v); MALDI-HRMS *m*/*z* 828.2828 ($[M+Na]^+$, $C_{50}H_{39}N_5O_6{\cdot}Na^+$, calc. 828.2798); ^{1}H NMR (DMSO-d_6) δ 8.89 (d, 1H, J = 9.5 Hz, Ar), 8.15-8.49 (m, 9H, Ar, H2), 7.60 (br s, 2H, ex, NH_2), 7.26-7.28 (m, 2H, Ar), 6.99-7.15 (m, 7H, Ar), 6.53-6.59 (2d, 4H, J = 9.0 Hz, Ar), 6.37 (s, 1H, H1′), 5.89 (d, 1H, ex, J = 5.0 Hz, 3′-OH), 5.21 (s, 1H, H2′), 4.61 (d, 1H, J = 5.0 Hz, H3′), 4.38-4.41 (d, 1H, J = 8.0 Hz, H5″), 4.17-4.20 (d, 1H, J = 8.0 Hz, H5″), 3.50 (s, 3H, CH_3O), 3.46 (s, 3H, CH_3O), 3.42-3.45 (d, 1H, J = 11.0 Hz, H5′), 3.19-3.22 (d, 1H, J = 11.0 Hz, H5′); ^{13}C NMR (DMSO-d_6) δ 157.8, 157.7, 156.0, 153.7 (C2), 148.4, 144.4, 135.5, 135.1, 133.3, 131.93, 131.90, 130.7, 130.4, 129.8 (Ar), 129.6 (Ar), 129.42 (Ar), 129.37 (Ar), 129.1 (Ar), 127.6 (Ar), 127.5 (Ar), 127.1 (Ar), 126.9 (Ar), 126.4 (Ar), 125.0 (Ar), 124.4 (Ar), 123.5, 123.1, 118.9, 114.4, 112.85 (Ar), 112.83 (Ar), 93.8, 86.7, 86.6 (C1′), 85.2, 85.0, 78.9 (C2′), 72.9 (C3′), 72.5 (C5″), 60.9 (C5′), 54.68 (CH_3O), 54.66 (CH_3O).

(1S,3R,4R,7S)-1-(4,4′-Dimethoxytrityloxymethyl)-7-hydroxy-3-[6-N-(dimethylamino)methylene-8-(2-(1-pyrenyl)ethynyl)adenin-9-yl]-2,5-dioxabicyclo[2.2.1]heptane (15).

N,*N*-dimethylformamide dimethyl acetal (0.11 mL, 0.82 mmol) was added to a solution of nucleoside **14** (0.33 g, 0.41 mmol) in anhydrous DMF (10 mL) and the reaction mixture was stirred at 50 °C for 5 h. At this point, all volatile components were removed and the resulting residue was taken up in ethyl acetate (15 mL). The organic phase was washed with brine (2×25 mL) and sat. aq. $NaHCO_3$ (25 mL), dried (Na_2SO_4) and evaporated to dryness. The resulting residue was purified by silica gel column chromatography (0-5% MeOH in CH_2Cl_2, v/v) to obtain nucleoside **15** (0.32 g, 90%) as a bright yellow solid material. R_f = 0.6 (6% MeOH in CH_2Cl_2, v/v); MALDI-HRMS *m/z* 883.3243 ($[M+Na]^+$, $C_{53}H_{44}N_6O_6 \cdot Na^+$, calc. 883.3220); ^{1}H NMR (DMSO-d_6) δ 8.94 (s, 1H, $CH(NMe_2)$), 8.91 (d, 1H, *J* = 9.0 Hz, Ar), 8.15-8.48 (m, 9H, Ar, H2), 7.25-7.29 (m, 2H, Ar), 6.98-7.16 (m, 7H, Ar), 6.57 (d, 2H, *J* = 9.0 Hz, Ar), 6.54 (d, 2H, *J* = 9.0 Hz, Ar), 6.40 (s, 1H, H1′), 5.90 (d, 1H, ex, *J* = 5.0 Hz, 3′-OH), 5.25 (s, 1H, H2′), 4.61 (d, 1H, *J* = 5.0 Hz, H3′), 4.41-4.43 (d, 1H, *J* = 7.5 Hz, H5″), 4.19-4.21 (d, 1H, *J* = 7.5 Hz, H5″), 3.49 (s, 3H, CH_3O), 3.47 (s, 3H, CH_3O), 3.42-3.45 (d, 1H, *J* = 11.0 Hz, H5′), 3.24 (s, 3H, NCH_3), 3.18-3.22 (m, 4H, H5′, NCH_3); ^{13}C NMR (DMSO-d_6) δ 159.1, 157.81 ($CH(NMe_2)$), 157.76, 157.69, 152.7 (C2), 150.3, 144.4, 135.6, 135.2, 135.1, 132.03, 131.97, 130.6, 130.4, 129.9 (Ar), 129.6 (Ar), 129.4 (Ar), 129.3 (Ar), 129.2 (Ar), 127.6 (Ar), 127.5 (Ar), 127.1 (Ar), 126.9 (Ar), 126.46 (Ar), 126.43 (Ar), 126.40 (Ar), 125.4, 125.0 (Ar), 124.4 (Ar), 123.5, 123.1, 114.3, 112.9 (Ar), 112.8 (Ar), 94.4, 86.7, 86.6 (C1′), 85.2, 85.1, 79.0 (C2′), 72.9 (C3′), 72.6 (C5″), 60.9 (C5′), 54.7 (CH_3O), 40.8 (NCH_3), 34.7 (NCH_3).

(1S,3R,4R,7S)-7-[2-Cyanoethoxy(diisopropylamino)phosphinoxy]-1-(4,4′-dimethoxytrityloxymethyl)-3-[6-N-(dimethylamino)methylene-8-(2-(1-pyrenyl)ethynyl)adenin-9-yl]-2,5-dioxabicyclo[2.2.1]heptane (16). Nucleoside **15** (0.32 g, 0.37 mmol) was dried through co-evaporation with anhydrous 1,2-dichloroethane (2×10 mL) and dissolved in anhydrous CH_2Cl_2 (8 mL). To this was added anhydrous *N*,*N*′-diisopropylethylamine (0.26 mL, 1.50 mmol) and 2-cyanoethyl-*N*,*N*-diisopropylchlorophosphoramidite (0.18 mL, 0.82 mmol) and the reaction mixture was stirred at rt for 3.5 h. The reaction mixture was diluted with CH_2Cl_2 (25 mL), washed with 5% aq. $NaHCO_3$ (2×10 mL) and the combined aqueous phase back-extracted with CH_2Cl_2 (2×10 mL). The combined organic layers were dried (Na_2SO_4), evaporated to dryness and the resulting residue purified by silica gel column chromatography (0-4% MeOH in CH_2Cl_2, v/v) and subsequent trituration from CH_2Cl_2 and petroleum ether to provide phosphoramidite **16** (0.28 g, 71%) as a yellow foam. R_f = 0.5 (4% MeOH in CH_2Cl_2, v/v); MALDI-HRMS *m/z* 1083.4299 ($[M+Na]^+$, $C_{62}H_{61}N_8O_7P{\cdot}Na^+$, calc. 1083.4315); ^{31}P NMR ($CDCl_3$) δ 150.0, 149.8.

4.4.2. Synthesis and purification of ONs. Synthesis of modified ONs was performed on a DNA synthesizer at a 0.2 μmol scale using succinyl linked LCAA-CPG (long chain alkyl amine controlled pore glass) columns with 500 Å pore size. Standard protocols for incorporation of DNA phosphoramidites were used. A ~50-fold molar excess of modified phosphoramidites in anhydrous acetonitrile (0.05 M – phosphoramidites **6a** and **6b**) or anhydrous dichloromethane (0.05 M – phosphoramidites **12**, **16** and the DNA analogue of **16**[33]) was used along with extended oxidation (45s) and the following hand-coupling conditions (activator, coupling time, coupling yield) for monomer **M** (4,5-dicyanoimidazole, 15 min, ~95%), monomer **N** (pyridinium hydrochloride, 15 min, ~90%), monomers **X**/**Y** (5-(ethylthio)-1*H*-tetrazole, 20

min, ~95%) and monomer **Z** (5-[3,5-bis(trifluoromethyl)phenyl]-1*H*-tetrazole, 20 min, ~95%). Cleavage from solid support and removal of nucleobase protecting groups was realized using 32% aq. ammonia (55 °C, ~18 h). ONs were purified (DMTr-on) by ion-pair reverse phase HPLC (XTerra MS C18 column) using a 0.05 mM triethylammonium acetate buffer - 25% water/acetonitrile (v/v) gradient. Purified ONs were detritylated using 80% aq. AcOH (~20 min) and precipitated from NaOAc/$NaClO_4$/acetone (-18 °C, 12-16 h). The identity of the synthesized ONs was verified through MALDI-MS recorded in positive ion mode on a quadrupole time-of-flight tandem mass spectrometer using anthranilic acid as a matrix (Tables 9 and 10), while purity (>80%) was verified by RP-HPLC running in analytical mode.

Thermal denaturation experiments. ON concentrations were estimated using the following extinction coefficients for DNA (OD/μmol): G (12.01), A (15.20), T (8.40), C (7.05); for RNA (OD/μmol): G (13.70), A (15.40), U (10.00), C (9.00), pyrene (22.4).[26c] The strands comprising a given duplex were mixed and annealed. Thermal denaturation temperatures of duplexes (1.0 μM final concentration of each strand) were determined on a temperature-controlled UV/VIS spectrophotometer using quartz optical cells with 1.0 cm path lengths. T_m's were determined as the first derivative maximum of thermal denaturation curves (A_{260} vs. T) recorded in medium salt buffer (100 mM NaCl, 0.1 mM EDTA, pH 7.0 adjusted with 10 mM Na_2HPO_4 and 5 mM Na_2HPO_4). The temperature of the denaturation experiments ranged from at least 15 °C below T_m to 20 °C above T_m (although not below 5 °C). A temperature ramp of 0.5 °C/min was used in all experiments. Reported T_m's are reported as averages of two experiments within ± 1.0 °C. *Absorption spectroscopy*. UV-vis absorption spectra were recorded at 5 °C using the same samples and instrumentation as in thermal denaturation experiments.

Fluorescence spectroscopy. Steady-state fluorescence emission spectra were recorded in non-deoxygenated thermal denaturation buffer (each strand 1.0 μM) using an excitation wavelength of λ_{ex} = 385 nm, excitation slit 5.0 nm, emission slit 5.0 nm and a scan speed of 600 nm/min. Experiments were performed at temperature (~5 °C).

Exonuclease studies. The change in absorbance at 260 nm as a function of time was monitored for a solution of ONs (3.3 μM) in magnesium buffer (600 μL, 50 mM Tris.HCl, 10 mM $MgCl_2$, pH 9.0) at 37 °C, to which snake venom phosphordiesterase (SVPDE, Worthington Biochemical Corporation) dissolved in H_2O was added (1.3 μL, 0.52 μg, 0.03 U). Rate constants were determined from -ln (1-*C*) versus time plots obtained for initial stages of degradation (Figure 39 and Table 12). *C* denotes the fraction of degraded oligonucleotide.

4.5. Supporting information.

General experimental section. Reagents and solvents were obtained from commercial suppliers and of analytical grade and used without further purification. Petroleum ether (60-80 °C) was used. Acetonitrile and *N*-methyl pyrrolidone was dried over activated molecular sieves (3Å). Dicholoromethane, 1,2-dichloroethane, Et_3N and *N,N′*-diisopropylethylamine were dried over activated molecular sieves (4Å). Anhydrous pyridine and DMF were obtained from commercial sources. Reactions were conducted under argon whenever anhydrous solvents were used. Reactions were monitored by TLC using silica gel plates coated with a fluorescence indicator (SiO_2-60, F-254). Plates were visualized under UV light and by dipping in 5% conc. H_2SO_4 in absolute ethanol (v/v) followed by heating. Silica gel column chromatography was performed with silica gel 60 (particle size 0.040–0.063 mm) using moderate pressure (pressure ball). Columns on DMTr-protected nucleosides were built in the listed starting eluent containing 0.5% v/v pyridine. Evaporation of solvents was carried out under reduced pressure at

temperatures below 45 °C. Following column chromatography, appropriate fractions were pooled, evaporated and dried at high vacuum for at least 12h to give the obtained products in high purity (>95%) as ascertained by 1D NMR techniques. Chemical shifts of ^{1}H NMR (500 MHz), ^{13}C NMR (125.6 MHz) and ^{31}P NMR (121.5 MHz) are reported relative to deuterated solvent or other internal standards (80% phosphoric acid for ^{31}P NMR). Exchangeable (ex) protons were detected by disappearance of ^{1}H NMR signals upon D_2O addition. Assignments of NMR spectra are based on 2D spectra (HSQC, COSY) and DEPT spectra. Quaternary carbons are not assigned in ^{13}C NMR but their presence was verified from HSQC and DEPT spectra (absence of signals). MALDI-HRMS spectra of compounds were recorded on a Q-TOF mass spectrometer using 2,5-dihydroxybenzoic acid as a matrix and a mixture of polyethylene glycol (PEG 600 or PEG 1000) as internal calibration standards.

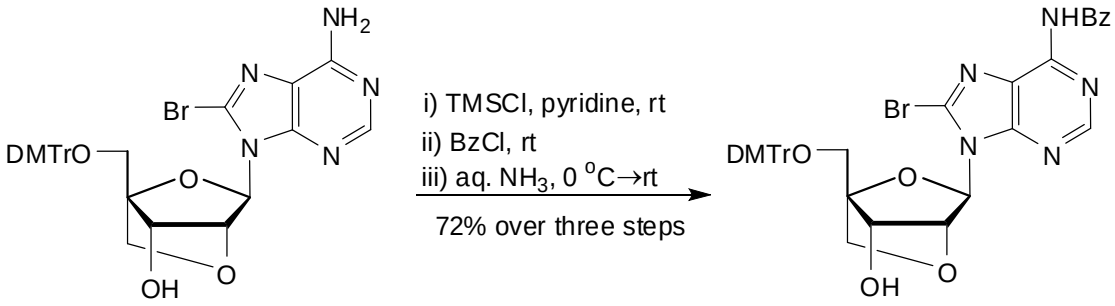

9 **S1**

Scheme 5. Synthesis of nucleoside **S1**.

(1R,3R,4R,7S)-1-(4,4′-Dimethoxytrityloxymethyl)-3-(6-N-benzoyl-8-bromo-adenin-9-yl)-7-hydroxy-2,5-dioxabicyclo[2.2.1]heptane (S1). Nucleoside **9** (0.25 g, 0.38 mmol) was dried through co-evaporation with pyridine (2×10 mL) and re-dissolved in anhydrous pyridine (5 mL). To this was added trimethylchlorosilane (0.14 mL, 1.14 mmol) and the reaction mixture was allowed to stir for 30 min at rt. At this point, BzCl (0.22 ml, 1.90 mmol) was added and the reaction mixture was stirred at rt for 5 h. The reaction mixture was then cooled to 0 °C and water (~1 mL) was added. After stirring for 15 min, aq. NH_3 (29%, 5.0 mL) was added and the suspension was stirred at rt for 30 min. The mixture was evaporated to near dryness and the resulting taken up in CH_2Cl_2 (25 ml) and washed with 5% aq. $NaHCO_3$ (2×10 mL). The organic layer was evaporated to dryness and the resulting residue was purified using silica gel column chromatography (0-5% MeOH in CH_2Cl_2, v/v) to obtain nucleoside **S1** (210 mg, 72%) as a pale brown solid material. R_f = 0.7 (5% MeOH in CH_2Cl_2, v/v); ESI-HRMS: *m/z* 786.1534 ($[M+Na]^+$, $C_{53}H_{44}N_6O_6{\cdot}Na^+$, calc. 786.1539); ^{1}H NMR (DMSO-d_6) δ 11.26 (s, 1H, ex, NH), 8.70 (s, 1H, H2), 8.02-8.05 (d, 2H, *J* = 7.0 Hz, Ar), 7.63-7.67 (t, 1H, *J* = 7.0 Hz, Ar), 7.53-7.58 (d, 2H, *J* = 7.0 Hz, Ar), 7.34-7.38 (m, 2H, Ar), 7.18-7.30 (m, 7H, Ar), 6.84-6.88 (m, 4H, Ar), 5.95 (s, 1H, H1′), 5.87 (d, 1H, ex, *J* = 5.0 Hz, 3′-OH), 5.16 (s, 1H, H2′), 4.62 (d, 1H, *J* = 5.0 Hz, H3′), 4.06-4.08 (d, 1H, *J* = 8.0 Hz, H5″), 4.02-4.05 (d, 1H, *J* = 8.0 Hz, H5″), 3.72 (br s, 6H, CH_3O), 3.38-3.42 (d, 1H, *J* = 11.0 Hz, H5′), 3.22-3.25 (d, 1H, *J* = 11.0 Hz, H5′); ^{13}C NMR (DMSO-d_6) δ 165.6, 158.0, 152.4, 151.5 (C2), 149.2, 144.7, 135.5, 135.3, 133.1, 132.5 (Ar), 132.1, 129.7 (Ar), 129.6 (Ar), 128.5 (Ar), 128.4 (Ar), 127.8 (Ar), 127.6 (Ar), 126.6 (Ar), 125.4, 113.2 (Ar), 87.3 (C1′), 86.9, 85.2, 78.9 (C2′), 72.7 (C3′), 72.1 (C5″), 60.3 (C5′), 55.0 (CH_3O).

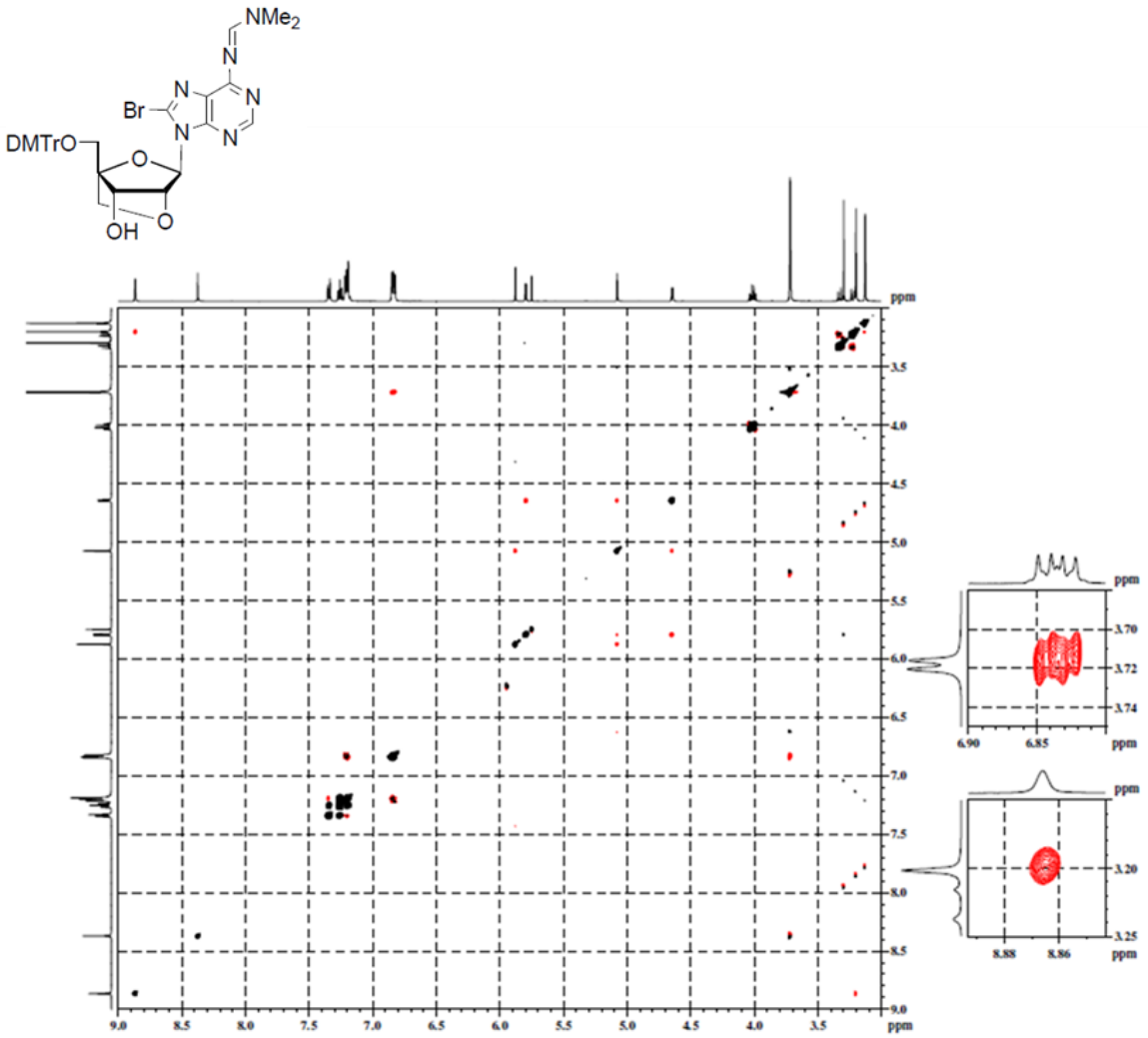

Figure 34. ROESY spectrum of **10**.

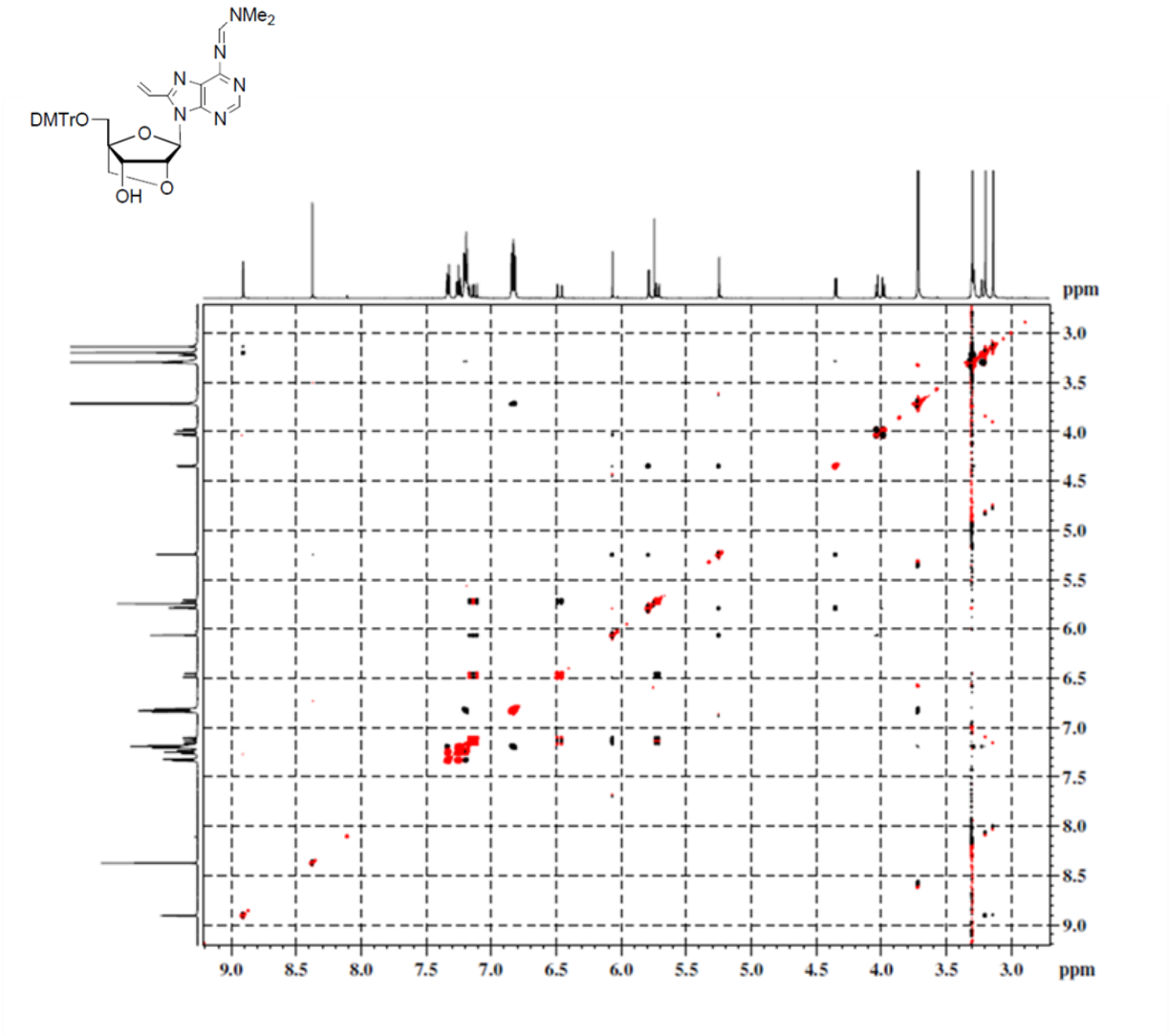

Figure 35. ROESY spectrum of **11**.

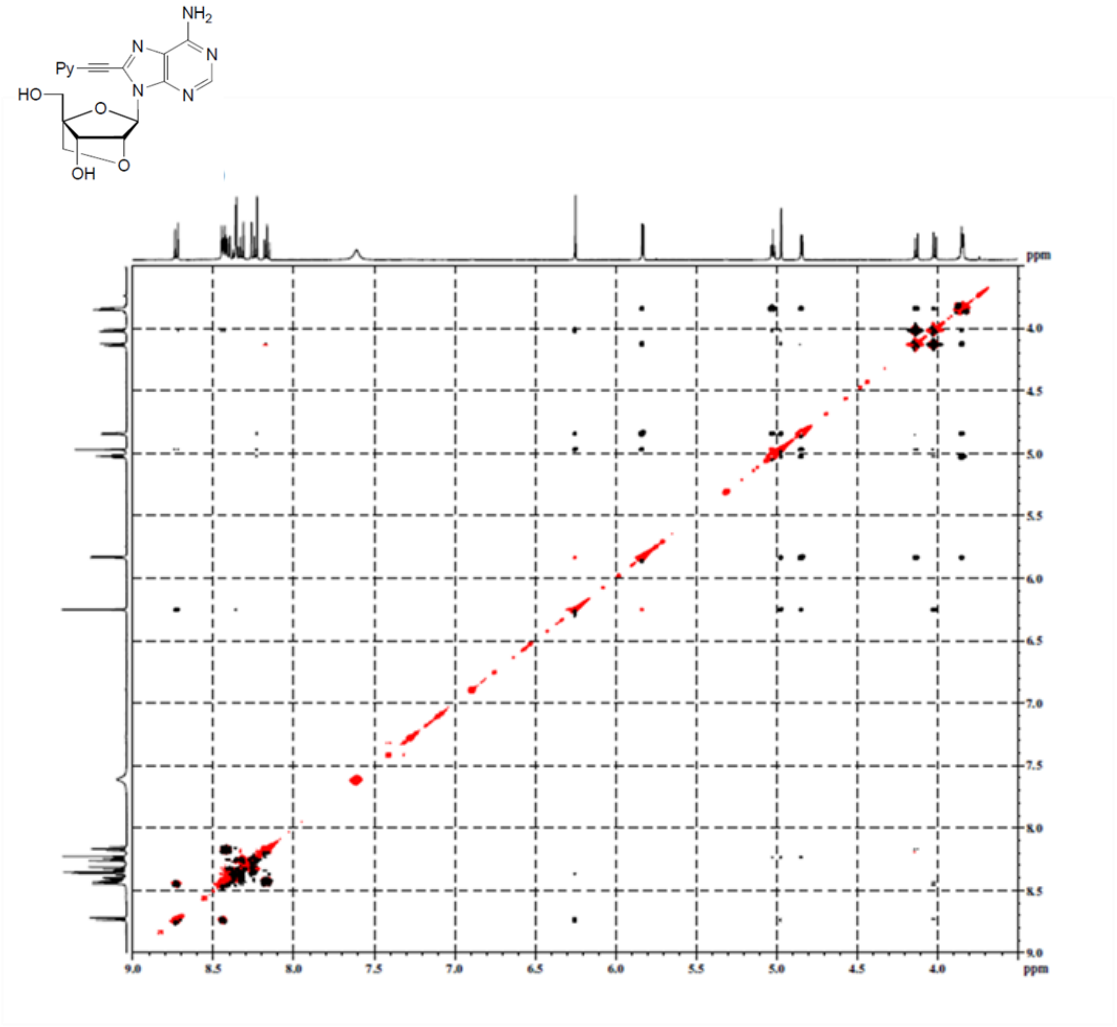

Figure 36. ROESY spectrum of **13**.

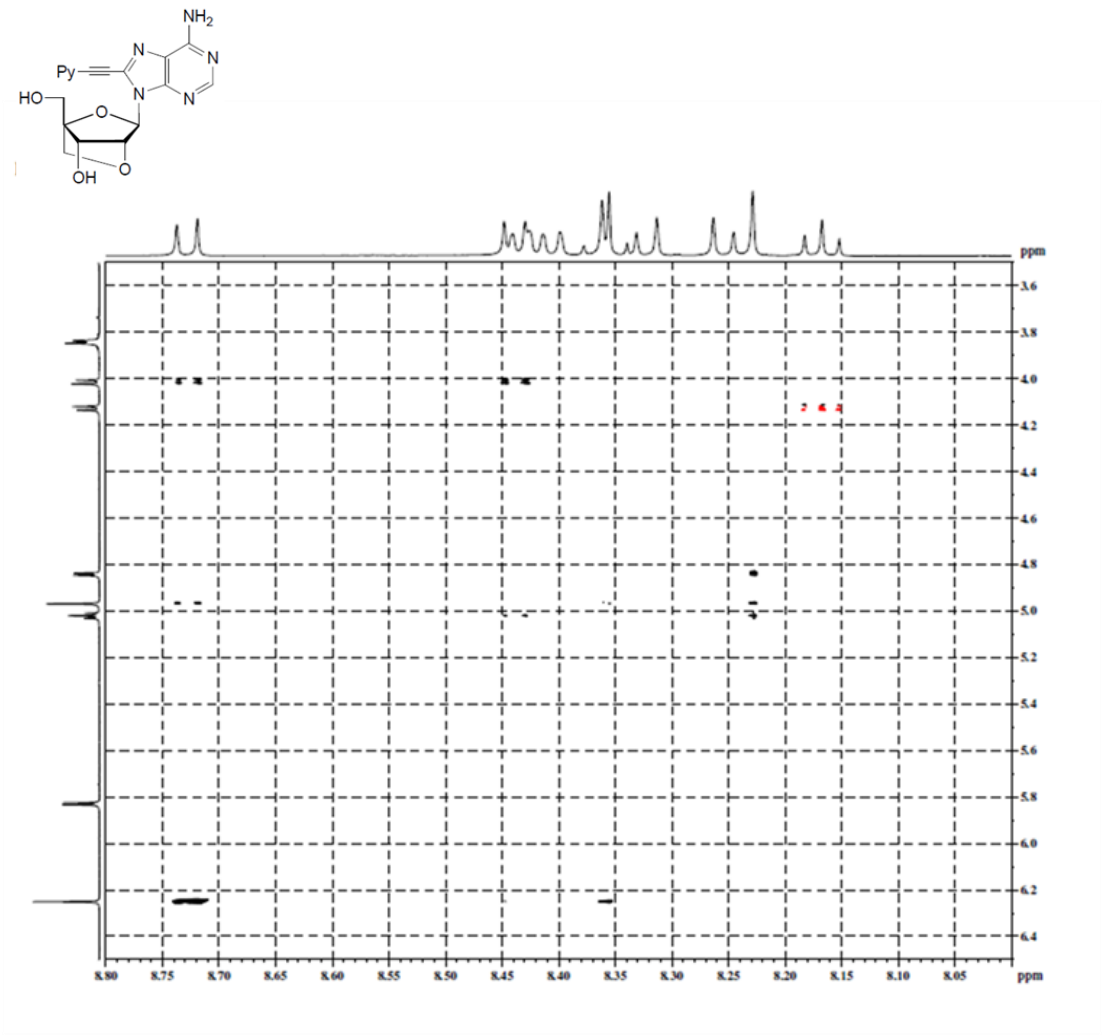

Figure 37. ROESY spectrum of **13** – expanded view.

Table 9. MALDI-ToF MS of **L**/**M**/**N**-modified ONs.[a]

ON	Sequence	Calc. $(M+H)^+$	Exp. $(M+H)^+$
L1	5′-G**L**A TCT CAC	2701	2701
L2	5′-GCA T**L**T CAC	2701	2701
L3	5′-GCA TCT **L**AC	2701	2701
L4	5′-G**L**A T**L**T **L**AC	2785	2785
M1	5′-G**M**A TCT CAC	2711	2710
M2	5′-GCA T**M**T CAC	2711	2711
M3	5′-GCA TCT **M**AC	2711	2711
M4	5′-G**M**A T**M**T **M**AC	2815	2815
N1	5′-G**N**A TCT CAC	2740	2740
N2	5′-GCA T**N**T CAC	2740	2739
N3	5′-GCA TCT **N**AC	2740	2739
N4	5′-G**N**A T**N**T **N**AC	2902	2902

[a] For structures of monomer **L**, **M** and **N** see Figure 30 in main manuscript.

Table 10. MALDI-ToF MS of **X**/**Y**/**Z**-modified ONs.[a]

ON	Sequence	Calc. $(M+H)^+$	Exp. $(M+H)^+$
X5	5′-GCGTT A**X**A TTGCG	4060	4063
X6	5′-GCGTT C**X**C TTGCG	4012	4016
X7	5′-GCGTT G**X**G TTGCG	4092	4095
X8	5′-GCGTT T**X**T TTGCG	4042	4045
Y5	5′-GCGTT A**Y**A TTGCG	4241	4241
Y6	5′-GCGTT C**Y**C TTGCG	4193	4193
Y7	5′-GCGTT G**Y**G TTGCG	4273	4274
Y8	5′-GCGTT T**Y**T TTGCG	4223	4224
Z5	5′-GCGTT A**Z**A TTGCG	4213	4212
Z6	5′-GCGTT C**Z**C TTGCG	4165	4164
Z7	5′-GCGTT G**Z**G TTGCG	4245	4244
Z8	5′-GCGTT T**Z**T TTGCG	4196	4194

[a] For structures of **X**, **Y** and **Z** monomer, see main manuscript, Figure 30.

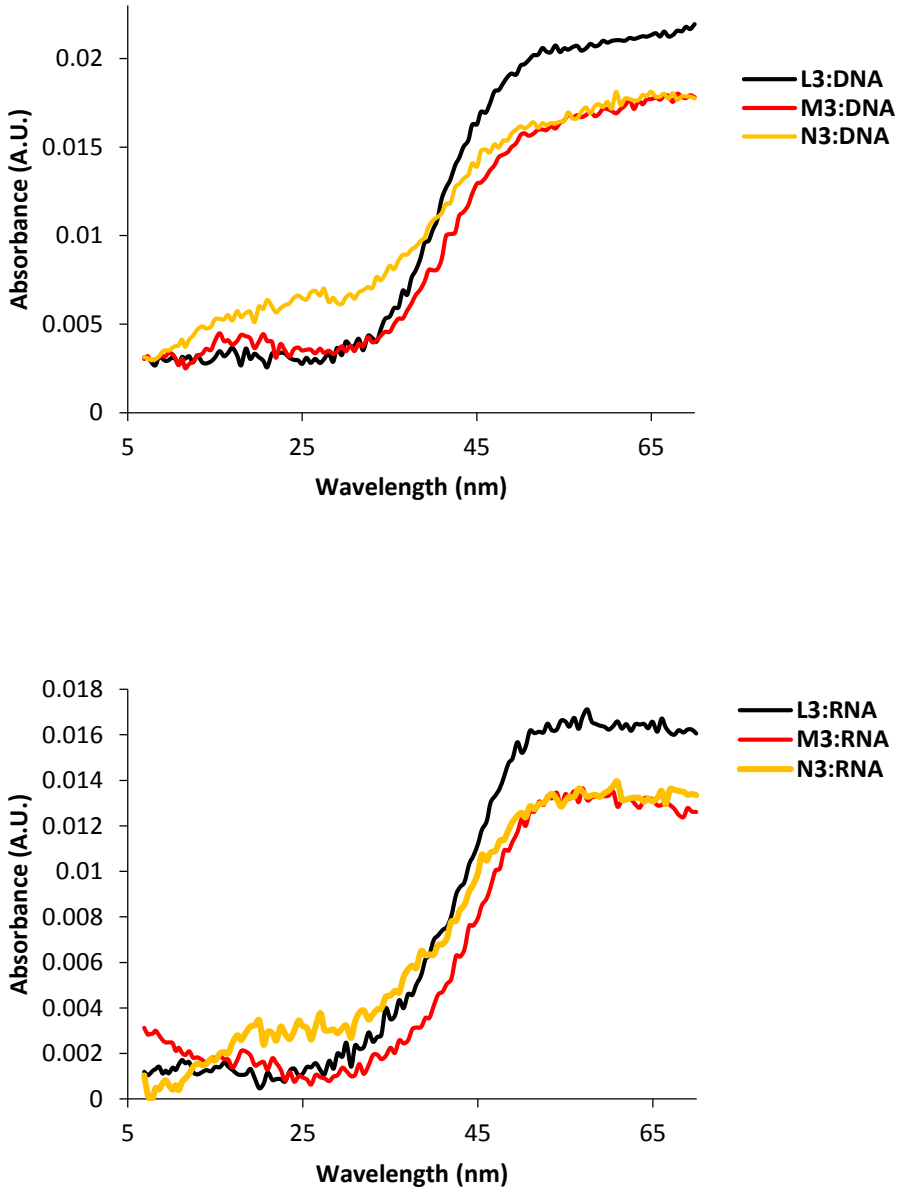

Figure 38. Representative thermal denaturation curves of duplexes between **L3**-**N3** and complementary DNA (upper panel) or RNA (lower panel).

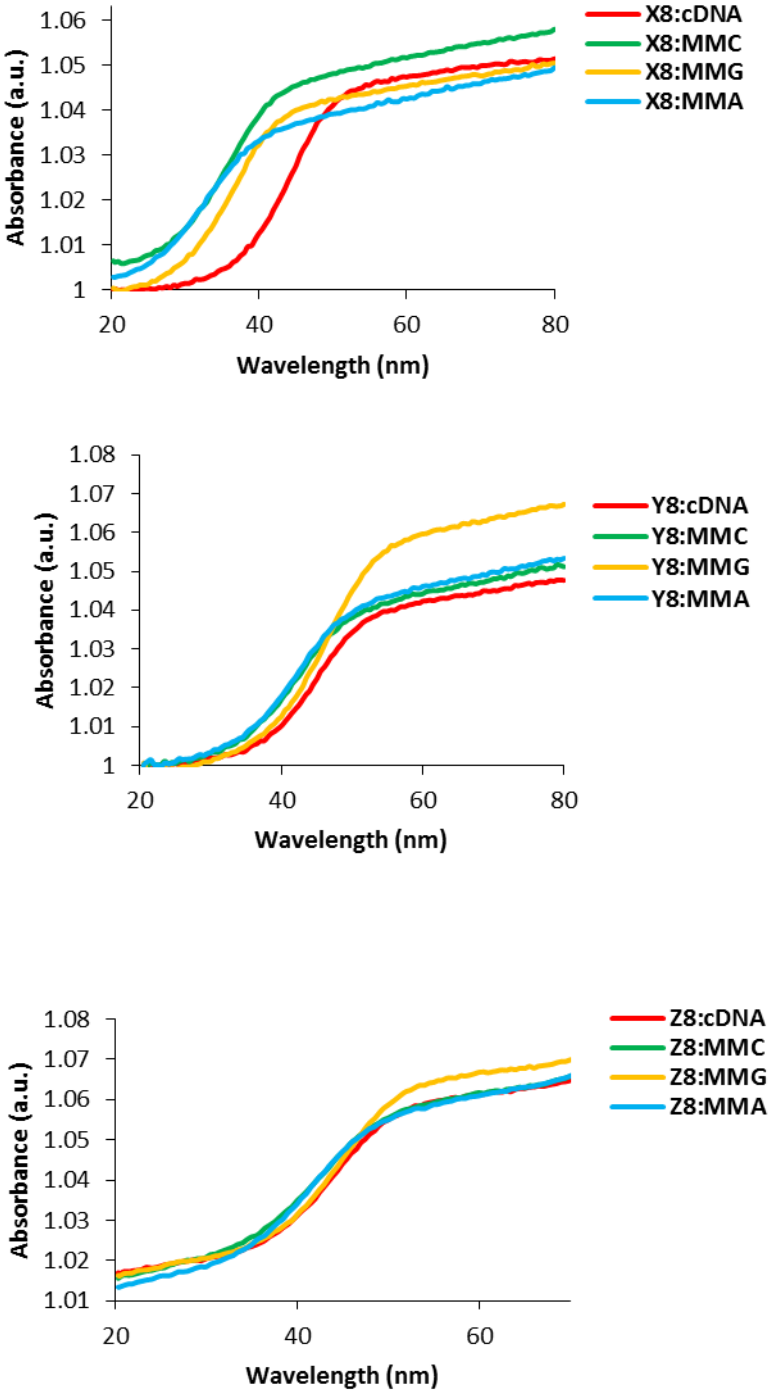

Figure 39. Representative thermal denaturation curves of duplexes between **X8**/**Y8**/**Z8** and complementary (cDNA) or mismatched DNA targets (MM – central mismatched nucleotide is specified).

Table 11. Pyrene absorption maxima in the ~420 nm region of **Y**/**Z**-modified ONs in absence or presence of matched/mismatched DNA targets[a]

		λ_{max}/nm	$\Delta\lambda_{max}$/nm			
ON	Sequence	SSP	+cDNA	+MM (C)	+MM (G)	+MM (T)
Y5	5′-GCGTT A**Y**A TTGCG	417	+1	+1	+1	+1
Y6	5′-GCGTT C**Y**C TTGCG	421	±0	-1	-1	-1
Y7	5′-GCGTT G**Y**G TTGCG	419	±0	±0	±0	±0
Y8	5′-GCGTT T**Y**T TTGCG	419	±0	-2	-1	-1
Z5	5′-GCGTT A**Z**A TTGCG	416	±0	±0	-1	-1
Z6	5′-GCGTT C**Z**C TTGCG	418	+2	+2	+2	+2
Z7	5′-GCGTT G**Z**G TTGCG	418	-1	+1	-1	-1
Z8	5′-GCGTT T**Z**T TTGCG	416	+3	+4	+4	+4

[a] Recorded in T_m buffer at T = 5 °C. $\Delta\lambda_{max}$ measured relative to "SSP", which denotes single-stranded probe. Central mismatched (MM) nucleotide is specified.

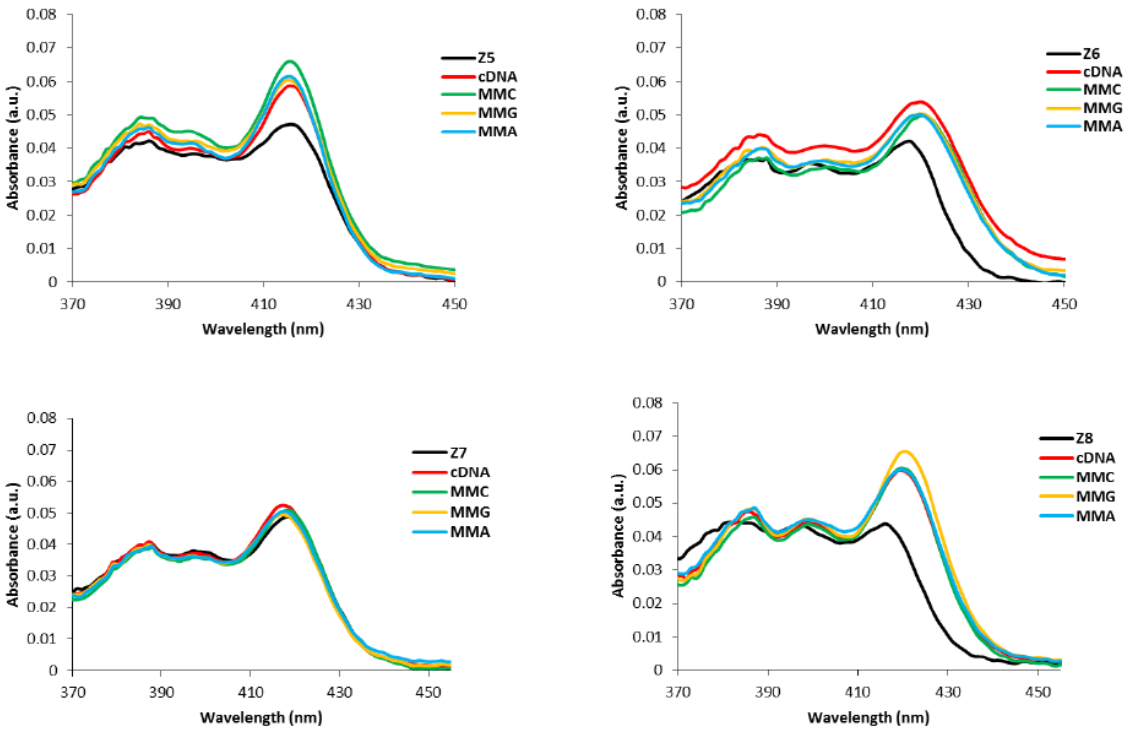

Figure 40. UV-Vis absorption spectra of single-stranded **Z5-Z8** and the corresponding duplexes with complementary (cDNA) or centrally mismatched DNA targets (MM – central

mismatched nucleotide is specified). Spectra were recorded in T_m buffer at T = 5 °C using each strand at 1.0 μM.

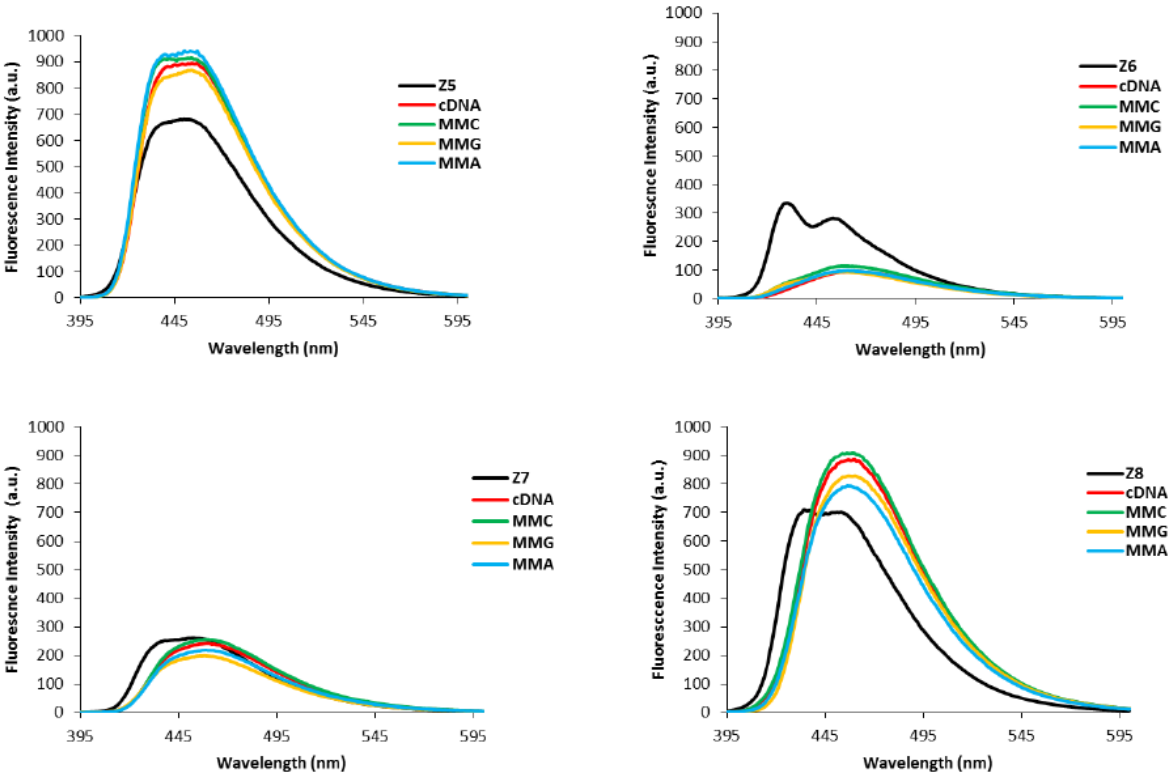

Figure 41. Steady-state fluorescence emission spectra of single-stranded **Z5**-**Z8** and the corresponding duplexes with complementary (cDNA) or centrally mismatched DNA targets (MM – central mismatched nucleotide is specified). Spectra were recorded in T_m buffer at T = 5 °C using each strand at 1.0 μM and λ_{ex} = 385 nm.

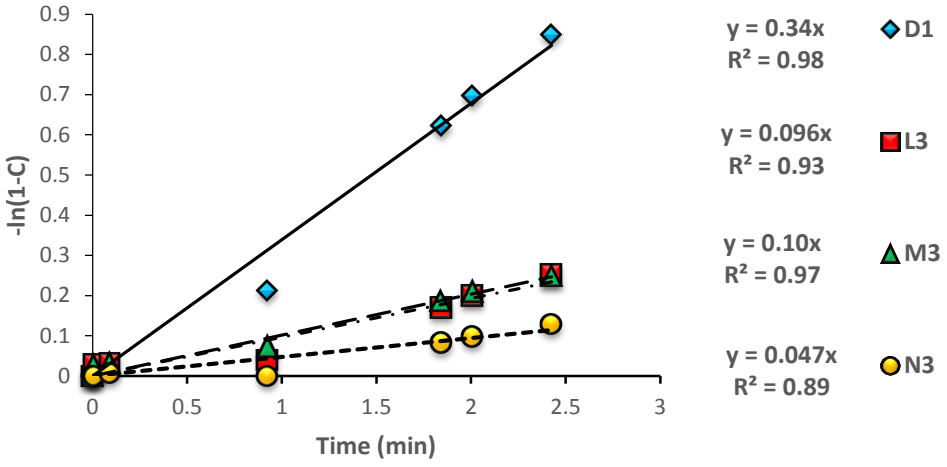

Figure 42. Plot of -ln (1-*C*) vs time (min) for SVPDE-mediated degradation of **B3** ONs. The linear fit shows that the reaction follows pseudo-first order kinetics during initial stages.

Table 12. Rate constants for enzymatic degradation of **B3** ONs.[a]

ON	5′-GCA TCT **B**AC	
	k_{obs} (min^{-1})	k_{rel}
D1	3.4×10^{-1}	1.0
L3	9.6×10^{-2}	0.28
M3	1.0×10^{-1}	0.29
N3	4.7×10^{-2}	0.14

[a] k_{rel}'s calculated relative to k_{obs} of **D1**.

4.6. References and Notes.

1. For recent reviews on conformationally restricted nucleotides, see e.g., a) Herdewijn, P. *Chem*. *Biodiv*. **2010**, *7*, 1-59. b) Obika, S.; Abdur Rahman, S. M.; Fujisaka, A.; Kawada, Y.; Baba T.; Imanishi, T. *Heterocycles* **2010**, *81*, 1347-1392. c) Prakash, T. P. *Chem*. *Biodiv*. **2011**, *8*, 1616-1641. d) Zhou, C.; Chattopadhyaya, J. *Chem*. *Rev*. **2012**, *112*, 3808-3832.

2. For recent examples, see: a) Upadhayaya, R.; Deshpande, S. A. Li, Q.; Kardile, R. A.; Sayyed, A. Y.; Kshirsagar, E. K.; Salunke, R. V.; Dixit, S. S.; Zhou, C.; Foldesi, A.; Chattopadhyaya, J. *J. Org*. *Chem*. **2011**, *76*, 4408-4431. b) Shrestha, A. R.; Hari, Y.; Yahara, A.; Osawa, T.; Obika, S. *J. Org*. *Chem*. **2011**, *76*, 9891-9899. c) Hanessian, S.; Schroeder, B. R.; Giacometti, R. D.; Merner, B. L.; Østergaard, M. E.; Swayze, E. E.; Seth, P. P. *Angew*. *Chem*., *Int*. *Ed*. **2012**, *51*, 11242-11245. d) Madsen, A. S.; Wengel, J. *J. Org*. *Chem*. **2012**, *77*, 3878-3886; e) Haziri, A. I.; Leumann, C. J. *J. Org*. *Chem*. **2012**, *77*, 5861-5869. f) Gerber, A-B.; Leumann, C. J. *Chem*. *Eur*. *J*. **2013**, *19*, 6990-7006. g) Morihiro, K.; Kodama, T.; Kentefu; Moai, Y.; Veedu, R. N.; Obika, S. *Angew*. *Chem*. *Int. Ed*. **2013**, *52*, 5074-5078. h) Hari, Y.; Osawa, T.; Kotobuki, Y.; Yahara, A.; Shrestha, A. R.; Obika, S. *Bioorg*. *Med*. *Chem*. **2013**, *21*, 4405-4412. i) Hari, Y.; Morikawa, T.; Osawa, T.; Obika, S. *Org*. *Lett*, **2013**, *15*, 3702-3705. j) Migawa, M. T.; Prakash, T. P.; Vasquez, G.; Seth, P. P.; Swayze, E. E. *Org*. *Lett*. **2013**, *15*, 4316-4319. k) Hanessian, S.; Schroeder, B. R.; Merner, B. L.; Chen. B.; Swayze, E. E.; Seth, P. P. *J. Org*. *Chem*. **2013**, *78*, 9051-9063. l) Hanessian, S.; Wagger, J.; Merner, B. L.; Giacometti, R. D.; Østergaard, M. E.; Swayze, E. E.; Seth, P. P. *J. Org*. *Chem*. **2013**, *78*, 9064-9075.

3. a) Duca, M.; Vekhoff, P.; Oussedik, K.; Halby, L.; Arimondo, P. B. *Nucleic Acids Res*. **2008**, *36*, 5123-5138. b) Bennett, C. F.; Swayze, E. E. *Annu*. *Rev*. *Pharmacol*. *Toxicol*. **2010**, *50*, 259-

293. c) Østergaard, M. E.; Hrdlicka, P. J. *Chem. Soc. Rev.*, **2011**, *40*, 5771-5788. d) Watts, J. K.; Corey, D. R. *J. Pathol*. **2012**, *226*, 365-379. e) Matsui, M.; Corey, D. R. *Drug Disc. Today* **2012**, *17*, 443-450. f) Dong, H.; Lei, J.; Ding, L.; Wen, Y.; Ju, H.; Zhang, X. *Chem. Rev*. **2013**, *113*, 6207-6233.

4. Kaur, H.; Babu, B. R.; Maiti, S. *Chem. Rev*. **2007**, *107*, 4672-4697.

5 Singh, S. K.; Nielsen, P.; Koshkin, A. A.; Wengel, J. *Chem. Commun*. **1998**, 455-456.

6 Obika, S.; Nanbu, D.; Hari, Y.; Andoh, J.-I.; Morio, K.-I.; Doi, T.; Imanishi, T. *Tetrahedron Lett*. **1998**, *39*, 5401-5404.

7 a) Wahlestedt, C.; Salmi, P.; Good, L.; Kela, J.; Johnsson, T.; Hokfelt, T.; Broberger, C.; Porreca, F.; Lai, J.; Ren, K. K.; Ossipov, M.; Koshkin, A.; Jacobsen, N.; Skouv, J.; Oerum, H.; Jacobsen, M. H.; Wengel, J. *Proc. Natl. Acad. Sci. U. S. A.* **2000**, *97*, 5633-5638. b) Graziewicz, M. A.; Tarrant, T. K.; Buckley, B.; Roberts, J.; Fulton, L.; Hansen, H.; Ørum, H.; Kole, R.; Sazani, P. *Mol. Ther.* **2008**, *16*, 1316-1322. c) Straarup, E. M.; Fisker, N.; Hedtjarn, M.; Lindholm, M. W.; Rosenbohm, C.; Aarup, V.; Hansen, H. F.; Ørum, H.; Hansen J. B.; Koch, T. *Nucleic Acids Res.* **2010**, *38*, 7100-7111. d) Lanford, R. E.; Hildebrandt-Eriksen, E. S.; Petri, A.; Persson, R.; Lindow, M.; Munk, M. E.; Kauppinen S.; Ørum, H. *Science*, **2010**, *327*, 198-201; e) Obad, S.; Dos Santos, C. O.; Petri, A.; Heidenblad, M.; Broom, O.; Ruse, C.; Fu, C.; Lindow, M.; Stenvang, J.; Straarup, E. M.; Hansen, H. F.; Koch, T.; Pappin, D.; Hannon G. J.; Kauppinen, S. *Nat. Genet.*, **2011**, *43*, 371-378.

8. For particularly important earlier examples see: a) Sørensen, M. D.; Kværnø, L.; Bryld, T.; Håkansson, A. E.; Verbeure, B.; Gaubert, G.; Herdewijn, P.; Wengel, J. *J. Am. Chem. Soc.* **2002**, *124*, 2164-2176. b) Sørensen, M. D.; Petersen, M.; Wengel, J. *Chem. Commun.* **2003**, 2130-2131. c) Morita, K.; Takagi, M.; Hasegawa, C.; Kaneko, M.; Tsutsumi, S.; Sone, J.;

Ishikawa, T.; Imanishi, T.; Koizumi, M. *Bioorg. Med. Chem.* **2003**, *11*, 2211-2226. d) Fluiter, K.; Frieden, M.; Vreijling, J.; Rosenbohm, C.; De Wissel, M. B.; Christensen, S. M.; Koch, T.; Ørum, H.; Baas, F. *ChemBioChem* **2005**, *6*, 1104-1109. e) Albæk, N.; Petersen, M.; Nielsen, P. *J. Org. Chem.* **2006**, *71*, 7731-7740. f) Varghese, O. P.; Barman, J.; Pathmasiri, W.; Plashkevych, O.; Honcharenko, D.; Chattopadhyaya, J. *J. Am. Chem. Soc.* **2006**, *128*, 15173-15187. g) Abdur Rahman, S. M.; Seki, S.; Obika, S.; Yoshikawa, H.; Miyashita, K.; Imanishi, T. *J. Am. Chem. Soc.* **2008**, *130*, 4886-4896. h) Mitsuoka, Y.; Kodama, T.; Ohnishi, R.; Hari, Y.; Imanishi, T.; Obika, S. *Nucleic Acids Res.* **2009**, *37*, 1225-1238. i) Zhou, C.; Liu, Y.; Andaloussi, M.; Badgujar, N.; Plashkevych, O.; Chattopadyaya, J. *J. Org. Chem.* **2009**, *74*, 118-134. j) Seth, P. P.; Siwkowski, A.; Allerson, C. R.; Vasquez, G.; Lee, S.; Prakash, T. P.; Wancewicz, E. V.; Witchell, D.; Swayze, E. E. *J. Med. Chem.* **2009**, *52*, 10-13. k) Seth, P. P.; Vasquez, G.; Allerson, C. A.; Berdeja, A.; Gaus, H.; Kinberger, G. A.; Prakash, T. P.; Migawa, M. T.; Bhat, B.; Swayze, E. E. *J. Org. Chem.* **2010**, *75*, 1569-1581. l) Li, Q.; Yuan, F.; Zhou, C.; Plashkevych, O.; Chattopadhyaya, J. *J. Org. Chem.* **2010**, *75*, 6122-6140. m) Liu, Y.; Xu, J.; Karimiahmadabadi, M.; Zhou, C.; Chattopadhyaya, J. *J. Org. Chem.* **2010**, *75*, 7112-7128.

9. Østergaard, M. E.; Kumar, P.; Baral, B.; Raible, D. J.; Kumar, T. S.; Anderson, B. A.; Guenther, D. C.; Deobald, L.; Paszczynski, A. J.; Sharma, P. K.; Hrdlicka, P. J. *ChemBioChem* **2009**, *10*, 2740-2743.

10. Kumar, P.; Østergaard, M. E.; Baral, B.; Anderson, B. A.; Guenther, D. C.; Kaura, M.; Raible, D. J.; Sharma, P. K.; Hrdlicka, P. J. J. *Org. Chem.* **2014**, *79*, 5047-5061.

11. Østergaard, M. E.; Kumar, P.; Baral, B.; Guenther, D. C.; Anderson, B. A.; Ytreberg, F. M.; Deobald, L.; Paszczynski, A. J.; Sharma P. K.; Hrdlicka, P. J.; *Chem. Eur. J.* **2011**, *17*, 3157-3165.

12. Kumar, P.; Baral, B.; Anderson, B. A.; Guenther, D. C.; Østergaard, M. E.; Sharma, P. K.; Hrdlicka, P. J. *J. Org. Chem*. **2014**, *79*, 5062−5073.

13. For reviews, see: a) Luyten, I.; Herdewijn, P. *Eur*. *J*. *Med*. *Chem*. **1998**, *33*, 515-576. b) M. Ahmadian, D. E. Bergstrom in *Modified Nucleotides in Biochemistry, Biotechnology and Medicine*, 1st ed (Ed: P. Herdewijn), Wiley-VCH, Weinheim, 2008, 251-276.

14. For particularly interesting examples from the original research literature, see: a) Wagner, R. W.; Matteucci, M. D.; Lewis, J. G.; Gutierrez, A. J.; Moulds, C.; Froehler B. C. *Science*, **1993**, *260*, 1510-1513. b) Hashimoto, H.; Nelson M. G.; Switzer, C. *J. Am. Chem. Soc.* **1993**, *115*, 7128-7134. c) Sagi, J.; Szemzo, A.; Ebinger, K.; Szabolcs, A.; Sagi, G.; Ruff, E.; Otvos, L. *Tetrahedron Lett.* **1993**, *34*, 2191-2194. d) Ahmadian, M.; Zhang, P. M.; Bergstrom, D. E. *Nucleic* Acids *Res*. **1998**, *26*, 3127-3135. e) Heystek, L. E.; Zhou, H. Q.; Dande P.; Gold, B. *J*. *Am*. *Chem*. *Soc*. **1998**, *120*, 12165-12166. f) Kottysch, T.; Ahlborn, C.; Brotzel, F.; Richert, C. *Chem*. *Eur*. *J*. **2004**, *10*, 4017-4028. g) Okamoto, A.; Kanatani, K.; Saito, I. *J. Am. Chem. Soc.* **2004**, *126*, 4820-4827. h) Booth, J.; Brown, T.; Vadhia, S. J.; Lack, O.; Cummins, W. J.; Trent, J. O.; Lane, A. N. *Biochemistry*, **2005**, *44*, 4710-4719. i) Skorobogatyi, M. V.; Malakhov, A. D.; Pchelintseva, A. A.; Turban, A. A.; Bondarev, S. L.; Korshun V. A. *ChemBioChem* **2006**, *7*, 810-816. j) Østergaard, M. E.; Guenther, D. C.; Kumar, P.; Baral, B.; Deobald, L.; Paszczynski, A. J.; Sharma P. K.; Hrdlicka, P. J. *Chem*. *Commun*. **2010**, 4929-4931.

15 a) Tavale, S. S.; Sobell, H. M. *J. Mol. Biol.*, **1970**, *48*, 109-123. b) Saenger, W. *Principles of Nucleic Acid Structure*; Springer-Verlag: Berlin, **1984**. pp. 51-104. c) Rao, S. N.; Kollman, P. A. *J*. *Am*. *Chem*. *Soc*. **1986**, *108*, 3048-3053. d) Eason, R. G.; Burkhardt, D. M.; Phillips, S. J.; Smith, D. P.; David, S. S. *Nucleic Acids Res.* **1996**, *24*, 890-897. e) Kuska, M. S.; Witham,

A. A.; Sproviero, M.; Manderville, R. A.; Yazdi, M. M.; Sharma, P.; Wetmore, S. D. *Chem. Res. Toxicol*. **2013**, *26*, 1397-1408.

16. a) Mayer, E.; Valis, L.; Wagner, C.; Rist, M.; Amann, N.; Wagenknecht, H.-A. *ChemBioChem* **2004**, *5*, 865-868. b) Seo, Y. J.; Ryu, J. H.; Kim, B. H. *Org. Lett*. **2005**, *7*, 4931-4933. c) Saito, Y.; Hanawa, K.; Motegi, K.; Omoto, K.; Okamoto, A.; Saito, I. *Tetrahedron Lett*. **2005**, *46*, 7605-7608. d) Seo, Y. J.; Hwang, G. T.; Kim, B. H. *Tetrahedron Lett*. **2006**, *47*, 4037-4039. e) Seo, Y. J.; Lee, I. J.; Yi, J. W.; Kim, B. H. *Chem. Commun*. **2007**, 2817-2819. f) Matsumoto, K.; Takahashi, N.; Suzuki, A.; Morii, T.; Saito, Y.; Saito, I. *Bioorg. Med. Chem. Lett*. **2011**, *21*, 1275-1278. g) Dierckx, A.; Diner, P.; El-Sagheer, A. H.; Kumar, J. D.; Brown, T.; Grøtli, M.; Wilhelmsson, L. M. Nucleic Acids Res. 2011. 39, 4513-4524. h) Suzuki, A.; Takahashi, N.; Okada, Y.; Saito, I.; Nemoto, N.; Saito, Y. *Bioorg. Med. Chem. Lett*. **2012**, *22*, 886-892.

17. Bartoszewicz, A.; Kalek, M.; Nilsson, J.; Hiresova, R.; Stawinski, J. *Synlett* **2008**, 37-40.

18. Xu, Y.-Z.; Zheng, Q.; Swann, P. F. *J. Org. Chem*. **1992**, *57*, 3839-3845.

19. Agrofoglio, L. A.; Gillaizeau, I.; Saito, Y. *Chem. Rev*. **2003**, *103*, 1875-1916.

20. a) Pfundheller, H. M.; Lomholt, *Curr. Protocols Nucleic Acid Chem*. **2002**, 4.12.1-4.12.16. b) Koshkin, A. A.; Fensholdt, J.; Pfundheller, H. M.; Lomholt, C. *J. Org. Chem*. **2001**, *66*, 8504-8512.

21. Clima, L.; Bannwarth, W. *Helv. Chim. Acta* **2008**, *91*, 165-175.

22. McBride, L. J.; Kierzek, R.; Beaucage, S. L.; Caruthers, M. H. *J. Am. Chem. Soc*. **1986**, *108*, 2040-2048.

23. Ti, G. S.; Gaffney, B. L.; Jones, R. A. *J. Am. Chem. Soc*. **1982**, *104*, 1316-1319.

24. Gaied, N. B.; Glasser, N.; Ramalanjaona, N.; Beltz, H.; Wolff, P.; Marquet, R.; Burger, A.; Mely, Y. *Nucleic Acids Res*. **2005**, *33*, 1031-1039.

25. Brown, T.; Hunter, W. N. *Biopolymers*, **1997**, *44*, 91-103.

26. a) Korshun, V. A.; Stetsenko, D. A.; Gait, M. J. *J. Chem. Soc., Perkin Trans. 1* **2002**, 1092-1104. b) Dohno, C.; Saito, I. *ChemBioChem* **2005**, *6*, 1075-1081. c) Kumar, T. S.; Madsen, A. S.; Østergaard, M. E.; Sau, S. P.; Wengel, J.; Hrdlicka, P. J., *J. Org. Chem.* **2009**, *74*, 1070-1081.

27. Asanuma, H.; Fujii, T.; Kato, T.; Kashida, H. *J. Photochem. Photobiol. C*. **2012**, *13*, 124-135.

28. Manoharan, M.; Tivel, K. L.; Zhao, M.; Nafisi, K.; Netzel, T. L. *J. Phys. Chem*. **1995**, *99*, 17461-17472.

29. Trybulski, E. J.; Zhang, J.; Kramss, R. H.; Mangano, R. M. *J. Med. Chem.* **1993**, *36*, 3533-3541.

30. ^{1}H NMR signals of H6 and the benzoyl group are very broad and/or split up due to slow interconversion (relative to NMR timescale) between the two rotameric benzamide forms.

31. The assignments of ^{13}C NMR signals 87.8 and 87.5 ppm are interchangeable.

32 Wenting, W.; Wanhua, W.; Shaomin, J.; Hunin, G.; Jiazhang, Z. *Eur. J. Inorg. Chem.* **2010**, 4470-4482.

33. The synthesis of this phosphoramidites will be presented elsewhere.

Chapter 5: Locked Nucleic Acid (LNA) Induced Conformational Tuning of ONs modified with C5-functionalized DNA monomers: Highly SNP discriminating probes.

The following paper by **Kaura**, **M** and Hrdlicka, P. J has been prepared for consideration in an international peer-reviewed journal.

Abstract. Single nucleotide polymorphisms (SNPs) are important markers for genetic diseases. Oligodeoxyribonucleotides (ONs) modified with 5-[3-(1-pyrenecarboxamido)propynyl]-2'-deoxyuridine monomer **X** have been utilized for SNP detection, based on different fluorescent levels upon hybridization with matched and mismatched DNA strands. LNA monomers carrying the pyrene-1-carboxamide fluorophore at the C5-position (monomer **Z)**, have been shown to produce large increases in fluorescence intensity and large quantum yields (Φ_F = 0.44-0.8) upon hybridization with cDNA. Here, we have developed LNA/DNA mixmer probes containing the 3-(1-pyrenecarboxamido)propynyl fluorophore attached to the C5-position of 2'-deoxyuridine (monomer **X**). We demonstrate that the presence of canonical LNAs near monomer **X** tunes the duplex toward a greater A-type character, i.e., more RNA like conformation. These probes display improved flurescence emission properties relative to **X** and **Z**-modified probes. These probes are easy to synthesize and hold promising SNP discriminating properties.

5.1. Introduction. Detection of single nucleotide polymorphisms is an important tool for the study of genetic mutations that relate to disease susceptibility and variations in drug response.[1] These mutations occur mainly at the level of single nucleotide. It is therefore of interest to develop efficient methods for SNP detection. Use of enzymatic methods[2a] and primer extension assays[2b] have been employed in the past for SNP typing. However, the complexity of these

methods has motivated researchers to develop simple, yet effective techniques for studying genetic disorders.[3] Fluorescence assays[4] based on molecular beacons,[5b,5c] base discriminating fluorescent probes (BDF),[5a] binary[5d] or intercalator-modified probes[5e] are a few examples of such approaches. These probes result in differential fluorescence emission depending on whether matched or mismatched duplex are formed. In particular, these probes are useful if they result in significantly increased fluorescence emission upon hybridization with a complementary target, but maintain low fluorescence intensity upon binding with mismatched targets. Pyrene-modified ONs have been extensively used as model systems due to the high quantum yield and position-dependent emission characteristics of pyrene.[6] These charactersitic features are due to different polarities of the grooves[6-7] and duplex interior which has led to the development of pyrene based BDF probes.[8]

It is well known from the literature that ONs, which are modified with 5-[3-(1-pyrenecarboxamido)propynyl]-2'-deoxyuridine monomers, result in increased fluorescence intensity upon hybridization with complementary DNA.[9] However, the corresponding LNA based monomer results in even greater increases in fluorescence intensity and larger quantum yields (0.44-0.80) upon duplex formation. Based on force-field calculations, we proposed that the bicyclic skeleton of LNA influences the conformational freedom about the glycosidic torsion angle, hence resulting in higher positional control of the fluorophore and its properties.[10] However, the involved synthesis of C5-functionalized LNA monomers[11] is a limiting factor to the use of these SNP probes for real applications such as detection of mutations in cancer cell lines.

In the present article, we set out to exploit LNA's well-known ability to influence the furanose conformation of flanking nucleotides toward greater North type conformations.[12] The goal of

the study was to tune the conformation and photophysical properties of ONs modified with 5-[3-(1-pyrenecarboxamido)propynyl]-2'-deoxyuridine monomer **X**, to obtain probes which emulate the properties of **Z**-modified probes.

Thus, canonical LNA monomers were incorporated near monomer **X** and the hybridization and fluorescence properties of the ONs studied. We demonstrate that such probes have interesting SNP-discriminating potential.

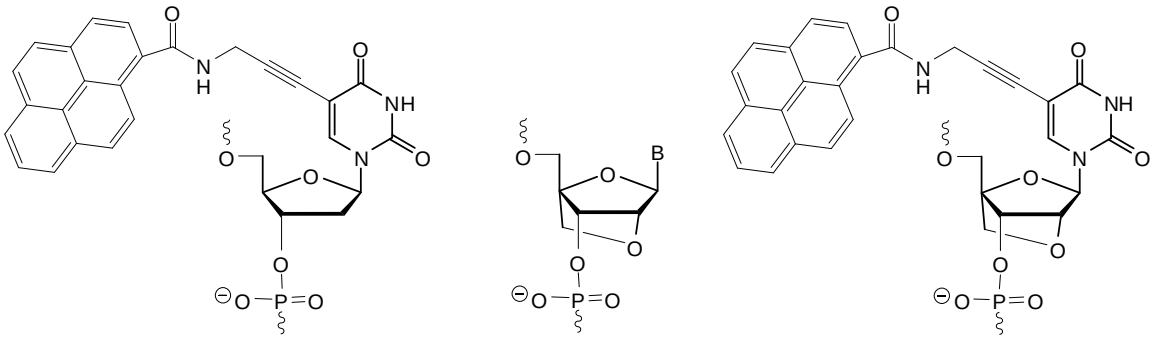

Figure 43. Chemical Structures of C5-Pyrene carboxamide functionalized DNA U, canonical LNA and C5-Pyrene carboxamide functionalized LNA U.

5.2. Results and discussion.

Experimental design. We designed 13-mer ONs in which a central **X** monomer is surrounded by canonical LNA nucleotides as direct (ON5-ON8, b**X**b, LNA in lower case letters) or next-nearest neighbors (ON9-ON12, bB**X**Bb, DNA in upper case letters) (Table 13). Unmodified reference strands (ON1-ON4, BTB) as well as benchmark probes from our previous studies[10a] featuring a central incorporation of either monomer **X** (ON13-ON16, BXB) or 5-[3-(1-pyrenecarboxamido)propynyl]-LNA-U, monomer **Z** (ON17-ON20, B**Z**B) were also included in the study. The nucleotides flanking the central pyrene-functionalized nucleotide were varied systematically as the four canonical nucleobases are known to quench pyrene fluorescence to

variable degrees.[13] For experimental details on machine-assisted solid phase synthesis of ON5-ON12, please refer to the experimental section.

Thermal denaturation studies. Thermal denaturation temperatures (T_m's) of duplexes between ON1-ON20 and complementary or centrally mismatched DNA targets were determined in a medium salt phosphate buffer ([Na^+] = 110 mM; pH 7.0). All denaturation curves displayed the expected monophasic sigmoidal transitions (Figures 46 and 47).

As previously reported, incorporation of a single **X** or **Z** monomer into ONs results in decreases in the thermostabilities of the resulting DNA duplexes (ΔT_m for ON13-ON20 between -6.0 and -1.5 °C, Table 13).[10a] Incorporation of two LNA nucleotides on either side of monomer **X** offsets the destabilization by 2.5-7.0 °C (ΔT_m for ON5-ON8 between -1.0 and +5.0 °C, Table 13). This stabilizing effect is even more pronounced in ONs with two LNA nucleotides positioned as next-nearest neighbors (ΔT_m for ON9-ON12 between +0.5 and +6.5 °C, Table 13). Hence, it appears that LNA's affinity-increasing properties[15] compensate for the destabilizing effects of the bulky pyrene moiety in the major groove.

Next, we examined the binding specificities of the modified ONs against DNA targets with centrally mismatched nucleotides. Our previous studies have shown that singly **X**- or **Z**-modified ONs display reduced binding specificity relative to the corresponding unmodified ONs, which is indicative of pyrene intercalation (compare mismatch ΔT_m for ON13-ON20 vs ON1-ON4, Table 13).[10a] Interestingly, incorporation of two LNA nucleotides as immediate or next-nearest neighbors of monomer **X** generally results in improved mismatch discrimination (compare mismatch ΔT_m for ON5-ON12 vs ON13-ON16, Table 13). Presumably, this is a consequence of LNA's long-ranging beneficial effect on binding specificity[15,16] and/or ability to tune the conformation of monomer **X** toward a more LNA-like North type conformation.[14]

Nonetheless, the hybrid probes generally display less efficient mismatch discrimination than unmodified ONs (compare mismatch ΔT_m for ON5-ON12 vs ON1-ON4, Table 13).

Table 13. T_m's of duplexes between **ON1**-**ON20** and complementary or centrally mismatched DNA targets.[a]

ON	Sequence	B =	T_m (ΔT_m) / A	mismatch ΔT_m / °C C	G	T
ON1	5′-CGCA AATAA ACGC		48.5	-10.0	-5.0	-9.0
ON2	5′-CGCA ACTCA ACGC		55.5	-13.5	-7.0	-9.0
ON3	5′-CGCA AGTGA ACGC		55.0	-13.0	-9.5	-10.0
ON4	5′-CGCA ATTTA ACGC		48.5	-11.0	-9.0	-11.0
ON5	5′-CGCA Aa**X**aA ACGC		47.5 (-1.0)	-6.5	-1.5	-3.5
ON6	5′-CGCA Ac**X**cA ACGC		60.5 (+5.0)	-14.0	-8.0	-9.5
ON7	5′-CGCA Ag**X**gA ACGC		56.0 (+1.0)	-8.0	-12.0	-9.0
ON8	5′-CGCA At**X**tA ACGC		47.5 (-1.0)	-7.5	-6.5	-4.5
ON9	5′-CGCA aA**X**Aa ACGC		50.0 (+1.5)	-5.0	-3.0	-2.0
ON10	5′-CGCA aC**X**Ca ACGC		62.0 (+6.5)	-13.0	-9.0	-9.0
ON11	5′-CGCA aG**X**Ga ACGC		60.0 (+5.0)	-9.0	-11.5	-8.5
ON12	5′-CGCA aT**X**Ta ACGC		49.0 (+0.5)	-5.0	-4.0	-4.0
ON13	5′-CGCA AA**X**AA ACGC		45.0 (-3.5)	-4.5	-2.0	-3.0
ON14	5′-CGCA AC**X**CA ACGC		54.0 (-1.5)	-8.0	-4.0	-5.5
ON15	5′-CGCA AG**X**GA ACGC		49.0 (-6.0)	-3.5	-7.0	-4.5
ON16	5′-CGCA AT**X**TA ACGC		44.0 (-4.5)	-5.0	-4.0	-3.5
ON17	5′-CGCA AA**Z**AA ACGC		45.5 (-3.0)	-5.5	-3.5	-4.5
ON18	5′-CGCA AC**Z**CA ACGC		53.5 (-2.0)	-9.0	-4.5	-7.0
ON19	5′-CGCA AG**Z**GA ACGC		51.5 (-3.5)	-3.5	-11.5	-6.5
ON20	5′-CGCA AT**Z**TA ACGC		44.0 (-4.5)	-7.5	-6.5	-6.0

[a] T_m's measured as maximum of first derivative plot of denaturation curves (A_{260} vs. T) recorded in medium salt phosphate buffer ([Na^+]= 110 mM, [Cl^-] = 100 mM, pH 7.0 (NaH_2PO_4/Na_2HPO_4), EDTA = 0.2 mM) using 1.0 mM of each strand. T_m's are averages of at least two measurements within ±1.0 °C. ΔT_m = change in T_m relative to corresponding unmodified reference duplex. Mismatch ΔT_m = difference in T_m between mismatched and complementary duplex. Target sequences: 3′-GCGT TT**B**TT TGCG (for **ON1**/**ON5**/**ON9**/**ON13**/**ON17**), 3′-GCGT TG**B**GT TGCG (for **ON2**/**ON6**/**ON10**/**ON14**/**ON18**), 3′-GCGT TC**B**CT TGCG (for **ON3**/**ON7**/**ON11**/**ON15**/**ON19**), and 3′-GCGT TA**B**AT TGCG (for **ON4**/**ON8**/**ON12**/**ON16**/**ON20**), where **B** is A (matched) or C/G/T (mismatched). Data for **ON**1-**ON4** and **ON13**-**ON20** are from reference 10a.

Photophysical studies. Having established that introduction of LNA nucleotides as direct or next-nearest neighbors of **X** monomers influences the binding characteristics of **X**-modified ONs, we set out to study if these structural motifs also influence the photophysical properties of **X**-modified ONs.

Steady-state fluorescence emission spectra of ON5-ON12, in the absence or presence of complementary or centrally mismatched DNA targets, were recorded at 5 °C to ensure maximal duplex formation and using an excitation wavelength of 344 nm (Figure 44 and S48). The spectra exhibit two broad fluorescence emission maxima at ~387 nm and ~402 nm. Hybridization with complementary DNA consistently results in increased fluorescence emission, whereas hybridization with mismatched targets generally results in decreased fluorescence emission relative to the corresponding single-stranded probes.

UV-vis absorption spectra of ON5-ON12 and their duplexes with complementary or mismatched DNA targets resulted in broad absorption spectra. Although the broadness of the pyrene peaks precluded a detailed analysis of absorption maxima, it is clear that hybridization with cDNA results in hypsochromic shifts of the absorption maxima, while no such shifts were observed upon hybridization with mismatched targets (Figure 49 and 50). These results are consistent with the previously proposed model for **X**-modified duplexes,[9] i.e., pyrene moieties are pointing into the major groove in matched duplexes (limited interactions with nucleobases;

blue-shifted absorbance; intense fluorescence; glycosidic torsion angle in *anti* range), while they are intercalating in mismatched duplexes (strong interaction with nucleobases; poor thermal mismatch discrimination; no blue-shifts in pyrene absorption; quenched fluorescence; glycosidic torsion angle in *syn* range).

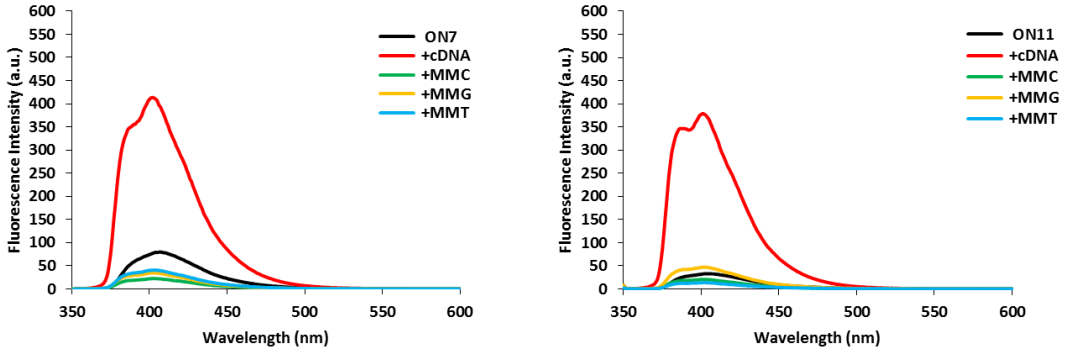

Figure 44. Steady-state fluorescence emission spectra of **ON7** (-Ag**X**gA-) and **ON11** (-aG**X**Ga-) in the presence or absence of complementary or centrally mismatched DNA targets (mismatched nucleotide specified). λ_{ex} = 344 nm; T = 5 °C; each strand used at 1.0 μM. Spectra of other b**X**b and bB**X**Bb probes are shown in Figure 50.

Further inspection of the fluorescence spectra reveal the following trends: (i) The fluorescence intensities of the matched duplexes are not very sensitive to the nature of the flanking nucleobases, which corroborates the hypothesis that the pyrene moieties are not in close contact with the nucleobases in matched duplexes (e.g., compare heights of red bars for ON9-ON12, Figure 45). (ii) Matched duplexes involving b**X**b ONs are more brightly fluorescent than those involving bB**X**Bb ONs, which indicates that directly flanking LNA nucleotides are more effective at directing the pyrene moiety of monomer **X** into the non-quenching major groove than LNA monomers positioned as next-nearest neighbors (compare heights of red bars for ON5-ON8 vs ON9-ON12, Figure 45). We speculate that this is due to more efficient restriction of monomer **X** in a North type conformation, which would reduce the degrees of freedom of

the glycosidic torsional angle and – concomitantly – of the pyrene moiety. (iii) The fluorescence intensities of single-stranded bB**X**Bb probes are significantly lower than those of b**X**b probes, presumably since the pyrene moieties are able to interact more efficiently with quenching nucleobases in ON5-ON8 (compare heights of black bars for ON5-ON8 vs ON9-ON12, Figure 45). As a result, significantly larger increases in fluorescence intensity are observed upon target binding with bB**X**Bb than b**X**b probes (between 1.7- and 12-fold vs 1.5- and 5-fold, respectively; compare values above black bars, Figure 45). Interestingly, the increases are less pronounced in ONs where monomer **X** is flanked by DNA-A or LNA-A monomers, most likely due to the fact that A is a weak quencher of pyrene fluorescence; (iv) Excellent fluorescent discrimination of mismatched targets is observed with both bB**X**Bb and b**X**b probes, although discrimination is slightly more efficient with the bB**X**Bb probes (discrimination factors I_m/I_{mm} between 2.3-18.3 and 2.0-28.0 for ON5-ON8 and ON9-ON12, respectively, Figure 45; for definition of I_m/I_{mm}, see legend of Figure 45). Targets with centrally mismatched 2′-deoxyribocytidines opposite of monomer **X** are slightly less efficiently discriminated (compare heights of yellow bars relative to green and blue bars, Figure 45). This is probably due to less efficient intercalation of the pyrene moiety in the duplex, leading to reduced quenching and less discrimination.

Comparison of the fluorescence properties of ON5-ON12 (Figure 45) and the **X**- and **Z**-modified benchmark probes ON13-ON20 (Figure 51) reveals the following trends: (i) The fluorescence brightness of the matched duplexes decreases in the order: b**X**b~B**Z**B>bB**X**Bb≥B**X**B (compare heights of red bars, Figure 45 and 51). (ii) The relative increase in fluorescence intensity upon hybridization with complementary DNA decreases in the following order: bB**X**Bb≥B**Z**B≥B**X**B>b**X**b. (iii) The efficiency in discriminating

mismatched targets via fluorescence decreases: bB**X**Bb>b**X**b>B**Z**B≥B**X**B. It is particularly interesting to note the improvement in SNP discrimination that introduction of LNA nucleotides as next-nearest neighbors brings in 'challenging' sequence contexts where the **X** monomer is flanked by 2′-deoxyadenosines or thymidines (compare I_m/I_{mm} for ON9/ON12 vs ON13/ON16, Figure 45 and 51).

In summary, these observations demonstrate that introduction of flanking LNA nucleotides indeed is a useful strategy for modulating the photophysical properties of **X**-modified ONs. ONs with bB**X**Bb motif (ON9-ON12) are emerging from this study as particularly interesting SNP-detection probes as they exhibit pronounced hybridization-induced increases in fluorescence intensity leading to the formation of brightly fluorescent duplexes, as well as excellent SNP-discriminatory properties.

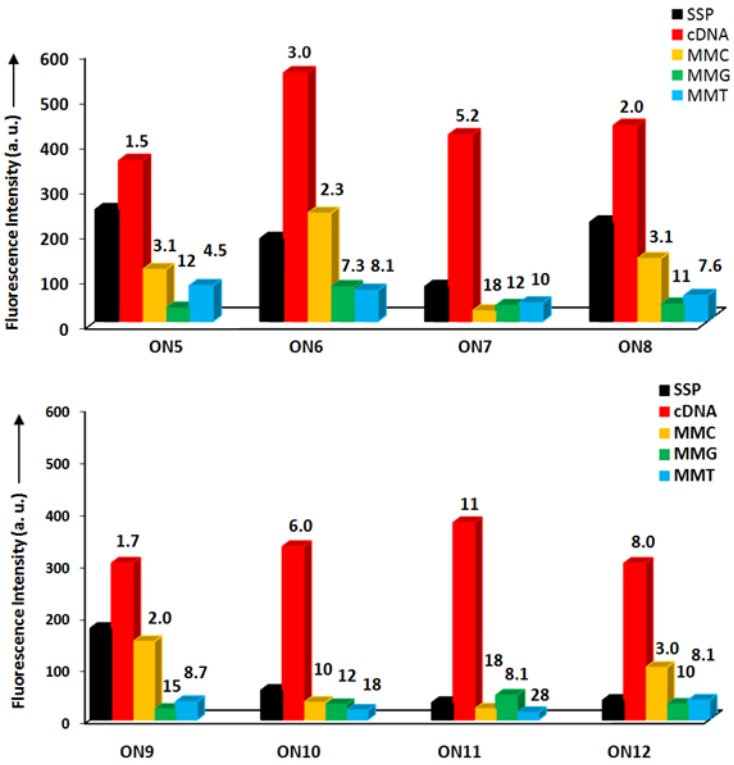

Figure 45. Fluorescence intensities at λ_{em} = 402 nm of **ON5-ON12** in the absence (single-stranded probe, SSP) or presence of complementary DNA targets. Hybridization-induced increases and discrimination factors (I_m/I_{mm}), defined as the fluorescence intensity of duplexes with complementary DNA divided by the fluorescence intensity of SSPs or duplexes with mismatched DNA, respectively, are listed above bars. For experimental conditions, see Figure 44.

5.3. Conclusion.

Introduction of canonical LNA nucleotides is able to improve the SNP discriminating photophysical properties of probes modified with 5-[3-(1-pyrene carboxamido)propynyl] 2'-deoxyuridines. Although we have previously utilized a similar strategy to design SNP discriminating probes for RNA detection,[17] with alternating segments of LNA. The current study demonstrates that the use of canonical LNA building blocks in combination with C5-pyrenecarboxamide fluorophore functionalized DNA can also be used to develop probes with interesting photophysical properties.

5.4. Supporting Information

Synthesis and purification of oligonucleotides (ONs). Modified ONs were prepared on a DNA synthesizer (0.2 μmol scale) using succinyl linked LCAA-CPG (long chain alkyl amine controlled pore glass) columns with 500 Å pore size. Standard protocols for incorporation of DNA phosphoramidites were used. Modified phosphoramidites were used in ~50-fold molar excess (0.05 M in anhydrous dichloromethane) along with extended oxidation (45 s) and the following hand-coupling conditions (activator, coupling time, coupling yield): phosphoramidite of monomer $\mathbf{X}$[9] (5-(ethylthio)-1*H*-tetrazole, 20 min, ~95%) and commercially available LNA A^{Bz}, $^{5\text{-Me}}C^{Bz}$, G^{DMF} and T phosphoramidites (4,5-dicyanoimidazole, 15 min or 5-[3,5-

bis(trifluoromethyl)phenyl]-1*H*-tetrazole, 20 min, ~95%). Cleavage from solid support and removal of nucleobase protecting groups was accomplished using 32% aq. ammonia (55 °C, ~18 h). ONs were purified (DMT-on) by ion-pair reverse-phase HPLC using a 0.05 mM triethylammonium acetate buffer - 25% water/acetonitrile (v/v) gradient. Purified ONs were detritylated using 80% aq. AcOH (~20 min) and precipitated from NaOAc/$NaClO_4$/acetone (-18 °C, 12-16 h). The identity of the synthesized ONs was verified through MALDI-MS recorded in positive ion mode on a quadrupole time-of-flight tandem mass spectrometer using anthranilic acid as a matrix (Table 14), while purity (>75%) was verified by RP-HPLC running in analytical mode.

Table 14. MALDI-ToF MS of new **X**-modified ONs[a]

ON	Sequence	Calc. $(M+H)^+$	Exp. $(M+H)^+$
ON5	5′-CGCA A**aXa**A ACGC	4258.8	4258.0
ON6	5′-CGCA A**cXc**A ACGC	4238.8	4238.0
ON7	5′-CGCA A**gXg**A ACGC	4290.7	4290.0
ON8	5′-CGCA A**tXt**A ACGC	4240.7	4241.5
ON9	5′-CGCA **a**AX**a**A **a** ACGC	4258.8	4258.5
ON10	5′-CGCA **a**C**X**C**a** ACGC	4210.7	4210.7
ON11	5′-CGCA **a**G**X**G**a** ACGC	4290.8	4290.5
ON12	5′-CGCA **a**T**X**T**a** ACGC	4240.7	4240.5

[a] For structure of monomer **X**, see Figure 43.

5.4.1. Experimental protocols for thermal denaturation studies, absorbance and fluorescence studies. ON concentrations were estimated using the following extinction coefficients (OD/μmol) for DNA: G (12.01), A (15.20), T (8.40), C (7.05); and pyrene (22.4).[S1] The strands

comprising a given duplex were mixed and annealed. Thermal denaturation temperatures of duplexes (1.0 µM final concentration of each strand) were determined on a temperature-controlled UV/Vis spectrophotometer using quartz optical cells with 1.0 cm path lengths. T_m's were determined as the first derivative maximum of thermal denaturation curves (A_{260} vs. T) recorded in medium salt phosphate buffer (100 mM NaCl, 0.1 mM EDTA, pH 7.0 adjusted with 10 mM NaH_2PO_4 and 5 mM Na_2HPO_4). The temperature of the denaturation experiments ranged from at least 15 °C below T_m to 20 °C above T_m (although not below 5 °C). A temperature ramp of 0.5 °C/min was used in all experiments. Reported T_m's are reported as averages of two experiments within ± 1.0 °C.

UV-vis absorption spectra were recorded at 5 °C using the same samples and instrumentation as in thermal denaturation experiments. Steady-state fluorescence emission spectra were recorded in non-deoxygenated thermal denaturation buffer (each strand used at 1.0 µM) using an excitation wavelength of λ_{ex} = 344 nm, excitation slit 5.0 nm, emission slit 5.0 nm and a scan speed of 600 nm/min. Experiments were performed at a temperature of 5 °C.

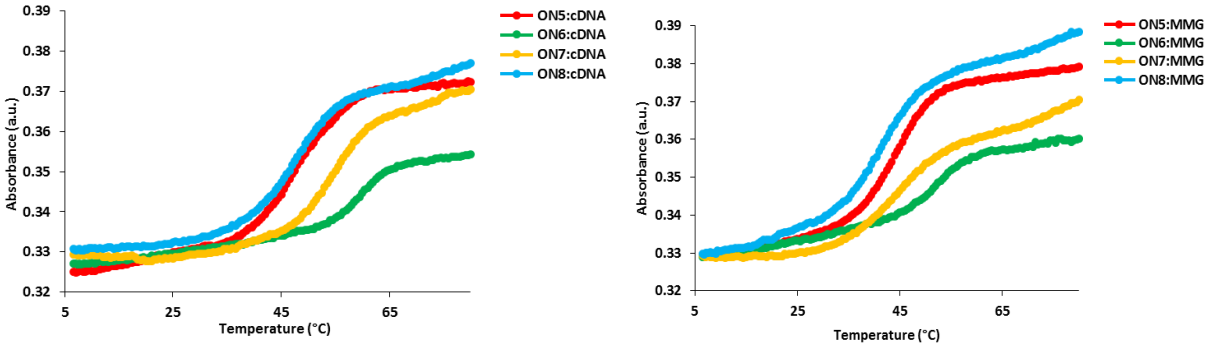

Figure 46. Representative thermal denaturation curves of duplexes formed between **ON5-ON8** and cDNA or centrally dG-mismatched DNA target (MMG).

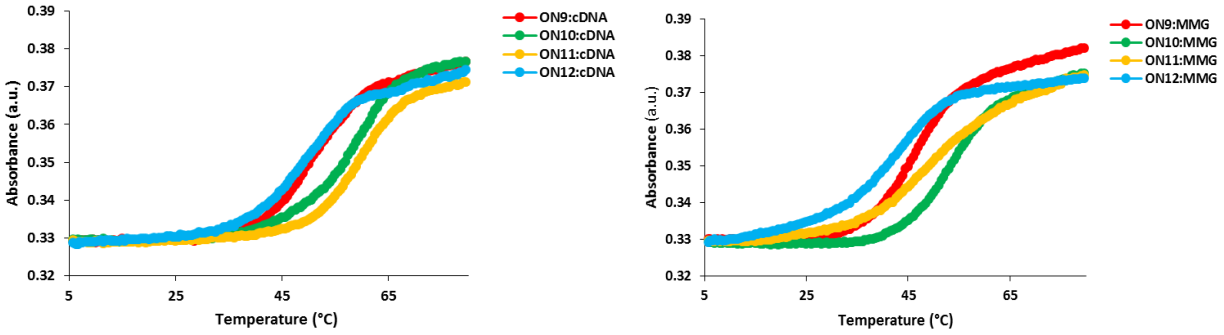

Figure 47. Representative thermal denaturation curves of duplexes between **ON9**-**ON12** and cDNA or centrally dG-mismatched DNA target (MMG).

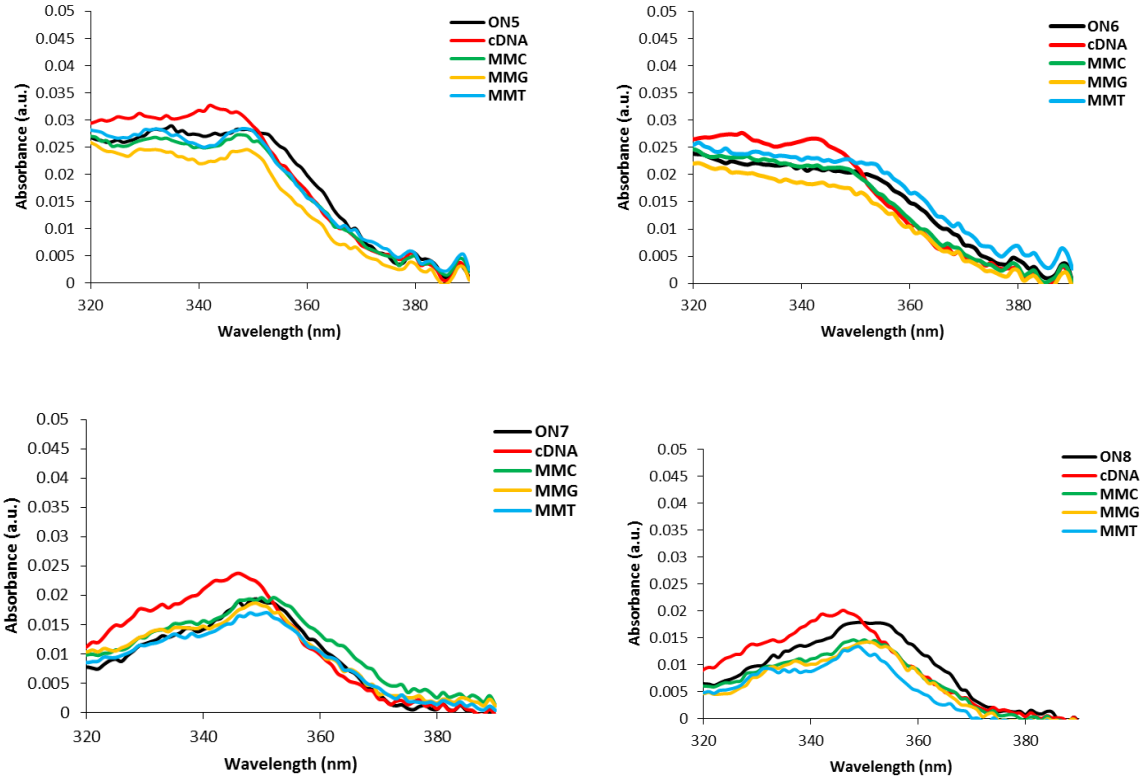

Figure 48. Absorption spectra of **ON5**-**ON8** in the presence or absence of cDNA or mismatched DNA targets (nature of central mismatched nucleotide is specified). Spectra were recorded at T = 5 °C using 1 μM concentration of each strand.

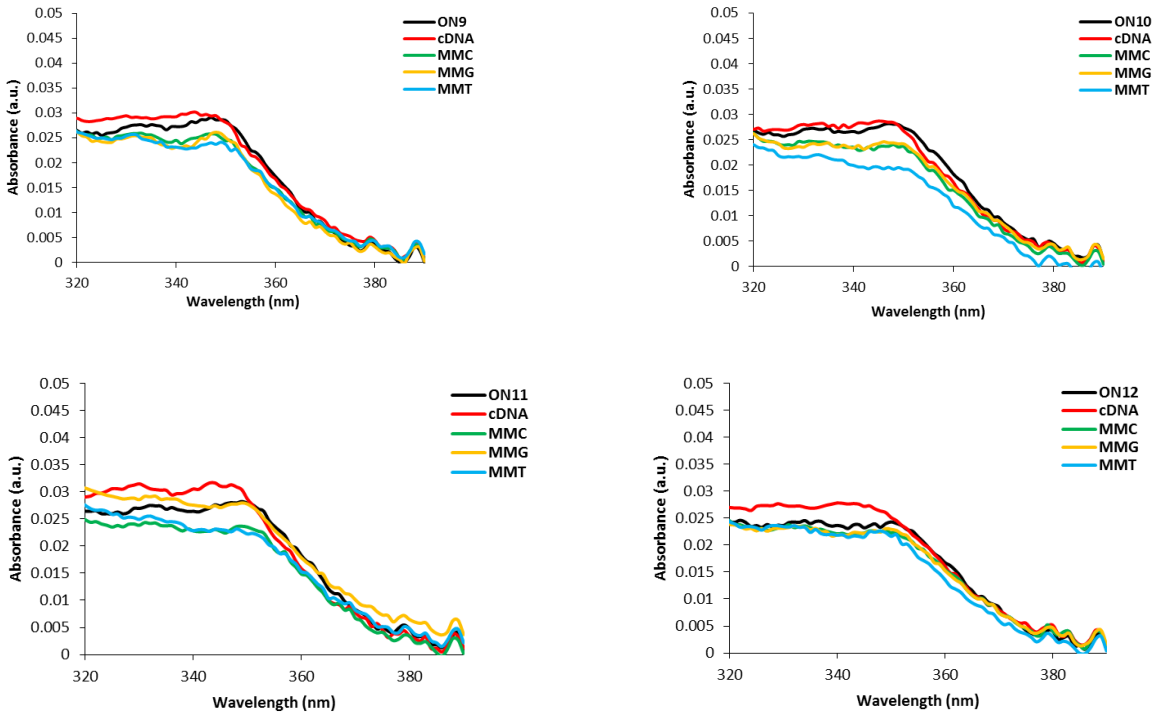

Figure 49. Absorption spectra of **ON9**-**ON12** in the presence or absence of cDNA or mismatched DNA targets (nature of central mismatched nucleotide is specified). Spectra were recorded at T = 5 °C using 1 µM concentration of each strand.

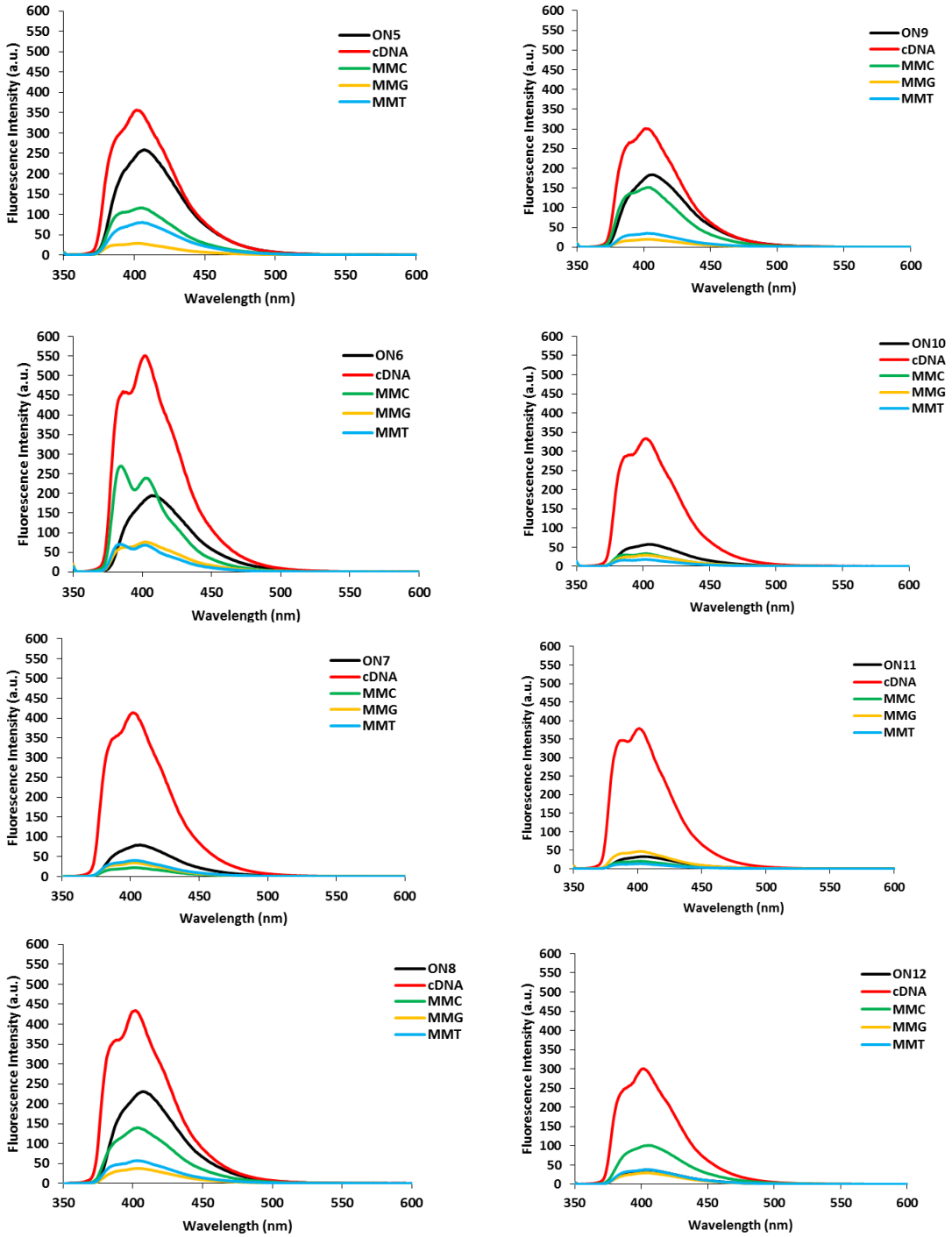

Figure 50. Steady-state fluorescence emission spectra of **ON5**-**ON8** (-b**X**b-) or **ON9**-**ON12** (-bB**X**Bb-) in the presence or absence of complementary or centrally mismatched DNA targets (mismatched nucleotide specified). λ_{ex} = 344 nm; T = 5 °C; each strand used at 1.0 μM.

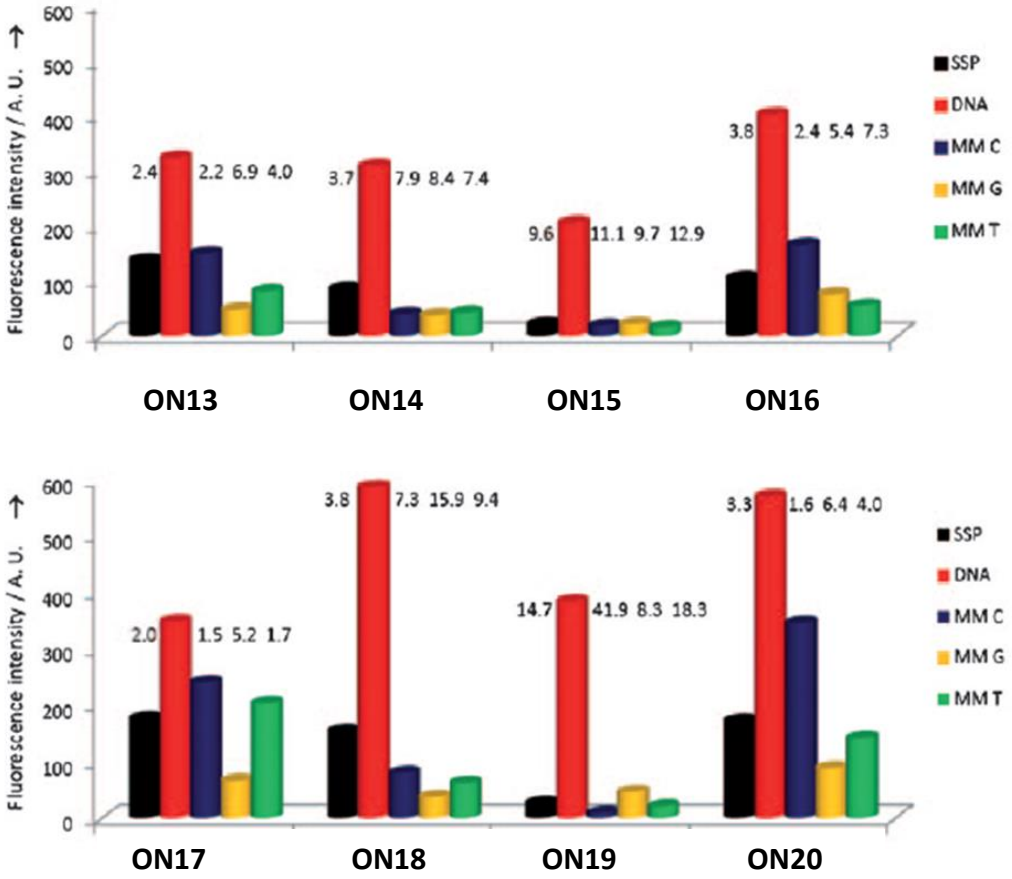

Figure 51. Fluorescence intensity of **X**- and **Z**-modified ONs in the absence (SSPs) or presence of complementary DNA or mismatched DNA targets.[S2] For experimental conditions, see Figure 44.

5.5. References and Footnotes.

1. Socher, E.; Jarikote, D.V.; Knoll, A.; Roglin, L.; Burmeister, J.; Seitz, O. *Anal. Biochem.* **2008**, *375*, 318-330; b) Kim, S.; Misra, A. *Annu. Rev. Biomed. Eng*. **2007**, *9*, 289-320.

2. a) Latif, S.; Bauer-Sardiña, I.; Ranade, K.; Livak, K.; Kwok, P. Y. *Genome Res*. **2001**, *11*, 436-440; b) Li, J.; Butler, J. M.; Tan, Y.; Lin, H.; Royer, S.; Ohler, L.; Shaler, T. A.; Hunter, J. M.; Pollart, D. J.; Monforte, J. A.; Becker, C. H. *Electrophoresis*. **1999**, *20*, 1258-1265.

3. a) Gray, I. C.; Campbell, D. A.; Spurr, N. K. *Hum. Mol. Genet.* **2000**, *9*, 2403 -2408; b) Syvnen, A. C. *Nat. Rev. Genet*. **2001**, 930-942; c) Haga, H.; Yamada, Y.; Ohnishi, Y.; Nakamura, Y.; Tanaka, T. *J. Hum.Genet*. **2002**, *47*, 605-610.

4. a) Levsky, J. M.; Singer, R. H. *J. Cell Sci*. **2003**, *116*, 2833-2838; b) Armitage, B. A. *Curr. Opin. Chem. Biol*. **2011**, *15*, 806-812; c) Tyagi, S. *Nat. Methods*. **2009**, *6*, 331-338; d) Marti, A. A.; Jockusch, S.; Stevens, N.; Ju, J.; Turro, N. J. *Acc. Chem. Res*. **2007**, *40*, 402-409.

5. a) Okamoto, A.; Saito, Y.; Saito, I. *J. Photo. Photobio. C*. **2005**, *6*, 108-122; b) Kolpashchikov, D. M. *Scientifica*. **2012**, *ID 928783*, 1-17; c) Wang, K.; Tang, Z.; Yang, C. J.; Kim, Y.; Fang, X.; Li, W.; Wu, Y.; Medley, C.D.; Cao, Z.; Li, J.; Colon, P.; Lin, H.; Tan, W. *Angew. Chem*. **2009**, *121*, 870-885; d) Kolpashchikov, D. M. *J. Am. Chem. Soc*. **2005**, *127*, 12442-12443; e) Umemoto, T.; Hrdlicka, P. J.; Babu, B. R.; Wengel, J. *ChemBioChem*. **2007**, *8*, 2240-2248.

6. a) Østergaard, M. E.; Hrdlicka, P. J. *Chem. Soc. Rev*. **2011**, *40*, 5771-5788; b) V. L. Malinovskii.; D. Wenger.; R. Häner. *Chem. Soc. Rev*. **2010**, *39*, 410-422.

7. a) Manoharan, M.; Tivel, K. L.; Zhao, M.; Nafisi, K.; Netzel, T. L. *J. Phys. Chem*. **1995**, *99*, 17461-17472; b) Kalyanasundaram, K.; Thomas, J. K. *J. Am. Chem. Soc*. **1977**, *99*, 2039-2044.

8. a) Boonlua, C.; Vilaivan, C.; Wagenknecht, H. A.; Vilaivan, T. *Chem. Asian J*. **2011**, *6*, 3251-3259; b) Saito, I.; Saito, Y.; Hanawa, K.; Hayashi, K.; Motegi, K.; Bag, S. S.; Ichiba, C. D. T, Tainaka, K.; Okamoto, A. *Pure Appl.Chem*. **2006**, *78*, 2305-2312; c) Okamoto, A.; Kanatani, K.; Saito, I. *J. Am. Chem. Soc*. **2004**, *126*, 4820-4827; d) Saito, Y.; Hanawa, K.; Motegi, K.; Omoto, K.; Okamto, A.; Saito, I. *Tetrahedron Lett*. **2005**, *46*, 7605-7608; e) Okamoto, A.; Tainaka, K.; Ochi, Y.; Kanatani, K.; Saito, I. *Mol. BioSyst*. **2006**, *2*, 122-127.

9. Okamoto, A.; Kanatani, K.; Saito, I. *J. Am. Chem. Soc*. **2004**, *126*, 4820-4827.

10. a) Østergaard, M. E; Kumar, P; Baral, B; Guenther, D. C; Anderson, B. A., Ytreberg, F. M; Deobald, L; Paszczynski, A. J; Sharma, P. K.; Hrdlicka, P. J. *Chem.Eur. J*. **2011**, *17*, 3157-3165; b) Østergaard, M. E; Guenther, D. C; Kumar, P; Baral, B; Paszczynski, A. J; Sharma, P. K; Hrdlicka, P. J. *Chem. Commun*. **2010**, *46*, 4929-4931.

11. Kumar, P.; Østergaard, M. E.; Baral, B.; Anderson, B.; Dale, C. G.; Kaura, M.; Raible, D. J.; Sharma, P. K.; Hrdlicka, P. J. *J. Org. Chem*. **2014**, *79*, 5047-5061.

12. a) Bhattacharyya, J.; Maiti, S.; Muhuri, S.; Nakano, S.; Miyoshi, D.; Sugimoto, N. *Biochemistry*, **2011**, *50*, 7414-7425; b) Owczarzy, R.; You, Y.; Groth, C. L.; Tataurov, A. V. *Biochemistry*, **2011**, *50*, 9352-9367.

13. Wilson, J. N.; Younjin, C.; Samuel, T.; Cuppoletti, A.; Kool, E. T. E. *ChemBioChem* **2008**, *9*, 279-285.

14 a) Bondensgaard, K.; Petersen, M.; Singh, S.K.; Rajwanshi, V. K.; Kumar, R.; Wengel, J.; Jacobsen, J. P. *Chem. Eur. J*. **2000**, *6*, 2687-2695; b) Bhattacharyya, J.; Maiti, S.; Muhuri, S.; Nakano, S.; Miyoshi, D.; Sugimoto, N. *Biochemistry* **2011**, *50*, 7414-7425; c) Owczarzy, R.; You, Y.; Christopher, L. G.; Tataurov, A. V. *Biochemistry* **2011**, *50*, 9352-9367.

15. a) You, Y; Moreira, B. G; Behlke, M. A; Owczarzy, R. *Nucleic Acids Res*. **2006**, *34*, 1-11; b) Koshkin, A. A.; Singh, S. K.; Nielsen, P.; Rajwanshi, V. K.; Kumar, R.; Meldgaard, M.; Olsen, C. E.; Wengel, J. *Tetrahedron*. **1998**, *54*, 3607-3630; c) Obika, S.; Uneda, T.; Sugimoto, T.; Nanbu, D.; Minami, T.; Doi, T.; Imanishi, T.; *Bioorg. Med. Chem*. **2001**, *9*, 1001-1011; d) Kaur, H.; Babu, B. R.; Maiti, S. *Chem. Rev*. **2007**, *107*, 4672-4697.

16. a) Dodd, D. W.; Hudson, R. H. E.; *Mini-Rev. Org. Chem*. **2009**, *6*, 378-391; b) Kumar, T.S.; Madsen, A. S.; Østergaard, M. E.; Sau, S. P.; Wengel, J.; Hrdlicka, P. J. *J. Org. Chem*. **2009**, *74*, 1070-1081; c) Dougherty, G.; Pilbrow, J. R. *Int. J. Biochem*. **1984**, *16*, 1179-1192; d) Astakhova, I. V.; Korshun, V. A.; Wengel, J. *Chem. Eur. J*. **2008**, *14*, 11010-11026.

17. Karmakar, S.; Hrdlicka. P. J. *Chem. Sci*. **2013**, *4*, 3447-3454.

S1. Dioubankova, N. N.; Malakhov, A. D.; Stetsenko, D. A.; Gait, M. J.; Volynsky, P. E.; Efremov, R. G.; Korshun, V. A. *ChemBioChem*. **2003**, *4*, 841-847.

S2. Østergaard, M. E.; Kumar, P.; Baral, B.; Guenther, D. C.; Anderson, B. A.; Ytreberg, F. M.; Deobald, L.; Paszczynski, A. J.; Sharma, P. K.; Hrdlicka, P. J. *Chem.Eur. J*. **2011**, *17*, 3157-3165.

Chapter 6: Locked Nucleic Acid (LNA) induced effect on thermal denaturation and fluorescence properties of oligonucleotides modified with nucleobase-functionalized DNA monomers

The following paper by **Kaura**, **M** and Hrdlicka, P. J has been prepared for consideration in an international peer-reviewed journal.

Abstract. Mixmer LNA/DNA probes comprising small and bulky moieties on the C5 and C8 positions of DNA (U) and DNA (A) monomers have been synthesized and studied. The effect of Locked Nucleic Acids (LNAs) on nucleobase-functionalized DNAs has been examined for potential application in antisense technology. Oligonucleotides modified with LNA monomers are known to display strong binding affinity towards RNA as they conformationally tune the duplex into a more RNA like (i.e., A-type) geometry. Here, we demonstrate that introduction of canonical LNAs into an oligonucleotide (ON) sequence results into the formation of duplexes with higher affinity towards cDNA/RNA and improved photophysical properties. We speculate that the relative increases are due to the shift of the duplexes from B-type to A-type.

6.1. Introduction.

Locked nucleic acid (LNA) modified oligonucleotides represent an interesting class of nucleic acids with an extensive therapeutic and diagnostic potential.[1,2] X-ray crystallography, NMR spectroscopy, and molecular modeling studies have shown that LNA has a fixed C3'-endo sugar pucker (N-type) conformation and can thus be classified as RNA mimics.[3,4] Thermodynamic and kinetic studies of LNA modified oligonucleotides in DNA:DNA or DNA:RNA duplexes suggest that incorporation of conventional LNA monomers into ONs, results in a gradual geometry shift toward A-type duplexes (RNA:RNA), which gives rise to higher affinity towards RNA.[5,6] As a result, LNA modified ON probes have been utilized in a wide range of nucleic

acid applications, such as mRNA antisense inhibition, DNA sequencing, SNP detection, RNA interference and mismatch discrimination.[7] However, LNAs are most prominently known for RNA targeting applications, inhibiting gene expression. In addition, the effects of LNA are sequence specific, and they vary with the sequence context, length and degree of modification.[8] For example, end modified LNA gapmers have been shown to have good antisense properties.[9] Hence, by using certain set of rules, one can design LNA modified probes to form a thermodynamically stable duplex.

Recently, we developed nucleobase-functionalized LNA analogs with the aim of improving the hybridization properties of LNA.[10-13] However, the challenging synthesis of these monomers,[14] is a limiting factor for their use in real world-applications. It would be desirable to develop ON probes using limited number of synthetic steps, while sharing the RNA targeting properties of C5-functionalized LNA modified sequences. Toward this end, we set out to synthesize probes modified with C5/C8-nucleobase-functionalized DNA monomers (Figure 52) in combination with commercially available canonical LNAs hypothesizing that LNA will tune the flanking nucleotides into N-type conformation to afford monomers that mimic the hybridization properties of C5/C8-functionalized LNA monomers.

We have previously utilized a similar strategy to modulate the photophysical properties of ONs modified with 5-[3-(1-pyrenecarboxamido)propynyl] DNA monomer with flanking LNAs resulting in probes with improved SNP discriminating properties. Phosphoramidites W/X/Y/Z and L/M/N were selected as synthetic targets to study the influence of C5/C8 modified labels on hybridization characteristics of ONs modified with corresponding monomers surrounded with flanking LNAs.

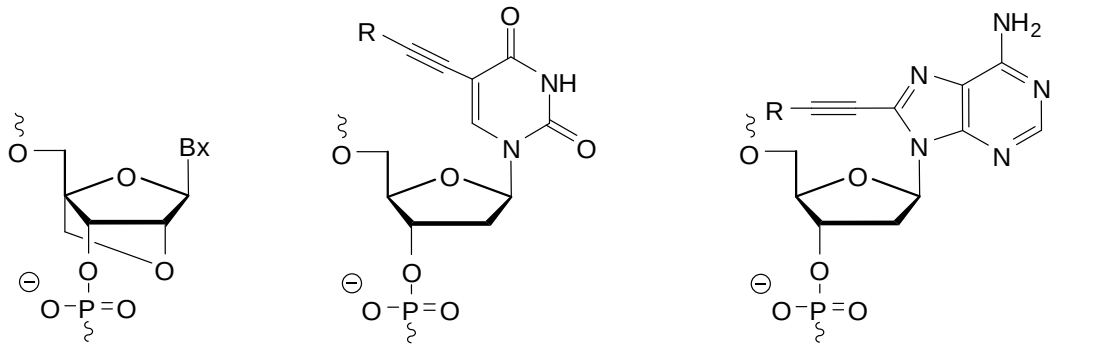

Figure 52. Structures of LNA, C5-functionalized 2′-deoxyuridines and C8-functionalized 2′-deoxyadenosines studied herein.

6.2. Results and discussion.

Synthesis of nucleobase-functionalized DNA phosphoramidites. The corresponding phosphoramidites of 2′-deoxyuridine monomers **W**-**Z** were prepared according to literature protocols,[15-18] while C8-functionalized 2′-deoxyadenosine phosphoramidites **L**-**N** were prepared as outlined in Schemes 6 and 7. Thus, 8-bromo 2′-deoxyadenosine derivative **1**[19,20] was coupled to *N*-(prop-2-ynyl)pyrene-1-carboxamide[21] under Sonogashira conditions to provide nucleoside **2** in 50% yield (Scheme 6). Subsequent O3′-phosphitylation using 2-cyanoethyl *N*,*N*-diisopropylchlorophosphoramidite (PCl reagent) and *N*,*N*-diisopropylethylamine (DIPEA) afforded target phosphoramidite **3N** in 60% yield.

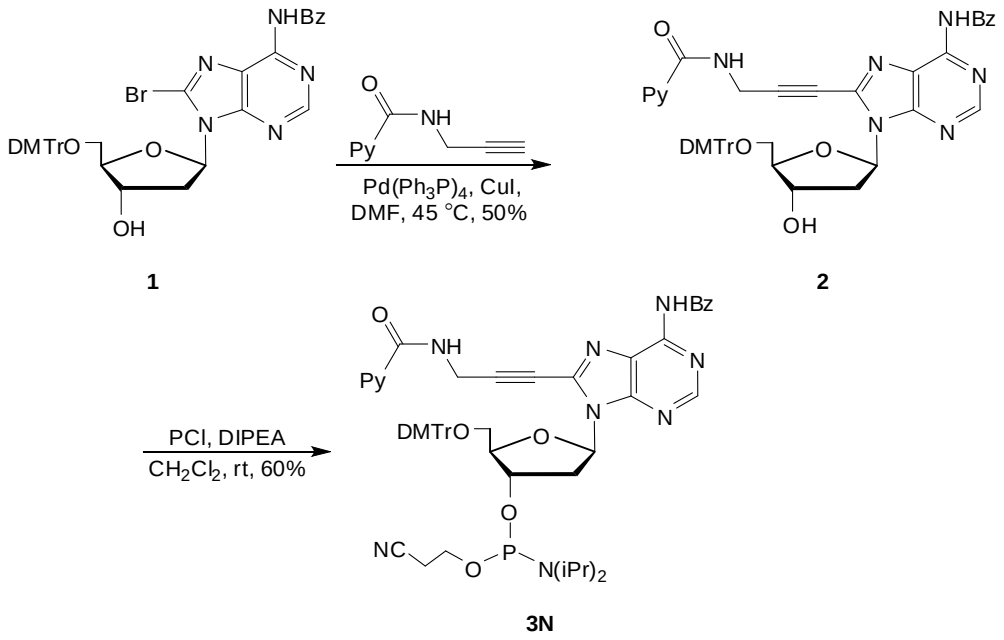

Scheme 6. Synthesis of C8-functionalized 2′-deoxyadenosine **3N**. PCl reagent = 2-cyanoethyl-*N*,*N*-diisopropylchlorophosphoramidite; DIPEA = *N*,*N*-diisopropylethylamine.

The reaction sequence had to be modified for the synthesis of phosphoramidites **3L** and **3M** since the Sonogashira couplings between nucleoside **1** and trimethylsilylacetylene or 1-ethynylpyrene were sluggish, resulting in incomplete reactions and low reaction yields. Nucleoside **4**[19], which features an unprotected adenine moiety, was found to be a more suitable substrate for Sonogashira couplings, furnishing nucleosides **5L** and **5M** in 68% and 80% yield, respectively. Attempts to benzoylate the N6-position using a transient protection protocol[22] were not satisfactory and the exocyclic amine of the adenine moiety was instead protected as an *N*,*N*-dimethylformamidine group[23] to afford nucleosides **6L** and **6M** in 83% and 87% yield, respectively. Phosphitylation of the 3′-position, using similar conditions as described for **3N**, provided target nucleosides **3L** and **3M** in 72% and 64% yield, respectively.

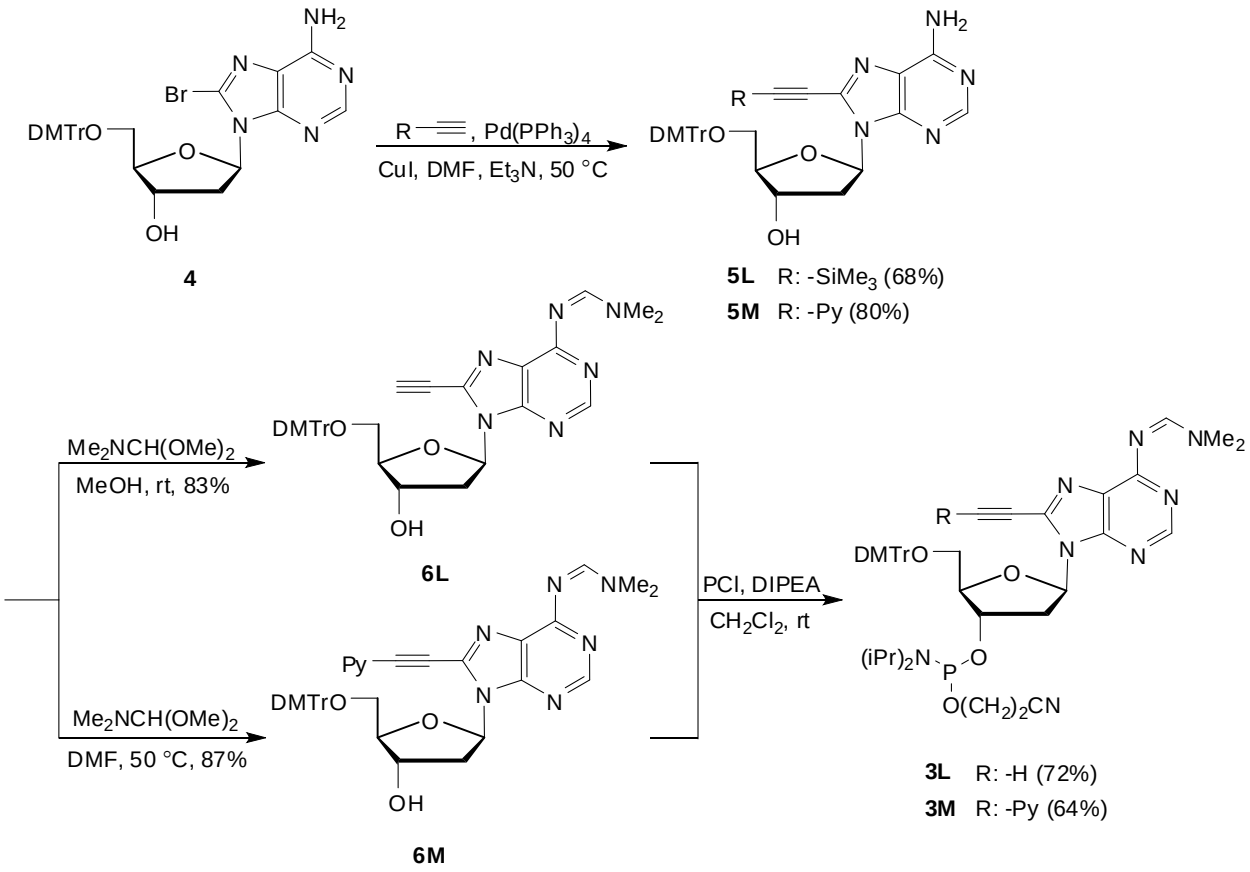

Scheme 7. Synthesis of C8-functionalized 2′-deoxyadenosines **3L** and **3M**.

Oligonucleotide synthesis. The nucleobase-functionalized phosphoramidites were used to prepare 9-mer ONs in which monomers **L**/**M**/**N**/**W**/**X**/**Y**/**Z** were incorporated with LNA nucleotides in two different relative positions; i) flanking LNA nucleotides (**B2/B5** series), or ii) LNA monomers as next-nearest neighbors (**B3/B6** series) (Tables 15 and 16). In addition, LNA free ONs (**B1**/**B4** series) were synthesized which were used as a reference to verify the effect of flnaking LNAs on 2'-deoxyribonucleotides. The following conditions were used during machine-assisted solid-phase DNA synthesis (activator/coupling time/coupling yield); 5-(ethylthio)-1*H*-tetrazole/20 min/~95% (monomers **M**/**N**), 4,5-dicyanoimidazole/20 min/~95% (monomers **L**/**W**/**X**) and 5-[3,5-bis(trifluoromethyl)phenyl]-1*H*-tetrazole/20

min/~95% (monomers **Y**/**Z** and LNA monomers). The composition and purity (>75 %) of all modified ONs was verified by MALDI-MS/MS analysis (Table 20 and Table 21) and ion-pair reverse-phase HPLC respectively.

Affinity toward cDNA/cRNA. Thermal denaturation temperatures (T_m's) of duplexes between ONs and complementary DNA and RNA (cDNA/cRNA) were determined in medium salt buffer ($[Na^+]$ = 110 mM, pH 7.0). All denaturation curves exhibited sigmoidal monophasic transitions (Figure 55). First, we investigated the binding affinities of C5-functionalized DNA ONs (B1-B3) with cDNA/cRNA (Table 15).

ONs that are modified with C5-ethynyl- or C5-aminopropynyl-functionalized 2′-deoxyuridine monomers **W** and **X** display moderately increased affinity toward cDNA and cRNA relative to unmodified ONs (ΔT_m up to +5 °C, Table 15). In contrast, ONs that are modified with bulky pyrene-functionalized monomers **Y** and **Z**[25] display greatly reduced cDNA/cRNA affinity (ΔT_m down to -11 °C, Table 15), presumably due to the steric bulk and/or hydrophobicity of the pyrene moieties. As expected,[24] incorporation of two canonical LNA monomers into 9-mer ONs strongly increases the affinity toward cDNA and especially cRNA (ΔT_m up to +20.5 °C, Table 15).

Although ONs in which two LNA nucleotides are incorporated as flanking or next nearest neighbors relative to C5-ethynyl 2′-deoxyuridine monomer **W** exhibit very high affinity toward cDNA and cRNA (ΔT_m between +7.5 °C and +17.5 °C, Table 15), the affinity-enhancing effects of the LNA and **W** monomers are not additive (e.g., compare ΔT_m of **W2** with **T2** and **W1**, Table 15). ONs with LNA nucleotides near C5-propargylamine 2′-deoxyuridine monomer **X** display higher cDNA/cRNA affinity but the effects upon combining these two chemistries are more complex. Synergistic stabilization is observed for **X3** vs cDNA, additive stabilization is

observed for **X2** vs cDNA and **X3** vs cRNA, while less-than-additive stabilization is seen for **X2** vs cRNA (Table 15). Introduction of LNA nucleotides in the vicinity of monomers **Y** and **Z** neutralizes the destabilizing effect of bulky pyrene moiety which results in very minor cDNA affinity increases, while far greater affinity increases are observed with cRNA (e.g., compare ΔT_m of **Y1**-**Y3** vs cDNA/cRNA, Table 15). One possible explanation is that the **Y** and **Z** monomers prefer *B*-type duplex geometries (compare ΔT_m of **Y1**/**Z1** vs cDNA and cRNA, Table 15), while introduction of LNA monomers is known to induce increasing *A*-type character[26], thus, forming stable duplexes with cRNA.

Table 15. Thermal denaturation data for duplexes between ONs modified with C5-functionalized DNA monomers and complementary DNA or RNA.[a]

			T_m (ΔT_m)/°C									
			cDNA: 3′-CAC TAT ACG					cRNA: 3′-CAC UAU ACG				
ON	**Sequence**	**B** =	**T**	**W**	**X**	**Y**	**Z**	**T**	**W**	**X**	**Y**	**Z**
B1	5′-GTG A**B**A TGC		29.5	31.0 (+1.5)	32.0 (+2.5)	22.5 (-7.0)	22.5 (-7.0)	27.0	30.0 (+3.0)	32.0 (+5.0)	16.0 (-11.0)	16.0 (-11.0)
B2	5′-GTG **aBa** TGC		38.5 (+9.0)	37.0 (+7.5)	41.0 (+11.5)	23.5 (-6.0)	21.5 (-8.0)	43.0 (+16.0)	42.0 (+15.0)	44.5 (+17.5)	34.0 (+7.0)	32.0 (+5.0)
B3	5′-GT**g** A**B**A **t**GC		39.5 (+10.0)	37.5 (+8.0)	44.5 (+15.0)	26.0 (-3.5)	31.5 (+2.0)	47.5 (+20.5)	46.0 (+19.0)	52.5 (+25.5)	29.0 (+2.0)	35.0 (+8.0)

[a] ΔT_m = change in T_m′s relative to unmodified reference duplexes. T_m's determined as the first derivative maximum of denaturation curves (A_{260} vs T) recorded in medium salt buffer ($[Na^+]$ = 110 mM, $[Cl^-]$ = 100 mM, pH 7.0 (NaH_2PO_4/Na_2HPO_4)), using 1.0 µM of each strand. T_m's are averages of at least two measurements within 1.0 °C; See Figure 52, for structures of monomers. LNA modifications are shown in lower case.

Incorporation of C8-ethynyl-functionalized 2′-deoxyadenosine monomer **L** – and in particular – C8-pyrene-functionalized monomers **M** and **N** into ONs dramatically reduces cDNA/cRNA affinity (see ΔT_m for **B4**-series, Table 16). While the affinity-decreasing effects of monomer **L** are compensated in an additive manner through incorporation of proximal LNA nucleotides

(e.g., compare ΔT_m of **L5** with **T5** and **L4**, Table 16), the effects on binding affinity upon combining LNA nucleotides and C8-pyrene-functionalized monomer **M** and **N** are more complex. For example, introduction of flanking LNA nucleotides results in additive or more-than-additive increases in cDNA/cRNA affinity for **M5** and **N5**, while LNA nucleotides positioned as next-nearest neighbors generally results in far smaller increases in cDNA/cRNA affinity (Table 16). These results indicate that the specific positioning of LNA nucleotides along the probe sequence has a remarkable influence on the T_m values. Thus, LNAs influence the binding mode and energetics of nearby C8-pyrene-functionalized monomers, but the effects are not clearly understood at a molecular level.

Table 16. Thermal denaturation data for duplexes between ONs modified with C8-functionalized DNA monomers and complementary DNA or RNA.[a]

			T_m (ΔT_m)/°C							
			DNA: 3′-CGT ATA GTG				RNA: 3′-CGU AUA GUG			
ON	Sequence	**B** =	T	L	M	N	T	L	M	N
ON4	5′-GCA T**B**T CAC		29.5	24.5 (-5.0)	17.5 (-12.0)	14.0 (-15.5)	27.0	25.0 (-2.0)	<15.0 (<-12.0)	20.0 (-7.0)
ON5	5′-GCA **tBt** CAC		41.5 (+12.0)	36.0 (+6.5)	29.5 (±0.0)	29.0 (-0.5)	40.5 (+13.5)	38.5 (+11.5)	32.0 (+5.0)	31.0 (+4.0)
ON6	5′-GC**a** T**B**T **c**AC		38.5 (+9.0)	34.0 (+4.5)	20.5 (-9.0)	17.0 (-12.5)	40.5 (+13.5)	40.0 (+13.0)	29.0 (+2.0)	15.0 (-12.0)

[a] ΔT_m = change in T_m's relative to unmodified reference duplexes. For experimental conditions, see Table 15.

Binding specificity. Next, we determined the binding specificity of the modified ONs using DNA targets with mismatched nucleotides in the central position (Table 17). Excellent discrimination is observed for control strand **T1** (see ΔT_m for **T1**, Table 17). Introduction of neighboring LNA nucleotides further increases binding specificity, whereas little improvement is achieved when LNA nucleotides are incorporated as next nearest neighbors (see ΔT_m's for

T1-**T3**, Table 17, and **T4**-**T6**, Table 18). Singly modified **W1** and **X1** display similar binding specificity as control strand **T1**, while the pyrene-modified **Y1** and **Z1** display severely compromised binding fidelity (see ΔT_m's for **B1** series, Table 17).

Incorporation of LNA nucleotides next to C5-functionalized 2′-deoxyuridine monomers **W** or **X** improves binding specificity relative to the corresponding "LNA-free" ONs (compare ΔT_m of **W2**/**X2** relative to **W1**/**X1**, Table 17). The improvements are less pronounced when LNA nucleotides are incorporated as next-nearest neighbors (compare ΔT_m of **W3**/**X3** relative to **W1**/**X1**, Table 17). Introduction of LNA nucleotides near pyrene-functionalized monomers **Y** or **Z** does not compensate for the poor binding fidelity of **W**/**Z**-modified ONs (compare ΔT_m of **Y2**/**Y3**/**Z2**/**Z3** relative to **Y1**/**Z1**, Table 17).

Table 17. Discrimination of mismatched DNA targets by ONs modified with C5-functionalized DNA monomers.[a]

			DNA: 3′-CAC T<u>M</u>T ACG			
			T_m/°C	ΔT_m/°C		
Sequence		**M** =	**A**	**C**	**G**	**T**
5′-GTG A**B**A TGC	**T1**		29.5	-16.5	-9.5	-17.0
	W1		31.0	-17.5	-11.5	-17.0
	X1		32.0	-15.0	-10.0	-16.5
	Y1		22.5	+2.0	-3.0	-1.0
	Z1		22.5	-8.0	-9.0	-4.0
5′-GTG **aBa** TGC	**T2**		38.5	-21.5	-14.5	-16.5
	W2		37.0	-21.0	-17.0	-16.0
	X2		41.0	-24.0	-19.5	-20.5
	Y2		23.5	-2.0	-4.0	-2.0
	Z2		21.5	-3.0	-8.0	-6.5
5′-GT**g** A**B**A **t**GC	**T3**		39.5	-17.5	-9.5	-15.5
	W3		37.5	-15.5	-10.0	-10.5
	X3		44.5	-19.5	-12.5	-12.5
	Y3		26.0	+5.5	+1.5	+2.5
	Z3		31.5	-9.0	-6.0	-2.0

[a] For experimental conditions, see Table 15. ΔT_m = change in T_m relative to fully matched ON:DNA duplex (**M**=A).

In case of C8-functionalized DNA ONs singly modified **L4** displays lower binding fidelity than control strand **T4** (Table 18). Incorporation of LNA nucleotides in the vicinity of C8-ethynyl-functionalized 2′-deoxyadenosine monomer **L** generally increases the binding specificity of **L**-modified ONs (compare ΔT_m of **L4** relative to **L5** and **L6**, Table 18). In contrast, incorporation of LNA nucleotides in the vicinity of C8-pyrene-functionalized 2′-deoxyadenosine monomers **M** and **N** does not reverse the poor binding specificity of **M**/**N**-modified ONs.

Table 18. Discrimination of mismatched DNA targets by ONs modified with C8-functionalized DNA monomers.[a]

			DNA: 3′-CGT A<u>M</u>A GTG			
			T_m/°C	ΔT_m/°C		
Sequence		**<u>M</u>** =	T	A	C	G
5′-GCA T**B**T CAC	**T4**		29.5	-17.0	-15.5	-9.0
	L4		24.5	-10.5	-10.0	-10.0
	M4		17.5	-0.5	+3.5	-3.5
	N4		14.0	<-4.0	-0.5	-1.5
5′-GCA **tBt** CAC	**T5**		41.5	-20.0	-19.0	-18.0
	L5		36.0	-15.5	-10.5	-13.5
	M5		29.5	-1.5	-1.5	+0.5
	N5		29.0	-5.5	+5.5	-4.5
5′-GC**a** T**B**T **c**AC	**T6**		38.5	-16.0	-17.0	-16.0
	L6		34.0	-17.5	-10.5	-17.5
	M6		20.5	+7.5	+5.5	-2.5
	N6		17.0	<-7.5	<-7.5	<-7.5

[a] For experimental conditions, see Table 15. ΔT_m = change in T_m relative to fully matched ON:DNA duplex (**<u>M</u>**=T).

Photophysical characterization. Next, we set out to determine if the presence of LNA nucleotides impacts the photophysical characteristics of pyrene constituting C5- and C8- DNA functionalized **Y**/**Z**/**M**/**N**–modified probes. UV-vis absorption spectra of single-stranded probes **Y1**-**Y3** display defined pyrene absorption maxima at ~375 nm and ~400 nm (Figure 56). Hybridization of **Y1** and **Y3** with cDNA/cRNA or centrally mismatched DNA targets results in bathochromic shifts of 2-6 nm (Table 19), which is indicative of strong interactions of pyrene moiety with neighboring nucleobases.[27] Interestingly, **Y2** probe, with LNAs at neighboring position, upon hybridization with mismatched DNA targets also results in bathochromic shifts, whereas, binding with cDNA/cRNA does not, suggesting that flanking LNA nucleotides reduce pyrene-nucleobase interactions in matched duplexes. We speculate that this is accomplished through LNA-induced tuning of the duplex toward *A*-type geometry and/or by increasingly shifting the nucleobase orientation of monomer **Y** from *syn* to *anti*, thereby changing the preferred binding mode of the pyrene moiety from intercalation to major groove placement.

The absorption maxima of ONs modified with C8-pyrenylacetylene DNA monomer **M** are observed at ~385 nm, ~400 nm and ~420 nm (Figure 58). Hybridization of **M4** with complementary or mismatched targets results in major bathochromic shifts (6-9 nm), whereas smaller shifts are observed for the LNA-modified **M5** or **M6** (Table 19), which may be the result of reduced pyrene-nucleobase interactions.

Absorption spectra of ONs and duplexes modified with the 3-(1-pyrenecarboxamido)propynyl chromophore on C5 and C8 position of DNA (**Z**- and **N**-series) are broad, which precludes a detailed analysis of absorption maxima (Figures 57 and 59).

Table 19. Absorption maxima of pyrene-modified ONs in the presence or absence of complementary DNA/RNA or singly mismatched DNA targets.[a]

		λ_{max}/nm	$\Delta\lambda_{max}$/nm				
ON	**Sequence**	SSP	+cDNA	+cRNA	+MM C	+MM G	+MM T
Y1	5′-GTG A**Y**A TGC	396	+4	+2	+5	+4	+5
Y2	5′-GTG **aYa** TGC	399	-2	+0	+3	+2	+4
Y3	5′-GT**g** A**Y**A **t**GC	395	+4	+2	+5	+4	+6
ON	**Sequence**	SSP	+cDNA	+cRNA	+MM A	+MM C	+MM G
M4	5′-GCA T**M**T CAC	412	+7	+7	+6	+7	+9
M5	5′-GCA **tMt** CAC	416	+3	+3	+3	+3	+3
M6	5′-GC**a** T**M**T **c**AC	416	+4	+4	+3	+0	+5

[a] Spectra were recorded in T_m buffer at T = 5 °C using each strand at 1 μM concentration.

Steady-state fluorescence emission spectra of pyrene-modified ONs were recorded at 5 °C in the absence or presence of cDNA/cRNA or centrally mismatched DNA targets. In line with literature reports,[28] **Y**-modified ONs display broad emission profiles that are centered at 460 nm, which is indicative of strong electronic interactions between the pyrene and nucleobase moiety (Figure 53). Hybridization of non LNA modified **Y1** with cDNA/cRNA results in approximately 1.3- and 2.7-fold increased emission at 460 nm, respectively. Insertion of LNAs at neighbouring position has greater influence as slightly larger increases are observed for **Y2** (approximately 2.0- and 4.5-fold increases vs cDNA and cRNA, respectively). In contrast, only minor hybridization-induced changes in fluorescence emission are observed for **Y3** having LNAs as next nearest neighbours.

Proximal LNA nucleotides also influence how efficiently mismatched targets are discriminated via fluorescence. Thus, the fluorescence intensities of mismatched DNA duplexes involving **Y1** and **Y3** range from slightly lower to considerably greater than matched duplexes. In contrast, mismatched duplexes are less emissive than matched duplexes when using **Y2**. This indicates

that flanking LNA nucleotides can be used to tune **Y**-modified ONs to yield probes with greater diagnostic potential. Similar results were observed for 13-mer probes, especially when monomer **Y** is flanked by ^{5Me}C LNA or G LNA monomers (Figure 62).

ONs modified with 5-[3-(1-pyrenecarboxamido)propynyl]-2′-deoxyuridine monomer **Z** exhibit two broad fluorescence emission maxima at ~387 nm and ~406 nm (Figure 53). Hybridization with cDNA/cRNA generally results in significantly increased fluorescence emission, especially with the LNA-containing probes. Thus, 11- and 9-fold increases in fluorescence intensity at 405 nm are observed for **Z2** upon cDNA/cRNA hybridization, while 3- and 7.5-fold increases are observed for **Z3**. Excellent mismatch discrimination is generally observed, especially for **Z2** where monomer **Z** is directly flanked by LNA monomers. We have recently explored the diagnostic potential of longer LNA-rich **Z**-modified probes and found them to display distinct advantages over regular **Z**-modified ONs, such as greater hybridization-induced increases in fluorescence intensity, formation of more brightly fluorescent duplexes and improved SNP discrimination (manuscript in preparation). Incorporation of flanking LNA monomers therefore appears to be an attractive strategy for improving the photophysical properties of ONs modified with C5-pyrene-functionalized 2′-deoxyuridine monomers.

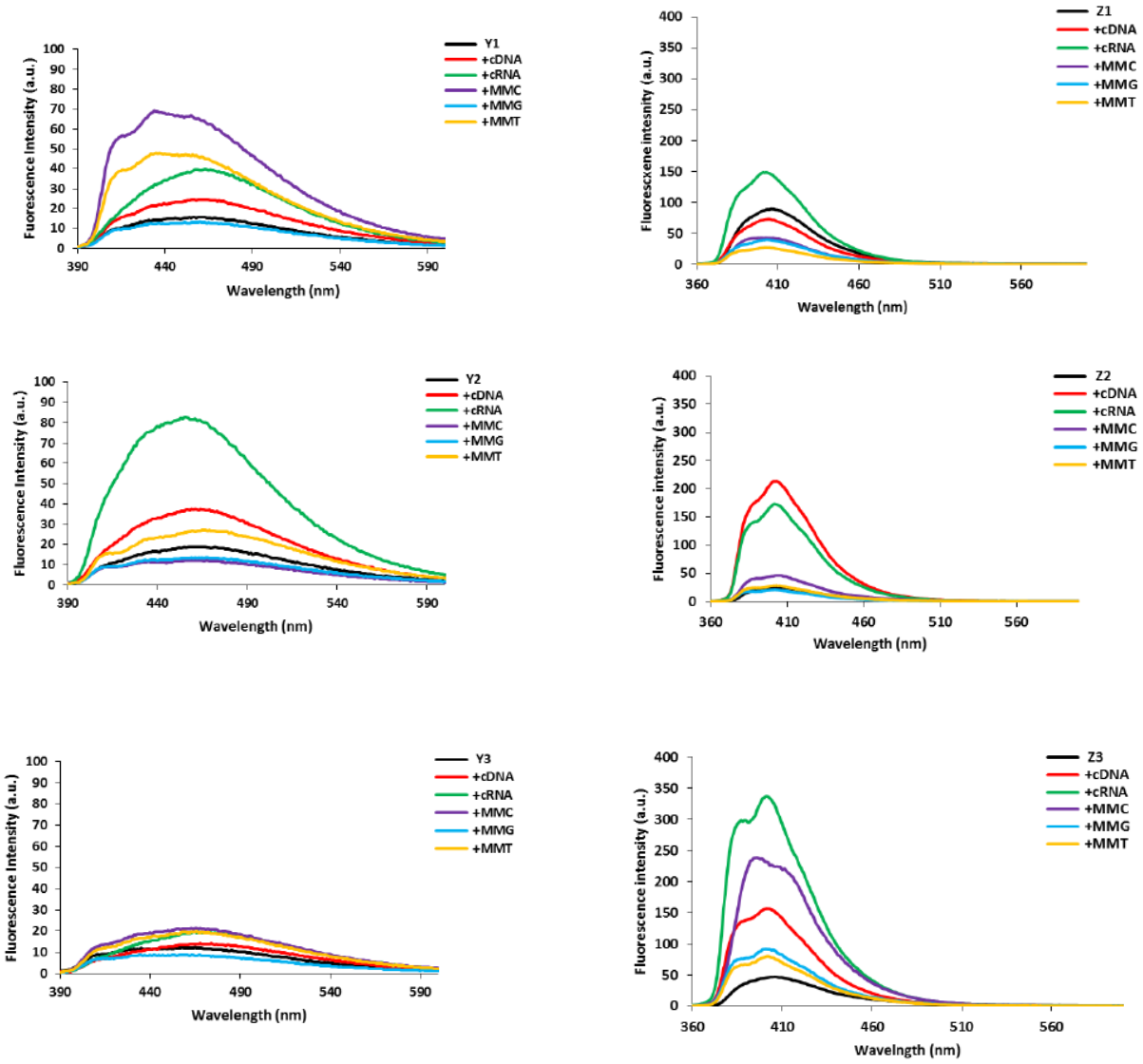

Figure 53. Steady-state fluorescence emission spectra of **Y1**-**Y3** or **Z1**-**Z3** in the presence or absence of complimentary DNA/RNA or centrally mismatched DNA targets (mismatched nucleoside specified). Spectra were recorded in T_m buffer at T = 5 °C using each strand at 1.0 μM and λ_{ex} = 380 nm and 340 nm for **Y**- and **Z**-modified ONs, respectively.

Steady-state fluorescence emission spectra of duplexes between **M4**-**M6** and complementary DNA/RNA or centrally mismatched DNA targets feature a broad emission maximum centered around 460 nm (Figure 54). Hybridization of **M4** with cDNA/cRNA is

accompanied by a ~1.5-fold increase in emission at ~460 nm, while the LNA-modified **M5** and **M6** display slightly greater hybridization-induced increases in fluorescence intensity (~3- and ~2-fold, respectively). Mismatched nucleotides opposite of monomer **M** are not discriminated efficiently as evidenced by the similar emission levels of matched and mismatched duplexes. The presence of nearby LNA nucleotides has limited influence on the photophysical properties of monomer **M**. Similar results were observed for 13-mer ONs with LNA-**M**-LNA motifs (Figure 63).

Fluorescence emission spectra of duplexes between **N4-N6** and complementary DNA/RNA or centrally mismatched DNA targets feature an emission maximum at ~410 nm with a shoulder at ~430 nm (Figure 54). Hybridization of **N4** or **N5** with matched or mismatched only results in minor intensity changes, whereas ~4- and ~7-fold increased emission at 410 nm is observed for **N6** upon cDNA and cRNA binding, respectively, because the single-stranded **N6** is only weakly fluorescent. Unfortunately, mismatched targets are not discriminated efficiently.

In summary, the above results indicate that incorporation of flanking LNA monomers is an interesting strategy for tuning the photophysical properties of ONs modified with C5-pyrene-functionalized DNA monomers, whereas the benefits are more limited with C8-pyrene-functionalized DNA monomers.

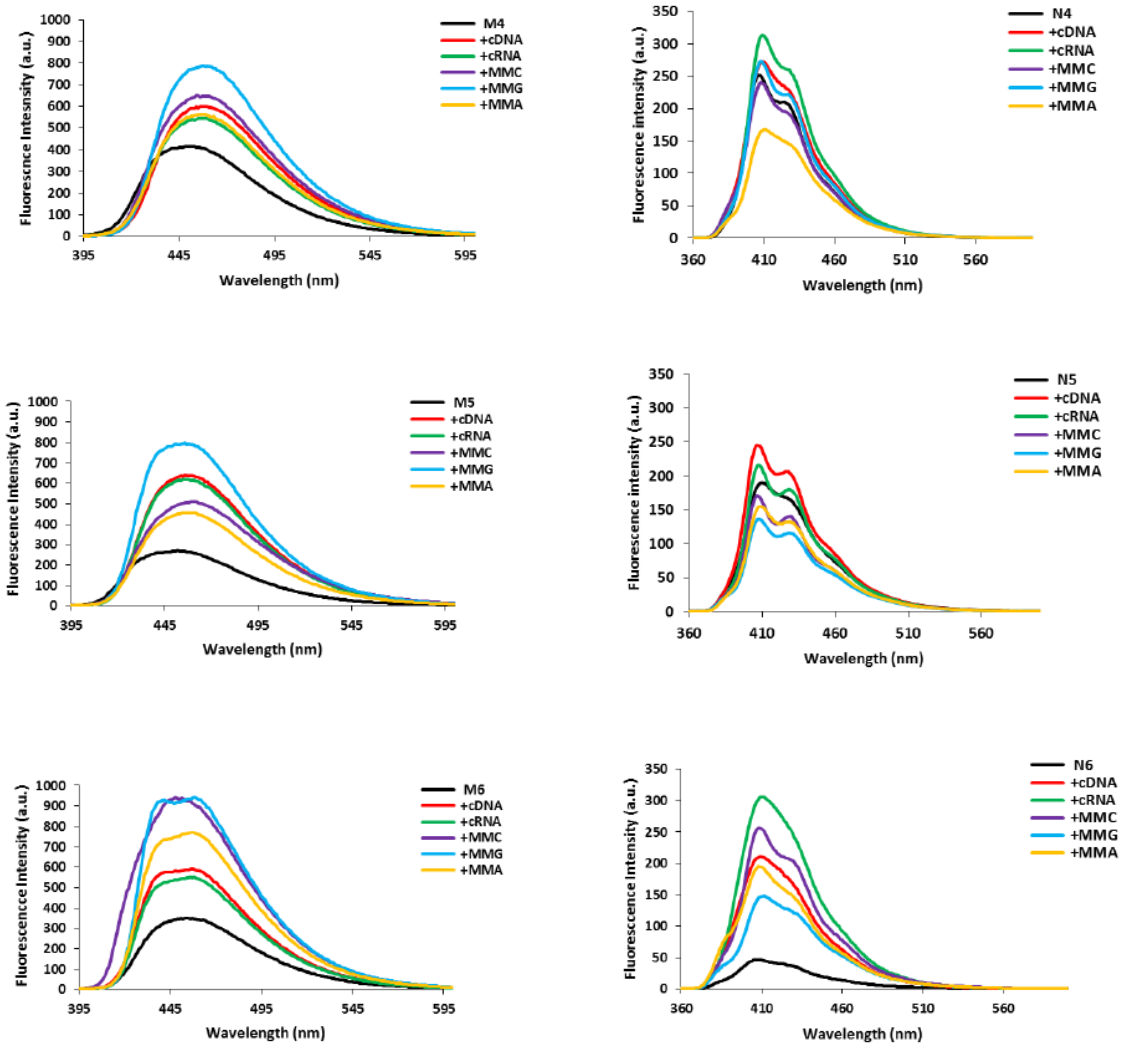

Figure 54. Steady-state fluorescence emission spectra of **M4**-**M6** or **N4**-**N6** in the presence or absence of complementary DNA/RNA or centrally mismatched DNA targets (mismatched nucleoside is specified). Spectra were recorded in T_m buffer at T = 5 °C using each strand at 1.0 μM and λ_{ex} = 385 nm and 350 nm for **M**- and **N**-modified ONs, respectively.

6.3. Conclusion.

The synthesis, hybridization and spectral properties of ONs modified with C5- and C8-functionalized DNA monomers in combination with LNAs at two different positions relative to

the modified DNA has been reported. We have shown that introduction of canonical LNAs into the probes resulted in strong binding affinity towards cDNA/RNA. Insertion of two LNA nucleotides at the neighboring position of C5/C8-functionalized DNA monomers produced a significant increase in T_m for small substituted ONs and reduced the destabilizing effect of bulky pyrene substituted moieties. The stabilizing effect of LNA was more pronounced for C5-functionalized pyrimidines relative to C8-functionalized purines. Besides, the influence of the position of LNA on the hybridization properties of ON reported herein, is an important detail, which needs to be considered while desigining LNA/DNA probes. Further, the excitation of pyrene substituted C5/C8-functionalized DNA ONs resulted in an improved fluorescence emission spectra, upon insertion of LNA nucleotides. As reported, the benefits of LNA are more pronounced with C5-pyrene functionalized DNAs and limited with C8-pyrene functionalized DNA.

In conclusion, the overall increase in binding ffinity towards cDNA/RNA and ability to modulate the photophysical properties of fluorophore labelled probes makes these C5- and C8-functionalized LNA/DNA probes promising constructs for antisense targeting applications.

6.4. Experimental Section

6-N-benzoyl,8-[3-(pyrene carboxamide)-1-propynyl]-5′-O-(4,4′-dimethoxytrityl)-DNA (2). Nucleoside **1**[19,20] (0.40 g, 0.54 mmol), $Pd(PPh_3)_4$ (63 mg, 0.05 mmol), CuI (21 mg, 0.11 mmol) and *N*-(prop-2-ynyl)pyrene-1-carboxamide[18] (0.38 g, 1.35 mmol) were added to anhydrous DMF (10 mL) and the reaction chamber was degassed and placed under an argon atmosphere. To this was added anhydrous Et_3N (0.35 mL, 2.51 mmol) and the reaction mixture was stirred at 45 °C for ~3 h at which point solvents were evaporated off. The resulting residue was taken up in EtOAc (100 mL) and washed with brine (2×50 mL) and saturated aqueous $NaHCO_3$ (50 mL). The combined aqueous layer was then extracted with EtOAc (100 mL). The combined organic layers were dried (Na_2SO_4), evaporated to dryness and the resulting residue purified by column chromatography (0-5% MeOH in CH_2Cl_2, v/v) to afford nucleoside **2** (0.26 g, 50%) as a yellow solid material. R_f = 0.4 (5% MeOH in CH_2Cl_2, v/v); ESI-HRMS *m*/*z* 961.3293 ($[M+Na]^+$, $C_{58}H_{46}N_6O_7{\cdot}Na^+$, Calc. 961.3326); ^{1}H NMR (500.1 MHz, DMSO-d_6) δ 11.26 (s, 1H, ex, NH), 9.41 (t, 1H, ex, J = 5.3 Hz, $NHCH_2$), 8.55-8.58 (m, 2H, Ar, H2), 8.10-8.38 (m, 8H, Ar), 8.05 (d, 2H, J = 7.5 Hz, Ar), 7.63-7.67 (m, 1H, Ar), 7.53-7.57 (m, 2H, Ar), 7.30-7.33 (m, 2H, Ar), 7.12-7.21 (m, 7H, Ar), 6.78 (d, 2H, J = 9.0 Hz, Ar), 6.75 (d, 2H, J = 9.0 Hz, Ar), 6.67 (m, 1H, H1′), 5.42 (d, 1H, ex, J = 4.5 Hz, 3′-OH), 4.71-4.76 (m, 1H, H3′), 4.61 (d, 2H, J = 5.3 Hz, CH_2NH), 4.06-4.10 (m, 1H, H4′), 3.70 (s, 3H, CH_3O), 3.68 (s, 3H, CH_3O), 3.34-3.40 (m, 1H, H2′), 3.22-3.29 (m, 2H, H5′), 2.35-2.41 (m, 1H, H2′); ^{13}C NMR (125.6 MHz, DMSO-d_6) δ 168.9, 165.5, 157.92, 157.90, 152.1 (C2), 151.1, 150.4, 144.9, 136.6, 135.7, 135.5, 133.2, 132.5 (Bz), 131.8, 130.7, 130.6, 130.1, 129.6 (DMTr), 128.50 (Ar), 128.45 (Ar), 128.41 (Ar), 128.3 (Ar), 127.9, 127.6 (DMTr), 127.5 (DMTr), 127.1 (Py), 126.6 (Py), 126.5 (DMTr), 125.9 (Py), 125.6 (Py), 125.3 (Py), 124.4 (Py), 123.8, 123.5, 113.0 (DMTr), 112.9 (DMTr), 95.4, 86.1 (C4′),

85.2, 84.9 (C1′), 71.0, 70.9 (C3′), 63.9 (C5′), 54.92 (CH_3O), 54.90 (CH_3O), 37.0 (C2′), 29.5 (CH_2NH).

8-[2-(trimethylsilyl)ethynyl]-5′-O-(4,4′-dimethoxytrityl) DNA-A (5L). Nucleoside **4**[19] (0.46 g, 0.73 mmol), $Pd(PPh_3)_4$ (84 mg, 0.07 mmol), CuI (28 mg, 0.15 mmol) and trimethylsilylacetylene (0.26 mL, 1.82 mmol) were added to anhydrous DMF (10 mL) and the reaction chamber was degassed and placed under an argon atmosphere. To this was added anhydrous Et_3N (0.42 mL, 3.00 mmol) and the reaction mixture was stirred at 50 °C for ~4 hr at which point solvents were evaporated off. The resulting residue was taken up in EtOAc (100 mL) and washed with brine (2×50 mL) and saturated aqueous $NaHCO_3$ (50 mL). The combined aqueous layer was then extracted with EtOAc (100 mL). The combined organic layer was dried (Na_2SO_4), evaporated to dryness, and the resulting residue purified by column chromatography (0-5% MeOH in CH_2Cl_2, v/v) to afford nucleoside **5L** (0.32 g, 68%) as an off-white solid material. R_f = 0.4 (5% MeOH in CH_2Cl_2, v/v); ESI-HRMS *m/z* 672.2626 ($[M+Na]^+$, $C_{36}H_{39}N_5O_5Si{\cdot}Na^+$, Calc. 672.2618); ^{1}H NMR (500.1 MHz, DMSO-d_6) δ 8.02 (s, 1H, H2), 7.49 (bs, 2H, ex, NH_2), 7.30-7.33 (m, 2H, DMTr), 7.14-7.22 (m, 7H, DMTr), 6.80 (d, 2H, J = 9.0 Hz, Ar), 6.76 (d, 2H, J = 9.0 Hz, Ar), 6.44 (dd, 1H, J = 7.0 Hz, 5.5 Hz, H1′), 5.33 (d, 1H, ex, J = 4.5 Hz, 3′-OH), 4.52-4.57 (m, 1H, H3′), 3.96-4.01 (m, 1H, H4′), 3.72 (s, 3H, CH_3O), 3.71 (s, 3H, CH_3O), 3.16-3.26 (m, 3H, H2′, 2×H5′), 2.25-2.31 (m, 1H, H2′), 0.24 (s, 9H, $(CH_3)_3Si$); ^{13}C NMR (125.6 MHz, DMSO-d_6) δ 157.93, 157.89, 155.9, 153.6 (C2), 148.5, 144.9, 135.7, 135.6, 132.5, 129.6 (DMTr), 129.5 (DMTr), 127.60 (DMTr), 127.56 (DMTr), 126.4 (DMTr), 119.0, 113.0 (DMTr), 112.9 (DMTr), 101.7, 93.8, 85.6 (C4′), 85.2, 83.9 (C1′), 70.9 (C3′), 64.0 (C5′), 54.95 (CH_3O), 54.93 (CH_3O), 37.0 (C2′), -0.77 ($(CH_3)_3Si$).

8-(2-(pyrenyl ethynyl)-5′-O-(4,4′-dimethoxytrityl) DNA-A (5M). Nucleoside **4**[19] (200 mg, 0.32 mmol), $Pd(PPh_3)_4$ (40 mg, 0.03 mmol), CuI (12 mg, 0.06 mmol) and 1-ethynylpyrene[29] (143 mg, 0.63 mmol) were added to anhydrous DMF (5.0 mL) and the reaction chamber was degassed and placed under an argon atmosphere. To this was added anhydrous Et_3N (200 µL, 1.30 mmol) and the reaction mixture was stirred at 50 °C for ~ 4 h at which point solvents were evaporated off. The resulting residue was taken up in EtOAc (50 mL) and washed with brine (2×25 mL) and saturated aqueous $NaHCO_3$ (25 mL). The combined aqueous layer was extracted with EtOAc (50 mL). The combined organic layers were dried (Na_2SO_4), evaporated to dryness, and the resulting residue purified by column chromatography (0-5% MeOH in CH_2Cl_2, v/v) to afford nucleoside **5M** (200 mg, 80%) as a bright yellow solid material. R_f = 0.5 (6% MeOH in CH_2Cl_2, v/v); MALDI-HRMS *m/z* 800.2877 ($[M+Na]^+$, $C_{49}H_{39}N_5O_5{\cdot}Na^+$, Calc. 800.2849); ^{1}H NMR (500.1 MHz, DMSO-d_6) δ 8.60-8.63 (d, 1H, *J* = 9.0 Hz, Py), 8.27-8.46 (m, 7H, Py), 8.17-8.21 (t, 1H, *J* = 7.8 Hz, Py), 8.14 (s, 1H, H2), 7.59 (br s, 2H, ex, NH_2), 7.24-7.27 (m, 2H, DMTr), 7.08-7.14 (m, 7H, DMTr), 6.78 (dd, 1H, *J* = 7.5 Hz, 5.5 Hz, H1′), 6.63-6.67 (m, 4H, DMTr), 5.42 (d, 1H, ex, *J* = 5.0 Hz, 3′-OH), 4.69-4.74 (ap quintet, 1H, *J* = 5.7 Hz, H3′), 4.09 (ap q, 1H, *J* = 5.0 Hz, H4′), 3.614 (s, 3H, CH_3O), 3.606 (s, 3H, CH_3O), 3.52-3.59 (m, 1H, H2′), 3.15-3.19 (m, 2H, H5′), 2.43-2.49 (m, 1H, H2′); ^{13}C NMR (125.6 MHz, DMSO-d_6) δ 157.8, 156.0, 153.6 (C2), 148.9, 144.9, 135.7, 135.5, 133.5, 132.0, 131.8, 130.7, 130.3, 129.9 (Py), 129.5 (Ar), 129.2 (Py), 127.6 (DMTr), 127.5 (DMTr), 127.2 (Py), 127.0 (Py), 126.5 (Py), 126.4 (Ar), 126.3 (Ar), 125.0 (Py), 124.3 (Py), 123.5, 123.2, 119.5, 114.2, 112.83 (DMTr), 112.81 (DMTr), 93.4, 85.7 (C4′), 85.1, 84.8, 84.5 (C1′), 70.7 (C3′), 63.8 (C5′), 54.8 (CH_3O), 37.1 (C2′).

6-N-(N,N-methyl methylene), 8-ethynyl-5′-O-(4,4′-dimethoxytrityl) DNA-A (6L). *N,N*-dimethylformamide dimethyl acetal (0.13 mL, 0.96 mmol) was added to a solution of

nucleoside **5L** (0.25 g, 0.38 mmol) in anhydrous MeOH (5.0 mL) and the reaction mixture was stirred for 5 h at rt. All volatile components were evaporated and the resulting residue was taken up in ethyl acetate (50 mL) and subsequently washed with brine (2×25 mL) and saturated aqueous $NaHCO_3$ (25 mL). The organic layer was dried (Na_2SO_4), evaporated to dryness and the resulting residue purified by silica gel column chromatography (0-6% MeOH in CH_2Cl_2, v/v) to furnish nucleoside **6L** (200 mg, 83%) as an off-white solid material. R_f = 0.5 (6% MeOH in CH_2Cl_2, v/v); ESI-HRMS *m/z* 655.2653 ($[M+Na]^+$, $C_{36}H_{36}N_6O_5 \cdot Na^+$, calc. 655.2645); ^1H NMR (500.1 MHz, DMSO-d_6) δ 8.90 (s, 1H, $CH(NMe_2)$), 8.28 (s, 1H, H2), 7.27-7.30 (m, 2H, DMTr), 7.13-7.21 (m, 7H, DMTr), 6.78 (d, 2H, *J* = 9.0 Hz, DMTr), 6.73 (d, 2H, *J* = 9.0 Hz, DMTr), 6.48 (dd, 1H, *J* = 7.0 Hz, 6.0 Hz, H1′), 5.35 (br s, 1H, ex, 3′-OH), 5.00 (s, 1H, HC≡C), 4.61-4.68 (m, 1H, H3′), 3.98-4.03 (dd, 1H, *J* = 10.0 Hz, 4.5 Hz, H4′), 3.72 (s, 3H, CH_3O), 3.70 (s, 3H, CH_3O), 3.30-3.38 (m, 1H, H2′), 3.23 (s, 3H, CH_3N), 3.16-3.19 (m, 2H, H5′), 3.15 (s, 3H, CH_3N), 2.26-2.32 (m, 1H, H2′); ^{13}C NMR (125.6 MHz, DMSO-d_6) δ 157.91, 157.89 ($CH(NMe_2)$), 157.8, 152.3 (C2), 150.4, 144.9, 135.7, 135.6, 134.7, 129.6 (DMTr), 129.4 (DMTr), 127.6 (DMTr), 127.5 (DMTr), 126.4 (DMTr), 125.3, 112.93 (DMTr), 112.87 (DMTr), 87.7 (HC≡C), 85.8 (C4′), 85.1, 84.7 (C1′), 73.1, 70.8 (C3′), 63.7 (C5′), 54.92 (CH_3O), 54.89 (CH_3O), 40.8 (CH_3N), 36.5 (C2′), 34.7 (CH_3N).

6-N-(N,N-methyl methylene), 8-(2-(pyrenyl ethynyl)-5'-O-(4,4'-dimethoxytrityl) DNA-A (6M). *N*,*N*-dimethylformamide dimethyl acetal (0.18 mL, 1.35 mmol) was added to a solution of nucleoside **5M** (200 mg, 0.27 mmol) in anhydrous DMF (5.0 mL) and the reaction mixture was stirred at 50 °C for ~4 h. Volatile components were removed through evaporation and the resulting residue was taken up in ethyl acetate (50 mL) and washed with brine (2×25 mL) and saturated aqueous $NaHCO_3$ (25 mL). The organic layer was dried (Na_2SO_4), evaporated to

dryness and the resulting residue purified by silica gel column chromatography (0-5% MeOH in CH_2Cl_2, v/v) to furnish nucleoside **6M** (190 mg, 87%) as a bright yellow solid material. R_f = 0.5 (6% MeOH in CH_2Cl_2, v/v); MALDI-HRMS *m/z* 855.3301 ($[M+Na]^+$, $C_{52}H_{44}N_6O_6 \cdot Na^+$, calc. 855.3271); ^{1}H NMR (500.1 MHz, DMSO-d_6) δ 8.95 (s, 1H, CH(NMe_2)), 8.65-8.68 (d, 1H, *J* = 9.0 Hz, Py), 8.29-8.47 (m, 8H, H2, Py), 8.20 (t, 1H, *J* = 7.5 Hz, Py), 7.24-7.27 (m, 2H, DMTr), 7.06-7.14 (m, 7H, DMTr), 6.83 (dd, 1H, *J* = 7.0 Hz, 5.5 Hz, H1′), 6.66 (d, 2H, *J* = 9.0 Hz, DMTr), 6.63 (d, 2H, *J* = 9.0 Hz, DMTr), 5.42 (d, 1H, ex, *J* = 5.0 Hz, 3′-OH), 4.71-4.75 (ap quintet, 1H, *J* = 5.4 Hz, H3′), 4.11 (ap q, 1H, *J* = 5.0 Hz, H4′), 3.609 (s, 3H, CH_3O), 3.605 (s, 3H, CH_3O), 3.54-3.59 (m, 1H, H2′), 3.26 (s, 3H, CH_3N), 3.17-3.22 (m, 5H, CH_3N, H5′), 2.48-2.51 (m, 1H, H2′ - overlap with DMSO-d_6 signal); ^{13}C NMR (125.6 MHz, DMSO-d_6) δ 159.1, 157.8, 157.7 (CH(NMe_2)), 152.7 (C2), 150.8, 144.8, 135.58, 135.55, 135.3, 132.0, 131.9, 130.7, 130.3, 130.0 (Py), 129.6 (Ar), 129.5, 129.4 (Ar), 129.3 (Ar), 127.55 (DMTr), 127.47 (DMTr), 127.2 (Py), 127.0 (Py), 126.52 (Py), 126.45 (Ar), 126.35 (Ar), 126.0, 125.0 (Py), 124.4 (Py), 123.5, 123.2, 114.0, 112.82 (DMTr), 112.79 (DMTr), 94.0, 85.8 (C4′), 85.1, 84.9, 84.6 (C1′), 70.7 (C3′), 63.8 (C5′), 54.8 (CH_3O), 40.7 (CH_3N), 37.0 (C2′), 34.7 (CH_3N).

Representative protocol for synthesis of phosphoramidites. Nucleosides **2**, **6L** and **6M** were dried through co-evaporation with anhydrous 1,2-dichloroethane (2×10 mL) and dissolved in anhydrous CH_2Cl_2. To this was added anhydrous *N*,*N*-diisopropylethylamine (DIPEA) and 2-cyanoethyl *N*,*N*-diisopropylchlorophosphoramidite (PCl reagent) (quantities and volumes specified below) and the reaction was stirred at rt for ~3.5 h when analytical TLC indicated complete conversion. The reaction mixture was diluted with CH_2Cl_2 (25 mL), washed with 5% aqueous $NaHCO_3$ (2×10 mL) and the combined aqueous layers back-extracted with CH_2Cl_2 (2×10 mL). The combined organic layers were dried (Na_2SO_4), evaporated to dryness, and the

resulting residue purified by silica gel column chromatography (0-4% MeOH/CH_2Cl_2, v/v) and subsequent trituration from CH_2Cl_2 and petroleum ether to afford phosphoramidites **3L-3N**.

8-[2-(ethynyl)]-5'-O-(4,4'-dimethoxytrityl) DNA-A phosphoramidite (3L). Nucleoside **6L** (220 mg, 0.35 mmol) in anhydrous CH_2Cl_2 (5 mL), DIPEA (0.24 mL, 1.40 mmol) and PCl reagent (0.18 mL, 0.77 mmol) were mixed, reacted, worked up and purified as described above to provide phosphoramidite **3L** (210 mg, 72%) as a white foam. R_f = 0.5 (2% MeOH in CH_2Cl_2, v/v); MALDI-HRMS *m/z* 855.3746 ($[M+Na]^+$, $C_{45}H_{53}N_8O_6P{\cdot}Na^+$, calc. 855.3723); ^{31}P NMR (121.5 MHz, $CDCl_3$) δ 148.9, 148.5.

6-N-(N,N-methyl methylene), 8-(2-(pyrenyl ethynyl)-5'-O-(4,4'-dimethoxytrityl) DNA-A phosphoramidite (3M). Nucleoside **6M** (250 mg, 0.30 mmol) in anhydrous CH_2Cl_2 (5 mL), DIPEA (0.16 mL, 1.20 mmol) and PCl reagent (0.15 mL, 0.66 mmol) were mixed, reacted, worked up and purified as described above to provide phosphoramidite **3M** (200 mg, 64%) as a white foam. R_f = 0.5 (2% MeOH in CH_2Cl_2, v/v); MALDI-HRMS *m/z* 1055.4387 ($[M+Na]^+$, $C_{61}H_{61}N_8O_6P{\cdot}Na^+$, calc. 1055.4349); ^{31}P NMR (121.5 MHz, $CDCl_3$) δ 149.1, 148.7.

6-N-benzoyl,8-[3-(pyrene carboxamide)-1-propynyl]-5'-O-(4,4'-dimethoxytrityl)-DNA-A (3N). Nucleoside **2** (0.32 g, 0.34 mmol) in anhydrous CH_2Cl_2 (5 mL), DIPEA (0.24 mL, 1.36 mmol) and PCl reagent (0.17 mL, 0.75 mmol) were mixed, reacted, worked up and purified as described above to provide phosphoramidite **3N** (233 mg, 60%) as a white foam. R_f = 0.5 (2% MeOH in CH_2Cl_2, v/v); MALDI-HRMS *m/z* 1161.4421 ($[M+Na]^+$, $C_{67}H_{63}N_8O_8P{\cdot}Na^+$, calc. 1161.4404); ^{31}P NMR (121.5 MHz, $CDCl_3$) δ 148.6, 148.5.

Synthesis and purification of ONs. ONs were prepared on a DNA synthesizer (0.2 μmol scale) using succinyl linked LCAA-CPG (long chain alkyl amine controlled pore glass) columns with

500Å pore size. Standard protocols for incorporation of DNA phosphoramidites were used. A ~50-fold molar excess of modified phosphoramidites in anhydrous dichloromethane (0.05 M) was used along with extended oxidation (45s) and hand-coupling, which resulted in coupling yields greater than 95% (20 min, 5-(ethylthio)-1*H*-tetrazole as activator for incorporation of monomers **M** and **N**; 20 min, 4,5-dicyanoimidazole as activator for incorporation of monomers **W/X/L**; 20 min, 5-(bis-3,5-trifluromethylphenyl)-1H-tetrazole, for incorporation of monomers **Y** and **Z**). Cleavage from solid support and removal of nucleobase protecting groups was accomplished using 32% aqueous ammonia (55 °C, ~18 h). Crude 5′-DMTr-ONs were purified on HPLC (XTerra MS C18 column) using a 0.05 mM triethylammonium acetate buffer - 25% water/acetonitrile (v/v) gradient. Purified ONs were detritylated using 80% aqueous AcOH (20 min) and precipitated ($NaOAc/NaClO_4$/acetone, -18 °C). The identity of the synthesized ONs was verified through MS analysis recorded in positive ion mode on a quadrupole time-of-flight tandem mass spectrometer equipped with a MALDI source using anthranilic acid as a matrix (Table 20 and 21), while purity (>80% for **L/M/W/X/Y**-modified ONs and ≥75% for **N/Z**-modified ONs) was verified by ion-pair reverse phase HPLC running in analytical mode.

Thermal denaturation experiments. ON concentrations were estimated using the following extinction coefficients (OD/μmol) for DNA: dG (12.01), dA (15.20), T (8.40), dC (7.05); for RNA: rG (13.70), rA (15.40), U (10.00), rC (9.00); and for pyrene (22.4).[30] The strands comprising a given duplex were mixed and annealed. Thermal denaturation temperatures of duplexes (1.0 μM final concentration of each strand) were determined using a temperature-controlled UV/vis spectrophotometer and quartz optical cells with 1.0 cm path lengths. T_m's were determined as the first derivative maximum of thermal denaturation curves (A_{260} vs. T) recorded in medium salt buffer (100 mM NaCl, 0.1 mM EDTA, pH 7.0 adjusted with 10 mM

Na_2HPO_4 and 5 mM Na_2HPO_4). The temperature of the denaturation experiments ranged from at least 15 °C below T_m to 20 °C above T_m (although not below 5 °C). A temperature ramp of 0.5 °C/min was used in all experiments. Reported T_m's are reported as averages of two experiments within ± 1.0 °C.

Absorption spectroscopy. UV-vis absorption spectra were recorded at 5 °C using the same samples and instrumentation as in thermal denaturation experiments.

Fluorescence spectroscopy. Steady-state fluorescence emission spectra were recorded in non-deoxygenated thermal denaturation buffer (each strand used in 1.0 μM concentration) using an excitation wavelength of λ_{ex} = 380 nm, 340 nm, 385 nm and 350 nm for **Y**-, **Z**-, **M**- and **N**-modified ONs, respectively, and excitation slit 5.0 nm, emission slit 5.0 nm and a scan speed of 600 nm/min. Experiments were performed at temperature (5 °C).

6.5. Supporting information

General experimental section. Reagents and solvents were obtained from commercial suppliers and of analytical grade and were used without further purification. Petroleum ether of the distillation range 60-80 °C was used. Dichloromethane, 1,2-dichloroethane, Et_3N and *N,N′*-diisopropylethylamine were dried over activated molecular sieves (4Å). Anhydrous pyridine and DMF were obtained from commercial sources. Reactions were conducted under argon whenever anhydrous solvents were used, and monitored by TLC using silica gel plates coated with a fluorescence indicator (SiO_2-60, F-254). Plates were visualized under UV light and by dipping in 5% conc. H_2SO_4 in absolute ethanol (v/v) followed by heating. Silica gel column chromatography was performed with silica gel 60 (particle size 0.040–0.063 mm) using moderate pressure (pressure ball). Columns on DMTr-protected nucleosides were built in the listed starting eluent containing 0.5% v/v pyridine. Evaporation of solvents was carried out

under reduced pressure at temperatures below 45 °C. Following column chromatography, appropriate fractions were pooled, evaporated and dried at high vacuum for at least 12 h to give the obtained products in high purity (>95%) as ascertained by 1D NMR techniques. Chemical shifts of ^{1}H NMR, ^{13}C NMR and ^{31}P NMR are reported relative to deuterated solvent or other internal standards (80% phosphoric acid for ^{31}P NMR). Exchangeable (ex) protons were detected by disappearance of ^{1}H NMR signals upon D_2O addition. Assignments of NMR spectra are based on 2D spectra (HSQC, COSY) and DEPT spectra. Quaternary carbons are not assigned in ^{13}C NMR but their presence was verified from HSQC and DEPT spectra (absence of signals). MALDI-HRMS spectra of compounds were recorded on a Q-TOF mass spectrometer using 2,5-dihydroxybenzoic acid as a matrix and a mixture of polyethylene glycol (PEG 600 or PEG 1000) as internal calibration standards.

Table 20. MALDI-ToF MS of 9-mer nucleobase-functionalized and LNA-modified ONs.[a]

		(M+H)	
ON	**Sequence**	**CALC**	**OBS**
T2	5′-GTG **a**T**a** TGC	2809.5	2810.7
T3	5′-GT**g** ATA **t**GC	2809.5	2810.6
W1	5′-GTG A**W**A TGC	2762.5	2763.6
W2	5′-GTG **aWa** TGC	2818.5	2819.6
W3	5′-GT**g** A**W**A **t**GC	2818.5	2819.6
X1	5′-GTG A**X**A TGC	2791.5	2793.0
X2	5′-GTG **aXa** TGC	2847.5	2848.0
X3	5′-GT**g** A**X**A **t**GC	2847.5	2848.7
Y1	5′-GTG A**Y**A TGC	2964.7	2962.1
Y2	5′-GTG **aYa** TGC	3020.7	3019.6
Y3	5′-GT**g** A**Y**A **t**GC	3020.7	3020.0
Z1	5′-GTG A**Z**A TGC	3019.6	3020.7
Z2	5′-GTG **aZa** TGC	3075.5	3076.6
Z3	5′-GT**g** A**Z**A **t**GC	3075.5	3076.6

[a] For structures of monomers **W/X/Y/Z** see Figure 52 in main manuscript. LNA modifications are shown in lower case ("c" = 5-methylcytosine LNA monomer).

Table 21. MALDI-ToF MS of 9-mer nucleobase-functionalized and LNA-modified ONs.[a]

		(M+H)	
ON	**Sequence**	**CALC**	**OBS**
T5	5′-GCA **t**A**t** CAC	2739.5	2738.2
T6	5′-GC**a** TAT **c**AC	2752.5	2751.2
L4	5′-GCA T**L**T CAC	2706.5	2706.3
L5	5′-GCA **tLt** CAC	2775.0	2776.0
L6	5′-GC**a** T**L**T **c**AC	2761.5	2762.3
M4	5′-GCA T**M**T CAC	2907.7	2906.7
M5	5′-GCA **tMt** CAC	2977.0	2977.0
M6	5′-GC**a** T**M**T **c**AC	2964.7	2964.0
N4	5′-GCA T**N**T CAC	2962.6	2963.3
N5	5′-GCA **tNt** CAC	3033.6	3033.3
N6	5′-GC**a** T**N**T **c**AC	3018.6	3021.0

[a] For structures of monomers **L**/**M/N** see Figure 52 in main manuscript. LNA modifications are shown in lower case ("c" = 5-methylcytosine LNA monomer).

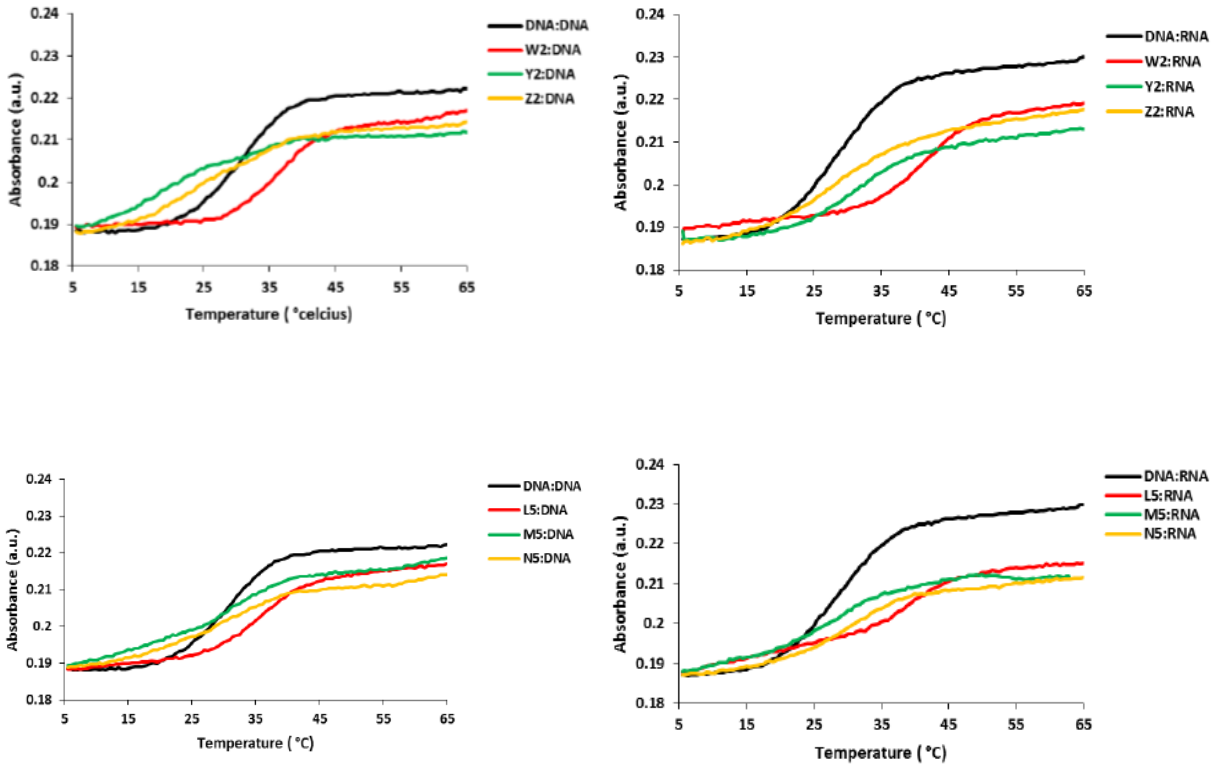

Figure 55. Representative thermal denaturation curves of duplexes between **W2**/**Y2**/**Z2**/**L5**/**M5**/**N5** and complimentary DNA (cDNA) or RNA (cRNA) targets. For experimental conditions, see Table 15.

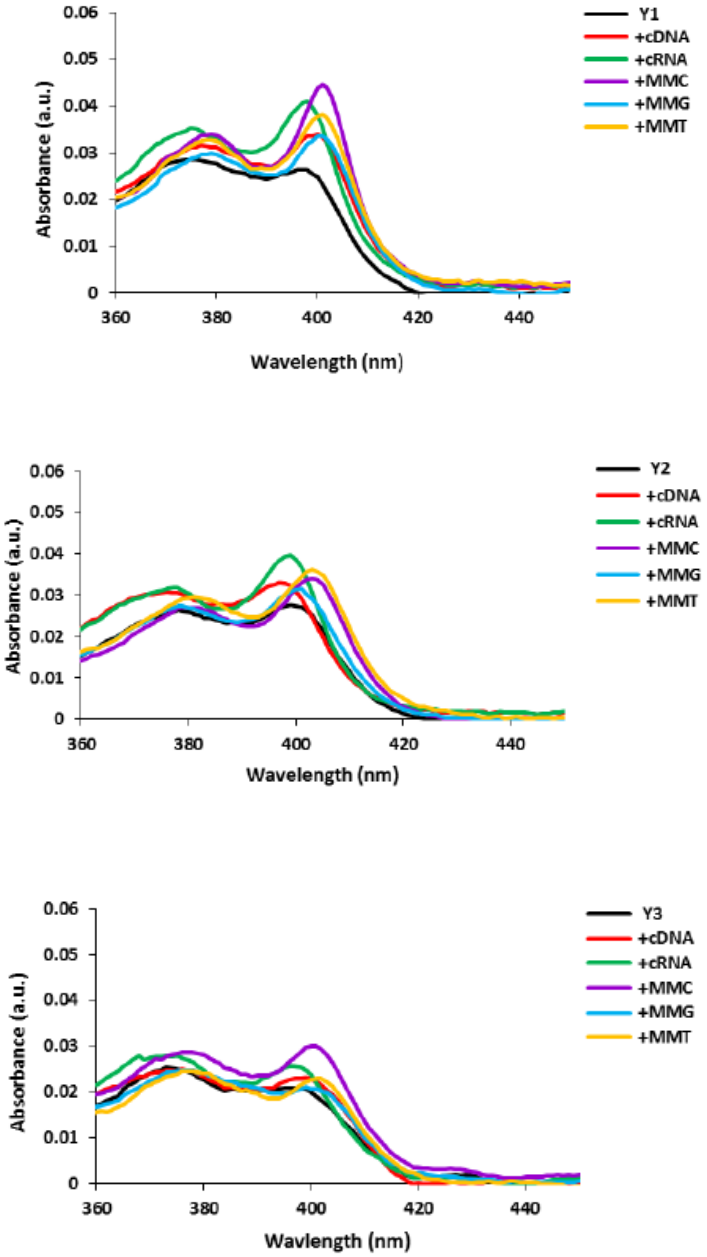

Figure 56. Absorption spectra of single-stranded **Y1**-**Y3** and the corresponding duplexes with complementary DNA/RNA or centrally mismatched DNA targets (mismatched nucleoside is specified). Spectra were recorded in T_m buffer at T = 5 °C using each strand at 1 μM concentration.

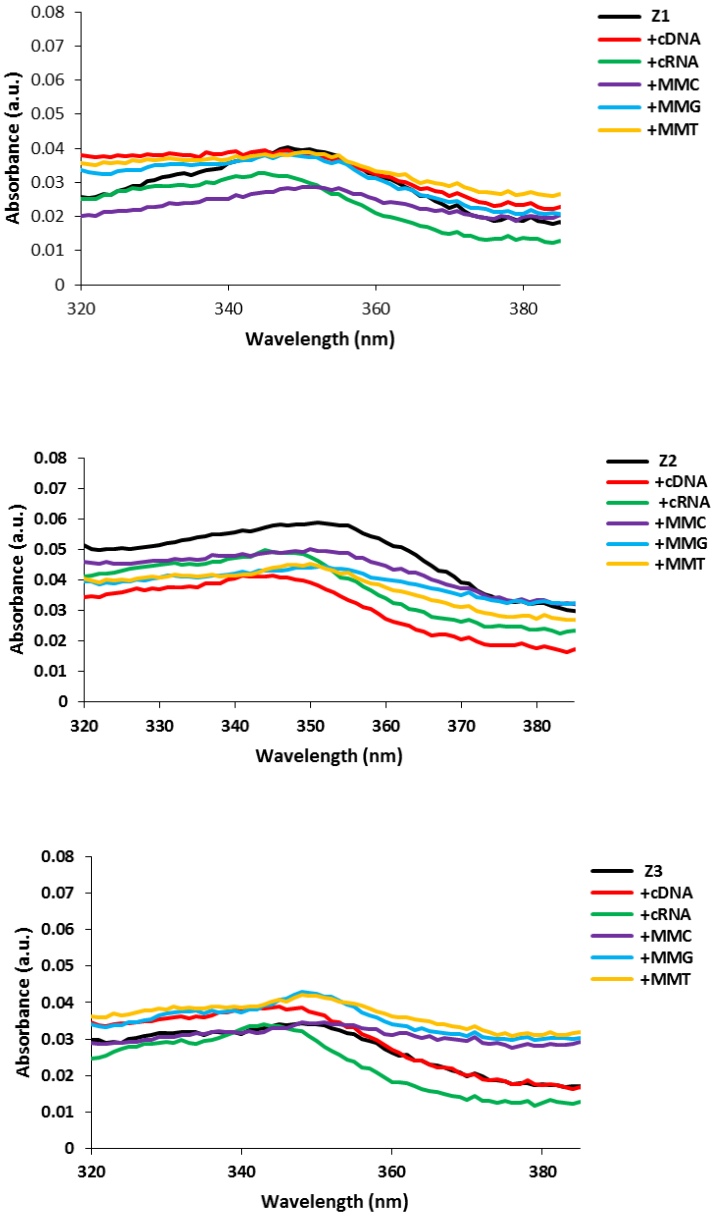

Figure 57. Absorption spectra of single-stranded **Z1**-**Z3** and the corresponding duplexes with complementary DNA/RNA or centrally mismatched DNA targets (mismatched nucleoside is specified). Spectra were recorded in T_m buffer at T = 5 °C using each strand at 1 μM concentration.

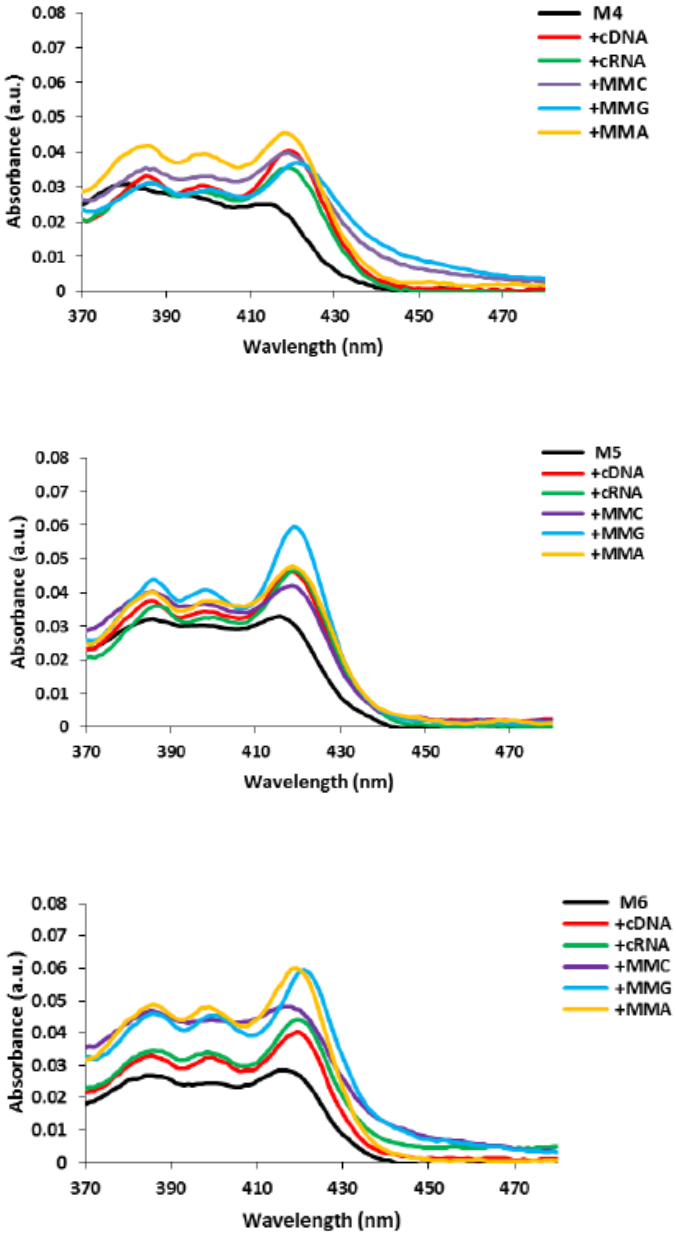

Figure 58. Absorption spectra of single-stranded **M4**-**M6** and the corresponding duplexes with complementary DNA/RNA or centrally mismatched DNA targets (mismatched nucleoside is specified). For experimental conditions, see Figure S20.

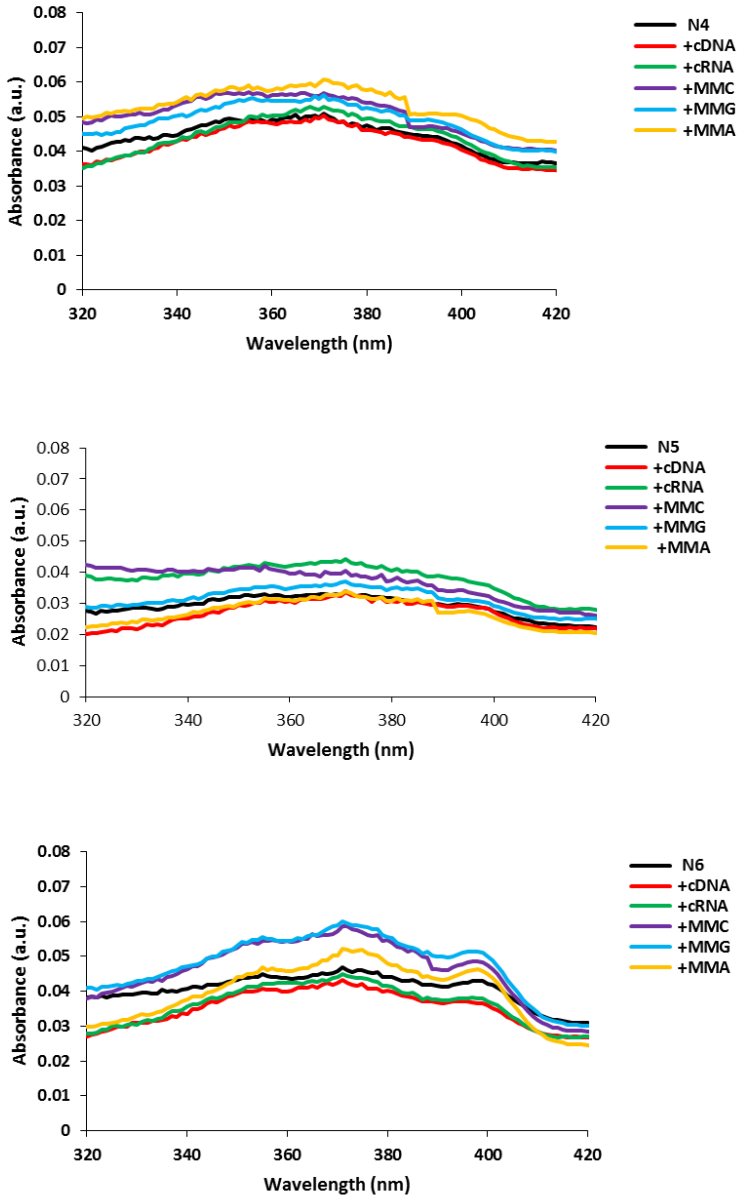

Figure 59. Absorption spectra of single-stranded **N4**-**N6** and the corresponding duplexes with complementary DNA/RNA or centrally mismatched DNA targets (mismatched nucleoside is specified). For experimental conditions, see Figure S20.

Biophysical characterization of 13-mer Y/M-modified ONs. Systematic studies of 13-mer ONs in which the C5- or C8-ethynylpyrene functionalized monomers **Y** or **M** are directly flanked by LNA nucleotides were performed (Table S8 and S9). Similar trends as in the 9-mer series were observed (see main manuscript).

Table 22. MALDI-ToF MS of 13-mer nucleobase-functionalized ONs.[a]

		(M+H)	
ON	**Sequence**	**CALC**	**OBS**
Y7	5′-CG CAA **aYa** AAC GC	4185.0	4184.0
Y8	5′-CG CAA **cYc** AAC GC	4232.7	4233.0
Y9	5′-CG CAA **gYg** AAC GC	4180.7	4182.0
Y10	5′-CG CAA **tYt** AAC GC	4200.0	4202.0
M11	3′-GCGTT **aMa** TTGCG	4249.7	4250.6
M12	3′-GCGTT **cMc** TTGCG	4299.7	4300.0
M13	3′-GCGTT **gMg** TTGCG	4247.7	4248.0
M14	3′-GCGTT **tMt** TTGCG	4267.8	4268.5

[a] Lower case letters denote canonical LNA monomers (**c** = 5-methylcytosine LNA). For structures of monomers **Y** and **M**, see Figure 52 in main manuscript.

Table 23. Thermal denaturation data for duplexes between **Y**-modified ONs and complementary or singly mismatched DNA targets.

			T_m/°C	ΔT_m/°C		
ON	Sequence	**B** =	**A**	**C**	**G**	**T**
Y7	5′-CG CAA **aYa** AAC GC 3′-GC GTT T**B**T TTG CG		45.0	0.0	+1.0	+1.0
Y8	5′-CG CAA **cYc** AAC GC 3′-GC GTT G**B**G TTG CG		57.0	-5.0	-2.0	-6.0
Y9	5′-CG CAA **gYg** AAC GC 3′-GC GTT C**B**C TTG CG		49.0	0.0	-8.0	-3.0
Y10	5′-CG CAA **tYt** AAC GC 3′-GC GTT A**B**A TTG CG		45.5	-1.0	-1.0	-3.0

[a] For experimental conditions, see Table 15 in main manuscript. T_m's of the corresponding unmodified matched duplexes are TAT (48.5 °C), GAG (55.5 °C), CAC (55.0 °C), AAA (48.5 °C), respectively. ΔT_m = change in T_m's relative to fully matched duplex (**B** = A).

Table 24. Thermal denaturation data for duplexes between **M**-modified ONs and complementary or singly mismatched DNA targets.

			T_m/°C	ΔT_m/°C		
ON	Sequence	**B** =	**T**	**A**	**C**	**G**
M11	5′-CGCAA T**B**T AACGC 3′-GCGTT **aMa** TTGCG		41.0	-0.5	+2.5	-0.5
M12	5′-CGCAA G**B**G AACGC 3′-GCGTT **cMc** TTGCG		54.0	-1.5	-2.5	-1.5
M13	5′-CGCAA C**B**C AACGC 3′-GCGTT **gMg** TTGCG		47.0	+1.5	+2.5	-3.5
M14	5′-CGCAA A**B**A AACGC 3′-GCGTT **tMt** TTGCG		42.0	-1.5	-0.5	+1.5

[a] For experimental conditions, see Table 15 in main manuscript. T_m's of the corresponding unmodified matched duplexes are TTT (48.5 °C), GTG (55.0 °C), CTC (55.5 °C), AAA (48.5 °C), respectively. ΔT_m = change in T_m's relative to fully matched duplex (**B** = T).

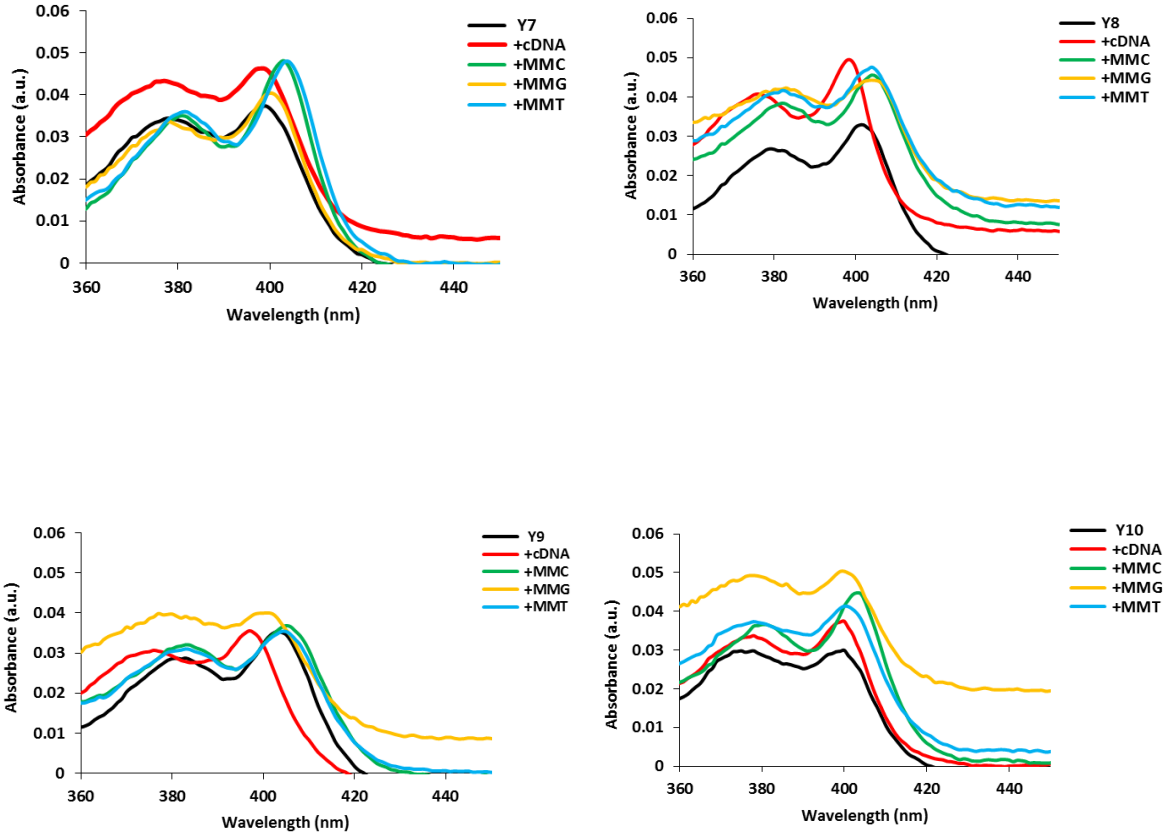

Figure 60. Absorption spectra of 13-mer **Y**-modified ONs and the corresponding duplexes with complementary or centrally mismatched DNA targets (nucleoside opposite of monomer **Y** is specified). Spectra were recorded in T_m buffer at T = 5 °C using each strand at 1 μM concentration.

Table 25. Absorption maxima of 13-mer **Y**-modified ONs in the presence or absence of complementary or singly mismatched DNA targets (nucleoside opposite of monomer **Y** is specified).

		λ_{max}/nm ($\Delta\lambda_{max}$)				
ON	**Sequence**	**SSP**	**+M (A)**	**+MM (C)**	**+MM (G)**	**+MM (T)**
Y7	5′-CG CAA **aYa** AAC GC 3′-GC GTT T**B**T TTG CG	399	-1	+4	+1	+5
Y8	5′-CG CAA **cYc** AAC GC 3′-GC GTT G**B**G TTG CG	402	-4	+2	+2	+2
Y9	5′-CG CAA **gYg** AAC GC 3′-GC GTT C**B**C TTG CG	403	-6	+2	-1	+1
Y10	5′-CG CAA **tYt** AAC GC 3′-GC GTT A**B**A TTG CG	400	+0	+4	±0	±0

[a] Recorded in T_m buffer at T = 5 °C using 1.0 μM of each strand.

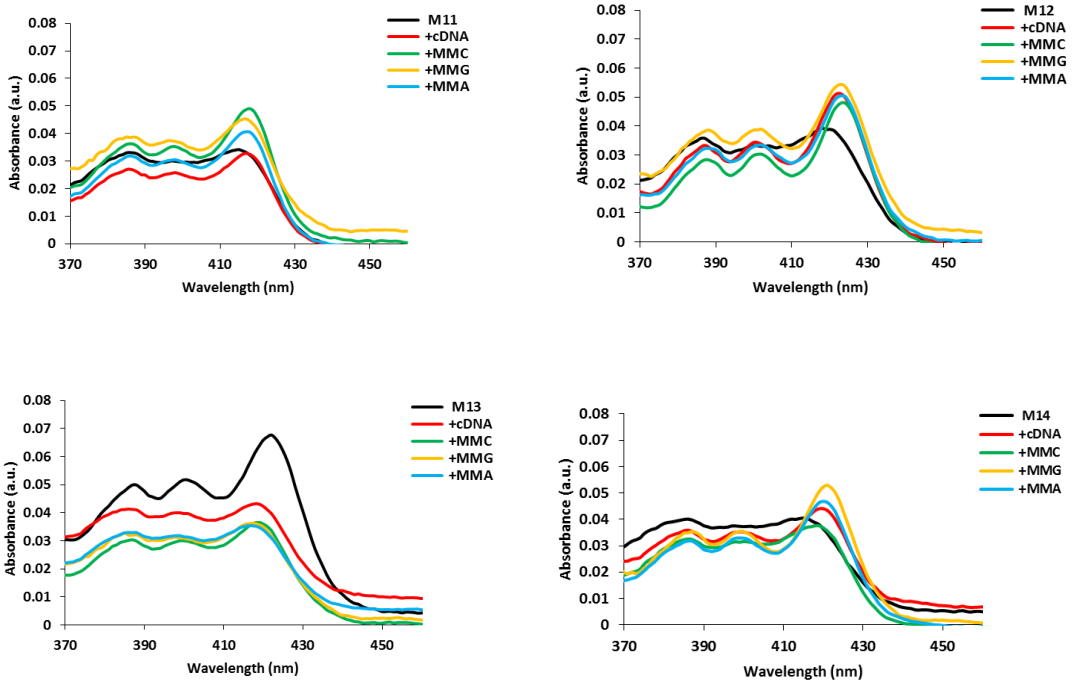

Figure 61. Absorption spectra of 13-mer **M**-modified ONs and the corresponding duplexes with complementary or centrally mismatched DNA targets (nucleoside opposite of monomer

M is specified). Spectra were recorded in T_m buffer at T = 5 °C using each strand at 1 μM concentration.

Table 26. Absorption maxima of 13-mer **M**-modified ONs in the absence (SSP) or presence of complementary or singly mismatched DNA targets (nucleoside opposite of monomer **M** is specified).[a]

		λ_{max}/nm ($\Delta\lambda_{max}$)				
ON	**Sequence**	**SSP**	**+M (T)**	**+MM (C)**	**+MM (G)**	**+MM (A)**
M11	3′-GCGTT **aMa** TTGCG 5′-CGCAA T**B**T AACGC	415	+2	+3	+2	+2
M12	3′-GCGTT **cMc** TTGCG 5′-CGCAA G**B**G AACGC	418	+4	+5	+5	+5
M13	3′-GCGTT **gMg** TTGCG 5′-CGCAA C**B**C AACGC	422	-4	-3	-5	-5
M14	3′-GCGTT **tMt** TTGCG 5′-CGCAA A**B**A AACGC	415	+4	+3	+3	+5

[a] Recorded in T_m buffer at T = 5 °C using 1.0 μM of each strand.

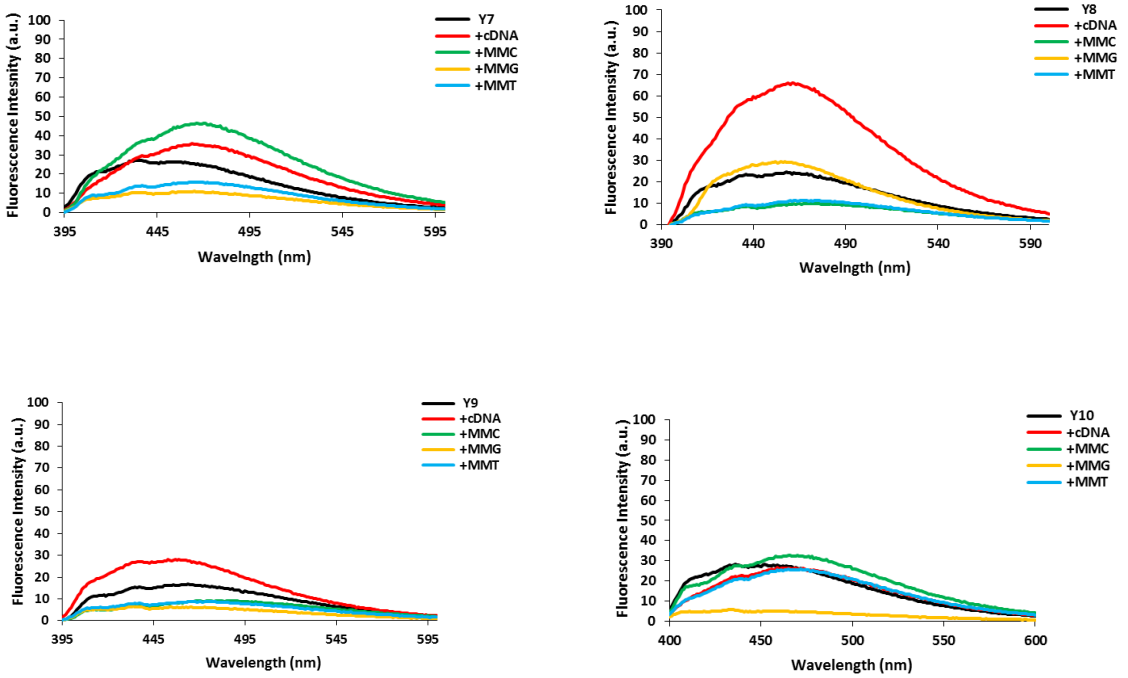

Figure 62. Steady-state fluorescence emission spectra of 13-mer **Y**-modified ONs in the presence or absence of complementary or centrally mismatched DNA targets (mismatched nucleoside opposite of monomer **Y** is specified). Spectra were recorded in T_m buffer at T = 5 °C using each strand at 1 µM concentration and λ_{ex} = 380 nm.

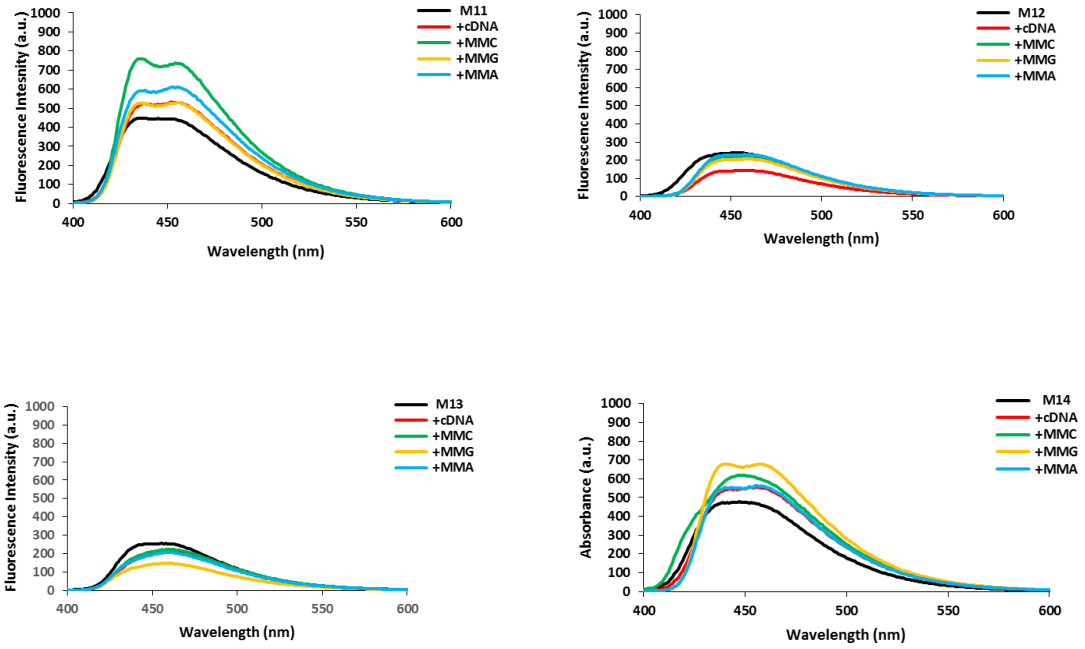

Figure 63. Steady-state fluorescence emission spectra of 13-mer **M**-modified ONs in the presence or absence of complementary or centrally mismatched DNA targets (mismatched nucleoside opposite of monomer **M** is specified). Spectra were recorded in T_m buffer at T = 5 °C using each strand at 1 µM concentration, λ_{ex} = 385 nm.

6.6. References.

1. a) Torigoe, H.; Hari, Y.; Sekiguchi, M.; Obika, S.; Imanishi, T. *J. Biol. Chem*. **2001**, *276*, 2354-2360; b) Braasch, D. A.; Corey, D. R. *Biochemistry*. **2001**, *41*, 4503-4510.

2. a) Tolstrup, N.; Nielsen, P. S.; Kolberg, J. G.; Frankel, A. M.; Vissing, H.; Kauppinen, S. *Nucleic Acids Res*. **2003**, *31*, 3758-3762; b) Umemoto, T.; Hrdlicka, P. J.; Babu, R. B.; Wengel, J. *ChemBioChem*. **2007**, *8*, 2240-2248.

3. a) Wengel, J. *Acc. Chem. Res*. **1998**, *32*, 301-310; b) Koshkin, A. A.; Neilsen, P.; Meldgaard, M.; Rajwanshi, V. K.; Singh, S. K.; Wengel, J. *J.Am.Chem.Soc*. **1998**, *120*, 13252-13253; b) Obika, S.; Nanbu, D.; Hari, Y.; Morio, K.; In, Y.; Ishida, T.; Imanishi, T. *Tetrahedron Lett*. **1997**, *38*, 8735-8739.

4. Petersen, M.; Nielsen, C. B.; Nielsen, K. E.; Jensen, G. A.; Bondensgaard, K.; Singh, S. K.; Rajwanshi, V. K.; Koshkin, A. A.; Dahl, B. M.; Wengel, J.; Jacobsen, J. P. *J. Mol. Recognit*. **2000**, *13*, 44-53.

5. Bondensgaard, K.; Petersen, M.; Singh, S. K.; Rajwanshi, V. K.; Kumar, R.; Wengel, J.; Jacobsen, J. P. *Chem. Eur. J*. **2000**, *6*, 2687-2695.

6. Egli, M.; Minasov, G.; Teplova, M.; Kumar, R.; Wengel, J. *J. Chem. Soc. Chem. Commun*. **2001**, *7*, 651-652.

7. Kaur, H.; Babu, B. R.; Maiti, S. *Chem. Rev*. **2007**, *107*, 4672-4697.

8. McTigue, P. M.; Peterson, R. J.; Kahn, J. D. *Biochemistry*. **2004**, *43*, 5388-5405.

9. Prakash, P. T.; Siwkowski, A.; Allerson, R. C.; Migawa, M. T.; Lee, S.; Gaus, H. J.; Black, C.; Seth, P. P.; Swayze, E. E.; Bhat, B. *J. Med. Chem*. **2010**, *53*, 1636-1650.

10. Østergaard, M. E.; Kumar, P.; Baral, B.; Raible, D. J.; Kumar, T. S.; Anderson, B. A.; Guenther, D. C.; Deobald, L.; Paszczynski, A. J.; Sharma, P. K.; Hrdlicka, P. J. *ChemBioChem*. **2009**, *10*, 2740-2743.

11. Kumar, P.; Østergaard, M. E.; Baral, B.; Anderson, B. A.; Guenther, D. C.; Kaura, M.; Raible, D. J.; Sharma, P. K.; Hrdlicka, P. J. *J. Org. Chem*. **2014**, *79*, 5047-5061.

12. Kaura, M.; Kumar, P.; Hrdlicka, P. J. *J. Org. Chem*. **2014**, *79*, 6256-6268.

13. Kaura, M.; Guenther, D. C.; Hrdlicka, P. J. *Org. Lett*. **2014**, *16*, 3308-3311.

14. Kumar, S. T.; Kumar, P.; Sharma, P. K.; Hrdlicka, P. J. *Tetrahedron Lett*. **2008**, *49*, 7168-7170.

15. Hurley, D. J.; Tor, Y. *J. Am. Chem. Soc*. **1998**, *120*, 2194-2195.

16. Cruickshank, K. A.; Stockwell, D. L.; *Tetrahedron lett*. **1988**, *29*, 5221-5224.

17. Malakhov, A. D.; Malakhova, E. V.; Kuznitsova, S. V.; Grechishnikova, I. V.; Prokhorenko, I. A.; Skorobogatyi, M. V.; Korshun, V. A.; Berlin, Yu. A. *Russ. J. Bioorg. Chem.* **2000**, *26*, 34-44.

18. Okamoto, A.; Kanatani, K.; Saito, I. *J. Am. Chem. Soc*. **2004**, *126*, 4820-4827.

19. Clima, L.; Bannwarth, W. *Helv. Chim. Acta*, **2008**, *91*, 165-175.

20. Tierney, M. T.; Grinstaff, M. W. *Org. Lett*. **2000**, *2*, 3413-3416.

21. Okamoto, A.; Kanatani, K.; Saito, I. *J. Am. Chem. Soc*. **2004**, *126*, 4820-4827.

22. Ti, G. S.; Gaffney, B. L.; Jones, R. A. *J. Am. Chem. Soc*. **1982**, *104*, 1316-1319

23. McBride, L. J.; Kierzek, R.; Beaucage, S. L.; Caruthers, M. H. *J. Am.Chem. Soc*. **1986**, *108*, 2040-2048.

24. Singh, S. K.; Nielsen, P.; Koshkin, A. A.; Wengel, J. *Chem. Commun*. **1998**, 455-456.

25. a) Bijapur, J.; Keppler, M. D.; Bergqvist, S.; Brown, T.; Fox, K. R. *Nucleic Acids Res*. **1999**, *27*, 1802-1809; b) Heystek, L. E.; Zhou, H. Q.; Dande, P.; Gold, B. *J. Am. Chem. Soc*. **1998**, *120*, 12165-12166; c) Seela, F.; Ramzaeva, N.; Leonard, P.; Chen, Y.; Debelak, H.; Feiling, E.; Kroschel, R.; Zulauf, M.; Wenzel, T.; Frohlich, T.; Kostrzewa, M. *Nucleos. Nucleot. Nucl*. **2001**, *20*, 1421-1424.

26. Sørensen, M. D.; Petersen, M.; Wengel, J. *Chem. Commun*. **2003**, 2130-2131.

27. a) Asanuma, H.; Fujii, T.; Kato, T.; Kashida, H. *J. Photochem. Photobiol*. **2012**, *13*, 124-135; b) Nakamura, M.; Fukunaga, Y.; Sasa, K.; Ohtoshi, Y.; Kanaori, K.; Hayashi, H.; Nakano, H.; Yamana, K. *Nucleic Acids Res*. **2005**, *33*, 5887-5895.

28. a) Mayer, E.; Valis, L.; Wagner, C.; Rist, M.; Amann, N.; Wagenknecht, H.-A. *Chem Bio Chem*. **2004**, *5*, 865-868; b) Saito, Y.; Hanawa, K.; Motegi, K.; Omoto, K.; Okamoto, A.; Saito, I. *Tetrahedron Lett*. **2005**, *46*, 7605-7608; c) Matsumoto, K.; Takahashi, N.; Suzuki, A.; Morii, T.; Saito, Y.; Saito, I. *Bioorg. Med. Chem. Lett*. **2011**, *21*, 1275-1278. d) Dierckx, A.; Diner, P.; El-Sagheer, A. H.; Kumar, J. D.; Brown, T.; Grøtli, M.; Wilhelmsson, L. M. *Nucleic Acids Res*. **2011**, *39*, 4513-4524. e) Suzuki, A.; Takahashi, N.; Okada, Y.; Saito, I.; Nemoto, N.; Saito, Y. *Bioorg. Med. Chem. Lett*. **2012**, *22*, 886-892.

29. Wu, W.; Wu, W.; Ji, S.; Guo, H.; Zhao, J. *Eur. J. Inorg. Chem*. **2010**, 4470-4482.

30. Kumar, T. S.; Madsen, A. S.; Østergaard, M. E.; Sau, S. P.; Wengel, J.; Hrdlicka, P. J. *J. Org. Chem*. **2009**, *74*, 1070-1081.

Chapter 7.0: Synthesis and Hybridization Properties of Oligonucleotides Modified with 5-(1-Aryl-1,2,3-Triazol-4-yl)-2'-Deoxyuridines

The following paper by **Kaura**, **M**.; Kumar, P and Hrdlicka, P. J. was published in *Org. Biomol. Chem.* **2012**, *10*, 8575-8578.

Abstract: Oligonucleotides modified with consecutive incorporations of 5-(1-aryl-1,2,3-triazol-4-yl)-2'-deoxyuridine monomers X-Z display high thermal affinity and binding specificity toward RNA targets, due to formation of chromophore arrays in the major groove.

7.1. Introduction.

The use of nucleic acids as scaffolds for organization of chromophore arrays is an area of considerable focus, which is fuelled by the promise for materials with interesting photophysical and electronic properties.[1-6] A frequently employed approach toward this end entails self-assembly of duplexes involving oligonucleotides (ONs), which are densely modified with chromophore-functionalized nucleotide monomers. Specific examples of building blocks include monomers where chromophores replace nucleobase moieties[7-9] or are attached to non-nucleosidic linkers,[10,11] sugar skeletons[12-14] or nucleobase moieties. Among the latter, C5-functionalized pyrimidine monomers in which chromophores are either directly attached to the nucleobase moiety or attached via an alkynyl linker, have been studied in particular detail and demonstrated to facilitate array formation in the major groove.[15-19] While array formation often partially counteracts the prominent duplex destabilization caused by these monomers, the resulting duplexes still only display moderate thermostability. Development of nucleotide building blocks, which enable formation of chromophore arrays in the major groove without compromising duplex thermostability, therefore remains a desirable goal.

Nielsen and coworkers have recently demonstrated that ONs, which are consecutively modified with 5-(1-phenyl-1,2,3-triazol-4-yl)-2'-deoxyuridine monomers, display strong and highly specific affinity toward RNA targets due to the formation of stabilizing chromophore arrays in the major groove.[20-22] While the influence of phenyl substitution on array formation has been studied in detail,[21,23] the question how the size of the aromatic moiety influences stacking efficiency and thermostability, has not been systematically addressed. Following a hypothesis that chromophores with larger aromatic surfaces are likely to result in stronger stacking interactions in the spacious major groove, we set out to study the hybridization properties of ONs, which are modified with 5-(1-aryl-1,2,3-triazol-4-yl)-2'-deoxyuridine monomers X-Z featuring three differentially sized aromatic moieties at the 1-position of the triazole ring (Figure. 64).

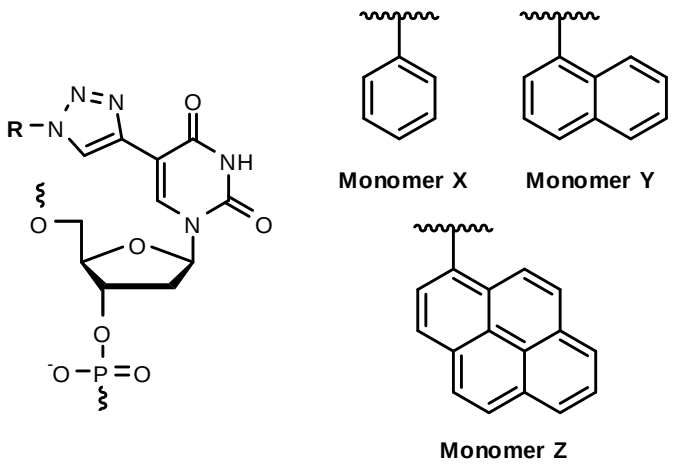

Figure 64. Structures of 5-(1-aryl-1,2,3-triazol-4-yl)-2'-deoxyuridines studied herein.

7.2. Results and Discussion.

Phosphoramidites 3X and 3Y were obtained via the same general strategy, which we recently used for the synthesis of 3Z (Scheme 8).[24] Thus, O5'-protected 5-ethynyl-2'-deoxyuridine 1[25] was reacted with azidobenzene[26] or 1-azidonapthalene[27] in a CuI catalyzed [3+2] azide-alkyne

cycloaddition[28] to afford nucleosides 2X and 2Y in 74% and 78% yield. Subsequent O3'-phosphitylation using 2-cyanoethyl-N,N'-diisopropylchlorophosporamidite (i.e., PCl-reagent) and N,N'-diisopropylethylamine (DIPEA), provided 5-(1-aryl-1,2,3-triazol-4-yl)-2'-deoxyuridine phosphoramidites 3X[20] and 3Y in 60% and 73% yield, respectively.

The phosphoramidites were incorporated into ONs via machine-assisted solid-phase DNA synthesis (hand-coupling 20 min, 4,5-dicyanoimidazole as activator; coupling yields >95%, >95% and ~92% for monomers X, Y and Z, respectively). The composition and purity of the modified ONs was verified by MALDI-ToF MS analysis (Table 29) and ion-pair reverse-phase HPLC, respectively.

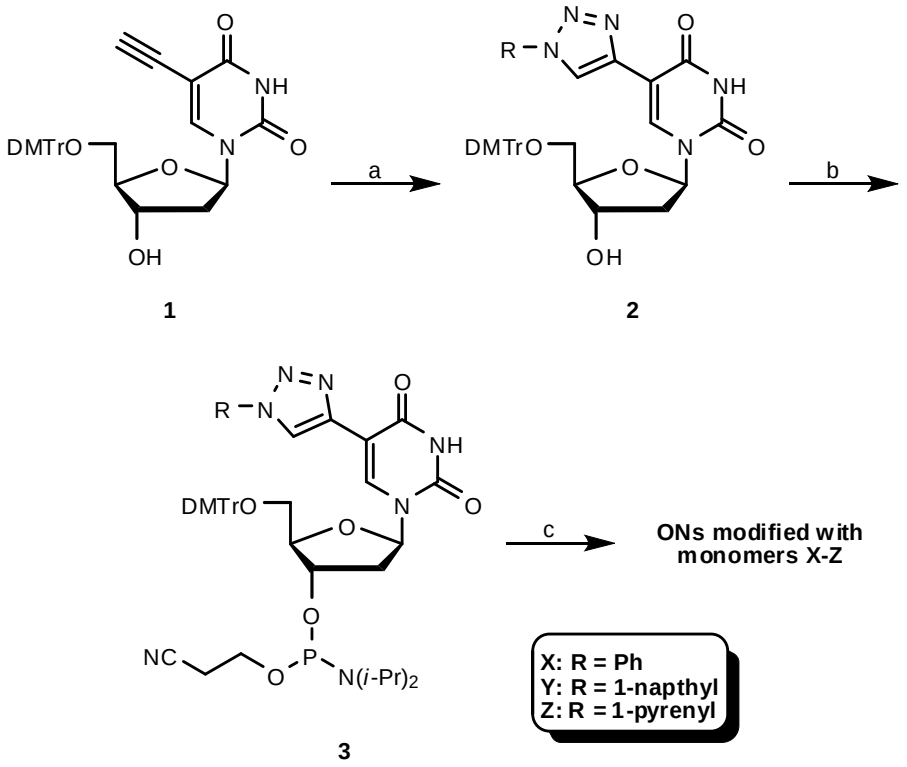

Scheme 8. a) RN_3, aq. sodium ascorbate, aq. $CuSO_4$, THF:H_2O:tBuOH, rt (2X: 74%; 2Y: 78%; 2Z[24]: 52%); b) PCl-reagent, DIPEA, CH_2Cl_2, rt (3X: 60%; 3Y: 73%; 3Z[24]: 73%); c) machine-assisted DNA synthesis. R = phenyl, 1-napthyl and 1-pyrenyl for X-, Y- and Z-series, respectively.

Monomers X-Z were incorporated once, twice or four times into a 9-mer T-rich sequence that has been used to study and prepare self-assembling chromophore arrays.[20] Thermal denaturation temperatures (T_m's) of duplexes between modified ONs and complementary DNA/RNA targets were determined in buffers of high or medium ionic strength (Tables 27 and 30‡, respectively).

Singly modified ONs display substantially lower thermal affinity toward DNA and RNA complements than corresponding unmodified ONs (see ΔT_m's for B1-series, Table 27), which is commonly observed for ONs modified with C5-chromophore-functionalized pyrimidine monomers.[15,16,29-31] Duplex thermostability decreases progressively as the size of the aryl substituent increases, most likely due to increased perturbation of the hydration spine in the major groove. Incorporation of two 5-(1-aryl-1,2,3-triazol-4-yl)-2'-deoxyuridine monomers as next-nearest neighbors, results in further duplex destabilization, although the energetic penalty associated with monomer Y is partially reversed (see ΔT_m/mod for B2-series, Table 27). In contrast, incorporation of two or four consecutive X or Y monomers strongly reverses duplex destabilization, especially in X-modified duplexes with RNA targets (compare ΔT_m/mod trends for X1→X3→X4 and Y1→Y3→Y4, Table 13). Interestingly, Z4, which features four consecutive incorporations of monomer Z, displays very high affinity toward RNA as well as DNA targets (see ΔT_m/mod for Z4, Table 27) although broad transitions are observed (Figs. 66-69)‡.

Computational studies have previously linked the increased thermostability of X4:RNA to formation of chromophore arrays in the major groove.[21] This, combined with the observed Tm trends for Y/Z-modified duplexes, suggests that 5-(1-aryl-1,2,3-triazol-4-yl) moieties are predisposed toward formation of stabilizing chromophore arrays. The inherently destabilizing

effect of 5-(1-aryl-1,2,3-triazol-4-yl)-2'-deoxyuridine monomers, is counteracted by energetically favorable hydrophobic interactions between chromophores upon array formation. However, the complex relationship between duplex/array stability and size/hydrophobicity of the aryl moiety is not fully understood (trend in ΔT_m/mod values: Z4≥X4>Y4).

Table 27. Thermal denaturation temperatures (T_m values) for duplexes between B1-B4 and complementary DNA/RNA in high salt buffer.[a]

			T_m (ΔT_m/mod) [°C]					
			DNA 3'-CAC AAA ACG			RNA 3'-CAC AAA ACG		
ON	Sequence	B =	**X**	**Y**	**Z**	**X**	**Y**	**Z**
B1	5'-GTGT **B** TTGC		35.5 [-4.5]	32.0 [-8.0]	25.0[b] [-15.0]	35.0 [-3.0]	29.0 [-9.0]	25.0[b] [-13.0]
B2	5'-GTG **B**T**B** TGC		28.5 [-5.8]	27.5 [-6.3]	-	29.5 [-4.3]	29.5 [-4.3]	-
B3	5'-GTGT **BB** TGC		32.5 [-3.8]	29.5 [-5.8]	-	40.0 [+1.0]	32.0 [-3.0]	-
B4	5'-GTG **BBBB** GC		38.0 [-0.5]	26.0[b] [-3.5]	52.5[b] [+3.0]	55.0 [+4.3]	39.0 [+0.3]	55.5[b] [+4.4]

[a] T_m's determined as the first derivative maximum of thermal denaturation curves (A_{260} vs T) recorded in high salt buffer ($[Na^+]$ = 710 mM, $[Cl^-]$ = 700 mM, pH 7.0 (adjusted with NaH_2PO_4/Na_2HPO_4), using 1.0 µM of each strand. T_m's are averages of at least two measurements within 1.0 °C. ΔT_m/mod = change in T_m's per modification relative to unmodified reference duplexes (+DNA complement: T_m = 40.0 °C; +RNA complement: T_m = 38.0 °C). "-" denotes no transition. [b] weak/broad transition.

Next, the thermostability of duplexes between B1- or B4-series ONs and RNA targets featuring a centrally mismatched nucleotide was determined to study the binding specificity of these probes (Table 28). Singly modified ONs display mismatch discrimination profiles that differ from the corresponding unmodified ONs in the following manner: i) X1 and Y1 display less efficient discrimination of U-mismatches; ii) Z1 displays markedly poorer discrimination of rC-

mismatches, and iii) X1 and Z1 display improved discrimination of rG-mismatches (Table 28). More interestingly, the target specificity of X4, Y4 and, possibly, Z4 is markedly improved relative to their singly modified counterparts (compare ΔT_m for B4- vs B1-series, Table 28). In fact, X4 and Y4 display base pairing fidelity that compares favorably with the unmodified reference strand, suggesting that chromophore arrays have beneficial impacts on target affinity as well as target specificity. Interestingly, while ONs with stretches of 5-ethynyl-2'-deoxyuridine monomers are known to display improved target specificity due to long-range cooperativity,[32] ONs with stretches of C5-chromophore-functionalized 2'-deoxyuridine monomers typically display poor mismatch discrimination.[15,17]

Table 28. T_m values for duplexes between B1/B4-series and centrally mismatched RNA targets.[a]

			RNA: 3'-CAC A**M**A ACG			
			T_m / °C	ΔT_m / °C		
ON	Sequence	**M** =	**A**	**C**	**G**	**U**
D1	5'-GTGTTTTGC		38.0	-14.0	-6.0	-20.0
X1	5'-GTGT **X** TTGC		35.0	-14.5	-11.0	-13.0
X4	5'-GTG **XXXX** GC		55.0	-20.0	-13.5	-20.0
Y1	5'-GTGT **Y** TTGC		29.0	-11.0	-7.0	-12.5
Y4	5'-GTG **YYYY** GC		39.0	-13.5	-7.0	-22.0
Z1	5'-GTGT **Z** TTGC		25.0	-3.0[b]	<-10.0[c]	<-10.0[c]
Z4	5'-GTG **ZZZZ** GC		55.5	-12.5[b]	-12.5[b]	-12.5[b]

[a] For conditions of thermal denaturation experiments, see Table 27. ΔT_m = change in T_m relative to matched DNA:RNA duplex (M = A).[b] Weak transition. [c] No transition above 15 °C.

The following structural model accounts for the observed trends (Fig. 65): i) hybridization of X4/Y4/Z4 with complementary RNA targets results in the formation of a stabilizing chromophore array in the major groove, whereas ii) hybridization with mismatched targets results in array disruption, reduced duplex stability and improved mismatch specificity.

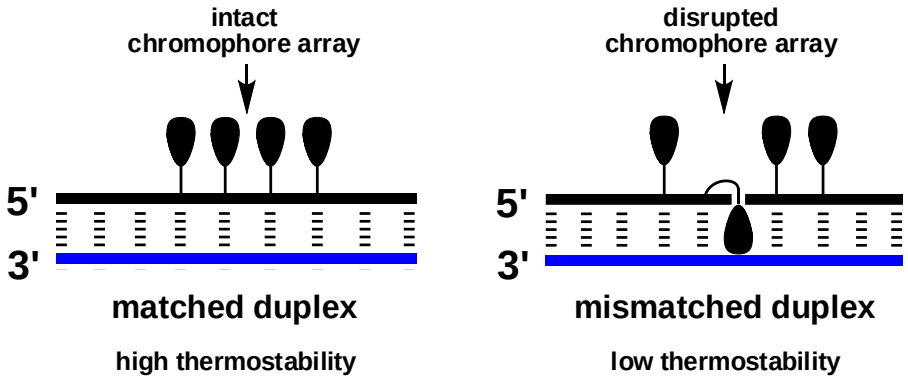

Figure 65. Proposed structural model rationalizing increased affinity and specificity of ONs modified with four consecutive 5-(1-aryl-1,2,3-triazol-4-yl)-2'-deoxyuridine monomers.

7.3. Conclusion.

In summary, we demonstrate that ONs with stretches of 5-(1-aryl-1,2,3-triazol-4-yl)-2'-deoxyuridine monomers, display improved RNA affinity and specificity relative to reference strands, presumably due to formation of stabilizing chromophore arrays in the major groove. This design principle is likely to have important implications in the design of supramolecular nucleic acid based π-functional materials and antisense ONs.

Acknowledgements

We appreciate support from Idaho NSF EPSCoR and the BANTech Center (Univ. Idaho). We thank Drs. Lee Deobald and Sujay P. Sau (both Univ. Idaho) for mass spectrometric analyses.

7.4. Supporting information.

General experimental section. Unless otherwise noted, reagents and solvents were commercially available, of analytical grade and used without further purification. Petroleum ether of the distillation range 60-80 °C was used. Dicholoromethane, 1,2-dichloroethane and *N,N'*-diisopropylethylamine were dried over activated molecular sieves (4Å). Reactions were monitored by TLC using silica gel coated plates with a fluorescence indicator (SiO_2-60, F-254) which were visualized under UV light and by dipping in 5% conc. H_2SO_4 in absolute ethanol (v/v) followed by heating. Silica gel column chromatography was performed with silica gel 60 (particle size 0.040–0.063 mm) using moderate pressure (pressure ball). Columns were built in the listed starting eluent containing 0.5% v/v pyridine. Evaporation of solvents was carried out under reduced pressure at temperatures below 45 °C. Following column chromatography, appropriate fractions were pooled, evaporated and dried at high vacuum for at least 12h to give the obtained products in high purity (>95%) as ascertained by 1D NMR techniques. Chemical shifts are reported relative to deuterated solvent or other internal standards (80% phosphoric acid for ^{31}P NMR). Exchangeable (ex) protons were detected by disappearance of signals upon D_2O addition. Assignments of NMR spectra are based on 2D spectra (HSQC, COSY) and DEPT-spectra. Quaternary carbons are not assigned in ^{13}C NMR but verified from HSQC and DEPT spectra (absence of signals). MALDI-HRMS spectra of compounds were recorded on a Q-TOF mass spectrometer using 2,5-dihydroxybenzoic acid as a matrix and mixture of polyethylene glycol (PEG 600) and (PEG 1000) as internal calibration standards.

Experimental protocols for preparation of nucleosides.

5-(1-phenyl-1*H*-1,2,3-triazol-4-yl)-2'-deoxyuridine (2X). Aqueous sodium ascorbate (1.0 M, 1.0 mL, 1.00 mmol), aq. $CuSO_4$ (0.73 mL, 7.5% w/v, 0.21 mmol) and 1-azidobenzene[S1] (83

mg, 0.70 mmol) were added to nucleoside **1** (200 mg, 0.35 mmol) in THF:H_2O:*t*BuOH (10 mL, 3:1:1, v/v/v). The reaction mixture was stirred for 4h at rt, whereupon it was diluted with EtOAc (30 mL) and brine (30 mL). The phases were separated and the organic phase was washed with sat. aq. $NaHCO_3$ (30 mL), dried (Na_2SO_4) and evaporated to dryness. The resulting crude was purified by column chromatography (0-100% EtOAc in petroleum ether, v/v) to afford **2X** (180 mg, 74%) as a pale yellow solid material. R_f = 0.5 (80% EtOAc in petroleum ether, v/v); MALDI-HRMS: *m/z* 696.2456 ($[M+Na]^+$, $C_{38}H_{35}N_5O_7Na^+$, calc. 696.2434); ^{1}H NMR (500 MHz, DMSO-d_6) δ 11.79 (s, 1H, ex, NH), 8.81 (s, 1H, H6/Tz), 8.40 (s, 1H, H6/Tz), 7.91 (d, 2H, *J* = 7.8Hz, Ph), 7.60 (t, 2H, *J* = 7.8 Hz, Ph), 7.51-7.48 (t, 1H, *J* = 7.8 Hz, Ph), 7.38-7.37 (d, 2H, *J* = 7.5 Hz, DMTr), 7.29-7.23 (m, 6H, DMTr), 7.16-7.13 (m, 1H, DMTr), 6.84-6.81 (m, 4H, DMTr), 6.20 (ap t, 1H, *J* = 6.5 Hz, H1'), 5.35 (d, 1H, ex, *J* = 4.7 Hz, 3'-OH), 4.23-4.21 (m, 1H, H3'), 3.97-3.96 (m, 1H, H4'), 3.68-3.67 (2s, 6H, CH_3O), 3.25-3.23 (m, 2H, H5'), 2.30-2.28 (m, 2H, H2'); ^{13}C NMR (125 MHz, DMSO-d_6) δ 161.1, 158.0, 157.9, 149.5, 144.7, 139.8, 136.5, 136.3 (Ar), 135.5, 135.4, 129.8 (Ar), 129.7 (Ar), 129.6 (Ar), 128.6 (Ar), 127.7 (Ar), 127.6 (Ar), 126.5 (Ar), 120.1 (Ar), 120.0 (C6), 113.1 (Ar), 104.7, 85.72, 85.67 (C4'), 85.3 (C1'), 70.3 (C3'), 63.6 (C5'), 54.85 (CH_3O), 39.9 (C2'; overlap with DMSO, visible in DEPT).

5-[1-(Napth-1-yl)-1*H*-1,2,3-triazol-4-yl]-2'-deoxyuridine (2Y). Aqueous sodium ascorbate (1.0 M, 1.2 mL, 1.20 mmol), aq. $CuSO_4$ (1.1 mL, 7.5% w/v, 0.32 mmol) and 1-azidonapthalene[S2] (200 mg, 0.80 mmol) were added to nucleoside **1**(0.30 g, 0.53 mmol) in THF:H_2O:*t*BuOH (10 mL, 3:1:1, v/v/v). The reaction mixture was stirred for 4h at rt, whereupon it was diluted with EtOAc (30 mL) and brine (30 mL). The phases were separated and the organic phase was washed with sat. aq. $NaHCO_3$ (30 mL). The combined aqueous phase was back-extracted with EtOAc (30 mL). The combined organic phase was dried (Na_2SO_4),

evaporated to dryness and the resulting crude purified by column chromatography (0-100% EtOAc in petroleum ether, v/v) to afford **2Y** (0.30 g, 78%) as a yellow solid material. R_f = 0.3 (70% EtOAc in petroleum ether, v/v); MALDI-HRMS: *m/z* 746.2625 ($[M+Na]^+$, $C_{42}H_{37}N_5O_7Na^+$ calc.746.2591); ^{1}H NMR (500 MHz, DMSO-d_6) δ 11.81 (s, 1H, ex, NH), 8.65 (s, 1H, H6/Tz), 8.49 (s, 1H, H6/Tz), 8.22-8.18 (m, 1H, Ar), 8.13 (d, 1H, *J* = 8.2 Hz, Ar), 7.72-7.70 (m, 2H, Ar), 7.69-7.65 (m, 1H, Ar), 7.61-7.57 (m, 1H, Ar), 7.48-7.46 (d, 1H, *J* = 8.5 Hz, Ar), 7.41-7.39 (m, 2H, Ar), 7.31-7.24 (m, 6H, Ar), 7.18-7.14 (m, 1H, Ar), 6.87-6.84 (m, 4H, Ar), 6.24 (ap t, 1H, *J* = 6.3 Hz, H1'), 5.37 (d, 1H, ex, *J* = 4.7 Hz, 3'-OH), 4.26-4.22 (m, 1H, H3'), 4.00-3.97 (m, 1H, H4'), 3.68-3.67 (2s, 6H, CH_3O), 3.27-3.26 (m, 2H, H5'), 2.34-2.31 (m, 2H, H2'); ^{13}C NMR (125 MHz, DMSO-d_6) δ 161.1, 157.97, 157.96, 149.6, 144.8, 139.0, 136.1 (Ar), 135.5, 135.4, 133.6, 133.1, 130.2 (Ar), 129.7 (Ar), 129.6 (Ar), 128.3 (Ar), 127.9, 127.8 (Ar), 127.7 (Ar), 127.6 (Ar), 127.0 (Ar), 126.5 (Ar), 125.4 (Ar), 124.4 (C6), 123.8 (Ar), 121.9 (Ar), 113.1 (Ar), 104.8, 85.74, 85.71(C4'), 85.2 (C1'), 70.4 (C3'), 63.7 (C5'), 54.9 (CH_3O), 39.9 (C2'; overlap with DMSO, visible in DEPT).

3'-*O*-(*N*,*N*-diisopropylamino-2-cyanoethoxyphosphinyl)-5-(1-phenyl-1*H*-1,2,3-triazol-4-yl)-2'-deoxyuridine (3X). Nucleoside **2X** (0.30 g, 0.44 mmol) was co-evaporated with anhydrous 1,2-dichloroethane (3×10 mL) and redissolved in anhydrous CH_2Cl_2 (6.0 mL). To this was dropwise added *N*,*N'*-diisopropylethylamine (DIPEA; 300 µL, 1.75 mmol) and 2-cyanoethyl-*N*,*N'*-diisopropylchlorophosporamidite (PCl-reagent; 200 µL, 0.60 mmol). The reaction mixture was stirred under an argon atmosphere for 3.5h at rt, evaporated to dryness and the resulting crude purified by column chromatography (0-3% MeOH in CH_2Cl_2, v/v) to afford phosphoramidite **3X** (230 mg, 60%) as a slightly yellow solid material. R_f = 0.7 (5% MeOH in CH_2Cl_2, v/v); MALDI-HRMS *m/z:* 896.3505 ($[M+Na]^+$, $C_{47}H_{52}N_7O_8PNa^+$,

calc.896.3512); ^{31}P NMR (121MHz, $CDCl_3$) δ 149.4, 149.0. The NMR data are in close agreement with previously published data.[S3]

3'-*O*-(*N*,*N*-diisopropylamino-2-cyanoethoxyphosphinyl)-5-[1-(napth-1-yl)-1*H*-1,2,3-triazol-4-yl]-2'-deoxyuridine (3Y). Nucleoside **2Y** (200 mg, 0.24mmol) was co-evaporated with anhydrous 1,2-dichloroethane (3×10 mL) and redissolved in anhydrous CH_2Cl_2 (4.0 mL). DIPEA (170 μL, 0.98 mmol) and PCl-reagent (76 μL, 0.34 mmol) were added dropwise and the reaction mixture was stirred under an argon atmosphere for 3.5h at rt, evaporated to dryness and the resulting crude purified by column chromatography (0-3% MeOH in CH_2Cl_2, v/v) to afford phosphoramidite **3Y** (180 mg, 73%) as a slightly yellow solid material. R_f = 0.5 (5% MeOH in CH_2Cl_2, v/v); MALDI-HRMS: *m/z* 946.3685 ($[M+Na]^+$, $C_{51}H_{54}N_7O_8PNa^+$, calc.946.3669; ^{31}P NMR (121 MHz, $CDCl_3$) δ 149.4, 149.0.

Synthesis and purification of ONs. ONs were made on a DNA synthesizer (0.2 μmol scale) using succinyl linked LCAA-CPG (long chain alkyl amine controlled pore glass) columns with 500Å pore size. Standard protocols for incorporation of DNA phosphoramidites were used. A ~50-fold molar excess of modified phosphoramidites in anhydrous acetonitrile (0.05M) was used along with extended oxidation (45s) and hand-coupling (20 min, 4,5-dicyanoimidazole as activator), which resulted in coupling yields of >95%, >95% and ~92% for monomers **X**, **Y** and **Z**, respectively. Cleavage from solid support and removal of nucleobase protecting groups was realized using 32% aq. ammonia (55 °C, 16 h). Crude 5'-DMTr-ONs were purified on HPLC (XTerra MS C18 10 μm 7.8 × 10 mm pre-column; XTerra MS C18 10 μm, 7.8 × 150 mm column) using a 0.05 mM TEAA (triethylammonium acetate) buffer - 25% water/acetonitrile (v/v) gradient. Purified ONs were detritylated using 80% aq. AcOH (20 min) and precipitated

from acetone (1 mL) at -18 °C for 12-16h. The identity of the synthesized ONs was established through MS analysis recorded in positive ion mode on a quadrupole time-of-flight tandem mass spectrometer equipped with a MALDI source using anthranilic acid as a matrix (Table 29), while purity (>80%) was verified by analytical RP-HPLC running in analytical mode.

Table 29. MALDI-ToF MS and ε_{260} of synthesized ONs.[a]

ONSequence	Calc. $(M+H)^+$	Exp. $(M+H)^+$	ε_{260} (OD/μmol)
X1 5'-GTGT **X** TTGC	2864	2864	84.5
X2 5'-GTG**X**T**X** TGC	2993	2993	84.0
X3 5'-GTGT**XX** TGC	2993	2993	84.0
X4 5'-GTG **XXXX**GC	3251	3251	83.0
Y1 5'-GTGT **Y** TTGC	2914	2914	89.0
Y2 5'-GTG**Y**T**Y** TGC	3094	3094	92.5
Y3 5'-GTGT**YY** TGC	3094	3093	92.5
Y4 5'-GTG **YYYY**GC	3452	3452	100.0
Z1 5'-GTGT **Z** TTGC	2988	2988	107.5
Z2 5'-GTG**Z**T**Z** TGC	3242	3242	130.0
Z3 5'-GTGT**ZZ** TGC	3242	3242	130.0
Z4 5'-GTG **ZZZZ**GC	3748	3748	175.0

[a] For structures of monomer **X** ,**Y** and **Z** see Figure 64 in main manuscript.

Experimental protocol for thermal denaturation studies. ON concentrations were estimated using the following extinction coefficients for DNA (OD/μmol): G (12.01), A (15.20), T (8.40), C (7.05); for RNA (OD/μmol): G (13.70), A (15.40), U (10.00), C (9.00). The contributions

from the chromophores were estimated at (OD/μmol): phenyl-1*H*-1,2,3-triazol-4-yl (7.8),[S4]naphthalene (3.8)[S5] and pyrene (22.4).[S6]The strands comprising a given duplex were mixed and annealed. Thermal denaturation temperatures of duplexes (1.0 μM final concentration of each strand) were determined on a temperature-controlled UV/VIS spectrophotometer using quartz optical cells with 1.0 cm pathlengths. T_m's were determined as the first derivative maximum of thermal denaturation curves (A_{260} vs. T) recorded in either medium or high salt buffer (100 mM or 710 mM NaCl, 0.1 mM EDTA, pH 7.0 adjusted with 10 mM Na_2HPO_4 and 5 mM Na_2HPO_4). The temperature of the denaturation experiments ranged from at least 15 °C below T_m to 20 °C above T_m (although not below 5 °C). A temperature ramp of 0.5 °C/min was used in all experiments. Reported T_m-values are reported as averages of two experiments within ± 1.0 °C.

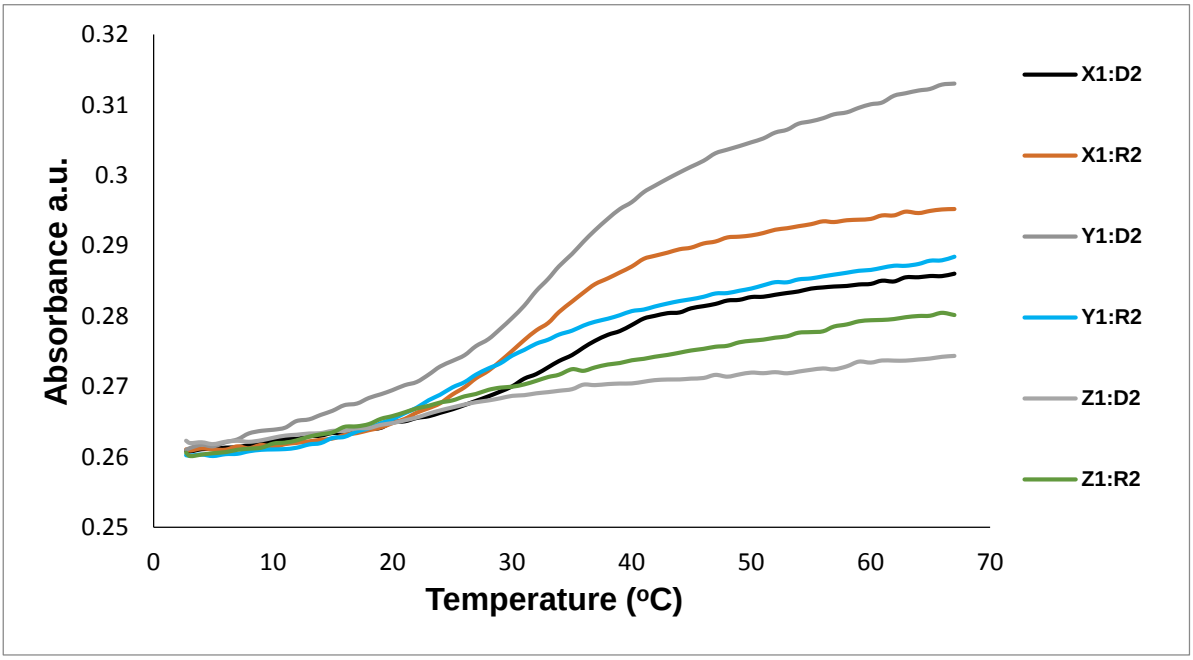

Figure 66. Thermal denaturation curves of duplexes involving **B1**-series ONs.

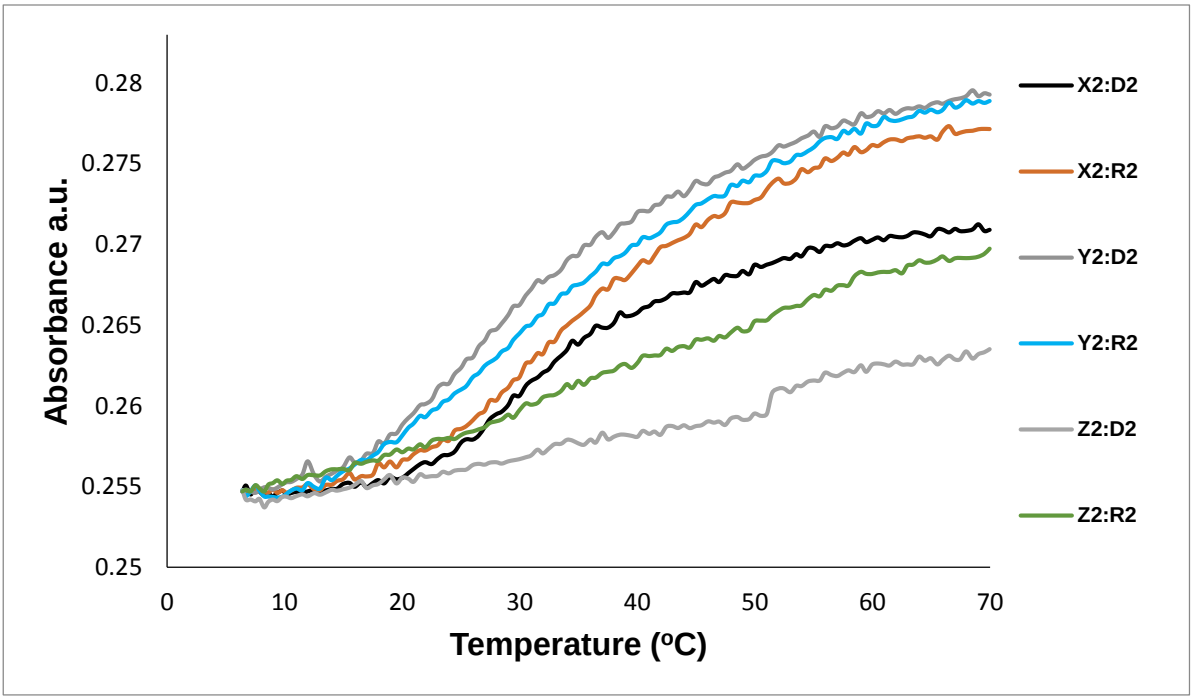

Figure 67. Thermal denaturation curves of duplexes involving **B2**-series ONs.

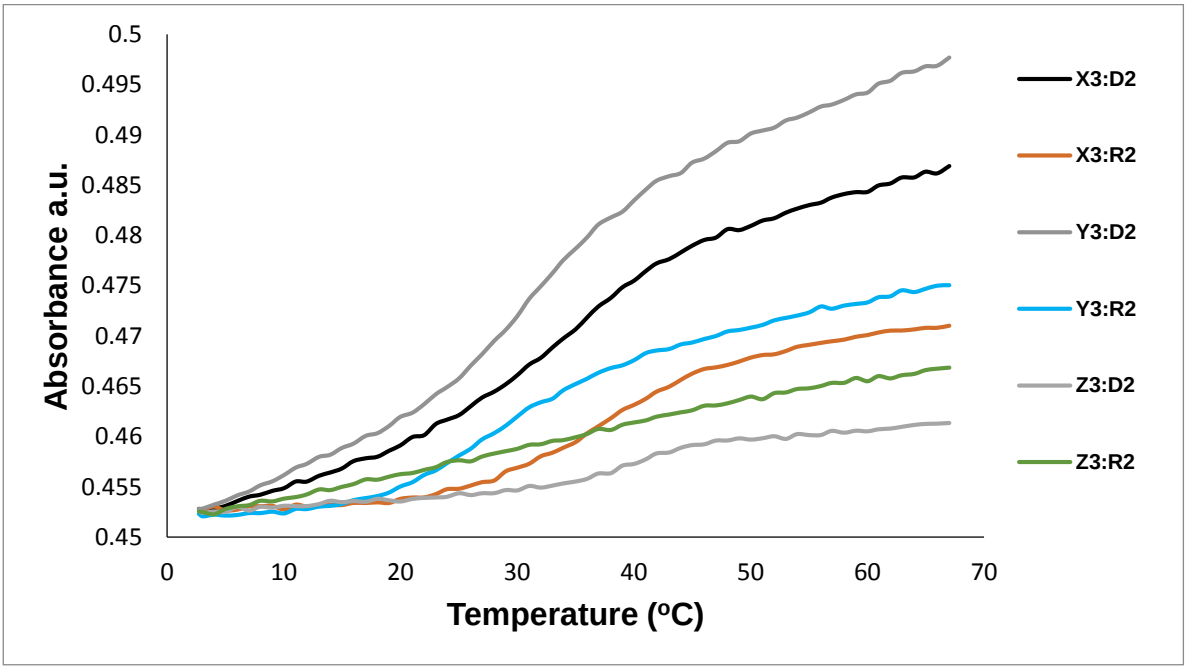

Figure 68. Thermal denaturation curves of duplexes involving **B3**-series ONs.

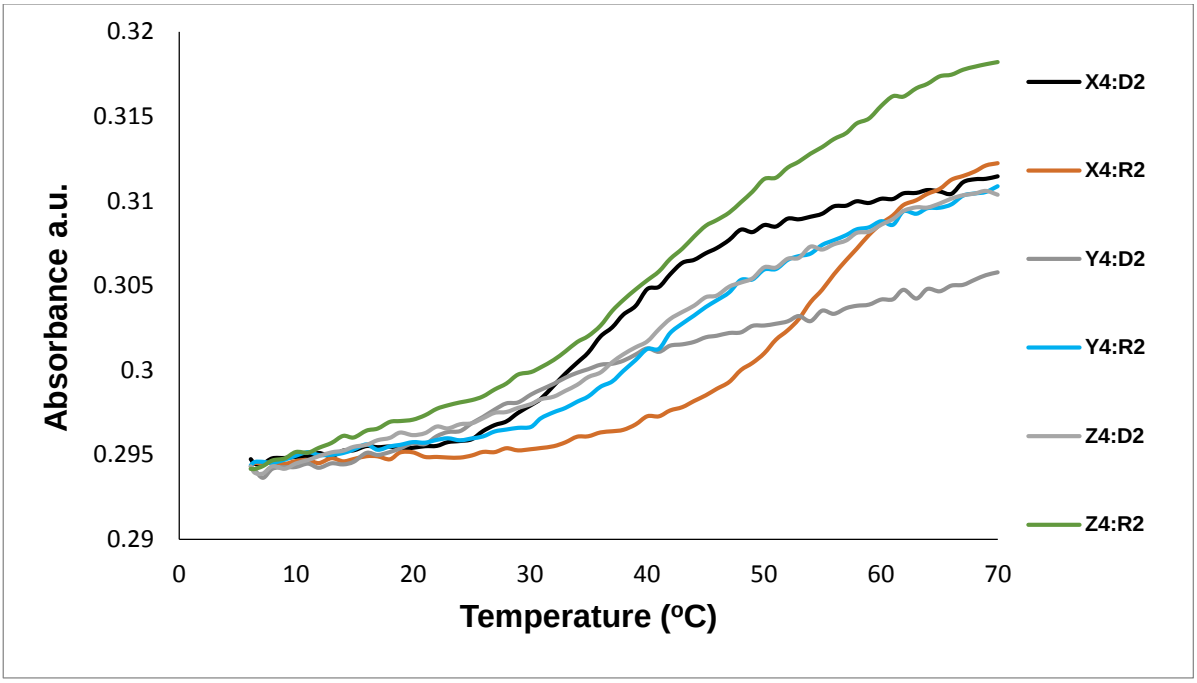

Figure 69. Thermal denaturation curves of duplexes involving **B4**-series ONs.

Table 30. Thermal denaturation temperatures (T_m values) for duplexes between **B1/B2/B4** and complementary DNA or RNA in medium salt buffer.[a]

			T_m (ΔT_m/mod) [°C]					
			DNA			RNA		
			3'-CAC AAA ACG			3'-CAC AAA ACG		
ON	Sequence	B =	**X**	**Y**	**Z**	**X**	**Y**	**Z**
B1	5'-GTGT **B** TTGC		27.0 [-6.0]	22.5 [-10.5]	14.5 [-18.5]	28.0 [-3.0]	-	-
B2	5'-GTGT **BB** TGC		26.0 [-3.5]	22.0 [-5.5]	-	34.5 [+1.8]	27.5 [-1.8]	-
B4	5'-GTG **BBBB** GC		28.0 [-1.3]	17.5 [-3.9]	-	45.5 [+3.6]	37.5 [+1.6]	-

[a]T_m's determined as the first derivative maximum of thermal denaturation curves (A_{260} vs T) recorded in medium salt buffer ([Na^+] = 110 mM, [Cl^-] = 100 mM, pH 7.0 (NaH_2PO_4/Na_2HPO_4)), using 1.0 µM of each strand. T_m's are averages of at least two measurements within 1.0 °C. ΔT_m/mod = change in T_m's per modification relative to unmodified reference duplexes (+cDNA: T_m= 33.0 °C; +cRNA: T_m = 31.0 °C). "-" denotes weak or no transition.

7.5. References.

1. D. G. Rodriguez and A. P. H. J. Schenning, *Chem. Mater*., **2011**, *23*, 310.

2. R. Varghese and H. A. Wagenknecht, *Chem. Commun*., **2009**, 2615.

3. V. L. Malinovskii, D. Wenger and R. Häner, *Chem. Soc. Rev*., **2010**, *39*, 410.

4. H. Kashida, and H. Asanuma, *Phys. Chem. Chem. Phys*., **2012**, *14*, 7196.

5. Y. N. Teo and E. T. Kool, *Chem. Rev*., **2012**, *112*, 4221.

6. M. E. Østergaard and P. J. Hrdlicka, *Chem. Soc. Rev*., **2011**, *40*, 5771.

7. C. Brotschi, G. Mathis and C. J. Leumann, *Chem. Eur. J*., **2005**, *11*, 1911.

8. C. Verhagen, T. Bryld, M. Raunkær, S. Vogel, K. Buchalova and J. Wengel, *Eur. J. Org. Chem*., **2006**, 2538.

9. Y. N. Teo, J. N. Wilson and E. T. Kool, *J. Am. Chem. Soc*., **2009**, *131*, 3923.

10. R. Häner, F. Samain and V. L. Malinovskii, *Chem. Eur. J*., **2009**, *15*, 5701.

11. H. Asanuma, K. Shirasuka, T. Takarada, H. Kashida and M. Komiyama, *J. Am Chem. Soc*., **2003**, *125*, 2217.

12. P. J. Hrdlicka, B. R. Babu, M. D. Sørensen and J. Wengel, *Chem. Commun*., **2004**, 1478.

13. M. Nakamura, Y. Shimomura, Y. Ohtoshi, K. Sasa, H. Hayashi, H. Nakano and K. Yamana, *Org. Biomol. Chem*., **2007**, *5*, 1945.

14. M. Nakamura, Y. Murakami, K. Sasa, H. Hayashi and K. Yamana, *J. Am. Chem. Soc*., **2008**, *130*, 6904.

15. E. Mayer-Enthart and H. A. Wagenknecht, *Angew. Chem. Int. Ed*., **2006**, *45*, 3372.

16. J. Barbaric and H. A. Wagenknecht, *Org. Biomol. Chem*., **2006**, *4*, 2088.

17. E. Mayer-Enthart, C. Wagner, J. Barbaric and H. A. Wagenknecht, *Tetrahedron*, **2007**, *63*, 3434.

18. L. A. Fendt, I. Bouamaied, S. Thoni, N. Amiot and E. Stulz, *J. Am. Chem. Soc*., **2007**, *129*, 15319.

19. T. N. Nguyen, A. Brewer and E. Stulz, *Angew. Chem. Int. Ed*., **2009**, *48*, 1974.

20. P. Kocalka, N. K. Andersen, F. Jensen and P. Nielsen, *Chem. Bio. Chem*., **2007**, *8*, 2106.

21. N. K. Andersen, N. Chandak, L. Brulikova, P. Kumar, M. D. Jensen, F. Jensen, P. K. Sharma and P. Nielsen, *Bioorg. Med. Chem*., **2010**, *18*, 4702.

22. N. K. Andersen, H. Dossing, F. Jensen and P. Nielsen, *J. Org. Chem*., **2011**, *76*, 6177.

23. P. Kumar, N. Chandak, P. Nielsen and P. K. Sharma, *Bioorg. Med. Chem*., **2012**, *20*, 3843.

24. M. E. Østergaard, D. C. Guenther, P. Kumar, B. Baral, L. Deobald, A. J. Paszczynski, P. K. Sharma and P. J. Hrdlicka, *Chem. Commun*., **2010**, *46*, 4929.

25. D. J. Hurley and Y. Tor, *J. Am. Chem. Soc*., **1998**, *120*, 2194.

26. G. Colombano, C. Travelli, U. Galli, A. Caldarelli, M. G. Chini, P. L. Canonico, G. Sorba, G. Bifulco, G. C. Tron and A. A. Genazzani, *J. Med. Chem*., **2010**, *53*, 616.

27. M. Hu, J. Li and S. Q. Yao, *Org. Lett*., **2008**, *10*, 5529.

28. V. V. Rostovtsev, L. G. Green, V. V. Fokin and K. B. Sharpless, *Angew. Chem. Int. Ed*., **2002**, *41*, 2596.

29. T. Kottysch, C. Ahlborn, F. Brotzel and C. Richert, *Chem. Eur J*., **2004**, *10*, 4017.

30. M. V. Skorobogatyi, A. D. Malakhov, A. A. Pchelintseva, A. A. Turban, S. L. Bondarev and V. A. Korshun, *Chem. Bio. Chem*., **2006**, *7*, 810.

31. M. E. Østergaard, P. Kumar, B. Baral, D. C. Guenther, B. A. Anderson, F. M. Ytreberg, L. Deobald, A. J. Paszczynski, P. K. Sharma and P. J. Hrdlicka, *Chem. Eur. J*., **2011**, *17*, 3157.

32. T. W. Barnes III and D. H. Turner, *Biochemistry*, **2001**, *40*, 12738.

S1 G. Colombano, C. Travelli, U. Galli, A. Caldarelli, M. G. Chini, P. L. Canonico, G. Sorba, G. Bifulco, G. C. Tron and A. A. Genazzani, *J. Med. Chem*., 2010, **53**, 616.

S2 M. Hu, J. Li and S. Q. Yao, *Org. Lett*., 2008, **10**, 5529.

S3 P. Kocalka, N. K. Andersen, F. Jensen and P. Nielsen, *Chem. Bio. Chem.*, 2007, **8**, 2106.

S4 N. K. Andersen, N. Chandak, L. Brulikova, P. Kumar, M. D. Jensen, F. Jensen, P. K. Sharma and P. Nielsen, *Bioorg. Med. Chem*., 2010, **18**, 4702.

S5 R. K. Sehgal and S. Kumar, *Org. Prep. Proc. Int.*, 1989, **21**, 223.

S6 T. S. Kumar, A. S. Madsen, M. E. Østergaard, J. Wengel and P. J. Hrdlicka, *J. Org. Chem*., 2008, **73**, 7060.

Appendix

Appendix 1: Publications

1. Kumar, P.; Østergaard, M.; Baral, B.; Andersen, B.; Guenther, D. C.; **Kaura**, **M**.; Raible, D. J.; Sharma, P. K.; Hrdlicka, P. J. "Synthesis and biophysical properties of C5-functionalized LNA (Locked Nucleic Acids)." *J. Org. Chem*. **2014**, *79*, 5047-5061.

2. Kengne, F, B. A.; Karmakar, S.; **Kaura**, **M**.; Sai, V.V. R.; Corti, G.; Niraula, I. B.; Larin, A.; Hall, J.; Sowell, D.; Hrdlicka, P.J., Dobrokhotov, V.; McIlroy, D. N. Self-Assembled Monolayers of Thiols Adsorbed on Au/ZnO-Functionalized Silica Nanosprings: Photoelectron Spectroscopy Analysis and detection of Vaporized Explosives. *ACS Appl. Mater. Interfaces*. **2014**, *6*, 13355-13366.

1. Synthesis and biophysical properties of C5-functionalized LNA (Locked Nucleic Acid)

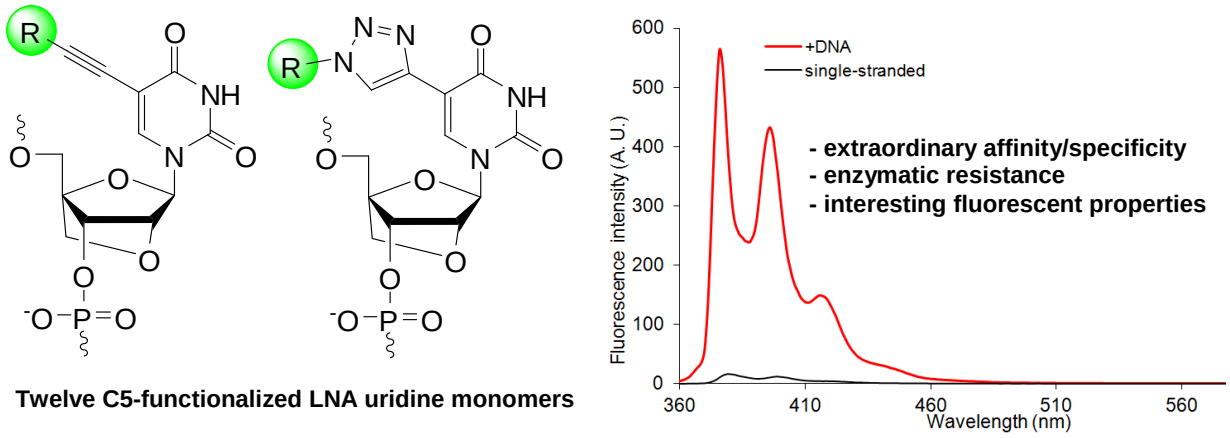

Abstract. Oligonucleotides that are modified with conformationally restricted nucleotides such as Locked Nucleic Acid (LNA) monomers, are used extensively in molecular biology and medicinal chemistry to modulate gene expression at the RNA level. Major efforts have been devoted to design LNA derivatives that induce even higher binding affinity and specificity, greater enzymatic stability and more desirable pharmacokinetic characteristics. Most of this work has focused on modifications of LNA's oxymethylene bridge. Here, we describe a different approach toward modulating the properties of LNA, i.e., through functionalization of LNA nucleobases. Twelve structurally diverse C5-functionalized LNA uridine (U) phosphoramidites were synthesized and incorporated into oligodeoxyribonucleotides (ONs), which were then characterized with respect to thermal denaturation, enzymatic stability and fluorescence properties. ONs modified with monomers that are conjugated to small alkynes display significantly increased affinity toward DNA/RNA targets, improved mismatch discrimination and markedly increased protection against 3′-exonucleases relative to conventional LNA. In contrast, ONs modified with monomers that are conjugated to bulky

hydrophobic alkynes, display significantly lower affinity toward DNA/RNA targets but also much greater resistance against 3′-exonucleases. ONs modified with C5-fluorophore-functionalized LNA-U monomers enable excellent fluorescent discrimination of targets with single nucleotide polymorphisms (SNPs). In concert, these properties render C5-functionalized LNA as a promising class of building blocks for RNA-targeting applications and nucleic acid diagnostics.

Introduction. Development of novel conformationally restricted nucleotides is a vibrant area of research.[1,2] Efforts are driven by the interesting properties of oligodeoxyribonucleotides (ONs) modified with classic examples of conformationally restricted nucleotides such as homo-DNA,[3] hexitol nucleic acid (HNA),[4] cyclohexane nucleic acid (CeNA),[5] bicyclo DNA,[6] tricyclo DNA[7] or Locked Nucleic Acid (LNA),[8,9] which is also known as Bridged Nucleic Acid (BNA).[10] ONs comprising these building blocks display high affinity toward complementary DNA/RNA due to reduced entropic binding penalties[11] and are accordingly in high demand for a wide range of nucleic acid targeting applications in molecular biology, biotechnology and pharmaceutical science.[12] Their use as RNA-targeting antisense oligonucleotides to decrease gene expression is a particularly prominent example hereof.[12b]

LNA is a particularly interesting member of this compound class because it induces some of the greatest duplex stabilizations observed till date (Figure 1).[8-10] Modulation of gene expression through LNA-mediated targeting of mRNA, pre-mRNA or miRNA has accelerated gene function studies and led to the development of LNA-based drug candidates against diseases of genetic origin.[13,14] Other applications of LNA include its use as an *in situ* hybridization probe to monitor spatiotemporal expression patterns of miRNAs.[15]

Many analogues of LNA have been synthesized with the aim of further improving the binding affinity/specificity, enzymatic stability and pharmokinetic characteristics of LNA.[1,2,16] The vast majority of these efforts have focused on modifying the oxymethylene bridge spanning the C2′/C4′-positions and/or introducing minor-groove-oriented substituents on the bridge. These structural perturbations have resulted in improved enzymatic stability, altered biodistribution and/or toxicity profiles, but have generally not resulted in major improvements in binding affinity and specificity.

C5-functionalized pyrimidine DNA monomers have also attracted considerable attention,[17,18] as they enable predictable positioning of functional entities in the major groove of nucleic acid duplexes.[19] Small C5-alkynyl substituents such as propyn-1-yl and 3-aminopropyn-1-yl induce considerable duplex thermostabilization relative to unmodified duplexes, while larger and more hydrophobic substituents typically decrease duplex thermostability. Attachment of polarity-sensitive fluorophores to the C5-position of DNA pyrimidine monomers has produced several interesting oligonucleotide probes for structural studies of nucleic acids and applications in nucleic acid diagnostics.[12c,20]

In light of the above - and our ongoing interest in LNA chemistry[12c,21] - we recently set out to study C5-alkynyl-functionalized LNA uridine (U) monomers, based on the hypothesis that these monomers will exhibit beneficial properties from both compound classes, i.e., high affinity toward RNA complements and good mismatch discrimination (LNA), along with the ability to position blocking groups in the major groove to confer protection against enzymatic degradation (C5-substituent). The results from our preliminary studies have been very encouraging.[22] ONs modified with small C5-alkynyl-functionalized LNA-U monomers display high affinity toward complementary RNA and moderate protection against 3′-exonucleases,

while ONs modified with large C5-alkynyl-functionalized LNA-U monomers display greatly increased enzymatic stability but decreased RNA affinity.

In the present article, we describe full experimental details concerning the synthesis of twelve different C5-functionalized LNA-U phosphoramidites, their incorporation into ONs and the characterization of these modified ONs by means of thermal denaturation experiments, analysis of thermodynamic parameters, enzymatic stability experiments and fluorescence spectroscopy. The monomers in question were selected to ensure a representation of substituents with different sizes, polarities, linker chemistries and fluorescence characteristics (Figure 1).

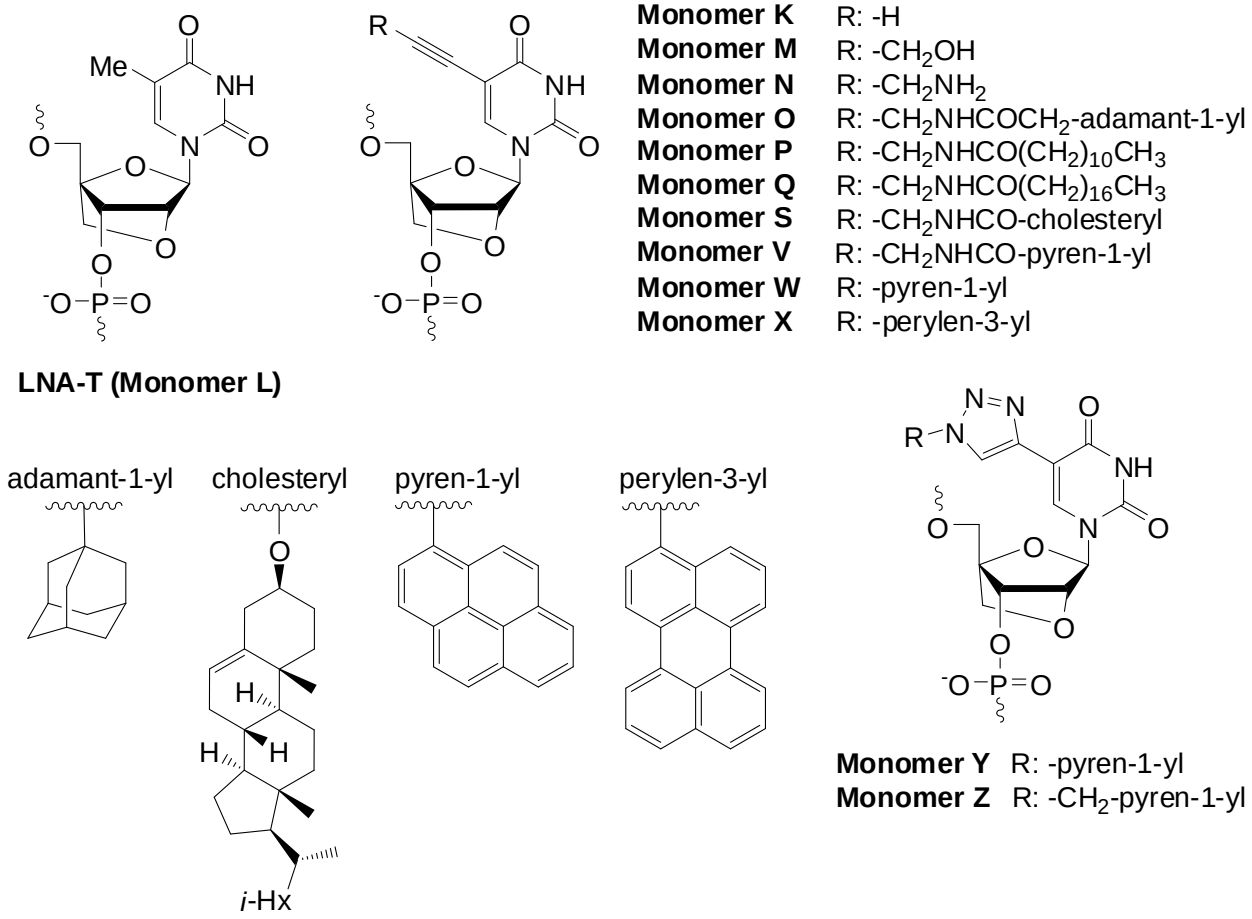

Figure 1. Structure of LNA-T and C5-functionalized analogues thereof studied herein.

Results and Discussion.

Synthesis of phosphoramidites. Our route to target phosphoramidites **5b-5l** initiates from LNA uridine diol **1**, which is obtained from commercially available diacetone-α-D-allose in ~52% yield (Scheme 1).[23] C5-iodination of **1** was accomplished through treatment with iodine and cerium ammonium nitrate (CAN) in acetic acid at 80 °C for ~45 min to afford nucleoside **2** in 87% yield. Prolonged heating and/or higher reaction temperatures result in the formation of non-polar impurities, which complicate purification and reduce product yield. Subsequent O5′-dimethoxytritylation using standard conditions afforded key intermediate **3** in 84% yield. Terminal alkynes[24] were then coupled with **3** under typical Sonogashira conditions[25] to provide

C5-alkynyl functionalized LNA uridines **4a**-**4j** in 53-87% yield. Careful deoxygenation is critical to the outcome of these reactions as they otherwise do not proceed to completion. Finally, O3′-phosphitylation using 2-cyanoethyl-*N*,*N*′-diisopropylchlorophosphoramidite afforded target phosphoramidites **5b**-**5j** in 43-83% yield.

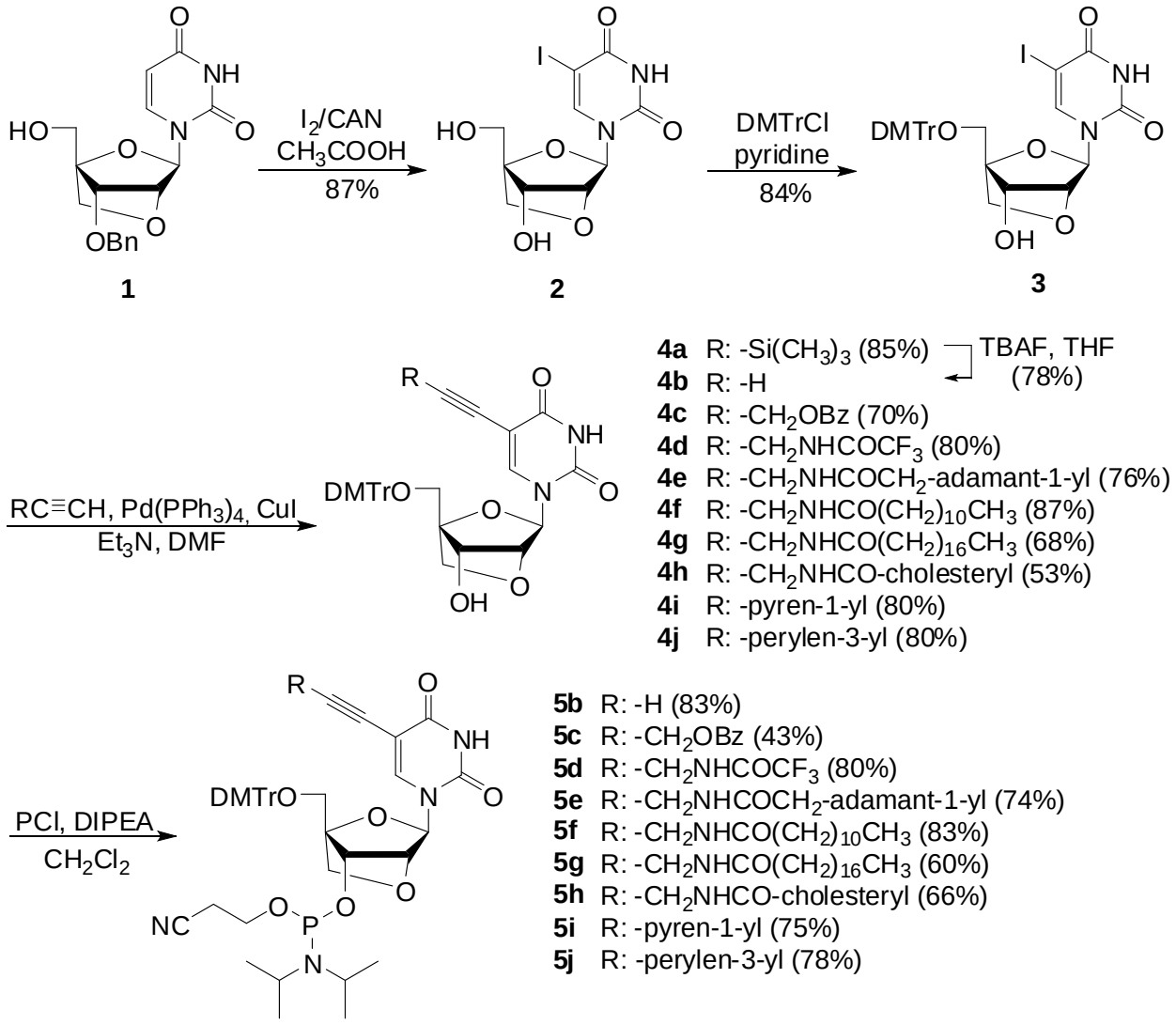

Scheme 1. Synthesis of C5-alkynyl-functionalized LNA uridine phosphoramidites. CAN = ceric ammonium nitrate; DMTrCl = 4,4′-dimethoxytrityl chloride; PCl = 2-cyanoethyl-*N*,*N*-diisopropylchlorophosphoramidite; DIPEA = *N*,*N*′-diisopropylethylamine.

In order to obtain C5-triazoyl-functionalized LNA uridine phosphoramidites **5k** and **5l**, C5-ethynyl functionalized LNA uridine **4b** (obtained via standard TBAF-mediated desilylation of **4a**) was reacted with 1-azidopyrene[26] or 1-azidomethylpyrene[27] in a Cu(I)-catalyzed azide alkyne Huisgen 1,3-dipolar cycloaddition,[28] followed by standard O3′-phosphitylation (Scheme 2).

ON synthesis. Phosphoramidites **5b**-**5l** were used in machine-assisted solid-phase DNA synthesis (0.2 μmol scale) to incorporate monomers **K**-**Z** into ONs. Standard conditions were used except for extended hand-coupling (generally 15 min with 4,5-dicyanoimidazole or 5-[3,5-bis(trifluoromethyl)phenyl]-1*H*-tetrazole as activator) when using **5b**-**5l**, which typically resulted in stepwise coupling yields of >95%. The composition and purity of all modified ONs was ascertained by MALDI MS analysis (Table S1) and ion-pair reversed-phase HPLC, respectively. ONs containing a single incorporation in the 5′-GTGA**B**ATGC context are denoted **K1**, **L1**, **M1** and so on. Similar conventions apply for ONs in the **B2**-**B4** series (Table 1). Reference DNA and RNA strands are denoted **D1**/**D2** and **R1**/**R2**, respectively.

Thermal denaturation experiments – binding affinity. The thermostabilities of duplexes between modified ONs and complementary DNA/RNA were evaluated by determining their thermal denaturation temperature (T_m) in medium salt buffer ([Na^+] = 110 mM, pH 7.0). T_m's of modified duplexes are discussed relative to T_m's of unmodified reference duplexes (Table 1).

As anticipated, ONs modified with one or two conventional LNA-T monomers form very thermostable duplexes with RNA targets in particular (see ΔT_m's for **L1**-**L4**, Table 1). Interestingly, ONs modified with LNA monomers featuring small C5-alkynyl moieties generally result in the formation of even more thermostable duplexes (compare ΔT_m's of

K/**M**/**N**-series with **L**-series, Table 1). The effect is most pronounced for ONs modified with aminopropynyl-functionalized monomer **N**, which display increases in T_m's of up to +13 °C per modification. The greater thermostability of duplexes modified with **K**/**M**/**N** monomers is most likely the result of enhanced stacking interactions[18a] and – in the case of monomer **N** – favorable electrostatic interactions and hydration in the major groove, in a similar manner as previously suggested for C5-aminopropynyl-modified DNA.[18e,18h]

In contrast, duplexes modified with LNA monomers that are conjugated to medium-sized hydrophobic C5-alkynyl substituents, are less thermostable than the corresponding LNA-modified duplexes (compare ΔT_m's of **O**/**P**-series with **L**-series, Table 1). The trend is particularly prominent in DNA:RNA duplexes, presumably due to a suboptimal fit of the C5-alkynyl substituent in the narrow major groove of *A*/*B*-type duplexes. However, other factors, such as different influences on hydration,[18c] cannot be ruled out. The resulting duplexes are, nevertheless, still significantly more stable that the unmodified reference duplexes.

ONs modified with LNA monomers that are conjugated to long hydrophobic C5-alkynyl substituents display even lower affinity toward their targets (see ΔT_m's of **Q**/**S**-series, Table 1). It is particularly noteworthy that duplexes involving the doubly modified **Q4** or **S4** do not display transitions above 10 °C. Similar observations have been made with doubly cholesterol-modified 2′-amino-LNA.[29] We hypothesize that interactions between the hydrophobic groups in single-stranded **Q4** or **S4** interfere with duplex formation. The fact that DNA duplexes with interstrand zipper arrangements of two **S** monomers are rather thermostable supports this hypothesis (see Table S2).

Similarly, ONs modified with LNA monomers that are conjugated to large hydrophobic fluorophores, generally form very thermolabile duplexes, regardless of whether the fluorophore

is attached via an alkynyl or triazoyl linker (see ΔT_m's of **V**-**Z**-series, Table 1). The use of monomers in which the fluorophore is attached to the nucleobase via a short rigid linker - such as in monomers **W**, **X** and **Y** - results in particularly unstable duplexes. Once again, we speculate that these trends reflect a poor fit of the fluorophore in the major groove; short rigid linkers between the fluorophore and nucleobase moieties may prevent the fluorophore from sampling more suitable conformational space. Interestingly, with the exception of pyreneethynyl- and perylene-functionalized **W4** and **X4**, duplexes entailing the doubly modified **B4** ONs are considerably more stable than those entailing their singly modified counterparts (e.g., compare ΔT_m/mod of **B4**:**D1** relative to **B2**:**D1** and **B3**:**D1**, Table 1). Similar stabilizing trends have been reported for other densely fluorophore-modified duplexes and were attributed to the formation of chromophore arrays in the major groove.[19] The presence of pyrene excimer signals in the steady-state fluorescence emission spectra of duplexes between **V4**/**Y4**/**Z4** and DNA/RNA complements supports this hypothesis (Figure S3).

Table 1. ΔT_m values of duplexes between ONs modified with C5-functionalized LNA monomers and complementary DNA/RNA measured relative to unmodified duplexes.[a]

		ΔT_m/mod (°C)												
ON	**Duplex B=**	**L**	**K**	**M**	**N**	**O**	**P**	**Q**	**S**	**V**	**W**	**X**	**Y**	**Z**
B1 **D2**	5′-GTG A**B**A TGC 3′-CAC TAT ACG	+5.0	+7.0	+7.0	+8.0	+4.5	+4.0	+1.0	-5.5	-6.5	-8.5	-12.5	-10.5	-5.5
D1 **B2**	5′-GTG ATA TGC 3′-CAC **B**AT ACG	+4.0	+5.5	+5.5	+6.5	+3.0	+1.0	+0.5	-5.0	-7.5	-9.5	<-10.0	-13.5	-6.5
D1 **B3**	5′-GTG ATA TGC 3′-CAC TA**B** ACG	+6.5	+5.5	+7.0	+9.5	+4.5	+3.5	+1.0	-3.5	-4.0	-10.5	-11.5	-12.5	-5.5
D1 **B4**	5′-GTG ATA TGC 3′-CAC **B**A**B** ACG	+5.5	+5.5	+5.5	+8.0	-	+3.0	<-10.0	<-10.0	+0.5	-6.5	<-10.0	-4.0	-2.0
B1 **R2**	5′-GTG A**B**A TGC 3′-CAC UAU ACG	+9.5	+11.0	+9.5	+13.0	+6.0	+5.5	+4.0	-2.0	-4.0	-2.0	-12.0	-2.0	-1.5
R1 **B2**	5′-GUG AUA UGC 3′-CAC **B**AT ACG	+6.5	+8.5	+8.0	+10.0	-0.5	+2.0	+3.5	±0	-6.0	-1.5	-12.0	-10.0	-5.0
R1 **B3**	5′-GUG AUA UGC 3′-CAC TA**B** ACG	+9.5	+8.5	+10.0	+12.5	+2.5	+2.0	+2.5	-1.0	±0	-5.5	-11.0	-9.0	-1.0
R1 **B4**	5′-GUG AUA UGC 3′-CAC **B**A**B** ACG	+8.0	+8.5	+8.0	+11.0	-	+4.5	<-8.5	<-8.5	+2.0	-5.5	<-8.5	-2.0	-0.5

[a] ΔT_m = change in T_m's relative to unmodified reference duplexes **D1**:**D2** ($T_m \equiv 29.5$ °C), **D1**:**R2** ($T_m \equiv 27.0$ °C) and **D2**:**R1** ($T_m \equiv 27.0$ °C); T_m's determined as the first derivative maximum of denaturation curves (A_{260} vs T) recorded in medium salt buffer ([Na^+] = 110 mM, [Cl^-] = 100 mM, pH 7.0 (NaH_2PO_4/Na_2HPO_4)), using 1.0 μM of each strand. T_m's are averages of at least two measurements within 1.0 °C; See Figure 1 for structures of monomers. "-" = not determined. Data for duplexes between **L**/**K**/**N**/**Q**/**S**-modified ONs and complementary RNA has been previously published in reference 22.

Thermodynamic analysis of duplexes modified with C5-functionalized LNA-U monomers. The T_m based conclusions are largely corroborated by analysis of the thermodynamic parameters for duplex formation, which were derived from thermal denaturation curves through curve-fitting.[30] Thus, formation of duplexes between conventional LNA **L1**-**L3** and complementary DNA or RNA is 4-7 kJ/mol and 8-13 kJ/mol more favorable, respectively, compared to unmodified reference duplexes (see $\Delta\Delta G^{298}$ values for **L1**-**L3**, Table 2). The greater stability of LNA-modified duplexes is generally a result of lower enthalpy ($\Delta\Delta H < 0$ kJ/mol for **L1**-**L3**, Table 2).

Formation of duplexes entailing ONs modified with **K**/**M**/**N** monomers - which are conjugated to small and/or relatively polar alkynyl substituents - is 1-7 kJ/mol more favorable than the corresponding LNA-modified duplexes (compare $\Delta\Delta G^{298}$ values for **K**/**M**/**N**-series vs **L**-series, Table 2). The additional duplex stabilization is generally enthalpic in origin, which is consistent with improved base-stacking due to the extended π-surface of the C5-alkynyl-functionalized LNA monomers (compare $\Delta\Delta H$ values for **K**/**M**/**N**-series vs **L**-series, Table 2); similar trends have been previously reported for C5-propynyl-functionalized DNA monomers.[31]

Duplexes involving ONs modified with monomers **O**/**P**/**Q**, which are conjugated to moderately large hydrophobic alkynyl substituents, are 0-7 kJ/mol less favorable than the corresponding LNA-modified duplexes (compare $\Delta\Delta G^{298}$ values for **O**/**P**/**Q**-series vs **L**-series, Table 2). Comparison with **K**-modified duplexes suggests that the hydrophobic substituents counteract the favorable enthalpy of the extended π-surfaces (compare $\Delta\Delta H$ values for **O**/**P**/**Q**-series vs **K**-series, Table 2). One possible interpretation of this is that the hydrophobic substituents disrupt hydration in the major groove.

DNA duplexes modified with C5-cholesterol-functionalized LNA monomer **S** are less stable than the control duplex, whereas duplexes with RNA are slightly more stable (see $\Delta\Delta G^{298}$ values for **S1**-**S3**, Table 2). The favorable enthalpic contribution of the alkyne functionality is fully counteracted by low entropy in DNA duplexes but only partially counteracted in DNA:RNA duplexes (compare $\Delta\Delta H$ vs $\Delta(T^{298}\Delta S)$ for **S1**-**S3**, Table 2).

Table 2. Thermodynamic parameters for formation of duplexes modified with C5-functionalized LNA monomers.[a]

		+ complementary DNA			+ complementary RNA		
		ΔG^{298} [$\Delta\Delta G^{298}$]	ΔH [$\Delta\Delta H$]	$-T^{298}\Delta S$ [$\Delta(T^{298}\Delta S)$]	ΔG^{298} [$\Delta\Delta G^{298}$]	ΔH [$\Delta\Delta H$]	$-T^{298}\Delta S$ [$\Delta(T^{298}\Delta S)$]
ON	**Sequence**	(kJ/mol)	(kJ/mol)	(kJ/mol)	(kJ/mol)	(kJ/mol)	(kJ/mol)
D1	5′-GTG ATA TGC	-42	-314	271	-36	-278	241
D2	3′-CAC TAT ACG	-42	-314	271	-39	-293	254
L1	5′-GTG A**L**A TGC	-47 [-5]	-297 [+17]	250 [-21]	-49 [-13]	-309 [-31]	260 [+19]
L2	3′-CAC **L**AT ACG	-46 [-4]	-332 [-18]	286 [+15]	-47 [-8]	-331 [-38]	283 [+29]
L3	3′-CAC TA**L** ACG	-49 [-7]	-332 [-18]	283 [+12]	-50 [-11]	-340 [-47]	290 [+36]
K1	5′-GTG A**K**A TGC	-49 [-7]	-350 [-36]	301 [+30]	-53 [-17]	-424 [-146]	371 [+130]
K2	3′-CAC **K**AT ACG	-49 [-7]	-349 [-35]	300 [+29]	-48 [-9]	-319 [-26]	270 [+16]
K3	3′-CAC TA**K** ACG	-52 [-10]	-372 [-58]	319 [+48]	-57 [-18]	-414 [-121]	357 [+103]
M1	5′-GTG A**M**A TGC	-51 [-9]	-390 [-76]	339 [+68]	-52 [-16]	-386 [-108]	334 [+93]
M2	3′-CAC **M**AT ACG	-50 [-8]	-394 [-80]	344 [+73]	-51 [-12]	-398 [-105]	347 [+93]
M3	3′-CAC TA**M** ACG	-51 [-9]	-360 [-46]	309 [+38]	-51 [-12]	-367 [-74]	316 [+62]
N1	5′-GTG A**N**A TGC	-51 [-9]	-353 [-39]	302 [+31]	-51 [-15]	-324 [-46]	272 [+31]
N2	3′-CAC **N**AT ACG	-49 [-7]	-362 [-48]	313 [+42]	-52 [-13]	-364 [-71]	312 [+58]
N3	3′-CAC TA**N** ACG	-52 [-10]	-361 [-47]	309 [+38]	-52 [-13]	-325 [-32]	272 [+18]
O1	5′-GTG A**O**A TGC	-47 [-5]	-337 [-23]	290 [+19]	-46 [-10]	-337 [-59]	291 [+50]
O2	3′-CAC **O**AT ACG	-44 [-2]	-322 [-8]	278 [+7]	-43 [-4]	-366 [-73]	322 [+68]
O3	3′-CAC TA**O** ACG	-46 [-4]	-324 [-10]	278 [+7]	-44 [-5]	-340 [-47]	296 [+42]
P1	5′-GTG A**P**A TGC	-45 [-3]	-334 [-20]	289 [+18]	-45 [-9]	-327 [-49]	282 [+41]
P2	3′-CAC **P**AT ACG	-43 [-1]	-324 [-10]	281 [+10]	-43 [-4]	-351 [-58]	308 [+54]
P3	3′-CAC TA**P** ACG	-44 [-2]	-339 [-25]	294 [+23]	-43 [-4]	-365 [-72]	321 [+67]
Q1	5′-GTG A**Q**A TGC	-45 [-3]	-346 [-32]	301 [+30]	-45 [-9]	-347 [-69]	302 [+61]
Q2	3′-CAC **Q**AT ACG	-45 [-3]	-411 [-97]	371 [+100]	-46 [-7]	-377 [-84]	331 [+77]
Q3	3′-CAC TA**Q** ACG	-43 [-1]	-287 [+27]	243 [-28]	-43 [-4]	-360 [-67]	317 [+63]
S1	5′-GTG A**S**A TGC	-37 [+5]	-317 [-3]	280 [+9]	-39 [-3]	-333 [-55]	294 [+53]
S2	3′-CAC **S**AT ACG	-39 [+3]	-380 [-66]	342 [+71]	-42 [-3]	-359 [-66]	316 [+62]
S3	3′-CAC TA**S** ACG	-40 [+2]	-380 [-66]	339 [+68]	-40 [-1]	-355 [-62]	315 [+61]

[a] Parameters were determined from thermal denaturation curves, which were recorded as described in Table 1. $\Delta\Delta G^{298}$, $\Delta\Delta H$ and $\Delta(T^{298}\Delta S)$ are calculated relative to reference duplexes **D1:D2**, **D1:R2** and **D2:R1**.

Thermal denaturation studies – binding specificity. The binding specificities of centrally modified ONs (**B1**-series) were determined by using DNA/RNA targets with mismatched nucleotides opposite of the modified monomer. As expected,[8-10] LNA-modified ON **L1** displays improved binding specificity relative to unmodified reference strand **D1** as evidenced by the more pronounced drops in T_m's of mismatched duplexes (compare ΔT_m's for **L1** and **D1**, Table

3). Interestingly, many of the C5-functionalized LNA monomers induce additional improvements in binding specificity (note ΔT_m's of **K1/M1/N1/O1/P1/Q1**, Table 3). It is well-established that nucleotide modifications, which improve target affinity as well as binding specificity, are desirable for nucleic acid targeting applications.[32] Cholesterol-functionalized LNA **S1** and fluorophore-functionalized LNAs **V1**/**W1**/**X1**/**Y1**/**Z1** display poor discrimination of mismatched DNA targets but maintain reasonable specificity against RNA targets (Table 3). These trends are indicative of different binding modes of the pyrene and perylene moieties in DNA:DNA vs DNA:RNA duplexes. Intercalation of aromatic units - which is known to stabilize mismatched base-pairs[33] - is more favorable in DNA:DNA than DNA:RNA duplexes.[34] For a discussion of the binding specificities of double modified ONs (**B4**-series), see the Supporting Information (Table S3).

Table 3. Discrimination of mismatched DNA/RNA targets by singly modified LNAs and reference ONs.[a]

		DNA: 3′-CAC T**B**T ACG				RNA: 3′-CAC U**B**U ACG			
		T_m	ΔT_m			T_m	ΔT_m		
ON	**Sequences**	**A**	C	G	T	**A**	C	G	U
D1	5′-GTG ATA TGC	**29.5**	-16.5	-8.0	-15.5	**27.0**	<-17.0	-4.5	<-17.0
L1	5′-GTG A**L**A TGC	**34.5**	-18.0	-11.0	-16.0	**36.5**	-19.0	-8.0	-18.5
K1	5′-GTG A**K**A TGC	**36.5**	-20.0	-15.5	-18.5	**38.0**	-20.5	-13.5	-22.0
M1	5′-GTG A**M**A TGC	**36.5**	-20.0	-11.5	-18.5	**36.5**	-18.5	-9.5	-20.0
N1	5′-GTG A**N**A TGC	**37.5**	-19.0	-12.0	-17.5	**40.0**	-18.5	-11.5	-22.5
O1	5′-GTG A**O**A TGC	**34.0**	-20.5	-16.5	-18.0	**33.0**	-20.0	-9.5	-20.0
P1	5′-GTG A**P**A TGC	**33.5**	-21.5	-17.0	-20.5	**32.5**	-20.5	-11.5	-19.5
Q1	5′-GTG A**Q**A TGC	**30.5**	-18.0	-13.0	-16.5	**31.0**	-19.5	-10.0	-20.0
S1	5′-GTG A**S**A TGC	**24.0**	-11.5	-10.0	-11.0	**25.0**	-15.0	-9.0	<-15.0
V1	5′-GTG A**V**A TGC	**23.0**	-7.5	-10.0	-7.5	**23.0**	<-13.0	-10.5	<-13.0
W1	5′-GTG A**W**A TGC	**21.0**	+6.0	-7.0	+3.0	**25.0**	<-15.0	<-15.0	<-15.0
X1	5′-GTG A**X**A TGC	**17.0**	+4.5	±0.0	+3.5	**15.0**	<-5.0	<-5.0	<-5.0
Y1	5′-GTG A**Y**A TGC	**19.0**	-1.0	-4.0	-2.5	**25.0**	<-15.0	-8.0	<-15.0

Z1	5′-GTG A**Z**A TGC	**24.0**	-10.0	<-14.0	-9.5	**25.5**	-1.5	<-15.5	<-15.5

[a] For experimental conditions and sequences see Table 1. ΔT_m = change in T_m value relative to fully matched ON:DNA or ON:RNA duplex (**B**=A). Data for **L1**/**K1**/**N1**/**Q1**/**S1** against mismatched RNA has been previously published in reference 22.

3′-Exonuclease stability of C5-functionalized LNA. Next, we examined the enzymatic stability of select C5-functionalized LNAs and reference strands in the presence of snake venom phosphordiesterase (SVPDE), a 3′-exonuclease. As expected, unmodified **D2** is quickly degraded (>95% cleavage after 15 min) while the singly modified LNA **L2** offers moderate protection against SVPDE (>95% cleaved after 50 min) (Figure 2). ONs modified with a single C5-ethynyl or C5-aminopropynyl functionalized LNA monomer, are markedly more resistant toward SVPDE degradation (~55% and 35% cleavage of **K2** and **N2**, respectively after 2h). Interestingly, ONs that are modified with LNA monomers conjugated to large hydrophobic substituents are completely inert against SVPDE-mediated degradation, following a brief period of cleavage (see degradation profiles for **Q2** and **S2**, Figure 2). **M2**/**O2**/**P2** also display markedly increased 3′-exonuclease resistance (Figure S1). As expected, these trends are even more pronounced with the doubly modified **B4**-series. Thus, the data strongly suggests that large hydrophobic C5-alkynyl substituents offer effective protection from enzymatic degradation, which renders C5-functionalized LNA of considerable interest for antisense applications.

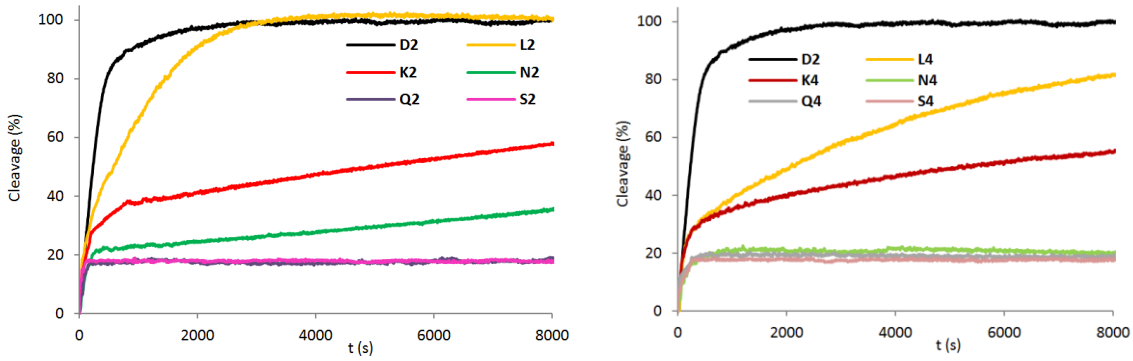

Figure 2. 3′-Exonuclease (SVPDE) degradation of singly (*left*, 3′-CAC BAT ACG) and doubly (*right*, 3′-CAC BAB ACG) modified C5-functionalized LNA and reference strands. Nuclease degradation studies were performed in magnesium buffer (50 mM Tris-HCl, 10 mM Mg^{2+}, pH 9.0) by using 3.3 μM ONs and 0.03 U of SVPDE. The data depicted in the left panel has been previously reported in reference 22.

Fluorescence properties of C5-functionalized LNA. Steady-state fluorescence emission spectra of ONs modified with C5-fluorophore-functionalized LNA monomers and the corresponding duplexes with complementary or mismatched DNA targets were recorded to gain further insight into the binding modes of the fluorophores. In addition to studying the fluorescence properties of **B1** and **B4** probes in the presence or absence of matched/mismatched DNA/RNA (Figures S2 and S3), we also studied centrally modified 13-mer ONs (**V5**-**Z5** series) and their duplexes with matched/mismatched DNA targets (Figure 3). The thermal denaturation characteristics of these ONs (Table S4) closely follow those of the singly modified 9-mer ONs, i.e., i) the corresponding duplexes with DNA/RNA targets are less stable than unmodified reference duplexes (only **Z5**-modified duplexes are slightly more stable) and ii) **W5**, **X5** and **Y5** display very poor thermal discrimination of mismatched DNA targets, while **V5** and **Z5** display similar binding specificity as the unmodified reference strands.

V/**Y**/**Z**-modified duplexes exhibit emission peaks of varying broadness at ~390/402 nm (**V**), ~381/398 nm (**Y**) and ~376/396/416 nm (**Z**), respectively, which are typical emission maxima for electronically isolated pyrene units (Figure 3). As expected for duplexes modified with the 1-ethynylpyrene fluorophore,[35] the duplex between **W5** and complementary DNA exhibits broad red-shifted emission centered around ~465 nm, which is indicative of strong electronic coupling between the pyrene and nucleobase moiety. Interestingly, the emission intensities of pyrene-functionalized ONs **V5**/**W5**/**Y5**/**Z5** increase upon binding to complementary DNA (~3.8, ~3.9, ~3.1 and ~51 fold increases for **V5**, **W5**, **Y5** and **Z5**, respectively, Figure 3). In contrast, much smaller increases are observed upon hybridization with mismatched DNA targets. The intensity differences are most likely due to different positioning of the pyrene moieties in matched vs mismatched duplexes, in a similar manner as proposed for the corresponding DNA analogues of monomers **V**/**W**/**Y**/**Z**.[18g,18j,35b] Thus, the pyrene moieties likely point into the non-quenching environment of the major groove in matched duplexes (nucleobase in *anti* conformation), while they are intercalating into mismatched duplexes leading to nucleobase-mediated quenching[36] of pyrene fluorescence (nucleobase in *syn* conformation). Regardless of the mechanism, the results strongly suggest that **V**/**W**/**Y**/**Z**-modified ONs are promising probes for detection of nucleic acid targets and fluorescent discrimination of single nucleotide polymorphisms (SNPs).

Duplexes between perylene-functionalized **X5** and complementary DNA display broad emission maxima at ~487 and ~517 nm, whereas the emission maxima are red-shifted by ~10 nm in mismatched DNA duplexes (Figure 3). The emission intensity of **X5** does not change significantly upon binding with complementary DNA, but reduces by 30-60% upon binding to

mismatched targets, presumably due to nucleobase-mediated quenching of intercalating perylene units.

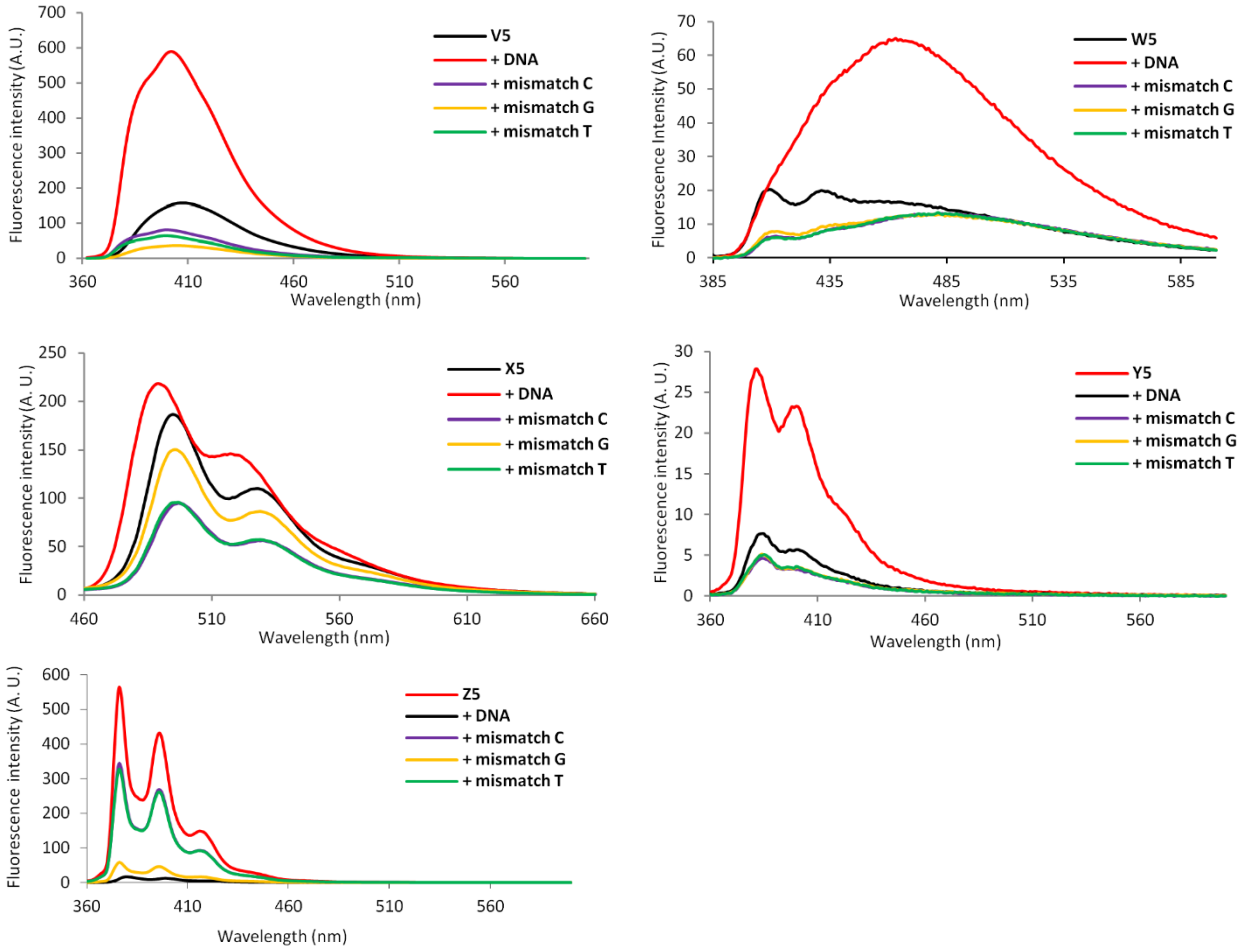

Figure 3. Steady-state fluorescence emission spectra of single stranded **B5** ONs (5′-CG CAA C**B**C AAC GC) and the corresponding duplexes with fully complementary or singly mismatched DNA strands (mismatched nucleotide opposite of modification is specified). λ_{ex} = 344 nm (**V5**/**Y5**/**Z5**), λ_{ex} = 375 nm (**W5**) or λ_{ex} = 448 nm (**X5**); T = 5 °C. Please note that different X- and Y-axis scales are used.

Recently, we examined the SNP-discriminating properties of **V**-modified ONs and compared them to probes modified with the corresponding DNA analogue of monomer **V**.[37] We found that there are distinct advantages to conjugating the 1-pyrenecarboxamido fluorophore to the C5-position of LNA-U, including i) greater increases in fluorescence intensity upon target binding, b) formation of more brightly fluorescent duplexes, and iii) stricter fluorescent discrimination of DNA targets with SNP sites. Force field calculations suggested that the extreme pucker of the LNA skeleton influences the rotational freedom around the N1-C1′ glycosyl bond due to steric hindrance between H6 and H3′, leading to different positioning and modulated photophysical properties of the C5-fluorophore relative to the analogous DNA monomer.[37]

Direct comparison of **Y5** and **Z5** with the corresponding DNA-based probes **Y5d** and **Z5d**[18j] (for structures of the DNA analogues of **V**/**Y**/**Z** monomers, see Figure S4) reveals similar advantages (Figure 4). Thus, the results suggests that conjugation of fluorophores to the C5-position of LNA monomers is a promising strategy toward probes with interesting photophysical properties.

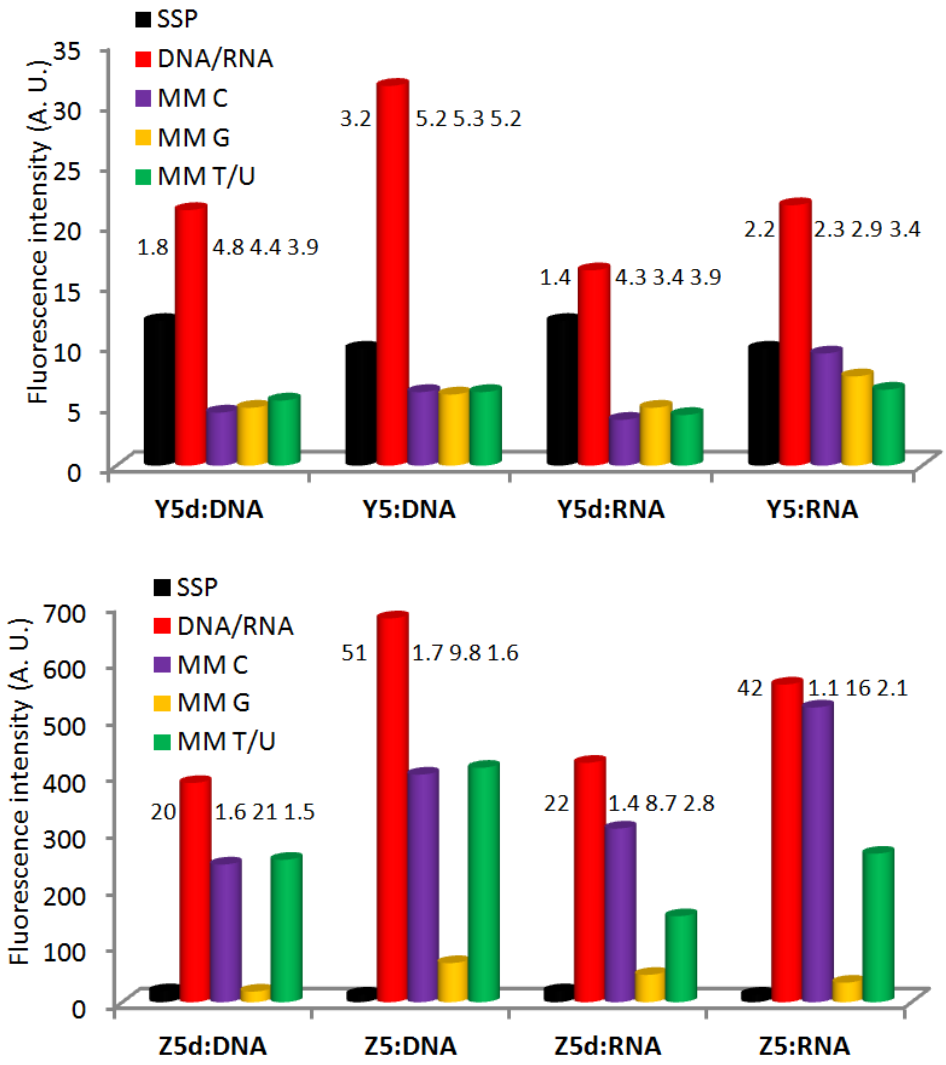

Figure 4. Fluorescence intensity of single stranded probes (SSPs) in the presence or absence of complementary or singly mismatched DNA/RNA strands. Mismatched nucleotide opposite of modification is specified. Hybridization-induced increases and discrimination factors (defined as the fluorescence intensity of duplexes with complementary DNA/RNA divided by the intensity of SSPs or duplexes with mismatched DNA/RNA, respectively) are listed above corresponding histograms. Intensity recorded at λ_{em} = 382 nm for **Y5**/**Y5d** and λ_{em} = 377 nm for **Z5**/**Z5d** at T = 5 °C. Note that different y-axis scales are used.

The large increases in fluorescence intensity upon hybridization of **Z5** with complementary targets prompted us to examine the potential of **Z**-modified ONs as hybridization probes[38] in greater detail. Three additional 13-mer ONs were therefore prepared in which the nucleotides flanking monomer **Z** were systematically varied (Table S4). Although the increases in fluorescence intensities upon hybridization with DNA targets are less pronounced (4-17 fold, Figure 5) and the resulting duplexes are significantly less fluorescent than with **Z5**,[39] moderate to excellent fluorescent discrimination of mismatched DNA targets is observed with all **Z**-modified probes (discrimination factors from 1.5 to 48, Figure 5). Accordingly, **Z**-modified ONs constitute an interesting addition to the existing pool of pyrene-based hybridization probes.[18j,40]

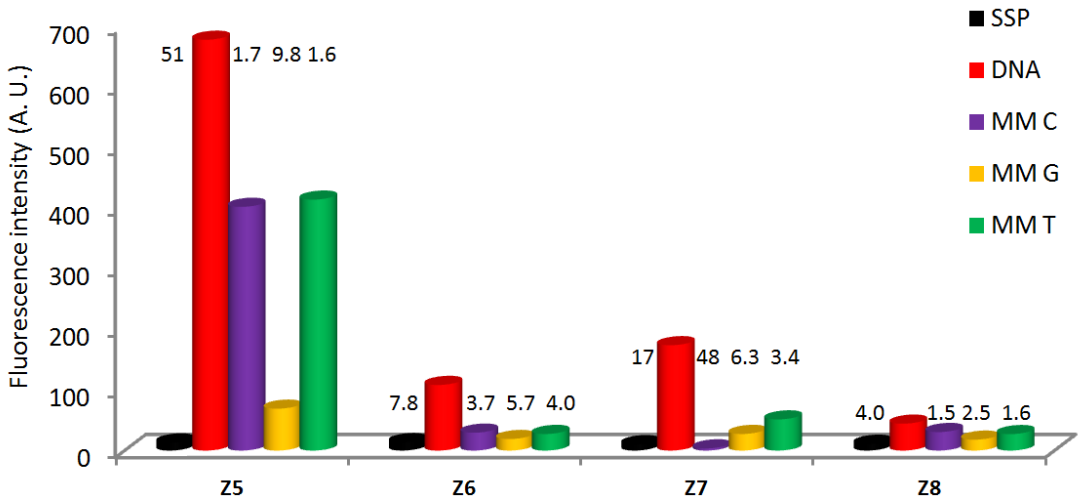

Figure 5. Fluorescence intensity of single stranded probes (SSPs) in the presence or absence of complementary or singly mismatched DNA strands. Mismatched nucleotide opposite of modification is specified. Hybridization-induced increases and discrimination factors are listed above corresponding histograms. Target: 5′-CG CAA B**Z**B AAC GC, where B = C/A/G/T for **ON5**-**ON8**, respectively. Intensity recorded at λ_{em} = 377 nm at T = 5 °C.

Conclusion. The hybridization characteristics and enzymatic stabilities of ONs modified with LNA pyrimidines can be extensively modulated through conjugation of different entities to the C5-position of the nucleobase. Only two extra steps, relative to conventional LNA synthesis, are needed. Monomers that are conjugated to small alkynyl substituents result in significantly greater target affinity and specificity than regular LNA monomers. Conjugation of bulky moieties confers complete protection against 3′-exonucleases but also decreases target affinity. ONs modified with C5-fluorophore-functionalized LNA uridines display improved photophysical characteristics relative to the corresponding DNA-based probes, including greater hybridization-induced increases in fluorescence intensity, formation of more brightly fluorescent duplexes and stricter fluorescent discrimination of single nucleotide polymorphisms.[20b] These properties render C5-functionalized LNA as promising building blocks for RNA-targeting applications and nucleic acid diagnostics, although concerns regarding potential toxicity of C5-alkynyl entities[41] must be alleviated prior to biological evaluation.

The present study suggests that it is possible to combine desirable properties from LNA (target affinity/specificity) and C5-functionalized DNA monomers (positioning of functional entities in the major groove) into one compound class. The subsequent article in this issue demonstrates that the properties of ONs modified with α-L-LNA uridines also can be modulated through functionalization of the nucleobase.[42] We therefore anticipate that C5-functionalization of pyrimidines will serve as a general and synthetically straightforward approach for modulation of pharmocodynamic and pharmacokinetic properties of oligonucleotides modified with LNA[8-10,13] or other conformationally restricted monomers.[1-7,16]

EXPERIMENTAL SECTION

(1*S*,3*R*,4*R*,7*S*)-7-Hydroxy-1-hydroxymethyl-3-(5-iodouracil-1-yl)-2,5-dioxabicyclo[2.2.1]heptane (2). To a solution of nucleoside **1**[23] (4.00 g, 15.62 mmol) in glacial AcOH (150 mL) was added iodine (2.40 g, 9.44 mmol) and ceric ammonium nitrate (4.26 g, 7.77 mmol), and the reaction mixture was stirred at 80 °C for ~40 min. After cooling to rt, the mixture was evaporated to dryness and the resulting residue was suspended in MeOH (150 mL). The mixture was concentrated at reduced pressure and purified by column chromatography (0-15% MeOH/CH_2Cl_2, v/v) to afford nucleoside **2** (5.21 g, 87%) as white solid material. R_f = 0.4 (10% MeOH/CH_2Cl_2, v/v); FAB-HRMS *m/z* 382.9732 ($[M+H]^+$, $C_{10}H_{11}IN_2O_6H^+$, Calcd 382.9735); ^{1}H NMR (DMSO-d_6) δ 11.69 (s, 1H, ex, NH), 8.13 (s, 1H, H6), 5.65 (d, 1H, ex, J = 4.5 Hz, 3′-OH), 5.40 (s, 1H, H1′), 5.27 (t, 1H, ex, J = 5.4 Hz, 5′-OH), 4.14 (s, 1H, H2′), 3.91 (d, 1H, J = 4.5 Hz, H3′), 3.79-3.82 (d, 1H, J = 8.5 Hz, H5″), 3.68-3.75 (m, 2H, H5′), 3.58-3.62 (d, 1H, J = 8.5 Hz, H5″); ^{13}C NMR (DMSO-d_6) δ 160.5, 149.6, 143.5 (C6), 88.8, 86.4 (C1′), 78.5 (C2′), 70.8 (C5″), 68.4, 68.2 (C3′), 55.3 (C5′).

(1*R*,3*R*,4*R*,7*S*)-1-(4,4′-Dimethoxytrityloxymethyl)-7-hydroxy-3-(5-iodouracil-1-yl)-2,5-dioxabicyclo[2.2.1]heptane (3). Diol **2** (5.00 g, 13.0 mmol) was coevaporated with anhydrous pyridine (100 mL) and redissolved in anhydrous pyridine (100 mL). To this was added 4,4′-dimethoxytrityl chloride (DMTr-Cl, 5.75 g, 16.9 mmol) and the reaction mixture was stirred at rt for 16 h, whereupon solvent was removed at reduced pressure. The residue was dissolved in CH_2Cl_2 (300 mL) and washed with sat. aq. $NaHCO_3$ (300 mL). The aqueous layer was back-extracted with CH_2Cl_2 (2×100 mL) and the combined organic layer was washed with sat. aq. $NaHCO_3$ (100 mL), dried (Na_2SO_4), evaporated to near dryness and coevaporated with toluene:abs. EtOH (100 mL, 1:2, v/v). The resulting residue was purified by column

chromatography (0-5 % MeOH in CH_2Cl_2, v/v) to afford key intermediate **3** (7.52 g, 82 %) as a slightly yellow solid material. R_f = 0.5 (5% MeOH in CH_2Cl_2, v/v); FAB-HRMS *m*/*z* 684.0977 ($[M]^+$, $C_{31}H_{29}IN_2O_8^+$, Calcd 684.0969); ^{1}H NMR (DMSO-d_6) δ 11.74 (s, 1H, ex, NH), 7.96 (s, 1H, H6), 7.23-7.45 (m, 9H, Ar), 6.91 (d, 4H, *J* = 8.5 Hz, Ar), 5.70 (d, 1H, ex, *J* = 4.5 Hz, 3′-OH), 5.44 (s, 1H, H1′), 4.24 (s, 1H, H2′), 4.07 (d, 1H, *J* = 4.5 Hz, H3′), 3.74-3.76 (m, 8H, 2×OCH_3, 2×H5″), 3.39-3.42 (d, 1H, *J* = 11.0 Hz, H5′), 3.28-3.31 (d, 1H, *J* = 11.0 Hz, H5′, overlap with H_2O); ^{13}C NMR (DMSO-d_6) δ 160.5, 158.1, 158.0, 149.7, 144.6, 142.7 (C6), 135.3, 135.2, 129.7 (Ar), 129.6 (Ar), 127.9 (Ar), 127.5 (Ar), 126.6 (Ar), 113.3 (Ar), 87.5, 86.9 (C1′), 85.6, 78.8 (C2′), 71.3 (C5″), 69.4 (C3′), 68.9, 58.9 (C5′), 55.0 (CH_3O).

Representative protocol for Sonogashira couplings (4a-4j). Key intermediate **3**, $Pd(PPh_3)_4$, CuI and alkyne were added to anhydrous DMF (quantities and volumes specified below) and the reaction chamber was degassed and placed under an argon atmosphere. To this was added Et_3N and the reaction mixture was stirred in the dark until analytical TLC indicated full conversion of the starting material (reaction time and temperature specified below), whereupon solvents were evaporated off. The resulting residue was taken in up in EtOAc (100 mL) and washed with brine (2×50 mL) and sat. aq. $NaHCO_3$ (50 mL). The combined aqueous phase was back-extracted with EtOAc (100 mL), the combined organic phase dried (Na_2SO_4) and evaporated to dryness, and the resulting residue purified by column chromatography (0-5 % MeOH in CH_2Cl_2 (v/v) to afford the desired product.

(1*R*,3*R*,4*R*,7*S*)-1-(4,4′-Dimethoxytrityloxymethyl)-7-hydroxy-3-[5-(trimethylsilylethynyl)uracil-1-yl]-2,5-dioxabicyclo[2.2.1]heptane (4a). After setting up nucleoside **3** (0.68 g, 1.00 mmol), $Pd(PPh_3)_4$ (120 mg, 0.10 mmol), CuI (40 mg, 0.20 mmol),

trimethylsilylacetylene (294 mg, 0.42 mL, 3.00 mmol) and Et_3N (0.60 mL, 4.27 mmol) in DMF (10 mL) as described in the representative Sonogashira protocol, the reaction mixture was stirred at rt for 12 h. After workup and purification, nucleoside **4a** (0.56 g, 85 %) was obtained as a brown solid material. R_f = 0.5 (5% MeOH in CH_2Cl_2, v/v); ESI-HRMS *m*/*z* 677.2297 ($[M+Na]^+$, $C_{36}H_{38}N_2O_8Si{\cdot}Na^+$, Calcd 677.2290); ^{1}H NMR (DMSO-d_6) δ 11.69 (s, 1H, ex, NH), 7.86 (s, 1H, H6), 7.20-7.45 (m, 9H, Ar), 6.89 (d, 4H, *J* = 8.5 Hz, Ar), 5.72 (d, 1H, ex, *J* = 4.5 Hz, 3′-OH), 5.39 (s, 1H, H1′), 4.28 (s, 1H, H2′), 4.08 (d, 1H, *J* = 4.5 Hz, H3′), 3.75-3.80 (m, 2H, 2×H5″), 3.73 (s, 6H, 2×OCH_3), 3.40-3.43 (d, 1H, *J* = 11.0 Hz, H5′), 3.30-3.33 (d, 1H, *J* = 11.0 Hz, H5′, overlap with H_2O signal), -0.04 (s, 9H, Me_3Si); ^{13}C NMR (DMSO-d_6) δ 161.5, 158.05, 158.03, 148.9, 144.6, 142.5 (C6), 135.4, 135.2, 129.7 (Ar), 129.5 (Ar), 127.8 (Ar), 127.6 (Ar), 126.6 (Ar), 113.2 (Ar), 97.9, 97.5, 96.9, 87.7, 87.1 (C1′), 85.5, 78.6 (C2′), 71.3 (C5″), 69.5 (C3′), 58.9 (C5′), 55.0 (CH_3O), -0.47 (Me_3Si).

(1*R*,3*R*,4*R*,7*S*)-1-(4,4′-Dimethoxytrityloxymethyl)-3-(5-ethynyluracil-1-yl)-7-hydroxy-2,5-dioxabicyclo[2.2.1]heptane (4b). To a solution of nucleoside **4a** (0.53 g, 0.81 mmol) in THF (20 mL) was added tetrabutylammonium fluoride in THF (TBAF, 1M, 1.2 mL, 1.2 mmol) and the reaction mixture was stirred at rt for 2h. EtOAc (50 mL) was added and the organic phase washed with brine (2×30 mL) and H_2O (30 mL). The aqueous phase was back-extracted with EtOAc (30 mL). The combined organic phase was dried (Na_2SO_4), evaporated to dryness and the resulting residue purified by column chromatography (0-5% MeOH in CH_2Cl_2, v/v) to afford nucleoside **4b** (0.37 g, 78%) as a lightly brown solid material. R_f = 0.4 (5% MeOH/ CH_2Cl_2, v/v); ESI-HRMS *m*/*z* 621.1666 ($[M+K]^+$, $C_{33}H_{30}N_2O_8{\cdot}K^+$, Calcd 621.1634); ^{1}H NMR (DMSO-d_6) δ 11.70 (s, 1H, ex, NH), 7.88 (s, 1H, H6), 7.21-7.45 (m, 9H, Ar), 6.88-6.92 (m, 4H, Ar), 5.70 (d, 1H, ex, *J* = 4.5 Hz, 3′-OH), 5.45 (s, 1H, H1′), 4.27 (s, 1H, H2′), 4.05 (d, 1H, *J* =

4.5 Hz, H3′), 3.95 (s, 1H, CH), 3.77 (s, 2H, 2×H5″), 3.75 (s, 6H, 2×CH_3O), 3.43-3.45 (d, 1H, *J* = 11.0 Hz, H5′), 3.28-3.31 (d, 1H, *J* = 11.0 Hz, H5′, overlap with H_2O signal); ^{13}C NMR (DMSO-d_6) δ 161.7, 158.1, 149.0, 144.6, 142.2 (C6), 135.3, 135.2, 129.7 (Ar), 129.6 (Ar), 127.9 (Ar), 127.5 (Ar), 126.7 (Ar), 113.3 (Ar), 97.2, 87.5, 86.9 (C1′), 85.7, 83.6, 78.9 (C2′), 76.2, 71.4 (C5″), 69.4 (C3′), 59.0 (C5′), 55.0 (CH_3O).

(1*R*,3*R*,4*R*,7*S*)-3-[5-(3-Benzoyloxypropyn-1-yl)uracil-1-yl]-1-(4,4′-dimethoxytrityloxymethyl)-7-hydroxy-2,5-dioxabicyclo[2.2.1]heptane (4c). After setting up nucleoside **3** (0.50 g, 0.73 mmol), $Pd(PPh_3)_4$ (90 mg, 0.07 mmol), CuI (30 mg, 0.14 mmol), prop-2-ynyl benzoate[43] (180 mg, 1.12 mmol) and Et_3N (0.40 mL, 2.84 mmol) in DMF (10 mL) as described in the representative Sonogashira protocol, the reaction mixture was stirred at rt for 12 h. After workup and purification, nucleoside **4c** (0.37 g, 70 %) was obtained as a light brown solid material. R_f = 0.5 (5% MeOH in CH_2Cl_2, v/v); ESI-HRMS *m/z* 739.2289 ($[M+Na]^+$, $C_{41}H_{36}N_2O_{10}$·Na, Calc 739.2262); ^{1}H NMR (DMSO-d_6) δ 11.72 (s, 1H, ex, NH), 7.91-7.93 (d, 2H, *J* = 7.7 Hz, Bz_{ortho}), 7.89 (s, 1H, H6), 7.65-7.70 (t, 1H, *J* = 7.7 Hz, Bz_{para}), 7.49-7.54 (t, 2H, *J* = 7.7 Hz, Bz_{meta}), 7.42-7.46 (d, 2H, *J* = 8.5 Hz, DMTr), 7.28-7.34 (m, 6H, DMTr), 7.18-7.22 (t, 1H, *J* = 7.5 Hz, DMTr), 6.87-6.91 (2d, 4H, *J* = 9.0 Hz, DMTr), 5.74 (d, 1H, ex, *J* = 4.5 Hz, 3′-OH), 5.42 (s, 1H, H1′), 4.93-4.97 (d, 1H, *J* = 16.0 Hz, CH_2OBz), 4.86-4.90 (d, 1H, *J* = 16.0 Hz, CH_2OBz), 4.25 (s, 1H, H2′), 4.10 (d, 1H, *J* = 4.5 Hz, H3′), 3.78-3.82 (d, 1H, *J* = 8.0 Hz, H5″), 3.75-3.76 (d, 1H, *J* = 8.0 Hz, H5″), 3.71 (s, 6H, 2×CH_3O), 3.53-3.56 (d, 1H, *J* = 11.0 Hz, H5′), 3.27-3.30 (d, 1H, *J* = 11.0 Hz, H5′, overlap with H_2O); ^{13}C NMR (DMSO-d_6) δ 164.9, 161.6, 158.1, 158.0, 149.0, 144.6, 142.7 (C6), 135.4, 135.0, 133.5 (CBz_{para}), 129.7 (DMTr), 129.6 (DMTr), 129.2 (CBz_{ortho}), 129.0, 128.7 (CBz_{meta}), 127.8 (DMTr), 127.5 (DMTr), 126.6

(DMTr), 113.20 (DMTr), 113.17 (DMTr), 96.8, 87.6, 86.9 (C1′), 86.3, 85.6, 79.2, 78.7 (C2′), 71.3 (C5″), 69.4 (C3′), 58.7 (C5′), 54.9 (CH_3O), 53.1 (CH_2OBz).

(1*R*,3*R*,4*R*,7*S*)-1-(4,4′-Dimethoxytrityloxymethyl)-7-hydroxy-3-[5-(3-trifluoroacetylaminopropyn-1-yl)uracil-1-yl]-2,5-dioxabicyclo[2.2.1]heptane (4d). After setting up nucleoside **3** (0.50 g, 0.73 mmol), $Pd(PPh_3)_4$ (90 mg, 0.07 mmol), CuI (30 mg, 0.14 mmol), 2,2,2-trifluoro-*N*-(prop-2-ynyl)acetamide[44] (180 mg, 1.46 mmol) and Et_3N (0.40 mL, 2.84 mmol) in DMF (10 mL) as described in the representative Sonogashira protocol, the reaction mixture was stirred at rt for 12 h. After workup and purification, nucleoside **4d** (0.41 g, 80 %) was obtained as a brown solid material. R_f = 0.5 (5% MeOH in CH_2Cl_2, v/v); ESI-HRMS *m/z* 714.2247 ($[M+Li]^+$, $C_{36}H_{32}F_3N_3O_9 \cdot Li^+$, Calc 714.2245); ^{1}H NMR (DMSO-d_6) δ 11.69 (s,1H, ex, NH(U)), 9.95 (t, 1H, ex, J = 5.5 Hz, $NHCH_2$), 7.78 (s, 1H, H6), 7.22-7.46 (m, 9H, Ar), 6.90 (dd, 4H, J = 9.0 Hz, 3.5 Hz, Ar), 5.73 (d, 1H, ex, J = 4.5 Hz, 3′-OH), 5.41 (s, 1H, H1′), 4.25 (s, 1H, H2′), 3.97-4.10 (m, 3H, H3′, CH_2NH), 3.79-3.83 (2d, 2H, J = 8.0 Hz, 2×H5″), 3.74 (s, 6H, 2×CH_3O), 3.56-3.58 (d, 1H, J = 11.0 Hz, H5′), 3.26-3.28 (d, 1H, J = 11.0 Hz, H5′); ^{13}C NMR (DMSO-d_6) δ 161.6, 158.11, 158.06, 155.9 (q, J = 36.1 Hz, $COCF_3$), 149.0, 144.6, 142.1 (C6), 135.4, 134.9, 129.8 (Ar), 129.6 (Ar), 127.8 (Ar), 127.5 (Ar), 126.6 (Ar), 115.6 (q, J = 287 Hz, CF_3), 113.22 (Ar), 113.20 (Ar), 97.2, 87.6, 87.2, 86.9 (C1′), 85.6, 78.7 (C2′), 75.4, 71.3 (C5″), 69.6 (C3′), 59.1 (C5′), 55.0 (CH_3O), 29.4 (CH_2NH); ^{19}F (DMSO-d_6, 470 MHz) δ -74.7.

(1*R*,3*R*,4*R*,7*S*)-3-[5-(3-(1-Adamantylmethylcarbonyl)aminopropyn-1-yl)uracil-1-yl]-1-(4,4′-dimethoxytrityloxymethyl)-7-hydroxy-2,5-dioxabicyclo[2.2.1]heptane (4e). After setting up nucleoside **3** (0.50 g, 0.73 mmol), $Pd(PPh_3)_4$ (90 mg, 0.05 mmol), CuI (30 mg, 0.10 mmol), *N*-(prop-2-ynyl)-1-adamantaneacetamide (220 mg, 1.00 mmol) and Et_3N (0.40 mL,

2.84 mmol) in DMF (10 mL) as described in the representative Sonogashira protcol, the reaction mixture was stirred at rt for 12h. After workup and purification, nucleoside **4e** (0.43 g, 76 %) was obtained as a white solid material. R_f = 0.5 (5% MeOH in CH_2Cl_2, v/v); MALDI-HRMS *m/z* 810.3330 ($[M + Na]^+$, $C_{46}H_{49}N_3O_9 \cdot Na^+$, Calcd 810.3361); ^{1}H NMR (DMSO-d_6) δ 11.66 (s, 1H, ex, NH(U)), 8.00 (t, 1H, ex, *J* = 5.5 Hz, NHCO), 7.75 (s, 1H, H6), 7.42-7.45 (m, 2H, Ar), 7.23-7.34 (m, 7H, Ar), 6.89-6.92 (2d, 4H, *J* = 9.0 Hz, Ar), 5.72 (d, 1H, ex, *J* = 4.5 Hz, 3′-OH), 5.42 (s, 1H, H1′), 4.24 (s, 1H, H2′), 4.01 (d, 1H, *J* = 4.5 Hz, H3′), 3.87-3.93 (dd, 1H, *J* = 17.5 Hz, 5.5 Hz, CH_2NHCO), 3.82-3.87 (dd, 1H, *J* = 17.5 Hz, 5.5 Hz, CH_2NHCO), 3.78-3.82 (2d, 2H, *J* = 8.2 Hz, H5″), 3.75 (s, 3H, CH_3O), 3.74 (s, 3H, CH_3O), 3.54-3.56 (d, 1H, *J* = 11.0 Hz, H5′), 3.27-3.30 (d, 1H, *J* = 11.0 Hz, H5′, overlap with H_2O), 1.82-1.87 (m, 5H, 3x ada-CH/CH_2CONH), 1.53-1.63 (m, 12H, 6x ada-CH_2); ^{13}C NMR (DMSO-d_6) δ 169.6, 161.7, 158.12, 158.07, 149.0, 144.7, 141.5 (C6), 135.4, 134.9, 129.8 (Ar), 129.6 (Ar), 127.9 (Ar), 127.5 (Ar), 126.7 (Ar), 113.24 (Ar), 113.23 (Ar), 97.7, 89.6, 87.5, 86.9 (C1′), 85.6, 78.8 (C2′), 74.2, 71.4 (C5″), 69.6 (C3′), 59.1 (C5′), 54.9 (CH_3O), 49.5 (CH_2CONH), 42.0 (ada-CH_2), 36.4 (ada-CH_2), 32.3, 28.4 (CH_2NHCO), 28.0 (ada-CH).

(1*R*,3*R*,4*R*,7*S*)-1-(4,4′-Dimethoxytrityloxymethyl)-3-[5-(3-dodecanoylaminopropyn-1-yl)uracil-1-yl]-7-hydroxy-2,5-dioxabicyclo[2.2.1]heptane (4f). After setting up nucleoside **3** (200 mg, 0.29 mmol), $Pd(PPh_3)_4$ (34 mg, 0.03 mmol), CuI (11 mg, 0.06 mmol), *N*-(prop-2-ynyl)lauroylamide (110 mg, 0.44 mmol) and Et_3N (0.18 mL, 1.29 mmol) in DMF (3 mL) as described in the representative Sonogashira protocol, the reaction mixture was stirred at rt for 15 h. After workup and purification, nucleoside **4f** (202 mg, 87 %) was obtained as a white solid material. R_f = 0.2 (5% MeOH in CH_2Cl_2, v/v); MALDI-HRMS *m/z* 816.3835 ($[M+Na]^+$, $C_{46}H_{55}N_3O_9P \cdot Na^+$, Calcd 816.3831); ^{1}H NMR (DMSO-d_6) δ 11.67 (s, 1H, ex, NH(U)), 8.08 (t,

1H, *J* = 5.4 Hz, $NHCH_2$), 7.76 (s, 1H, H6), 7.22-7.46 (m, 9H, Ar), 6.87-6.96 (m, 4H, Ar), 5.72 (d, 1H, ex, *J* = 4.7 Hz, 3′-OH), 5.42 (s, 1H, H1′), 4.25 (s, 1H, H2′), 4.03 (d, 1H, *J* = 4.7 Hz, H3′), 3.88-3.94 (dd, 1H, *J* = 12.4 Hz, 5.4 Hz, CH_2NHCO), 3.81-3.88 (dd, 1H, *J* = 12.4 Hz, 5.4 Hz, CH_2NHCO), 3.78-3.82 (2d, 2H, *J* = 8.0 Hz, H5″), 3.75 (s, 6H, 2×CH_3O), 3.55-3.57 (d, 1H, *J* = 10.9 Hz, H5′), 3.27-3.30 (d, 1H, *J* = 10.9 Hz, H5′, overlap with H_2O), 2.05 (t, 2H, *J* = 7.4 Hz,CH_2CONH), 1.43-1.48 (m, 2H, CH_2CH_2CONH), 1.19-1.28 (m, 16H, 8×CH_2), 0.85 (t, 3H, *J* = 7.0 Hz, CH_3); ^{13}C NMR (DMSO) δ 171.7, 161.7, 158.11, 158.06, 149.0, 144.6, 141.6 (C6), 135.4, 134.9, 129.8 (Ar), 129.6 (Ar), 127.9 (Ar), 127.5 (Ar), 126.6 (Ar), 113.22 (Ar), 113.21 (Ar), 97.7, 89.5, 87.5, 86.9 (C1′), 85.6, 78.8 (C2′), 74.3, 71.4 (C5”), 69.6 (C3′), 59.0 (C5′), 55.0 (CH_3O), 35.0 (CH_2CONH), 31.2 (CH_2), 28.94 (CH_2), 28.92 (CH_2), 28.8 (CH_2), 28.7 (CH_2), 28.63 (CH_2), 28.60 (CH_2), 28.52 (CH_2NHCO), 25.0 (CH_2CH_2CONH), 22.0 (CH_2CH_3), 13.9 (CH_3).

(1*R*,3*R*,4*R*,7*S*)-1-(4,4′-Dimethoxytrityloxymethyl)-7-hydroxy-3-[5-(3-octadecanoylaminopropyn-1-yl)uracil-1-yl]-2,5-dioxabicyclo[2.2.1]heptane (4g). After setting up nucleoside **3** (0.34 g, 0.50 mmol), $Pd(PPh_3)_4$ (60 mg, 0.05 mmol), CuI (20 mg, 0.10 mmol), *N*-(prop-2-ynyl)stearamide (0.28 g, 1.00 mmol) and Et_3N (0.30 mL, 2.13 mmol) in DMF (10 mL) as described in the representative Sonogashira protocol, the reaction mixture was stirred at 40 °C for 6 h. After workup and purification, nucleoside **4g** (0.29 g, 68 %) was obtained as a brown solid material, which was used in the next step without further purification. R_f = 0.5 (5% MeOH in CH_2Cl_2, v/v); FAB-HRMS *m/z* 877.4844 ($[M]^+$, $C_{52}H_{67}N_3O_9^+$, Calcd 877.4877); ^1H NMR ($CDCl_3$) δ 9.45 (br s, 1H, ex, NH(U)), 8.05 (s, 1H, H6), 7.22-7.50 (m, 9H, Ar), 6.85-6.89 (dd, 4H, *J* = 9.0 Hz, 1.5 Hz, Ar), 5.56-5.59 (m, 2H, 1 ex, H1′, $NHCH_2$), 4.53 (s, 1H, H2′), 4.29 (s, 1H, H3′), 3.78-4.01 (m, 10H, 2×H5″, CH_2NH, 2×CH_3O), 3.53-3.57 (d, 1H, *J*

= 11.0 Hz, H5′), 3.49-3.52 (d, 1H, *J* = 11.0 Hz, H5′), 3.35 (br s, 1H, ex, 3′-OH), 1.85-1.89 (m, 2H, CH_2CONH), 1.44-1.51 (m, 2H, CH_2CH_2CONH), 1.23-1.28 (m, 28H, 14 × CH_2), 0.89 (t, 3H, *J* = 6.5 Hz, CH_3); ^{13}C NMR ($CDCl_3$) δ 172.7, 162.1, 158.69, 158.67, 148.6, 144.6, 141.9 (C6), 135.5, 135.4, 130.02 (Ar), 130.01 (Ar), 128.1 (Ar), 128.0 (Ar), 127.0 (Ar), 113.45 (Ar), 113.43 (Ar), 99.1, 89.9, 88.4, 87.4 (C1′), 86.6, 79.1 (C2′), 74.2, 71.8 (C5″), 70.5 (C3′), 58.5 (C5′), 55.3 (CH_3O), 36.1 (CH_2CONH), 31.9 (CH_2), 29.9 (CH_2NH), 29.69 (CH_2), 29.68 (CH_2), 29.66 (CH_2), 29.6 (CH_2), 29.5 (CH_2), 29.4 (CH_2), 29.34 (CH_2), 29.33 (CH_2), 25.4 (CH_2CH_2CONH), 22.7 (CH_2), 14.1 (CH_3). A small impurity of silicon grease was observed at ~ 1 ppm in the ^{13}C NMR.[45]

(1*R*,3*R*,4*R*,7*S*)-3-[5-(3-Cholesterylcarbonylaminopropyn-1-yl)uracil-1-yl]-1-(4,4′-dimethoxytrityloxymethyl)-7-hydroxy-2,5-dioxabicyclo[2.2.1]heptane (4h). After setting up nucleoside **3** (0.34 g, 0.50 mmol), $Pd(PPh_3)_4$ (60 mg, 0.05 mmol), CuI (20 mg, 0.10 mmol), cholesteryl-prop-2-ynyl-carbamate[46] (0.47 g, 1.00 mmol) and Et_3N (0.30 mL, 2.13 mmol) in DMF (8 mL) as described in the representative Sonogashira protocol, the reaction mixture was stirred at rt for 12 h. After workup and purification, nucleoside **4h** (0.27 g, 53%) was obtained as a brown solid material, which was used in the next step without further purification. R_f = 0.5 (5% MeOH in CH_2Cl_2, v/v); FAB-HRMS *m/z* 1046.5560 ($[M+Na]^+$, $C_{62}H_{77}N_3O_{10}\cdot Na^+$, Calcd 1046.5507); ^1H NMR ($CDCl_3$) δ 9.40 (br s, 1H, ex, NH(U)), 7.97 (s, 1H, H6), 7.22-7.49 (m, 9H, Ar), 6.87 (d, 4H, *J* = 9.0 Hz, Ar), 5.58 (s, 1H, H1′), 5.34 (d, 1H, *J* = 5.0 Hz, HC=C-chol), 4.96 (bs, 1H, ex, $NHCH_2$), 4.53 (s, 1H, H2′), 4.40-4.47 (m, 1H, HC-O-chol) 4.23 (bs, 1H, H3′), 3.83-3.98 (m, 4H, 2×H5″, CH_2NH), 3.80 (s, 3H, CH_3O), 3.79 (s, 6H, 2×CH_3O), 3.58-3.61 (d, 1H, *J* = 11.0 Hz, H5′), 3.51-3.53 (d, 1H, *J* = 11.0 Hz, H5′), 3.27 (bs, 1H, ex, 3′-OH), 0.87-2.29 (m, 40 H, chol), 0.69 (s, 3H, CH_3-chol); ^{13}C NMR ($CDCl_3$) δ 162.1, 158.63, 158.60, 155.5,

148.7, 144.5, 141.8 (C6), 139.8, 135.44, 135.39, 130.0 (Ar), 128.1 (Ar), 128.0 (Ar), 127.0 (Ar), 122.5 (=CH, chol), 113.4 (Ar), 99.2, 90.1, 88.4, 87.4 (C1′), 86.6, 79.1 (C2′), 74.7 (OCH-chol), 74.1, 71.9 (C5″), 70.6 (C3′), 58.6 (C5′), 56.7 (CH-chol), 56.2 (CH-chol), 55.2 (CH_3O), 50.0 (CH-chol), 42.3, 39.8 (CH_2-chol), 39.5 (CH_2-chol), 38.5 (CH_2-chol), 37.0 (CH_2-chol), 36.5, 36.2 (CH_2-chol), 35.8 (CH-chol), 31.9 (CH-chol/CH_2NH), 28.2 (CH_2-chol), 28.1 (CH_2-chol), 28.0 (CH-chol), 24.3 (CH_2-chol), 23.8 (CH_2-chol), 22.8 (CH_3-chol), 22.5 (CH_3-chol), 21.0 (CH_2-chol), 19.3 (CH_3-chol), 18.7 (CH_3-chol), 11.8 (CH_3-chol). Signals at 41.4, 29.0, 22.6, 20.4, 19.4, 14.3 and 11.4 ppm - presumably arising from a small contamination of unreacted cholesteryl-prop-2-ynyl-carbamate - were also observed in the ^{13}C NMR spectrum.

(1*R*,3*R*,4*R*,7*S*)-1-(4,4′-Dimethoxytrityloxymethyl)-7-hydroxy-3-[5-(2-(1-pyrenyl)ethynyl)uracil-1-yl]-2,5-dioxabicyclo[2.2.1]heptane (4i). After setting up nucleoside **3** (0.34 g, 0.50 mmol), $Pd(PPh_3)_4$ (60 mg, 0.05 mmol), CuI (20 mg, 0.10 mmol), 1-ethynylpyrene[47] (0.28 g, 1.00 mmol) and Et_3N (0.30 mL, 2.84 mmol) in DMF (10 mL) as described in the representative Sonogashira protcol, the reaction mixture was stirred at rt for 12h. Following workup and purification, nucleoside **4i** (0.31 g, 80 %) was obtained as a slightly yellow solid, which was used in the next step without further purification. R_f = 0.5 (5% MeOH in CH_2Cl_2, v/v); MALDI-HRMS *m/z* 805.2554 ($[M+Na]^+$, $C_{49}H_{38}N_2O_8 \cdot Na^+$, Calcd 805.2520); ^1H NMR (DMSO-d_6) δ 11.89 (s, 1H, ex, NH), 8.35 (d, 1H, *J* = 8.5 Hz, Ar), 8.31-8.34 (d, 1H, *J* = 8.5 Hz, Ar), 8.25-8.28 (d, 1H, *J* = 8.0 Hz, Ar), 8.14-8.23 (m, 4H, H6, Ar), 8.09-8.12 (ap t, 1H, *J* = 8.0 Hz, Ar), 7.93 (d, 1H, *J* = 8.5 Hz, Ar), 7.67 (d, 1H, *J* = 8.0 Hz, Ar), 7.49-7.50 (m, 2H, Ar), 7.33-7.38 (m, 4H, Ar), 7.26-7.30 (ap t, 2H, *J* = 7.5 Hz, Ar), 7.03-7.06 (ap t, 1H, *J* = 7.5 Hz, Ar), 6.78-6.85 (m, 4H, Ar), 5.78 (d, 1H, ex, *J* = 4.5 Hz, 3′-OH), 5.53 (s, 1H, H1′), 4.34 (s, 1H, H2′), 4.24 (d, 1H, *J* = 4.5 Hz, H3′), 3.78-3.82 (2d, 2H, *J* = 7.5 Hz, H5″), 3.43-3.52 (m,

7H, OCH_3, H5′), 3.38-3.42 (d, 1H, *J* = 11.0 Hz, H5′); ^{13}C NMR (DMSO-d_6) δ 161.7, 158.02, 157.95, 149.1, 144.4, 141.4 (C6), 135.4, 130.8, 130.7, 130.6, 130.4, 129.6 (Ar), 129.5 (Ar), 128.8 (Ar), 128.2 (Ar), 128.1 (Ar), 127.8 (Ar), 127.7 (Ar), 127.1 (Ar), 126.63 (Ar), 126.58 (Ar), 125.7 (Ar), 125.6 (Ar), 124.8 (Ar), 124.5 (Ar), 123.5, 123.3, 116.9, 113.17 (Ar), 113.16 (Ar), 98.2, 91.3, 88.2, 87.8, 87.2 (C1′), 85.6, 78.8 (C2′), 71.4 (C5″), 69.4 (C3′), 58.7 (C5′), 54.7 (OCH_3), 54.6 (OCH_3). A trace of pyridine was observed in the ^{13}C NMR.[45]

(1*R*,3*R*,4*R*,7*S*)-1-(4,4′-Dimethoxytrityloxymethyl)-7-hydroxy-3-[5-(2-(3-perylenyl)ethynyl)uracil-1-yl]-2,5-dioxabicyclo[2.2.1]heptane (4j). After setting up nucleoside **3** (0.50 g, 0.73 mmol), $Pd(PPh_3)_4$ (90 mg, 0.07 mmol), CuI (30 mg, 0.14 mmol), 3-ethynylperylene[48] (0.27 g, 1.00 mmol) and Et_3N (0.40 mmol, 2.84 mmol) in DMF (10 mL) as described in the representative Sonogashira protocol, the reaction mixture was stirred at rt for 12 h. After workup and purification, nucleoside **4j** (0.49 g, 80 %) was obtained as a brown solid material. R_f = 0.5 (5% MeOH in CH_2Cl_2, v/v); MALDI-HRMS *m/z* 855.2675 ($[M+Na]^+$, $C_{53}H_{40}N_2O_8 \cdot Na^+$, Calcd 855.2677); ^1H NMR (DMSO-d_6) δ 11.86 (s, 1H, ex, NH), 8.34-8.40 (m, 3H, Ar), 8.22 (d, 1H, *J* = 8.0 Hz, Ar), 8.13 (s, 1H, H6), 8.02 (d, 1H , *J* = 8.5 Hz, Ar), 7.79-7.85 (m, 2H, Ar), 7.55 (dt, 2H, *J* = 8.0 Hz, 2.0 Hz, Ar), 7.48-7.51 (m, 2H, Ar), 7.28-7.37 (m, 7H, Ar), 7.22 (d, 1H, *J* = 8.0 Hz, Ar), 7.09-7.12 (t, 1H, *J* = 7.5 Hz, Ar), 6.83-6.88 (m, 4H, Ar), 5.77 (d, 1H, ex, *J* = 4.5 Hz, 3′-OH), 5.51 (s, 1H, H1′), 4.33 (s, 1H, H2′), 4.22 (d, 1H, *J* = 4.5 Hz, H3′), 3.77-3.83 (m, 2H, 2×H5″), 3.59 (s, 3H, OCH_3), 3.56 (s, 3H, OCH_3), 3.48-3.51 (d, 1H, *J* = 11.0 Hz, H5′), 3.35-3.39 (d, 1H, *J* = 11.0 Hz, H5′); ^{13}C NMR (DMSO-d_6) δ 161.7, 158.05, 158.00, 149.0, 144.4, 141.3 (C6), 135.43, 135.37, 134.2, 133.6, 130.9, 130.7, 130.4 (Ar), 130.1, 129.9, 129.6 (Ar), 129.5 (Ar), 128.5 (Ar), 128.2 (Ar), 127.9 (Ar), 127.7 (Ar), 127.60, 127.57, 127.47 (Ar), 127.0 (Ar), 126.9 (Ar), 126.7 (Ar), 125.7 (Ar), 121.5 (Ar), 121.2, 121.1 (Ar), 120.0

(Ar), 119.4, 113.2 (Ar), 98.1, 90.9, 88.5, 87.7, 87.1 (C1′), 85.6, 78.8 (C2′), 71.4 (C5″), 69.4 (C3′), 58.7 (C5′), 54.80 (CH_3O), 54.75 (CH_3O).

(1*R*,3*R*,4*R*,7*S*)-1-(4,4′-Dimethoxytrityloxymethyl)-7-hydroxy-3-[5-(1-(1-pyrenyl)-1*H*-1,2,3-triazol-4-yl)-uracil-1-yl]-2,5-dioxabicyclo[2.2.1]heptane (4k). To a solution of nucleoside **4b** (0.25 g, 0.36 mmol) and 1-pyrenylazide[26] (110 mg, 0.45 mmol) in THF:H_2O:*t*-BuOH (10 mL, 3:1:1, v/v/v) was added aq. sodium ascorbate (1M, 0.70 mL, 0.70 mmol) and aq. $CuSO_4$ (7.5 %, w/v, 0.65 mL, 0.19 mmol). The solution was stirred at rt for 2h, whereupon it was taken up in EtOAc (50 mL) and brine (50 mL). The layers were separated and the organic phase was washed with sat. aq. $NaHCO_3$ (50 mL). The combined aqueous phase was back-extracted with EtOAc (50 mL). The combined organic phase was then dried (Na_2SO_4), evaporated to dryness and the resulting residue purified by column chromatography (0-75 % EtOAc in petroleum ether, v/v) to afford nucleoside **4k** (230 mg, 76%) as a slightly yellow solid material. R_f = 0.4 (70 % EtOAc in petroleum ether, v/v); ESI-HRMS *m/z* 848.2712 ($[M+Na]^+$, $C_{49}H_{39}N_5O_8{\cdot}Na^+$, Calcd 848.2691); ^{1}H NMR (DMSO-d_6) δ 11.85 (s, 1H, ex, NH), 8.84 (s, 1H, H-Tz), 8.58 (s, 1H, H6), 8.48 (d, 1H, *J* = 8.0 Hz, Ar), 8.44-8.47 (d, 1H, *J* = 7.5 Hz, Ar), 8.40-8.43 (d, 1H, *J* = 8.0 Hz, Ar), 8.35-8.38 (d, 1H, *J* = 9.0 Hz, Ar), 8.32-8.35 (d, 1H, *J* = 9.0 Hz, Ar), 8.30 (d, 1H, *J* = 9.0 Hz, Ar), 8.16-8.20 (overlapping d and t, 2H, Ar), 7.79 (d, 1H, *J* = 8.0 Hz, Ar), 7.45-7.48 (d, 2H, *J* = 7.5 Hz, Ar), 7.28-7.39 (m, 6H, Ar), 7.17-7.20 (t, 1H, *J* = 7.5 Hz, Ar), 6.88-6.93 (2d, 4H, *J* = 9.0 Hz, Ar), 5.79 (d, 1H, ex, *J* = 4.5 Hz, 3′-OH), 5.64 (s, 1H, H1′), 4.43 (s, 1H, H2′), 4.13 (d, 1H, *J* = 4.5 Hz, H3′), 3.94-3.97 (d, 1H, *J* = 9.0 Hz, H5″), 3.86-3.90 (d, 1H, *J* = 9.0 Hz, H5″), 3.681 (s, 3H, CH_3O), 3.675 (s, 3H, CH_3O), 3.57-3.60 (d, 1H, *J* = 11.0 Hz, H5′), 3.34-3.37 (m, 1H, *J* = 11.0 Hz, H5′); ^{13}C NMR (DMSO-d_6) δ 161.3, 158.05, 158.02, 149.4, 144.6, 139.4, 135.3, 135.2, 135.0 (C6), 131.6, 130.6, 130.14, 130.09, 129.7 (Ar), 129.6

(Ar), 129.5 (Ar), 128.7 (Ar), 127.8 (Ar), 127.6 (Ar), 127.0 (Ar), 126.6 (Ar), 126.5 (Ar), 126.1 (Ar), 125.3, 125.1 (Ar), 124.8 (CH-Tz), 124.0, 123.7 (Ar), 123.3, 120.9 (Ar), 113.24 (Ar), 113.19 (Ar), 104.3, 87.6, 87.2 (C1′), 85.6, 79.0 (C2′), 71.5 (C5″), 70.0 (C3′), 59.5 (C5′), 54.9 (CH_3O).

(1*R*,3*R*,4*R*,7*S*)-1-(4,4′-Dimethoxytrityloxymethyl)-7-hydroxy-3-[5-(1-(pyren-1-ylmethyl)-1*H*-1,2,3-triazol-4-yl)-uracil-1-yl]-2,5-dioxabicyclo[2.2.1]heptane (4l). To a solution of nucleoside **4b** (0.33 g, 0.56 mmol) and 1-azidomethylpyrene[27] (200 mg, 0.78 mmol) in THF:H_2O:*t*-BuOH (10 mL, 3:1:1, v/v/v), was added aq. sodium ascorbate (1M, 1.00 mL, 1.00 mmol) and aq. $CuSO_4$ (7.5 %, w/v, 1.00 mL, 0.30 mmol). The reaction mixture was stirred at rt for 2 h, whereupon it was taken up in EtOAc (50 mL) and brine (50 mL). The layers were separated and the organic phase was washed with sat. aq. $NaHCO_3$ (50 mL). The combined aqueous phase was back-extracted with EtOAc (50 mL). The combined organic phase was dried (Na_2SO_4), evaporated to dryness and the resulting residue purified by column chromatography (0-75 % EtOAc in petroleum ether, v/v) to afford nucleoside **4l** (0.43 g, 91%) as a slightly yellow solid material. R_f = 0.4 (70 % EtOAc in petroleum ether, v/v); ESI-HRMS *m/z* 862.2869 ($[M+Na]^+$, $C_{50}H_{41}N_5O_8{\cdot}Na^+$, Calc 862.2847); ^{1}H NMR (DMSO-d_6) δ 11.70 (s, 1H, ex, NH), 8.56 (d, 1H, *J* = 9.0 Hz, Ar), 8.44 (s, 1H, H-Tz), 8.29-8.36 (m, 5H, H6, Ar), 8.20-8.23 (d, 1H, *J* = 9.0 Hz, Ar), 8.17-8.20 (d, 1H, *J* = 9.0 Hz, Ar), 8.09-8.12 (t, 1H, *J* = 8.0 Hz, Ar), 8.07 (d, 1H, *J* = 8.0 Hz, Ar), 7.39-7.42 (d, 2H, *J* = 7.5 Hz, Ar), 7.22-7.33 (m, 6H, Ar), 7.09-7.12 (t, 1H, *J* = 7.5 Hz, Ar), 6.88 (d, 4H, *J* = 8.0 Hz, Ar), 6.40 (s, 2H, CH_2Py), 5.69 (d, 1H, ex, *J* = 4.5 Hz, 3′-OH), 5.55 (s, 1H, H1′), 4.32 (s , 1H, H2′), 3.91-3.96 (m, 2H, H3′, H5″), 3.81-3.84 (d, 1H, *J* = 8.0 Hz, H5″), 3.70 (s, 3H, CH_3O), 3.68 (s, 3H, CH_3O), 3.50-3.54 (d, 1H, *J* = 11.0 Hz, H5′), 3.25-3.29 (d, 1H, *J* = 11.0 Hz, H5′); ^{13}C NMR (DMSO-d_6) δ 161.2, 158.1, 158.0, 149.2, 144.7,

138.9, 135.1, 134.2 (C6), 131.0, 130.7, 130.1, 129.7 (Ar), 129.6 (Ar), 129.1, 128.4, 128.2 (Ar), 127.8 (Ar), 127.6 (Ar), 127.5 (Ar), 127.2 (Ar), 126.52 (Ar), 126.45 (Ar), 125.7 (Ar), 125.5 (Ar), 125.0 (Ar), 124.0, 123.7, 122.7 (Ar), 122.4 (CH-Tz), 113.3 (Ar), 113.2 (Ar), 104.5, 87.5, 87.1 (C1′), 85.6, 79.0 (C2′), 71.6 (C5″), 70.0 (C3′), 59.8 (C5′), 54.9 (CH_3O), 54.8 (CH_3O), 50.7 (CH_2Py).

Representative procedure for O3′-phosphitylation. Alcohols **5b-5l** were dried by co-evaporation with anhydrous 1,2-dichloroethane and dissolved in anhydrous CH_2Cl_2. To this was added anhydrous *N*,*N*′-diisopropylethylamine (DIPEA) and 2-cyanoethyl-*N*,*N*-diisopropylchlorophosphoramidite (PCl-reagent) [quantities and volumes specified below] and the reaction was stirred at rt until analytical TLC indicated complete conversion (2 h unless otherwise mentioned). Unless otherwise mentioned, the reaction mixture was diluted with CH_2Cl_2 (25 mL), washed with aq. $NaHCO_3$ (2×10 mL), the combined aqueous phase back-extracted with CH_2Cl_2 (2×10 mL) and the combined organic phase dried (Na_2SO_4) and evaporated to dryness. Regardless of the workup procedure, the resulting residue was purified by silica gel column chromatography (typically 0-4 % MeOH/CH_2Cl_2, v/v) and subsequent trituration from CH_2Cl_2 and petroleum ether to provide the target phosphoramidites.

(1*R*,3*R*,4*R*,7*S*)-7-[2-Cyanoethoxy(diisopropylamino)phosphinoxy]-1-(4,4′-dimethoxytrityloxymethyl)-3-(5-ethynyluracil-1-yl)-2,5-dioxabicyclo[2.2.1]heptane (5b). Nucleoside **4b** (0.34 g 0.58 mmol), DIPEA (0.50 mL, 2.90 mmol), PCl-reagent (0.20 mL, 0.87 mmol) and anhydrous CH_2Cl_2 (10 mL) were mixed, reacted, worked up and purified as described in the representative protocol to provide nucleoside **5b** (0.38 g, 83 %) as a white foam. R_f = 0.5 (2% MeOH in CH_2Cl_2, v/v); ESI-HRMS *m/z* 805.2973 ($[M+Na]^+$, $C_{42}H_{47}N_4O_9P{\cdot}Na^+$, Calcd 805.2958); ^{31}P NMR ($CDCl_3$) δ 149.8, 149.3.

(1*R*,3*R*,4*R*,7*S*)-3-[5-(3-Benzoyloxypropyn-1-yl)uracil-1-yl]-7-[2-cyanoethoxy(diisopropylamino)phosphinoxy]-1-(4,4′-dimethoxytrityloxymethyl)-2,5-dioxabicyclo[2.2.1]heptane (5c). Nucleoside **4c** (0.30 g, 0.42 mmol), DIPEA (300 μL, 1.67 mmol), PCl-reagent (121 μL, 0.54 mmol) and anhydrous CH_2Cl_2 (5 mL) were mixed and reacted (5 h) as described above. At this point the reaction mixture was concentrated to 1/3 volume, diluted with diethyl ether (100 mL) and the organic phase sequentially washed with H_2O (35 mL), H_2O:DMF (70 mL, 1:1, v/v), H_2O (35 mL) and brine (35 mL). The organic phase was evaporated to dryness and the resulting residue purified as described in the representative protocol to provide nucleoside **5c** (150 mg, 43%) as a white foam. R_f = 0.6 (5% MeOH in CH_2Cl_2, v/v); ESI-HRMS *m/z* 939.3356 ($[M+Na]^+$, $C_{50}H_{53}N_4O_{11}P{\cdot}Na^+$, Calcd 939.3341); ^{31}P NMR ($CDCl_3$) δ 149.8, 149.3.

(1*R*,3*R*,4*R*,7*S*)-7-[2-Cyanoethoxy(diisopropylamino)phosphinoxy]-1-(4,4′-dimethoxytrityloxymethyl)-3-[5-(3-trifluoroacetylaminopropyn-1-yl)uracil-1-yl]-2,5-dioxabicyclo[2.2.1]heptane (5d). Nucleoside **4d** (0.37 g 0.52 mmol), DIPEA (0.44 mL, 2.52 mmol), PCl-reagent (0.18 mL, 0.78 mmol) and anhydrous CH_2Cl_2 (10 mL) were mixed, reacted, worked up and purified as described in the representative protocol to provide nucleoside **5d** (0.39 g, 80%) as a white foam. R_f = 0.5 (2% MeOH in CH_2Cl_2, v/v); ESI-HRMS *m/z* 930.3068 ($[M+Na]^+$, $C_{45}H_{49}F_3N_5O_{10}P{\cdot}Na^+$, Calcd 930.3061); ^{31}P NMR ($CDCl_3$) δ 149.7, 149.1.

(1*R*,3*R*,4*R*,7*S*)-3-[5-(3-(1-Adamantylmethylcarbonyl)aminopropyn-1-yl)uracil-1-yl]-7-[2-cyanoethoxy(diisopropylamino)phosphinoxy]-1-(4,4′-dimethoxytrityloxymethyl)-2,5-dioxabicyclo[2.2.1]heptane (5e). Nucleoside **4e** (204 mg, 0.26 mmol), DIPEA (184 μL, 1.06 mmol) and PCl-reagent (106 μL, 0.48 mmol) in anhydrous CH_2Cl_2 (4 mL) were mixed and reacted as described in the representative protocol. At this point, ice-cold EtOH (1 mL) was

added and the solvents were evaporated off. Purification as described in the representative protocol provided nucleoside **4e** (190 mg, 74%) as a slightly yellow foam. R_f = 0.4 (5% MeOH in CH_2Cl_2, v/v); MALDI-HRMS *m/z* 1010.4408 ($[M+Na]^+$, $C_{51}H_{66}N_5O_{10}P{\cdot}Na^+$, Calcd 1010.4440); ^{31}P NMR ($CDCl_3$) δ 149.8, 149.2. A minor impurity at ~14 ppm was observed.

(1*R*,3*R*,4*R*,7*S*)-7-[2-Cyanoethoxy(diisopropylamino)phosphinoxy]-1-(4,4′-dimethoxytrityloxymethyl)-3-[5-(3-dodecanoylaminopropyn-1-yl)uracil-1-yl]-2,5-dioxabicyclo[2.2.1]heptane (5f). Nucleoside **4f** (175 mg, 0.22 mmol), DIPEA (154 μL, 0.88 mmol), N-methylimidazole (14 μL, 0.18 mmol), PCl-reagent (75 μL, 0.33 mmol) and anhydrous CH_2Cl_2 (3 mL) were mixed and reacted (2.5h). The solvents were evaporated off and the resulting residue purified as described in the representative protocol to provide nucleoside **5f** (183 mg, 83%) as a white foam. R_f = 0.4 (4% MeOH in CH_2Cl_2, v/v); MALDI-HRMS *m/z* 1016.4983 ($[M+Na]^+$, $C_{55}H_{72}N_5O_{10}P{\cdot}Na^+$, Calcd 1016.4909); ^{31}P NMR ($CDCl_3$) δ 149.8, 149.2.

(1*R*,3*R*,4*R*,7*S*)-7-[2-Cyanoethoxy(diisopropylamino)phosphinoxy]-1-(4,4′-dimethoxytrityloxymethyl)-3-[5-(3-octadecanoylaminopropyn-1-yl)uracil-1-yl]-2,5-dioxabicyclo[2.2.1]heptane (5g). Nucleoside **4g** (0.25 g, 0.28 mmol), DIPEA (0.24 mL, 1.37 mmol), PCl-reagent 0.10 mL, 0.42 mmol) and anhydrous CH_2Cl_2 (10 mL) were mixed, reacted, worked up and purified as described in the representative protocol to provide nucleoside **5g** (180 mg, 60%) as a white foam. R_f = 0.5 (2% MeOH in CH_2Cl_2, v/v); ESI-HRMS *m/z* 1100.5836 ($[M+Na]^+$, $C_{61}H_{84}N_5O_{10}P{\cdot}Na^+$, Calcd 1100.5848); ^{31}P NMR ($CDCl_3$) δ 149.8, 149.2.

(1*R*,3*R*,4*R*,7*S*)-3-[5-(3-Cholesterylcarbonylaminopropyn-1-yl)uracil-1-yl]-7-[2-cyanoethoxy(diisopropylamino)phosphinoxy]-1-(4,4′-dimethoxytrityloxymethyl)-2,5-dioxabicyclo[2.2.1]heptane (5h). Nucleoside **4h** (240 mg, 0.23 mmol), DIPEA (0.19 mL, 1.08 mmol), PCl-reagent (0.08 mL, 0.34 mmol) and anhydrous CH_2Cl_2 (10 mL) were mixed, reacted, worked up and purified as described in the representative protocol to provide nucleoside **5h** (190 mg, 66%) as a white foam. R_f = 0.5 (2% MeOH in CH_2Cl_2, v/v); ESI-HRMS *m/z* 1246.6571 ($[M+Na]^+$, $C_{71}H_{94}N_5O_{11}P{\cdot}Na^+$, Calcd 1246.6579); ^{31}P NMR ($CDCl_3$) δ 149.8, 149.3.

(1*R*,3*R*,4*R*,7*S*)-7-[2-Cyanoethoxy(diisopropylamino)phosphinoxy]-1-(4,4′-dimethoxytrityloxymethyl)-3-[5-(2-(1-pyrenyl)ethynyl)uracil-1-yl]-2,5-dioxabicyclo[2.2.1]heptane (5i). Nucleoside **4i** (0.20 g, 0.26 mmol), DIPEA (225 μL, 1.28 mmol), PCl-reagent (114 μL, 0.51 mmol) and anhydrous CH_2Cl_2 (4 mL) were mixed and reacted (4.5h) as described in the representative protocol. Solvents were evaporated off and the resulting residue purified as described in the representative protocol to provide nucleoside **5i** (188 mg, 75%) as a pale yellow foam. R_f = 0.5 (5% MeOH in CH_2Cl_2, v/v); MALDI-HRMS *m/z* 1005.3661 ($[M+Na]^+$, $C_{58}H_{55}N_4O_9P{\cdot}Na^+$, Calcd 1005.3606); ^{31}P NMR ($CDCl_3$) δ 149.7, 149.3.

(1*R*,3*R*,4*R*,7*S*)-7-[2-Cyanoethoxy(diisopropylamino)phosphinoxy]-1-(4,4′-dimethoxytrityloxymethyl)-3-[5-(2-(3-perylenyl)ethynyl)uracil-1-yl]-2,5-dioxabicyclo[2.2.1]heptane (5j). Nucleoside **4j** (0.47 g, 0.56 mmol), DIPEA (0.40 mL, 2.26 mmol), PCl-reagent (165 μL, 0.73 mmol) and anhydrous CH_2Cl_2 (4 mL) were mixed, reacted (3h), worked up and purified as described in the representative protocol to provide nucleoside **5j** (0.43 g, 78%) as a yellow foam. R_f = 0.4 (4% MeOH in CH_2Cl_2, v/v); ESI-HRMS *m/z* 1055.3751 ($[M+Na]^+$, $C_{62}H_{57}N_4O_9P{\cdot}Na^+$, Calcd 1055.3763); ^{31}P NMR ($CDCl_3$) δ 149.7, 149.3

(1*R*,3*R*,4*R*,7*S*)-7-[2-Cyanoethoxy(diisopropylamino)phosphinoxy]-1-(4,4′-dimethoxytrityloxymethyl)-3-[5-(1-(1-pyrenyl)-1*H*-1,2,3-triazol-4-yl)-uracil-1-yl]-2,5-dioxabicyclo[2.2.1]heptane (5k). Nucleoside **4k** (180 mg, 0.22 mmol), DIPEA (160 μL, 0.88 mmol), PCl-reagent (63 μL, 0.28 mmol) and anhydrous CH_2Cl_2 (1.5 mL) were mixed and reacted (2.5 h) as described in the representative protocol. At this point, the reaction mixture was diluted with EtOAc (20 mL) and washed with H_2O (2×25 mL). The organic phase was dried (Na_2SO_4), evaporated to dryness and the resulting residue purified as described in the representative protocol to provide nucleoside **5k** (184 mg, 82%) as a white foam. R_f = 0.7 (5% MeOH in CH_2Cl_2, v/v); ESI-HRMS *m/z* 1048.3789 ($[M+Na]^+$, $C_{58}H_{56}N_7O_9P{\cdot}Na^+$, Calcd 1048.3769); ^{31}P NMR ($CDCl_3$) δ 149.8, 149.1.

(1*R*,3*R*,4*R*,7*S*)-7-[2-Cyanoethoxy(diisopropylamino)phosphinoxy]-1-(4,4′-dimethoxytrityloxymethyl)-3-[5-(1-(pyren-1-ylmethyl)-1*H*-1,2,3-triazol-4-yl)-uracil-1-yl]-2,5-dioxabicyclo[2.2.1]heptane (5l). Nucleoside **4l** (0.41 g, 0.49 mmol), DIPEA (345 μL, 1.95 mmol), PCl-reagent (165 μL, 0.73 mmol) and anhydrous CH_2Cl_2 (5 mL) were mixed, reacted (2.5h), worked up and purified as described in the representative protocol to provide nucleoside **5l** (190 mg, 40%) as a white foam. R_f = 0.5 (3% MeOH in CH_2Cl_2, v/v); ESI-HRMS *m/z* 1062.3909 ($[M+Na]^+$, $C_{59}H_{58}N_7O_9P{\cdot}Na^+$, Calcd 1062.3934); ^{31}P NMR ($CDCl_3$) δ 149.6, 149.1.

Synthesis and purification of ONs. **L1**-**L4**, **K1**-**K4**, **N1**-**N4**, **Q1**-**Q4**, **S1**-**S4** and **V5** were prepared and characterized with respect to identity (MALDI-MS) and purity (>80%, ion-pair reverse-phase HPLC) in previous studies.[22,37] All other ONs were synthesized, worked-up, purified and characterized essentially as previously described.[37] Briefly, ONs were synthesized on a 0.2 μmol scale using an automated DNA synthesizer and long chain alkyl amine controlled pore glass columns with a pore size of 500 Å. Standard reagents were used. The following hand-

coupling conditions were employed to incorporate monomers **K**-**Z** into ONs, which generally resulted in coupling yields in excess of 95% (coupling time/activator/solvent): monomers **K**/**L**/**M**/**N**/**O**/**Q**/**S**/**W**/**Z** (15 min/4,5-dicyanoimidazole/CH_3CN), monomer **P** (15 min/4,5-dicyanoimidazole/CH_2Cl_2), monomer **V** (30 min/4,5-dicyanoimidazole/ CH_2Cl_2) and monomers **X**/**Y**/**Z** (15 min/5-[3,5-bis(trifluoromethyl)phenyl]-1*H*-tetrazole/CH_2Cl_2). ONs were cleaved from solid support and protecting groups removed through treatment with concentrated aq. ammonia (55 °C, 24 h). ONs were purified by ion-pair reverse phase HPLC (XTerra MS C18 column) using a gradient of 0.05 M triethyl ammonium acetate in water and 25% water in CH_3CN, followed by detritylation (80% aq. AcOH) and precipitation (NaOAc/$NaClO_4$/acetone, -18 °C for 12-16 h). The identity of all synthesized ONs was verified by MALDI MS analysis (Table S1) recorded in positive ions mode on a Quadrupole Time-Of-Flight tandem Mass Spectrometer (Q-TOF Premiere) equipped with a MALDI source (Waters Micromass LTD., U.K.). Purity (>80%) was verified by ion-pair reverse phase HPLC running in analytical mode.

Biophysical characterization studies. Thermal denaturation temperatures and steady-state fluorescence emission spectra were determined essentially as previously described.[37] Briefly, thermal denaturation temperatures were determined as the maximum of the first derivative of the thermal denaturation curve (A_{260} vs. T) recorded in medium salt buffer (T_m buffer: 110 mM NaCl, 0.1 mM EDTA, pH adjusted with 10 mM Na_2HPO_4/ NaH_2PO_4). A temperature ramp of 0.5 °C/min was used in all experiments. Reported thermal denaturation temperatures are an average of at least two experiments within ±1.0 °C.

Thermodynamic parameters for duplex formation were determined through baseline fitting of denaturation curves (van't Hoff analysis) using software provided with the UV/VIS

spectrometer. Bimolecular reactions, two-state melting behavior, and a heat capacity change of $\Delta C_p = 0$ upon hybridization were assumed. A minimum of two experimental denaturation curves were each analyzed to minimize errors arising from baseline choice. Averages are listed.

3′-Exonuclease degradation studies were performed by observing the change in absorbance at 260 nm and 37 °C as a function of time for a solution of ONs (3.3 μM) in magnesium buffer (600 μL, 50 mM Tris·HCl, 10 mM $MgCl_2$, pH 9.0) to which SVPDE (snake venom phosphordiesterase, Worthington Biochemical Corporation) dissolved in H_2O was added (12 μL, 0.52 μg, 0.03 U).

Steady state fluorescence emission spectra were recorded using the same buffers and ON concentrations (1.0 μM) as in thermal denaturation studies. Fluorescence emission spectra were recorded at 5 °C to ensure maximal hybridization. Deoxygenation was deliberately not applied to the samples since the scope of the work was to determine fluorescence under aerated condition prevailing in bioassays. Steady state fluorescence emission spectra were obtained as an average of five scans using λ_{ex} = 344 nm for **V/Y/Z**-modified ONs, λ_{ex} = 375 nm for **W**-modified ONs, λ_{ex} = 448 nm for **X**-modified ONs, excitation slit 5.0 nm, emission slit 5.0 nm and a scan speed of 600 nm/min.

Supporting Information: General experimental section; experimental protocols for functionalized alkynes; NMR spectra for all new compounds; MS data for all new modified ONs; additional T_m data, 3′-exonuclease degradation and fluorescence data; structure of modified DNA monomers. This material is available free of charge via the Internet at http://pubs.acs.org/.

ACKNOWLEDGEMENTS. We appreciate financial support from Idaho NSF EPSCoR, the BANTech Center at the Univ. of Idaho and Award Number R01 GM088697 from the National Institute of General Medical Sciences, National Institutes of Health. Scholarships from the College of Graduate Studies (M.E.Ø) and the National Science Foundation under award number 0648202 and the Department of Defense ASSURE (Awards to Stimulate and Support Undergraduate Research Experiences) Program (D.J.R) are appreciated. We thank Dr. Alexander Blumenfeld (Dept. Chemistry), Dr. Gary Knerr (Dept. Chemistry) and Dr. Lee Deobald (EBI Murdock Mass Spectrometry Center, Univ. Idaho) for NMR and mass spectrometric analyses.

REFERENCES and NOTES

(1) For recent reviews on conformationally restricted nucleotides, see e.g., (a) Herdewijn, P. *Chem*. *Biodiv*. **2010**, *7*, 1-59. (b) Obika, S.; Abdur Rahman, S. M.; Fujisaka, A.; Kawada, Y.; Baba T.; Imanishi, T. *Heterocycles* **2010**, *81*, 1347-1392. (c) Prakash, T. P. *Chem*. *Biodiv*. **2011**, *8*, 1616-1641. (d) Zhou, C.; Chattopadhyaya, J. *Chem*. *Rev*. **2012**, *112*, 3808-3832.

(2) For recent representative examples, see: (a) Seth, P. P.; Vasquez, G.; Allerson, C. A.; Berdeja, A.; Gaus, H.; Kinberger, G. A.; Prakash, T. P.; Migawa, M. T.; Bhat, B.; Swayze, E. E. *J. Org*. *Chem*. **2010**, *75*, 1569-1581. (b) Li, Q.; Yuan, F.; Zhou, C.; Plashkevych, O.; Chattopadhyaya, J. *J. Org*. *Chem*. **2010**, *75*, 6122-6140. (c) Liu, Y.; Xu, J.; Karimiahmadabadi, M.; Zhou, C.; Chattopadhyaya, J. *J. Org*. *Chem*. **2010**, *75*, 7112-7128. (d) Upadhayaya, R.; Deshpande, S. A. Li, Q.; Kardile, R. A.; Sayyed, A. Y.; Kshirsagar, E. K.; Salunke, R. V.; Dixit, S. S.; Zhou, C.; Foldesi, A.; Chattopadhyaya, J. *J. Org*. *Chem*. **2011**, *76*, 4408-4431. (e) Shrestha, A. R.; Hari, Y.; Yahara, A.; Osawa, T.; Obika, S. *J. Org*. *Chem*. **2011**, *76*, 9891-9899.

(f) Hanessian, S.; Schroeder, B. R.; Giacometti, R. D.; Merner, B. L.; Østergaard, M. E.; Swayze, E. E.; Seth, P. P. *Angew*. *Chem*., *Int. Ed*. **2012**, *51*, 11242-11245. (g) Madsen, A. S.; Wengel, J. *J*. *Org*. *Chem*. **2012**, *77*, 3878-3886; (h) Haziri, A. I.; Leumann, C. J. *J*. *Org*. *Chem*. **2012**, *77*, 5861-5869. (i) Gerber, A-B.; Leumann, C. J. *Chem*. *Eur*. *J*. **2013**, *19*, 6990-7006. (j) Morihiro, K.; Kodama, T.; Kentefu; Moai, Y.; Veedu, R. N.; Obika, S. *Angew*. *Chem*. *Int*. *Ed*. **2013**, *52*, 5074-5078. (k) Hari, Y.; Osawa, T.; Kotobuki, Y.; Yahara, A.; Shrestha, A. R.; Obika, S. *Bioorg*. *Med*. *Chem*. **2013**, *21*, 4405-4412. (l) Hari, Y.; Morikawa, T.; Osawa, T.; Obika, S. *Org*. *Lett*, **2013**, *15*, 3702-3705. (m) Migawa, M. T.; Prakash, T. P.; Vasquez, G.; Seth, P. P.; Swayze, E. E. *Org*. *Lett*. **2013**, *15*, 4316-4319. (n) Hanessian, S.; Schroeder, B. R.; Merner, B. L.; Chen. B.; Swayze, E. E.; Seth, P. P. *J*. *Org*. *Chem*. **2013**, *78*, 9051-9063. (o) Hanessian, S.; Wagger, J.; Merner, B. L.; Giacometti, R. D.; Østergaard, M. E.; Swayze, E. E.; Seth, P. P. *J*. *Org*. *Chem*. **2013**, *78*, 9064-9075.

(3) Eschenmoser, A. *Science* **1999**, *284*, 2118-2124.

(4) Hendrix, C.; Rosemeyer, H.; Verheggen, I.; Van Aerschot, A.; Seela, F.; Herdewijn, P. *Chem*. *Eur*. *J*. **1997**, *3*, 110-120.

(5) Wang, J.; Verbeure, B.; Luyten, I.; Lescrinier, E.; Froeyen, M.; Hendrix, C.; Rosemeyer, H.; Seela, F.; Van Aerschot, A.; Herdewijn, P. *J*. *Am*. *Chem*. *Soc*. **2000**, *122*, 8595-8602.

(6) Bolli, M.; Trafelet, H. U.; Leumann, C. *Nucleic Acids Res*. **1996**, *24*, 4660-4667.

(7) Renneberg, D.; Leumann, C. J. *J*. *Am*. *Chem*. *Soc*. **2002**, *124*, 5993-6002.

(8) Singh, S. K.; Nielsen, P.; Koshkin, A. A.; Wengel, J. *Chem*. *Commun*. **1998**, 455-456.

(9) Kaur, H.; Babu, B. R.; Maiti, S. *Chem*. *Rev*. **2007**, *107*, 4672-4697.

(10) Obika, S.; Nanbu, D.; Hari, Y.; Andoh, J.-I.; Morio, K.-I.; Doi, T.; Imanishi, T. *Tetrahedron Lett*. **1998**, *39*, 5401-5404.

(11) Kool, E. T. *Chem*. *Rev*. **1997**, *97*, 1473-1487.

(12) (a) Duca, M.; Vekhoff, P.; Oussedik, K.; Halby, L.; Arimondo, P. B. *Nucleic Acids Res*. **2008**, *36*, 5123-5138. (b) Bennett, C. F.; Swayze, E. E. *Annu*. *Rev*. *Pharmacol*. *Toxicol*. **2010**, *50*, 259-293. (c) Østergaard, M. E.; Hrdlicka, P. J. *Chem*. *Soc*. *Rev*., **2011**, *40*, 5771-5788. (d) Watts, J. K.; Corey, D. R. *J*. *Pathol*. **2012**, *226*, 365-379. (e) Matsui, M.; Corey, D. R. *Drug Disc*. *Today* **2012**, *17*, 443-450. (f) Dong, H.; Lei, J.; Ding, L.; Wen, Y.; Ju, H.; Zhang, X. *Chem*. *Rev*. **2013**, *113*, 6207-6233.

(13) (a) Wahlestedt, C.; Salmi, P.; Good, L.; Kela, J.; Johnsson, T.; Hokfelt, T.; Broberger, C.; Porreca, F.; Lai, J.; Ren, K. K.; Ossipov, M.; Koshkin, A.; Jacobsen, N.; Skouv, J.; Oerum, H.; Jacobsen, M. H.; Wengel, J. *Proc*. *Natl*. *Acad*. *Sci*. *U*. *S*. *A*. **2000**, *97*, 5633-5638. (b) Graziewicz, M. A.; Tarrant, T. K.; Buckley, B.; Roberts, J.; Fulton, L.; Hansen, H.; Ørum, H.; Kole, R.; Sazani, P. *Mol. Ther.* **2008**, *16*, 1316-1322. (c) Straarup, E. M.; Fisker, N.; Hedtjarn, M.; Lindholm, M. W.; Rosenbohm, C.; Aarup, V.; Hansen, H. F.; Ørum, H.; Hansen J. B.; Koch, T. *Nucleic Acids Res.* **2010**, *38*, 7100-7111. (d) Lanford, R. E.; Hildebrandt-Eriksen, E. S.; Petri, A.; Persson, R.; Lindow, M.; Munk, M. E.; Kauppinen S.; Ørum, H. *Science*, **2010**, *327*, 198-201; (e) Obad, S.; Dos Santos, C. O.; Petri, A.; Heidenblad, M.; Broom, O.; Ruse, C.; Fu, C.; Lindow, M.; Stenvang, J.; Straarup, E. M.; Hansen, H. F.; Koch, T.; Pappin, D.; Hannon G. J.; Kauppinen, S. *Nat. Genet.*, **2011**, *43*, 371-378.

(14) For an updated clinical status of LNA, see http://www.santaris.com/product-pipeline

(15) Wienholds, E.; Kloostermann, W. P.; Misk, W. P.; Alvarez-Saavedra, E.; Berezikov, E.; Bruijn, E.; Horvitz, H. R.; Kauppinen S.; Plasterk, R. H. A. *Nature*, **2005**, *309*, 310-311.

(16) For particularly interesting earlier examples see: (a) Sørensen, M. D.; Kværnø, L.; Bryld, T.; Håkansson, A. E.; Verbeure, B.; Gaubert, G.; Herdewijn, P.; Wengel, J. *J. Am. Chem. Soc.* **2002**, *124*, 2164-2176. (b) Sørensen, M. D.; Petersen, M.; Wengel, J. *Chem. Commun.* **2003**, 2130-2131; (c) Morita, K.; Takagi, M.; Hasegawa, C.; Kaneko, M.; Tsutsumi, S.; Sone, J.; Ishikawa, T.; Imanishi, T.; Koizumi, M. *Bioorg. Med. Chem.* **2003**, *11*, 2211-2226; (d) Fluiter, K.; Frieden, M.; Vreijling, J.; Rosenbohm, C.; De Wissel, M. B.; Christensen, S. M.; Koch, T.; Ørum, H.; Baas, F. *ChemBioChem* **2005**, *6*, 1104-1109; (e) Albæk, N.; Petersen, M.; Nielsen, P. *J. Org. Chem.* **2006**, *71*, 7731-7740; (f) Varghese, O. P.; Barman, J.; Pathmasiri, W.; Plashkevych, O.; Honcharenko, D.; Chattopadhyaya, J. *J. Am. Chem. Soc.* **2006**, *128*, 15173-15187; (g) Abdur Rahman, S. M.; Seki, S.; Obika, S.; Yoshikawa, H.; Miyashita, K.; Imanishi, T. *J. Am. Chem. Soc.* **2008**, *130*, 4886-4896; (h) Mitsuoka, Y.; Kodama, T.; Ohnishi, R.; Hari, Y.; Imanishi, T.; Obika, S. *Nucleic Acids Res.* **2009**, *37*, 1225-1238; (i) Zhou, C.; Liu, Y.; Andaloussi, M.; Badgujar, N.; Plashkevych, O.; Chattopadyaya, J. *J. Org. Chem.* **2009**, *74*, 118-134; (j) Seth, P. P.; Siwkowski, A.; Allerson, C. R.; Vasquez, G.; Lee, S.; Prakash, T. P.; Wancewicz, E. V.; Witchell, D.; Swayze, E. E. *J. Med. Chem.* **2009**, *52*, 10-13.

(17) For reviews, see: (a) Luyten, I.; Herdewijn, P. *Eur. J. Med. Chem.* **1998**, *33*, 515-576. (b) Ahmadian, M.; Bergstrom D. E. in *Modified Nucleotides in Biochemistry, Biotechnology and Medicine*, 1st ed (Ed: P. Herdewijn), Wiley-VCH, Weinheim, **2008**, 251-276.

(18) For particularly interesting examples from the original research literature, see: (a) Wagner, R. W.; Matteucci, M. D.; Lewis, J. G.; Gutierrez, A. J.; Moulds, C.; Froehler B. C. *Science*, **1993**, *260*, 1510-1513. (b) Hashimoto, H.; Nelson M. G.; Switzer, C. *J. Am. Chem. Soc.* **1993**,

115, 7128-7134. (c) Sagi, J.; Szemzo, A.; Ebinger, K.; Szabolcs, A.; Sagi, G.; Ruff, E.; Otvos, L. *Tetrahedron Lett.* **1993**, *34*, 2191-2194. (d) Ahmadian, M.; Zhang, P. M.; Bergstrom, D. E. *Nucleic* Acids *Res*. **1998**, *26*, 3127-3135. (e) Heystek, L. E.; Zhou, H. Q.; Dande P.; Gold, B. *J. Am. Chem. Soc*. **1998**, *120*, 12165-12166. (f) Kottysch, T.; Ahlborn, C.; Brotzel, F.; Richert, C. *Chem. Eur. J*. **2004**, *10*, 4017-4028. (g) Okamoto, A.; Kanatani, K.; Saito, I. *J. Am. Chem. Soc*. **2004**, *126*, 4820-4827. (h) Booth, J.; Brown, T.; Vadhia, S. J.; Lack, O.; Cummins, W. J.; Trent, J. O.; Lane, A. N. *Biochemistry*, **2005**, *44*, 4710-4719. (i) Skorobogatyi, M. V.; Malakhov, A. D.; Pchelintseva, A. A.; Turban, A. A.; Bondarev, S. L.; Korshun V. A. *ChemBioChem* **2006**, *7*, 810-816. (j) Østergaard, M. E.; Guenther, D. C.; Kumar, P.; Baral, B.; Deobald, L.; Paszczynski, A. J.; Sharma P. K.; Hrdlicka, P. J. *Chem. Commun*. **2010**, 4929-4931.

(19) (a) Barbaric J.; Wagenknecht, H. A. *Org. Biomol. Chem*. **2006**, *4*, 2088-2090. (b) Kocalka, P.; Andersen, N. K.; Jensen F.; Nielsen, P. *ChemBioChem.,* **2007**, *8*, 2106-2116. (c) Nguyen, T. N.; Brewer A.; Stulz, E. *Angew. Chem. Int. Ed*. **2009**, *48*, 1974-1977. (d) Kaura, M.; Kumar P.; Hrdlicka, P. J. *Org. Biomol. Chem*. **2012**, *10*, 8575-8578.

(20) Sinkeldam, R. W.; Greco N. J.; Tor, Y. *Chem. Rev*. **2010**, *110*, 2579-2619.

(21) For a recent example, see: Andersen, N. K.; Anderson, B. A.; Wengel J.; Hrdlicka, P. J. *J. Org. Chem*. **2013**, *78*, 12690-12702.

(22) Østergaard, M. E.; Kumar, P.; Baral, B.; Raible, D. J.; Kumar, T. S.; Anderson, B. A.; Guenther, D. C.; Deobald, L.; Paszczynski, A. J.; Sharma P. K.; Hrdlicka, P. J. *ChemBioChem*, **2009**, *10*, 2740-2743.

(23) Kumar, P.; Østerggard, M. E.; Hrdlicka, P. J. *Curr. Protocols Nucleic Acid Chem.*, **2011**, *44*, 4.43.1-4.43.22.

(24) Terminal alkynes were obtained from commercial vendors, synthesized via EDC-mediated coupling between functionalized carboxylic acids and propargylamine (see Scheme S1, Supporting Information) or prepared according to known literature protocols (see experimental protocols).

(25) Agrofoglio, L.A.; Gillaizeau I.; Saito, Y. *Chem. Rev.* **2003**, *103*, 1875-1916.

(26) Schrock, A. K.; Schuster, G. B. *J. Am. Chem. Soc.* **1984**, *106*, 5234-5240

(27) Park, S. Y.; Yoon, J. H.; Hong, C. S., Souane, R.; Kim, J. S.; Mathews, S. E.; Vicens, J. *J. Org. Chem.* **2008**, *73*, 8212-8218.

(28) Rostovtsev, V. V.; Green, L. G.; Fokin, V. V.; Sharpless, K. B. *Angew. Chem. Int. Ed.* **2002**, *41*, 2596-2599.

(29) Bryld, T.; Lomholt, C. *Nucleosides Nucleotides Nucleic Acids*, **2007**, *26*, 1645-1647.

(30) Mergny, J. L.; Lacroix, L. *Oligonucleotides* **2003**, *13*, 515-537.

(31) Gyi, J. I.; Gao, D.; Conn, G. L.; Trent, J. O.; Brown, T.; Lane, A. N. *Nucleic Acids Res.* **2003**, *31*, 2683-2693.

(32) Demidov V. V.; Frank-Kamenetskii, M. D. *Trends Biochemical Sci.* **2004**, *29*, 62-71.

(33) (a) Korshun, V. A.; Stetsenko, D. A.; Gait, M. J. *J. Chem. Soc. Perkin Trans. 1* **2002**, 1092-1104. (b) Dohno, C.; Saito, I. *ChemBioChem* **2005**, *6*, 1075-1081. (c) Kumar, T. S.; Madsen, A. S.; Østergaard, M. E.; Sau, S. P.; Wengel, J.; Hrdlicka, P. J. *J. Org. Chem.* **2009**, *74*, 1070-1081.

(34) Marin, V.; Hansen, H. F.; Koch, T. R.; Armitage, B. A. *J. Biomol. Struc. Dyn.* **2004**, *21*, 841-850.

(35) (a) Mayer, E.; Valis, L.; Wagner, C.; Rist, M.; Amann N.; Wagenknecht, H.-A. *ChemBioChem*, **2004**, *5*, 865-868. (b) Hwang, G. T; Seo, Y. J.; Kim S. J.; Kim, B. H. *Tetrahedron Lett.* **2004**, *45*, 3543-3546.

(36) (a) Dougherty, G.; Pilbrow, J. R. *Int. J. Biochem*. **1984**, *16*, 1179-1192. (b) Manoharan, M.; Tivel, K. L.; Zhao, M.; Nafisi, K.; Netzel, T. L. *J. Phys. Chem*. **1995**, *99*, 17461-17472. (c) Seo, Y. J.; Ryu, J. H.; Kim, B. H. *Org. Lett*. **2005**, *7*, 4931-4933.

(37) Østergaard, M. E.; Kumar, P.; Baral, B.; Guenther, D. C.; Anderson, B. A.; Ytreberg, F. M.; Deobald, L.; Paszczynski, A. J.; Sharma P. K.; Hrdlicka, P. J.; *Chem. Eur. J.* **2011**, *17*, 3157-3165.

(38) Seitz, O.; Schmuck, E. C.; Wennemers, H. Homogeneous DNA Detection, *Highlights in Bioorganic Chemistry*, Wiley-VCH Verlag GmbH & Co., **2004**, pp 311–328.

(39) Quantum yields were not determined for **Z**-modified duplexes. However, direct comparison with **Z5d**:DNA, which has a relative fluorescence quantum yield of ~16% (see reference 18j), suggests that **Z5**:DNA has a quantum yield of 20-30%.

(40) (a) Yamana, K.; Iwase, R.; Furutani, S.; Tsuchida, H.; Zako, H.; Yamaoka T.; Murakami, A. *Nucleic Acids Res*., **1999**, *27*, 2387-2392. (b) Yamana, K.; Zako, H.; Asazuma, K.; Iwase, R.; Nakano H.; Murakami, A. *Angew. Chem. Int. Ed*., **2001**, 40, 1104-1106. (c) Mahara, A.; Iwase, R.; Sakamoto, T.; Yamana, K.; Yamaoka, T.; Murakami, A. *Angew. Chem. Int. Ed*. **2002**, *41*, 3648-3650. (d) Hrdlicka, P. J.; Babu, B. R.; Sørensen, M. D.; Harrit N.; Wengel, J. *J. Am. Chem. Soc***. 2005**, *127*, 13293-13299. (e) Astakhova, I. V.; Korshun V. A.; Wengel, J. *Chem.*

Eur. J. **2008**, *14*, 11010-11026. (f) Wang, G.; Bobkov, G. V.; Mikhailov, S. N.; Schepers, G.; van Aerschot, A.; Rozenski, J.; van der Auweraer, M.; Herdewijn P.; Feyter, S. D. *ChemBioChem* **2009**, *10*, 1175-1185. (g) Østergaard, M. E.; Cheguru, P.; Papasani, M. R.; Hill R. A.; Hrdlicka, P. J. *J. Am. Chem. Soc*. **2010**, *132*, 14221-14228. (h) Astakhova, I. V.; Lindegaard, D.; Korshun V. A.; Wengel, J. *Chem. Commun*. **2010**, *46*, 8362-8364. (i) Förster, U.; Lommel, K.; Sauter, D.; Grünewald, C.; Engels, J. W.; Wachtveitl, J. *ChemBioChem*. **2010**, 11, 664-672. (j) Mansawat, W.; Boonlua, C.; Siriwong K.; Vilaivan, T. *Tetrahedron* **2012**, *68*, 3988-3995.

(41) Shen, L.; Siwkowski, A.; Wancewicz, E.V.; Lesnik, E.; Butler, M.; Witchell, D.; Vasquez, G.; Ross, B.; Acevedo, O.; Inamati, G.; Sasmor, H.; Manoharan, M.; Monia, B. P. *Antisense Nucleic Acid Drug Dev.* **2003**, *13*, 129-142.

(42) Kumar, P., et al…α-L-LNA manus

(43) Ott, K.; Schmidt, K.; Kircher, B.; Schumacher, P.; Wiglenda, T.; Gust, R. *J. Med. Chem.* **2005**, *48*, 622-629.

(44) Trybulski, E.; Zhang, J.; Kramss, R. H.; Mangano, R. M. *J. Med. Chem*. **1993**, *36*, 3533-3541.

(45) Gottlieb, H. E.; Kotlyar, V.; Nudelman, A. *J. Org. Chem.* **1997**, *62*, 7512-7515.

(46) Qu J.; Shiotsuki, M.; Sanda, F.; Masuda, T. *Macromol. Chem. Phys.* **2007**, *208*, 823-832.

(47) Wenting, W.; Wanhua, W.; Shaomin, J.; Hunin, G.; Jiazhang, Z. *Eur. J. Inorg. Chem.* **2010**, 4470-4482.

(48) Andronova, V. L.; Skorobogtyi, M. V.; Manasova, E. V.; Berlin, Y. A.; Korshun, V. A.; Galegov, G. A. *Russ. J. Bioorg. Chem.* **2003**, *29*, 262-266.

2. Self-Assembled Monolayers of Thiols Adsorbed on Au/ZnO-Functionalized Silica Nanosprings: Photoelectron Spectroscopy-Analysis and Detection of Vaporized Explosives

*Abstract.*Self-assembled monolayers (SAMs) of a series of thiols, i.e., L-cysteine, 6-mercaptohexanol, 4-mercaptobenzoic acid, DL-thioctic acid and 11-(1-pyrenyl)-1-undecathiol, which were selected for their propensity to interact with vaporized explosives, were grafted from solution onto gold decorated ZnO-coated nanosprings. X-ray and ultraviolet photoelectron spectroscopies (XPS and UPS) were used to investigate the surface electronic structure of the samples. Based on XPS analysis, characteristic functional groups such as amine, carboxylic acid, hydroxyl and aromatics are exposed at the monolayer-air interface. One or two sulfur signals were observed, which were assigned to sulfur-gold bonds (S-Au) and sulfur-zinc bonds (S-Zn). The C/S ratios agree well with the stoichiometry of the respective thiols. UPS analysis shows that the hybridization of sulfur p states and gold d states produces both bonding and antibonding orbitals, below and above the metal d band, which is characteristic of molecular chemisorption on metal surfaces. Samples treated with 4-mercaptobenzoic acid and 6-mercaptohexanol showed the strongest responses. The response to ammonium nitrate depends on the packing density and ordering of the SAMs. Functionalization of gold decorated ZnO-coated nanosprings with thiols is a promising approach for improving electronic noses for explosives detection.

Introduction.

Recently, major efforts are underway to harness the power of organic chemistry for tuning organic/inorganic interface properties for various materials used in nanoelectronics, chemical sensing, and passivation layers.[1] In fact, combining inorganic and organic materials into hybrid

structures enables one to take advantage of new "collective effects" (i.e. phenomena that the individual components comprising the interface do not exhibit).[2] SAMs on metal nanoparticles or semiconductors surfaces are one approach to tailor these interfaces with close-packed molecules with variable headgroups, chain lengths and film thicknesses.[3] SAMs of thiols on the surface of gold nanoparticles are widely used for the following reasons. First, gold is a relatively inert metal: it does not form a stable oxide surface and it resists atmospheric contamination. Second, gold has a strong specific interaction with sulfur that allows the formation of monolayers with different functional groups. Third, when suitably selected, the formed monolayers are coherent, densely packed, very stable, and crystalline or liquid-crystalline on gold.[4] Understanding, controlling and optimizing the properties of these hybrid materials are keys to developing an efficient device for explosives detection.

The adsorption of thiols onto gold surfaces has been studied by many analytical methods including IR spectroscopy, optical ellipsometry, electron diffraction, wetting contact angle measurements, electrochemistry, and photoelectron spectroscopy.[4-6] These studies have shown that defect-free monolayers are spontaneously adsorbed at Au surfaces with a mean tilt of 20-30°.[5] X-ray and ultraviolet photoelectron spectroscopies, XPS and UPS, respectively, are acutely sensitive to changes in surface morphology and surface functionalization due to their very shallow sampling depths on the order of 30Å. XPS is capable of giving direct and specific insight into the elemental composition, the oxidation states, and the chemical bonding of the elements within the surface region of the material. For example, Joseph et al.[6] analyzed the composition of alkanedithiols films assembled on gold nanoparticles and found that approximately 20 % of the adsorbed thiols were free groups, implying that only 60 % of the alkanedithiol molecules were bound at both ends to the nanoparticles. In terms of sensors, at

room temperature the resistance of these films increased reversibly when dosed with vapors of toluene and tetrachloroethylene and the response increased exponentially with increasing length of the alkanethiols. The presence of unattached thiols within the film is important to deciphering the sensing properties of thiol-based sensors. UPS is a powerful tool to probe the valence band density of states. Furthermore, given the large photoionization cross sections of p-type orbitals in the UV regime, UPS is ideal for probing the highest valence bands of organic materials.[7] Specifically, UPS can be used to identify chemisorbed molecules on solid surfaces and the orbital bonding mechanisms responsible for chemisorptions. Duwez et al.[7] have successfully used UPS to investigate molecular configurations and conformations of n-alkanethiols, α,ω-alkanedithiols, α-cycloalkyl-ω-alkanethiols adsorbed on gold. They found that for n greater than 16, where n is the number of carbon atoms in the hydrocarbon chain, the gold substrate does not disturb the spectral features of SAMs. In all the above-mentioned works, thiols are attached on gold nanoparticles evaporated onto flat surfaces.

The uniqueness of the work reported herein lies in the nature of the substrate, silica nanospring-mats coated with ZnO and subsequently decorated with Au nanoparticles, which is not only non-planar, but is also a hybrid material. ZnO nanosprings have already been shown to be very sensitive chemiresistors, as compared to their thin film, or nanowire, counterparts;[8] however, chemiresistors can sometimes give similar response to different chemicals. Molecular surface functionalization of sensor surface plays a pivotal role in imparting selectivity toward specific gaseous explosives in a complex background of carrier gases, atmospheric vapors, and degradation products. A wide range of coatings such as thiols, polymers, peptides or even antibodies have been demonstrated to exhibit selectivity for explosive analytes.[9] In this study, Au nanoparticles supported on ZnO-coated silica nanosprings have been functionalized with 6-

mercaptohexanol, L-cysteine, 4-mercaptobenzoic acid, DL-thioctic acid and 11-(1-pyrenyl)-1-undecathiol. The first objective of this study is to characterize the binding of thiols to gold nanoparticles and verify the presence of explosive specific receptors at the monolayer-air interface. The second objective is to test the vapor response of the functionalized sensors within the thermal stability range of the Au-S bond. These two objectives are aligned with the ultimate goal of developing a nanospring-based sensor platform capable of detecting vaporized explosives. Based on the success of the aforementioned XPS[6] and UPS[7] studies, we will employ these techniques to achieve our first objective. The vapor sensitivity of the samples will be investigated by exposing them to gaseous analytes while monitoring their conductance.

2. Experimental Details

2.1. Sample Synthesis

2.1.1. Synthesis of Nanospring-mats, Coating and Decoration

The process for producing mats of nanosprings and their subsequent coating with ZnO by atomic layer deposition (ALD) has been discussed in Ref.[8] The ZnO-coated silica nanosprings were decorated with gold nanoparticles by reducing gold salt to metallic gold through a pyrolysis-like process. A 19.5 mM solution was prepared by dissolving $AuCl_3$ in deionized water. Prior to use, the solution was mixed with 20% reagent grade ethanol to improve solvent evaporation and the adhesion of particles. The samples were dipped in the final solution and dried in air at room temperature. Next, they were baked in a preheated tube furnace at 300°C at atmospheric pressure under Ar/H_2 flow of 480 sccm (standard cubic centimeters per minute) and 38 sccm, respectively, for 15 minutes. In the last step, the samples were allowed to cool down to room temperature in Ar atmosphere to minimize condensation of water, CO, etc. A field emission scanning microscope (FESEM) micrograph of a Au/ZnO nanosprings sample is shown in Fig.1. While not visible in Fig. 1, the silica nanosprings consist of five to eight

intertwined silica nanowires.[10] The ZnO coating by ALD is very conformal to the underlying nanosprings and granular in nature, with an average grain size of 20 nm, in excellent agreement with the value of (18 ± 3) nm calculated from X-ray diffraction (XRD) data (not shown). The Au nanoparticles are not distinguishable from ZnO crystallites in the FESEM image due to absence of sufficient contrast. We could not rely on the XRD data for particle size calculation given the significant contribution to Au peaks arising from the underlying Au catalyst used for nanospring synthesis. We therefore resorted to TEM micrographs (not included here) where the mean particle size was measured to be (10 ± 4) nm.

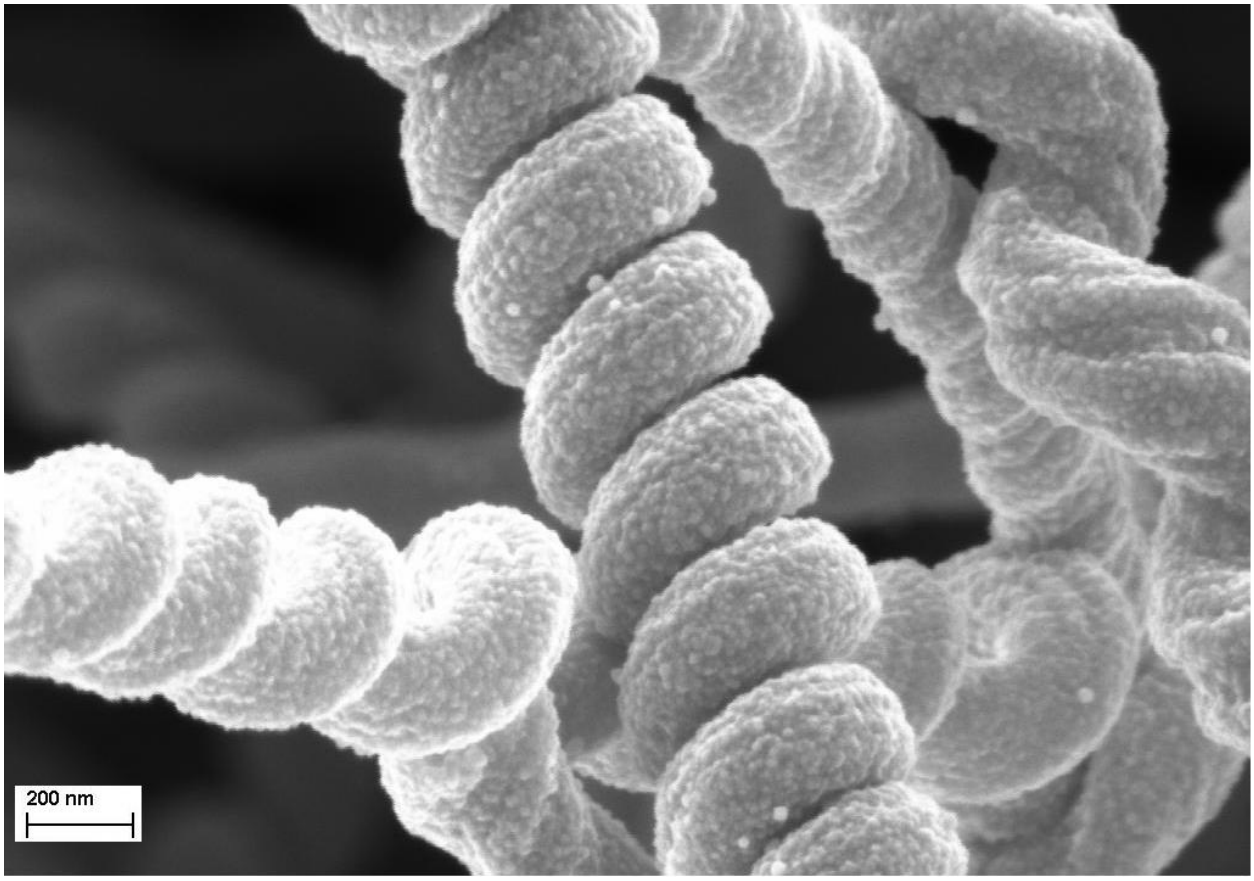

Figure 1. FESEM micrographs of silica nanosprings ALD coated with ZnO and subsequently decorated with Au nanoparticles. The original morphology of the nanosprings is retained during coating. The granular structure of the coating consists of ZnO and Au nanoparticles.

2.1.2. Molecular Functionalization

A total of five Au/ZnO coated silica nanospring mats (area ~ 1 cm^2 grown on Si wafer) were prepared and functionalized with either 6-mercaptohexanol, L-cysteine, 4-mercaptobenzoic acid, DL-thioctic acid, or 11-(1-pyrenyl)-1-undecathiol (selected for their propensity to interact with vaporized explosives[9,11,12]) through incubation of the mats with 10 mM of the selected thiol in an appropriate solvent (6-mercaptohexanol, 4-mercaptobenzoic acid, and DL-thioctic acid in ethanol, L-cysteine in DI water and 11-(1-pyrenyl)-1-undecathiol in toluene) for 48 h to allow uniform and dense SAM formation. The substrates were subsequently washed thrice in the respective solvents and dried under a stream of argon. Relatively highly concentrated thiol solutions were used due to the high surface-to-volume ratio of nanospring mats (~ 400 m^2/g) (10 µM are typically used when functionalizing flat gold surfaces). 11-(1-pyrenyl)-1-undecathiol was synthesized following the protocol in Supporting Information II. Fig. 2 illustrates the anticipated surface attachment of the thiols to the surface of the Au nanoparticles.

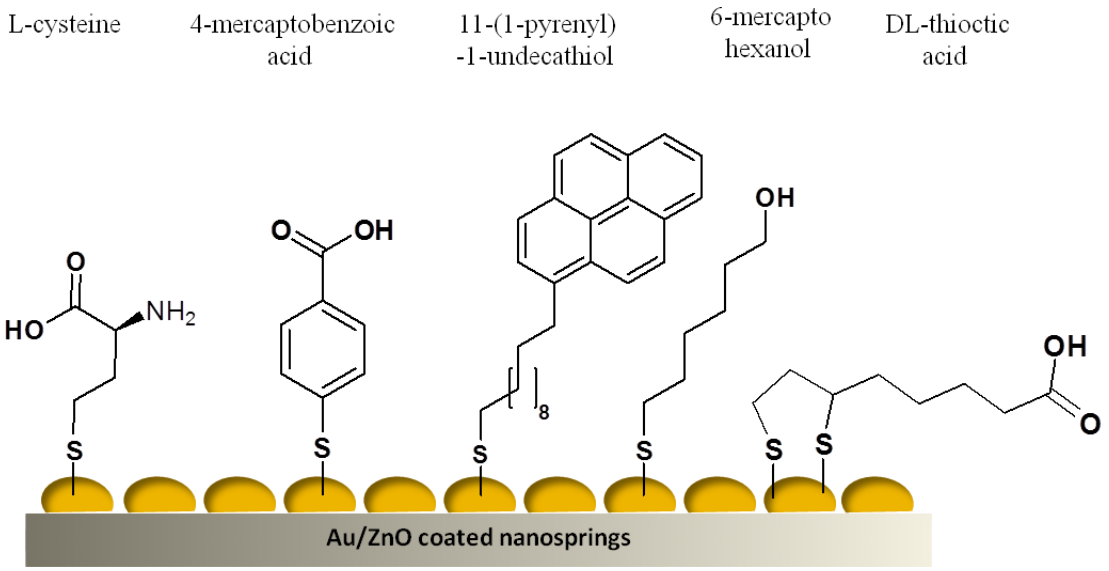

Figure 2. An illustration of idealized binding of thiol groups to the surface of Au/ZnO coated nanosprings.

2.2. X-ray and Ultraviolet Photoelectron Spectroscopies (XPS and UPS)

Photoelectron spectroscopy was performed in a custom built ultra-high vacuum (UHV) chamber with a base pressure of 1.5×10^{-10} Torr. The chamber is equipped with an Omicron model EA 125 hemispherical electron energy analyzer, a dual anode X-ray source, and a He UV lamp. Both the X-ray source and the UV lamp are at the so-called magic angle of 54.7° relative to the axis of the electron analyzer. The MgKα emission line (1253.6 eV) was used for XPS data acquisition. Given the highly disordered nature of the nanospring samples (randomly oriented nanosprings and a mat thickness of ~ 60 μm), in conjunction with the specifications of the X-ray source and electron analyzer, the upper resolution of the XPS spectra is estimated to no better than 300 meV based on the full width at half maximum (FWHM) of the Au $4f_{7/2}$ core level state of the bare Au/ZnO nanosprings sample. To avoid spurious charging the sample was grounded and exposed to a 153 eV electron beam using an electron flood gun. Note, dissociation of the thiols directly by the primary electrons of the flood gun, or subsequent low energy secondary electrons, with extended exposure was not observed. The data pertaining to the use of the electron flood gun is available as Supporting Information I. The binding energy was referenced to the C 1s peak at 285 eV. UPS spectra were acquired with the He I line (21.2 eV) from a Specs UVS 10/35 source, using ultra-pure He (99.999%) that was passed through a liquid nitrogen cold trap. The Fermi edge of a polycrystalline Au specimen was used for binding

energy calibration. In both experiments the takeoff angle was 90°, corresponding to photoelectron emission normal to the sample surface. All spectra were acquired at room temperature. The fitting of the XPS spectra consisted of subtracting a Shirley background prior to peak fitting with Voigt functions.

2.3. Gaseous Analytes Detection Measurements

The apparatus for sensor measurements, as well as test protocols, are described in detail in Ref.[8] Succinctly, a standard two-electrode was used for measuring the electrical response of the samples to chemical vapors. The sensor was connected to a thermocouple and placed on a variable temperature platform for temperature control. The sensor responses were acquired with a Keithley 2400 source-sense meter interfaced to a computer via Labview operated data acquisition software allowing for real time conductance measurements. The sensor was initially heated to the desired temperature. When a steady state resistance was obtained, pulses of vapor were produced by the VaporJet calibrator. Liquid analytes were evaporated while solid ones were sublimated. The VaporJet's ability to sublimate solids almost instantly allows for extremely short pulses in the order of milliseconds. Sensors were tested with vapors of ammonium nitrate (NH_4NO_3), 2,4-dinitrotoluene (DNT), acetone, toluene and ethanol, which are explosives or degradation products of explosive compounds. The experiments were carried out at 100°C and 150°C, below the maximum desorption temperature of the thiols as verified by the XPS analysis (Supporting Information I).

3. Results and discussion.

3.1. X-ray Photoelectron Spectroscopy (XPS)

Broad survey XPS scans of the four SAM-functionalized Au/ZnO nanosprings samples (not shown) exhibited core level states of Au (4f), C (1s), Zn (3d, 3p, 3s, 2p), O (1s) and S (2s,

2p).The sulfur signal of 11-(1-pyrenyl)-1-undecathiol was very weak, where the weakness is attributed to different molecular coverage relative to the other thiols, perhaps due to their long hydrophobic chain. The L-cysteine functionalized sample also included a N (1s) core level state associated with the amine group ($-NH_2$).To investigate the chemical environment of Au, C, S, O, Zn, and N, higher resolution scans for the corresponding specific core levels were acquired. Fig. 3 shows the overlapping Au 4f and Zn 3p core level states.

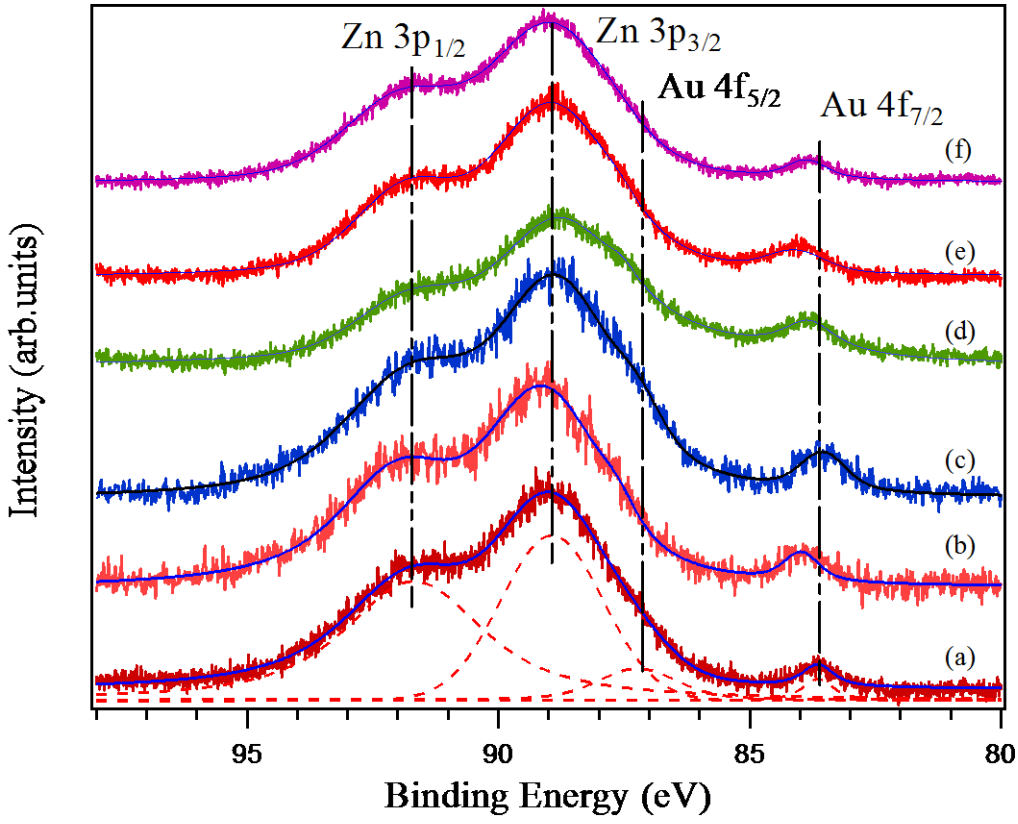

Figure 3. The Au 4f-Zn 3p core level states of an untreated Au/ZnO sample (a) and samples treated with DL-thioctic acid (b), 4-mercaptobenzoic acid (c), L-cysteine (d), 6-mercaptohexanol (e), and 11-(1-pyrenyl)-1-undodecathiol (f).

Quantitative analysis of the XPS spectra of the untreated Au/ZnO sample indicates an atomic ratio of Au/Zn of 0.05. The binding energy of Au 4f for the treated samples is in agreement with results reported for thiols assembled on gold nanoparticles [6-13]. For peak fitting of the spectra in Fig. 3 the spin-orbit splitting of Au 4f was held at 3.65 eV and the ratio of the Au $4f_{7/2}$:Au $4f_{5/2}$ intensity held at 4:3. The Au 4f binding energy shifts to higher values with thiol functionalization relative to the pristine Au/ZnO nanosprings sample, with the exception of 4-mercaptobenzoic acid. This is indicative of charge redistribution associated with the formation of the S-Au bond between the thiols and the Au nanoparticles.

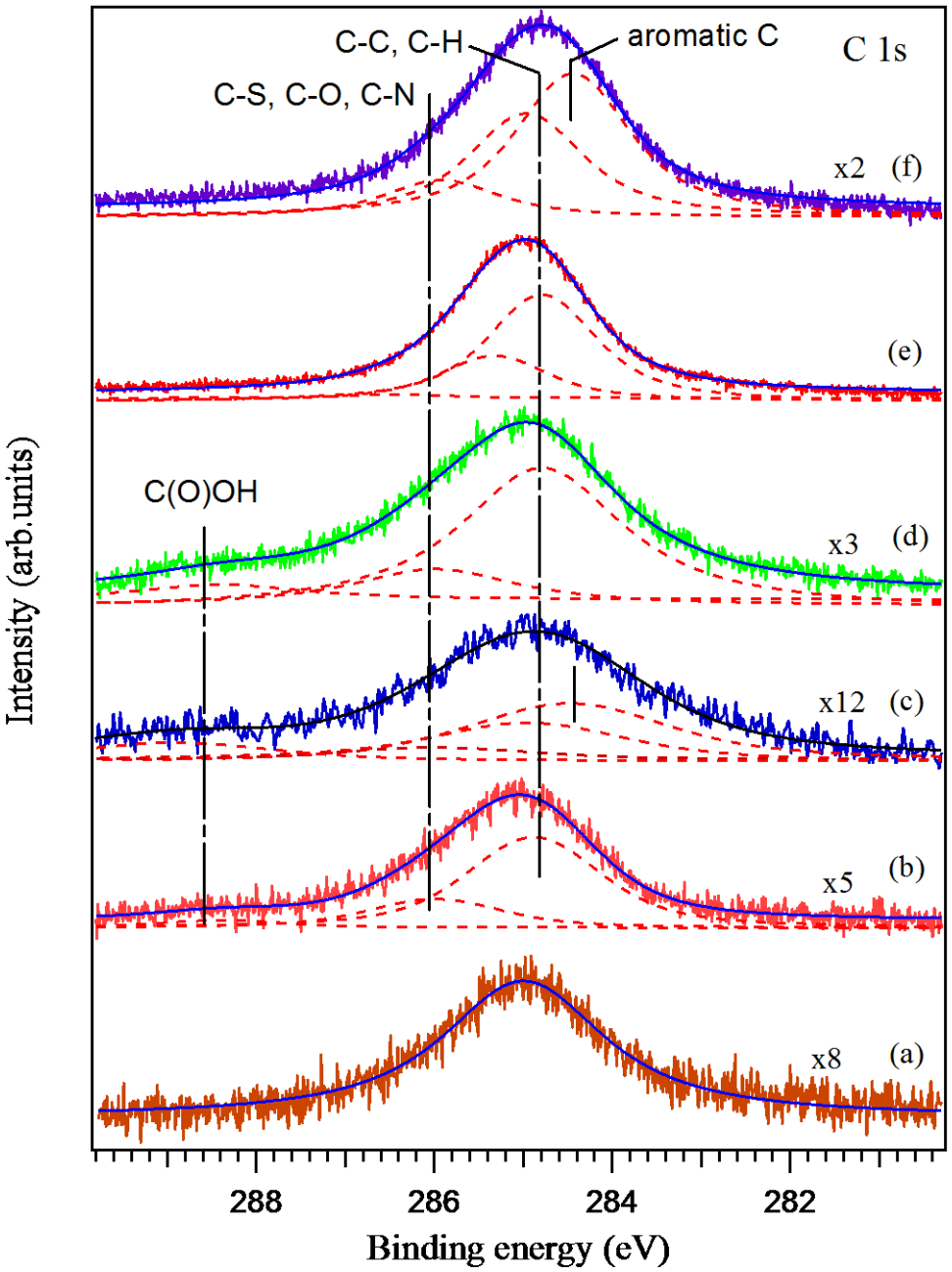

Figure 4. The C 1s core level states of an untreated Au/ZnO sample (a) and treated with DL-thioctic acid (b), 4-mercaptobenzoic acid (c), L-cysteine (d), 6-mercaptohexanol (e), and 11-(1-pyrenyl)-1-undodecathiol (f).

Treated samples contain a substantial amount of carbon due to the organic thiols. In order to achieve a satisfactory peak fitting the adventitious carbon as detected from the untreated sample

was included in the deconvolution of C 1s spectra. The position of a photoelectron peak is sensitive to the charge density on the un-ionized atom and to the degree of shielding of the core-hole generated by the loss of the electron. For carbon 1s, this sensitivity manifests itself as chemical shifts to higher binding energies for carbons in higher oxidation states or with electronegative substituents.[4] The peaks at 284.79 eV (L-cysteine), 284.80 eV (6-mercaptohexanol), 284.97 eV (11-(1-pyrenyl)-1-undecathiol) and 284.88 eV (DL-thioctic acid) are assigned to the C-C/C-H bonds of the aliphatic carbons in the respective thiols. The peak at 285.33 eV (6-mercaptohexanol) corresponds to C-S. The aromatic carbons are the singlets at 284.44 eV (11-(1-pyrenyl)-1-undecathiol) and 284.42 eV (4-mercaptobenzoic acid) since a chemical shift of ~ 0.5 eV occurs in the aromatic species relative to aliphatic unfunctionalized carbon atoms [14]. The contribution at a binding energy of ~ 286 eV is characteristic for C-S, C-O, or C-N bonds. Signals between 288-289 eV are assigned to carbon species involved in the carboxylic acid functional group (O=C-O) of L-cysteine, 4-mercaptobenzoic acid and DL-thioctic acid. These assignments are summarized in Table 1.

Table 1. C 1s spectral deconvolution results showing binding energy, possible assignment and reference.

Sample	Binding Energy (eV)	Assignment	Reference
L-cysteine	284.79	C-C, C-H	[1]
	285.99	C-N, C-O or C-S	[15,16]
	288.39	O=C-O	[14]
6-mercaptohexanol	284.80	C-C, C-H	[1]
	285.33	C-S	[16]
	286.43	C-O	[17]
11-(1-pyrenyl)-1-undecathiol	284.44	Aromatic carbon	[14]
	284.97	C-C, C-H	[14]
	285.92	C-S	[16]
DL-thioctic acid	284.88	C-C, C-H	[1]
	285.99	C-O, C-S	[16]
	288.39	O=C-O	[14]
4-mercaptobenzoic acid	284.42	Aromatic carbon	[14]
	284.72	C-C, C-H	[1]
	285.99	C-O, C-S	[16]
	288.90	O=C-O	[14]

Figure 5. The S 2p core level states as determined by XPS for 4-mercaptobenzoic acid (a), DL-thioctic acid (b), L-cysteine (c), and 6-mercaptohexanol (d) treated samples. The peaks were fitted using one or two doublets corresponding to two different sulfur species. These two sulfur species are assigned to sulfur bound to gold (~161.60 eV) and sulfur bound to zinc at higher binding energies.

The S 2p signal was fitted with two or four peaks which correspond to one doublet (S 2p3/2, S 2p1/2) or two sets of doublets. The fitting procedure of the S doublet consisted of using the same FWHM for both spin states, holding the spin-orbit splitting at 1.2 eV, and a branching ratio of 2:1 (S $2p_{3/2}$:S $2p_{1/2}$). The lower binding energy S doublet is ascribed to sulfur bound to Au. The second doublet is attributed to unbound free thiol groups, and/or bonding of the headgroup instead of S[16] or a Zn-S bond.[18] In the present work, the second doublet is attributed to the Zn-S bonds because alkanethiols are known to form monolayers on ZnO surfaces through Zn-S bonding [16,18]. A peak at 170 eV, which corresponds to a S-O bond, was not observed. The conclusion is that thiol bonding is either Au-S or Zn-S. The weakness of the sulfur signals of 4-mercaptobenzoic acid and 11-(1-pyrenyl)-1-undecathiol samples reflects the attenuation of the signal due to the hydrocarbon chain length and the density of the molecules on the surface of the nanoparticles. It is important to note that the large surface area of the substrate in these samples, notwithstanding, would result in a higher surface density of molecules compared with planar substrates. Furthermore, additional steric hindrance is expected due to the presence of aromatic rings in the headgroup resulting in greater attenuation of the sulfur photoelectrons. Bain et al.[4] reported a weak sulfur signal in the XPS characterization of the following thiols on gold: $HS(CH_2)_{10}CH_3$, $HS(CH_2)_{10}CH_2OH$, $HS(CH_2)_{10}CO_2H$, $HS(CH_2)CO_2CH_3$, $HS(CH_2)_{10}CH_2Cl$, and $HS(CH_2)_8CN$. They invoked monolayer orientation to explain the inelastic scattering of the S 2p electrons by the molecules within the monolayer.

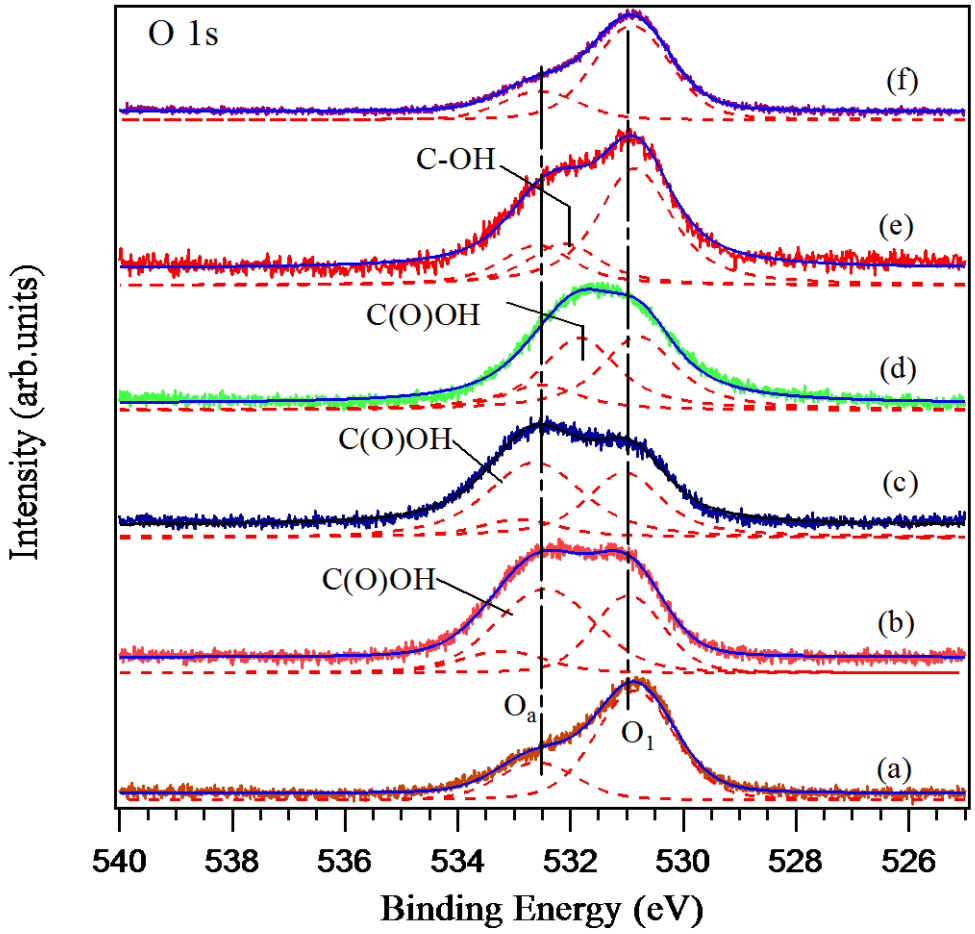

Figure 6. The O 1s core level states of an untreated Au/ZnO sample (a) and samples treated with DL-thioctic acid (b), 4-mercaptobenzoic acid (c), L-cysteine (d), 6-mercaptohexanol (e), and 11-(1-pyrenyl)-1-undodecathiol (f). O1 represent O2- in the wurtzite structure of ZnO and Oa chemisorbed oxygen.

Fig. 6 shows O 1s spectra, which were fitted with two to three components. The peak at ~530 eV (O_1) is due to the lattice oxygen in ZnO, which is the O^{2-} state while the peak at ~532.7 eV (O_a) originates from hydroxyl groups or chemisorbed oxygen[19-20]. The shape for 11-(1-pyrenyl)-1-undecathiol is virtually unchanged relative to the untreated Au/ZnO sample. Besides

the fact that 11-(1-pyrenyl)-1-undecathiol is not an oxygen-containing moiety, this suggests that the oxygen sites on ZnO are not involved in the chemisorption of those molecules onto the substrate. The significant change observed in the spectra of the other treated samples is due to large contributions from the COOH and/or OH groups. Maintaining a fixed ratio between O_1 and O_a allowed us to resolve these contributions. It can be seen that the chemisorbed oxygen shoulder is mainly affected, which suggests that those functional groups are located at the surface.

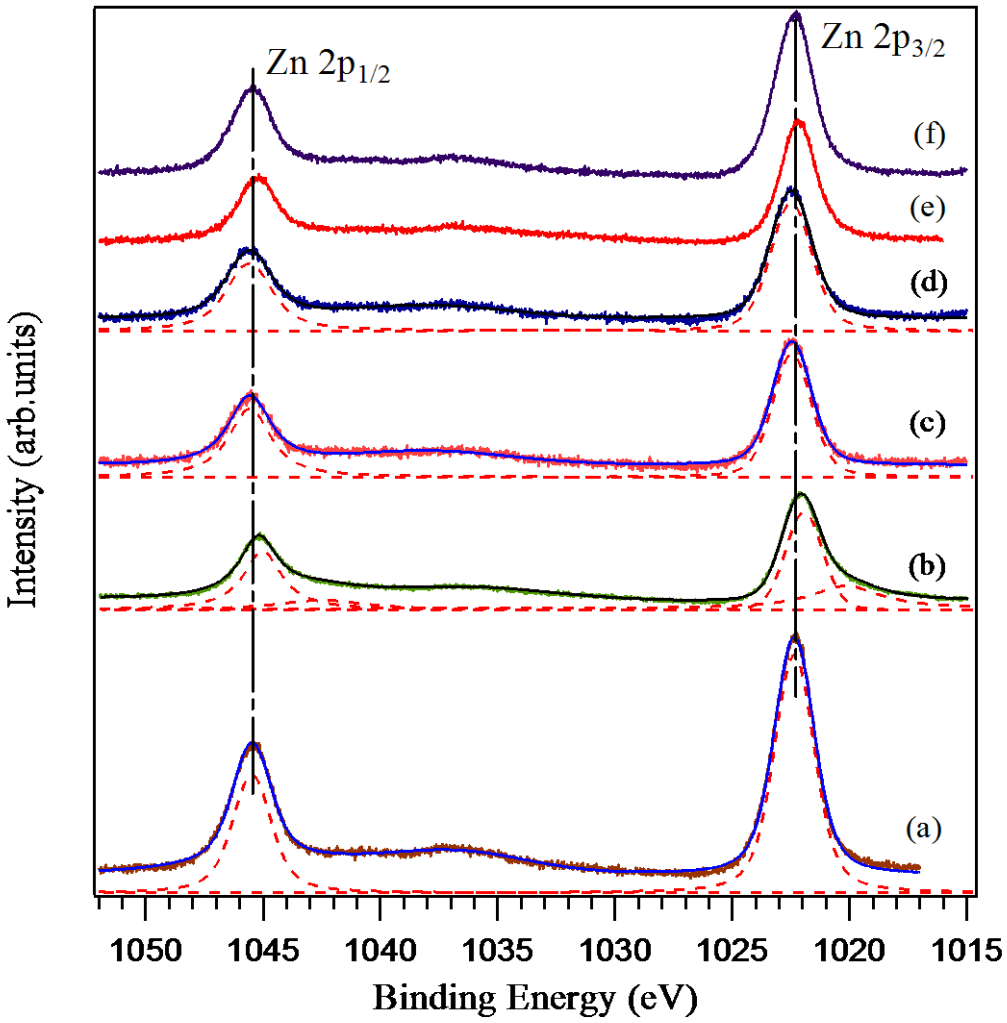

Figure 7. The Zn 2p core level states from Au/ZnO as determined by XPS for an untreated sample (a) and treated with L-cysteine (b), DL-thioctic acid (c), 4-mercaptobenzoic acid (d), 6-mercaptohexanol (e), and 11-(1-pyrenyl)-1-undodecathiol (f). The pronounced asymmetry in (b) is attributed to electrostatic interaction.

Zn $2p_{3/2}$ and Zn $2p_{1/2}$ core level states (Fig. 7) with peaks at ~1022 eV and ~1045 eV, respectively, correspond to zinc ions in ZnO. The peak position for Zn $2p_{3/2}$ is in good agreement with the wurtzite phase of ZnO at 1022.4 eV[21]. The absence of a peak at 1021.5 eV indicates that there is no metallic zinc, thus all the Zn atoms are in Zn^{2+} state.[19] There is a very small spectral contribution on the lower binding energy side of the L-cysteine treated sample. This might be attributed to the electrostatic interaction between Zn^{2+} ions and the electrically charges sites of L-cysteine which are (–COO-) and ($+NH^{3-}$) when L-cysteine exists in the zwitterionic form. Alternatively, it could be attributed to Zn-S bonds. However, the latter possibility is less likely since the four other thiols have been grafted following the same protocol, and the Zn-S bond therefore should have appeared in the Zn 2p core level states of all the samples. The attenuation of the Zn 2p photoelectrons upon treatment in conjunction with the peaks assignment of the S 2p core level states, demonstrates the formation of an overlayer and the potential formation of Zn-S bonds.

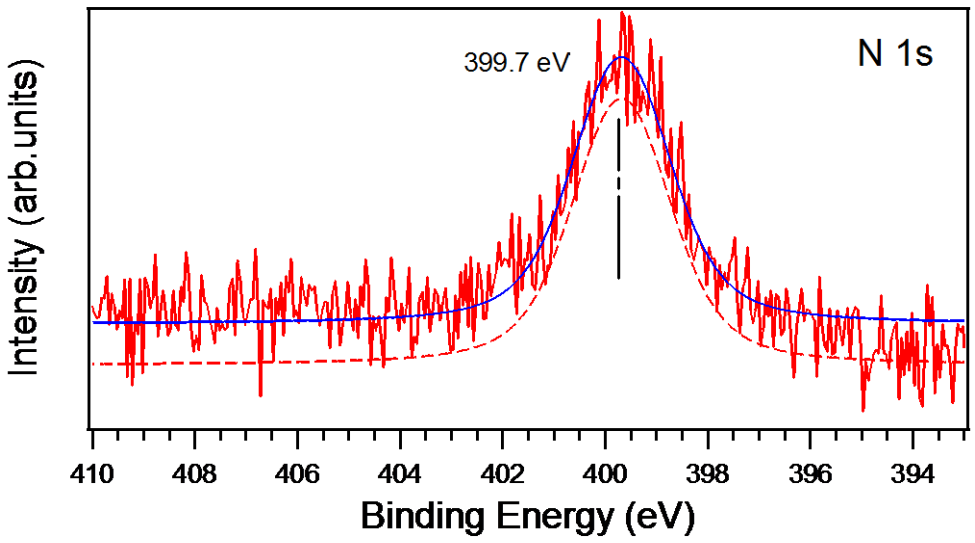

Figure 8. The N 1s core level for L-cysteine functionalized Au/ZnO nanospring sample.

The N 1s core level state for L-cysteine is shown in Fig. 8. The single peak at ~ 400 eV corresponds to NH_x species [1]. The N 1s signal provides confirmation for the location of the headgroup exclusively at the surface of the monolayer. Signals from oxidized nitrogen species (NO_x) at higher binding energies were not observed. This demonstrates the stability and resistance of L-cysteine to oxidation.

Table 2 summarizes the atomic ratios of the elements calculated from the integrals of the XPS signals which were corrected by Scofield sensitivity factors. These factors were obtained from the literature [22,23]. The area of carbon impurities, as detected in the untreated sample, was subtracted from the area of each C 1s core level prior to the elemental analysis.

Table 2. Atomic ratios of elements at the outer surface of treated samples

Sample	C1s/S2p		$\frac{S2p}{Au}$	$\frac{Au}{Zn}$	$\frac{S2p}{Zn2p+Au}$	$\frac{C1s+S2p}{Zn2p+Au}$
	Theoretical	XPS				
L-cysteine	1.12	1.40	46.06	0.014	0.64	2.09
6-mercaptohexanol	2.25	2.22	58.59	0.018	1.01	4.38
11-(1-pyrenyl)-1-undecathiol	10.5	10.1	5.88	0.028	0.16	2.59
4-mercaptobenzoic acid	2.62	2.47	6.59	0.057	0.36	1.69
DL-thioctic acid	1.50	1.42	64.73	0.028	1.17	3.67

The carbon to sulfur ratios (C1s/S2p) are close to the expected theoretical values corresponding to the stoichiometry of the linker molecules, which confirm the quality of monolayers and the reliability of the sensitivity factors used. The Au/ZnO ratios reflect the low content of Au in the samples. Compared with the value of 0.05 for the untreated sample, the relative decrease (except for 4-mercaptobenzoic acid) provides additional evidence of a monolayer on the Au nanoparticles. For 4-mercaptobenzoic acid the change is likely due to differences in chemical interactions with Au/ZnO and in molecular orientation. The S 2p/Au ratios follow the trend of the S 2p signal in the samples, with the exception of the values of 5.88 and 6.59 for11-(1-pyrenyl)-1-undecathiol and 4-mercaptobenzoic acid, respectively, where the signal should not be weak if sulfur bound exclusively to Au. Conversely, the S 2p/Au+Zn ratios are more reasonable, consistent with chemisorption through S-Au and S-Zn bonds.

The nature of the interface between Au/ZnO nanosprings and the adsorbed thiols is an important point of interest. X-ray absorption near-edge spectroscopy (XANES) studies of thiol-capped ZnO nanoparticles have demonstrated the existence of a ZnS-ZnO interface at the surface of the nanoparticles, with both ZnS and ZnO showing a wurtzite structure. [24,25,26] The S 2p core level states from L-cysteine and 6-mercaptohexanol treated samples clearly exhibited two sulfur signals, which were assigned to S-Au and S-Zn bonds. In the other samples the S-Au bonds (1-(1-pyrenyl)-1-undecathiol and 4-mercaptobenzoic acid) or S-Zn bonds (DL-thioctic acid) were dominant. The electron withdrawing power of the benzene rings in 1-(1-pyrenyl)-1-undecathiol and 4-mercaptobenzoic acid might explain the weakness of the S-Zn bond.

Packing density and order/disorder of SAMs:

Packing densities of thiols were calculated from XPS data following the method described in Ref.[27] Since XPS probes few atomic layers of the sample, to estimate the packing density of thiols on nanoparticles XPS integrals must be corrected for the electron escape depth ($\lambda\cos\theta$), where λ is the inelastic mean free path (IMFP) and θ the emission angle to the surface normal. For normal emission as in our experiments, the escape depth reduces to simply λ. From the NIST Electron Inelastic Free Path Database, the IMFPs of gold and zinc are 1.78 nm and 2 nm, respectively.[22]

The shell method models nanoparticles as a central atom surrounded by shells (layers) of atoms where the number of atoms in the nth shell is $10n^2+2$.[27] The total number of shells can then be determined from the diameters of the atom and the nanoparticles. The number of layers sampled by XPS is the ratio of the escape depth to the atom diameter. From these estimates, a 10 nm gold nanoparticles contains 18 shells but only 6 are samples, a zinc nanoparticles of 7 nm (size of coordinated zinc in a 18 nm ZnO crystal) 14 shells and 8 are signaled.

The S to Au or to Zn atomic ratios are corrected as follows:

$$\frac{S}{X_{Surface}} = \left(\frac{\sum_{n=n_i}^{n_o} (10n^2 + 2)}{10n_o^{\ 2} + 2} \right) \left(\frac{S}{X} \right) \qquad \text{X = Au, Zn} \qquad (1)$$

where n_i is the deepest layer sampled and n_o the outer layer. The surface of ~ 12 nm gold nanoparticles mostly contains (100) crystal planes.[27] Large grains ZnO (~20 nm) correspond to the growth mode with c-axis parallel to the substrate which privileges 100 and 110 orientations, and the surface planes are therefore predominantly (100).

The number of lattice points per unit area of a crystal plane is given by:

$$\rho_{hkl} = \frac{n d_{hkl}}{\Omega} \qquad (2)$$

where n is the number of lattice points per unit cell, Ω the volume of the unit cell, and d_{hkl} the interplanar spacing.

The packing density of atoms on a plane is calculated as follows:

$$\sigma_{hkl} = N_0 \rho_{hkl} \qquad (3)$$

where N_0 is the number of atoms per lattice point in the plane (hkl). These quantities for Au and Zn are:

$$\sigma_{hkl}(Au) = \frac{2}{a^2 \left(h^2 + k^2 + l^2 \right)^{1/2}} \qquad (4)$$

and

$$\sigma_{hkl}(Zn) = \frac{2}{\sqrt{3}a^2c\left(\frac{4}{3}\frac{h^2+hk+k^2}{a^2}+\frac{l^2}{c^2}\right)^{1/2}} \quad (5)$$

Finally, the packing density of thiols can be approximated from XPS data using the following:

$$PD = \left(\frac{S}{X_{Surface}}\right)\left(\frac{TH}{S}\right)\left(\sigma_{hkl}\right) \quad (6)$$

The factor $\frac{TH}{S}$ is 2 for DL-thioctic acid and 1 for the rest of the thiols.

The surface coverage and packing density calculated by the method described above are summarized in the table below.

Table 3. Surface coverage and packing density of thiols on Au and Zn as estimated from XPS data

Thiols	L-cysteine	6-mercaptohexanol	11-(1-pyrenyl)-1-undecathiol	DL-thioctic acid	4-mercaptobenzoic acid
Coverage on Au	0.451	0.271	0.0435	0.106	0.0791
PD on Au (molecule/cm^2)	5.42x10^{14}	3.26x10^{14}	5.23x10^{13}	2.55x10^{14}	9.50x10^{13}
Coverage on Zn	0.239	0.215	0.00164	0.0475	0.00676
PD on Zn (molecule/cm^2)	2.83x10^{14}	2.54x10^{14}	1.94x10^{11}	1.12x10^{14}	8x10^{12}

The values agree with the SAMs packing densities which are in the order of 10^{14} molecule/cm^2 on flat gold surface.[28] L-cysteine, 6-mercaptohexanol, and DL-thioctic acid are more densely packed than 4-mercaptobenzoic acid and 11-(1-pyrenyl)-1-undecathiol. The latter thiols do both have larger end groups, the reduced packing densities might be due to steric hindrance.

Ordering of thiols is another important factor in their effectiveness as receptors. It is reported that in 4-mercaptobenzoic acid, the proximity of the carboxyl group to the surface of the monolayer – compared to similar types of thiols - reduces its interaction with the substrate, resulting in an increased reactivity with vapors of analytes.[29,30] SAMs of DL-thioctic acid formed in ethanol are highly disordered due to hydrogen bonding between neighboring molecules with a tilt of 38° that results in the loose packing of the SAMs.[31] Unlike DL-thioctic, the higher degree of ordering of 6-mercaptohexanol SAMs is ascribed to complementary effects such as the solubility of solvents with the thiol chains and hydrogen bonding of adjacent –OH of thiols or –OH with solvents.[32] Note, a high packing density is required to order long chain molecules within a monolayer;[33] if this applies to SAMs of 11-(1-pyrenyl)-1-undecathiol, with an increased steric hindrance of the headgroups, they are likely to be disordered. Finally, SAMs of L-cysteine are highly ordered, most likely due to intermolecular and intramolecular interactions of hydrophilic ammonium and carboxylic groups that lead to the formation of hydrogen bonds among adsorbed molecules.[34]

3.2. Ultraviolet Photoelectron Spectroscopy (UPS)

UPS spectra (He I emission line) of untreated and the four treated samples are displayed in Fig. 9 (upper panel). The spectrum of the untreated sample is reminiscent of polycrystalline Au and ZnO valence bands with some attenuation and hybridization. The Au 5d electrons form a broad band between 2-8 eV and the 6s electrons are seen between 2 eV and the Fermi level. Note, the

6s band extends to much greater binding energy and is strongly hybridized with the 5d bands.[35] As for ZnO, the valence band extends from 3 to 8 eV; theory predicts that the emission from 3-5 eV corresponds to non-bonding O 2p orbitals, and between 5-8 eV to a bonding between the O 2p and Zn 4s orbitals.[36]A feature valence band spectra of bare ZnO at a binding energy of ~10 eV, which arises from the Zn 3d band, is attenuated upon decoration with Au nanoparticles. As previously pointed out by Duwez et al.[7], one of the difficulties one encounters when interpreting valence band spectra consisting of Au and organics is the superimposition of the Au 5d signal with the valence band structure of the organic material. There are, however, obvious changes to the shape of the Au/ZnO spectrum upon the thiol functionalization. For instance, the Au 5d and Zn 4s-O 2p bands are attenuated differently. For DL-thioctic acid and 4-mercaptobenzoic acid functionalization these bands are almost completely suppressed, yet may still be resolvable upon functionalization with L-cysteine, 6-mercaptohexanol and 11-(1-pyrenyl)-1-undecathiol. These modifications are indicative of the formation of an overlayer on the surface which is chemically bonded not only to gold, but also to Zn, as demonstrated by the change in the ZnO features in the range of 5-8 eV. The occurrence of the maximum at different binding energies is suggestive of different molecule orientations. The bond formation occurs through a rearrangement of the orbitals of the substrate and of the adsorbed molecules.[7] The thickness and the compactness of the film will affect the intensity of the photoemission of the underlying substrate. XPS analysis showed that the thiols have different packing densities on Au or ZnO. The presence of contributions from Au and ZnO in the valence spectra is related to the hydrocarbon chain length, the size of the end group and the molecular orientation. Finally the feature at ~15 eV is the background of secondary electrons that arise from the substrate

near-surface region, as well as the thiol layer.[3] The onset of secondary electrons was used to determine the change in the work function with respect to the untreated sample.

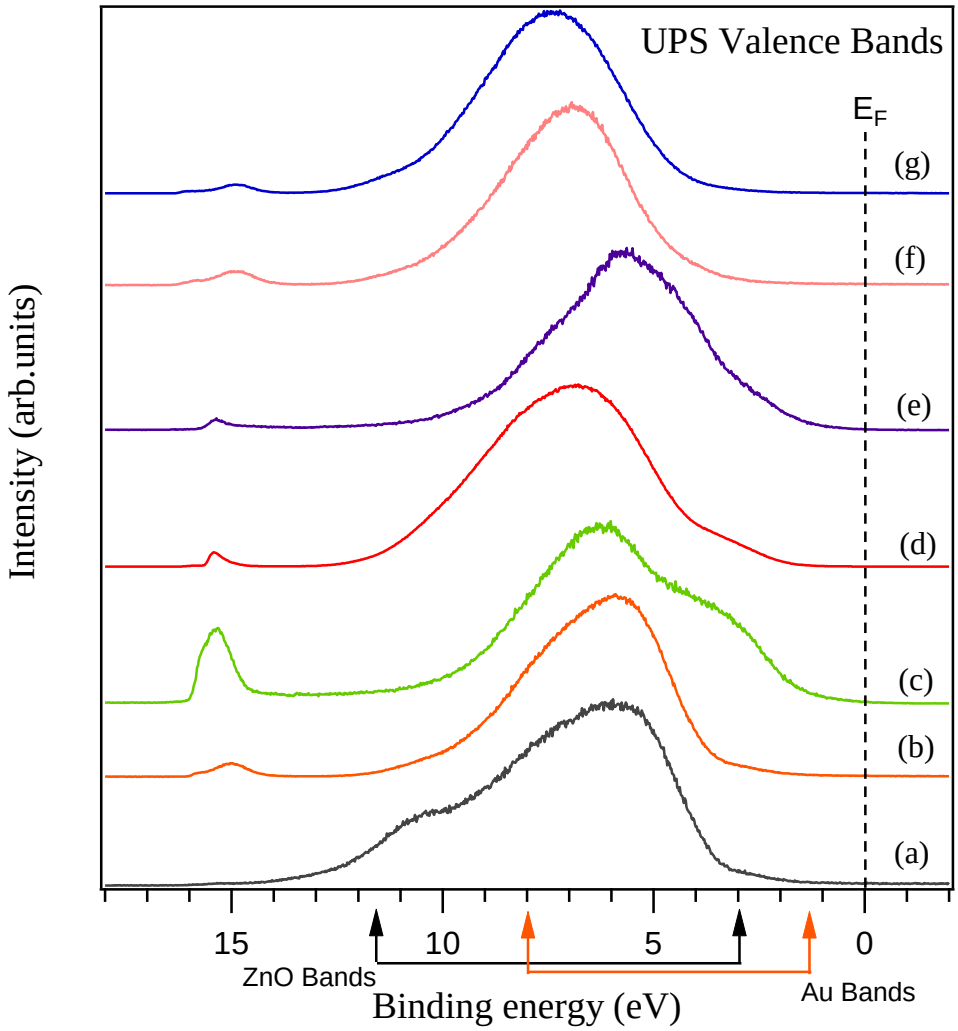

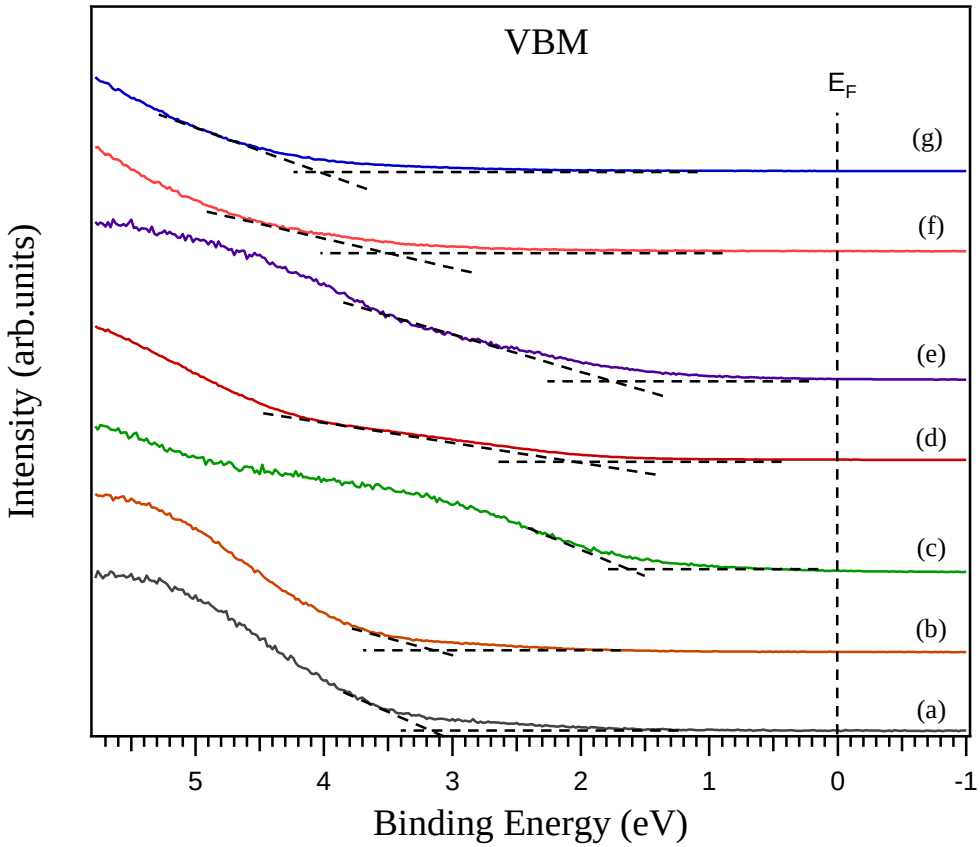

Figure 9. (Upper panel).The UPS (He I) valence bands spectra for a bare ZnO nanospring-mat (a), an untreated Au/ZnO nanospring-mat (b) and treated with L-cysteine (c), 6-mercaptohexanol (d), 11-(1-pyrenyl)-1-undecathiol (e), DL-thioctic acid (f), and 4-mercaptobenzoic acid (g). (Lower panel).The Valence band maximum (VBM) of the same samples obtained by linear extrapolations.

Table 4. Position of the VBM and change in the work function of the treated samples

Sample treated with	L-cysteine	11-(1-pyrenyl)-1-undecathiol	6-mercaptohexanol	4-mercaptobenzoic acid	DL-thioctic acid
VBM (eV)	1.50	1.45	1.80	3.10	3.05
ΔΦ(eV)	+0.17	-0.38	-0.02	+0.10	+0.22

Also shown in Fig. 9 (lower panel) are linear extrapolations of the leading edge to zero intensity to obtain VBM positions of the samples. Band bending and dipole layer formation upon chemisorptions lead to shifts in the VBM (due to band bending), in electron binding energies and in the energy cutoff (due to change in the work function (Table 4).[3] Different values of the VBM position and $\Delta\Phi$ illustrate differences in the self-assembled films.

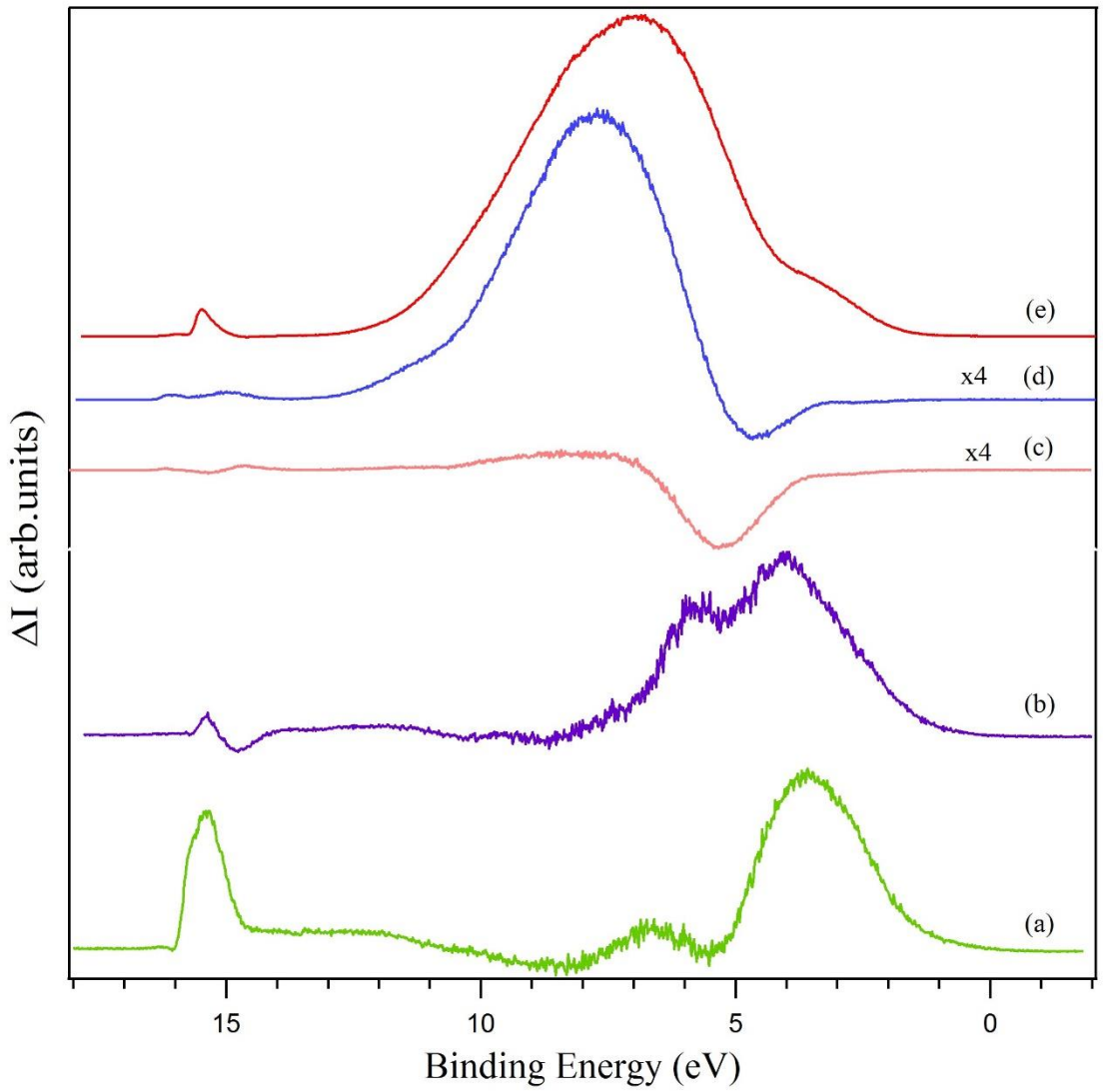

Figure 10. UPS difference spectra for chemisorbed (a) L-cysteine, (b) 11-(1-pyrenyl)-1-undecathiol, (c) DL-thioctic acid, (d) 4-mercaptobenzoic acid, and (e) 6-mercaptohexanol on Au/ZnO nanospring-mats.

Difference spectra analysis of the valence band spectra in Fig. 9 (upper panel) was performed to elucidate the changes in the valence band density of states of the five thiols. The procedure is described in detail in Ref. [37]. The results are shown in Fig. 10. Negative features in the difference curve arise from suppression of valence band density of states of the Au/ZnO nanosprings substrate. Note, attenuation is attributable to either electron scattering arising from disorder in the thiol layer or hybridization of S and Au surface atoms. The negative features at a binding energy of ~ 5eV of the difference curves of L-cysteine, DL-thioctic acid and 4-mercaptobenzoic acid correspond to Au d-bands prior to thiol functionalization. The attenuation of the Au d-bands in the case of DL-thioctic acid is due to electron scattering due to disorder within the layer (see section 3.1), which also accounts for the lack of distinguishable molecular orbitals of the adsorbate. The difference spectrum of 4-mercaptobenzoic acid, taken in conjunction with its low coverage (Table 3), suggests that the attenuation of the Au feature is due to hybridization of S with the Au surface, as opposed to electron scattering. The molecular orbitals of 4-mercaptobenzoic acid in the range of ~6-12 eV support this conclusion. The new density of states in range of 1-2 eV for L-cysteine, 11-(1-pyrenyl)-1-undecathiol, and 6-mercaptohexanol is attributed to hybridization of the antibonding S 3p-states with the Au 5d-bands, where the additional new states with binding energies > 2 eV are the molecular orbitals of the respective thiols, which may, or may not, hybridize with the Au d-bands. In the case of L-cysteine, there is a contribution from nitrogen p states above 1.5 eV.[38] Note, the assignments are based on the assumption that the S antibonding 3p orbital does not mix with the

wavefunctions on the hydrocarbon chain. The formation of hybrid orbitals of both bonding and antibonding type, below and above the metal d bands, is consistent with the Newns-Anderson model for atomic and molecular chemisorptions on metal surfaces.[39] This is clearly demonstrated by the L-cysteine difference spectrum, which confirms Felice and co-workers [40] theoretical predictions of the above mentioned model applied to cysteine chemisorbed on Au (111). The bonding and antibonding orbitals are both π-like and σ-like. In the outer valence band region ~6-12 eV, bands can be attributed to thiol orbitals with contributions from carbon 2p and nitrogen 2p states in the specific case of L-cysteine. These orbitals also contribute to the bonding of the molecule to the surface, especially the ZnO surface where the bonding primarily occurs via high-lying orbitals.[41]

3.3. Gaseous Analytes Detection Properties

To test the response of the functionalized samples with respect to vaporized explosive compounds, the sensors responses were measured as relative changes in conductance normalized with respect to a baseline signal level when no vapor was present. The results for exposures to different vapors are displayed in Fig. 11. The operational temperatures of the sensors functionalized with 11-(1-pyrenyl)-1-undecathiol and DL-thioctic acid were 100°C, and 150°C for the other four sensors. The sensors were heated for thermal activation of carriers.[42]

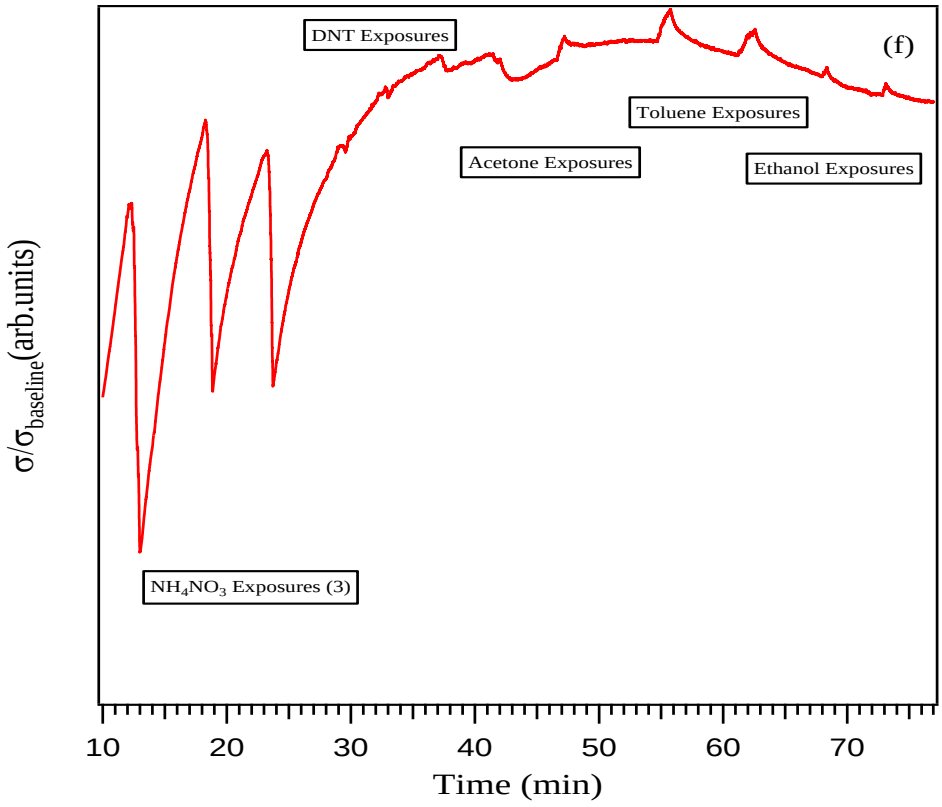
DNT Exposures
(f)
Toluene Exposures
Acetone Exposures
Ethanol Exposures
NH4NO3 Exposures (3)
σ/σbaseline(arb.units)
10
20
30
40
50
60
70
Time (min)

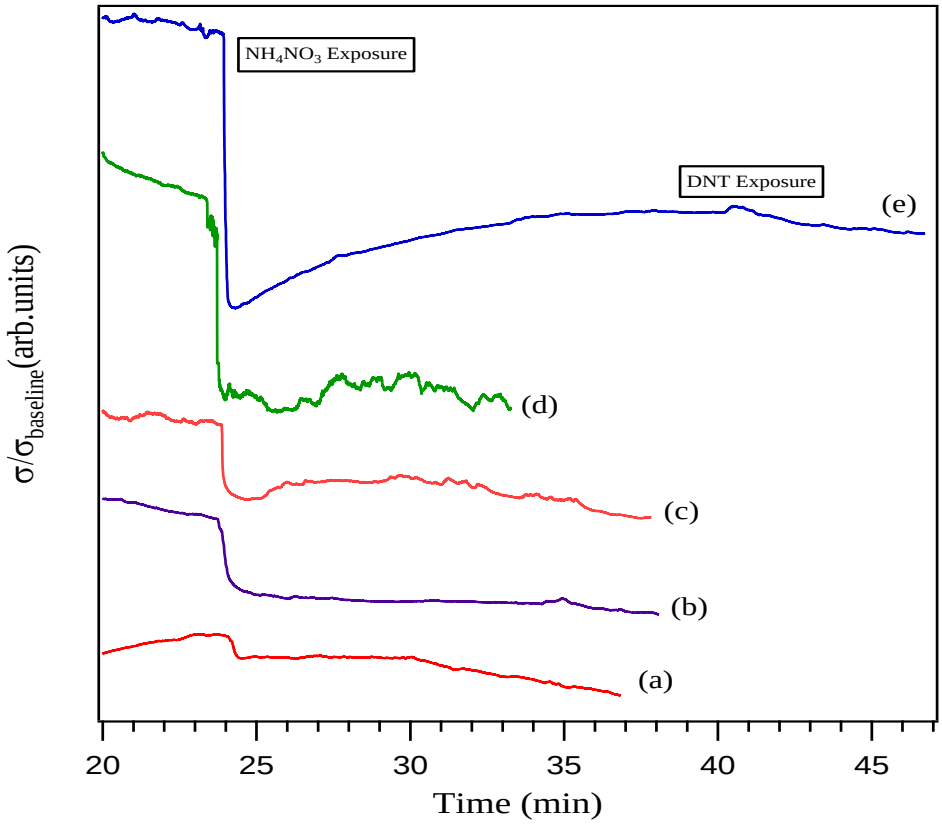
NH4NO3 Exposure
DNT Exposure
(e)
(d)
(c)
(b)
(a)
σ/σbaseline(arb.units)
20
25
30
35
40
45
Time (min)

Figure 11. The relative change in conductance of (a) untreated Au/ZnO nanospring-mat and samples treated with (b) 11-(1-pyrenyl)-1-undecathiol, (c) DL-thioctic acid, and (d) L-cysteine upon exposure to ammonium nitrate, (e) 4-mercaptobenzoic acid, and (f) 6-mercaptohexanol upon exposure to ammonium nitrate, DNT, acetone, toluene, and ethanol.

It is reported that upon heating to temperatures over 70 °C, monolayers of alkanethiols on gold start desorbing, but the rate of desorption is dependent on the temperature, ambient medium, and chain length of the adsorbate.[4] Desorption is most rapid in a hydrocarbon solvent, slower in ethanol and in still air. Long-chain thiols form monolayers that are more stable than those from short-chain thiols. The thermal stability of the adsorbate molecule is an issue for ZnO nanospring chemiresistors, which operate optimally at 400 °C. XPS was performed to verify the stability of the thiols on ZnO nanosprings at the above-mentioned operational temperatures. The results of these tests are presented in Supporting Information I. These results and the data in Fig. 11 demonstrate that the linker molecules were much more thermally stable than those adsorbed on gold and the plausible reason is the attachment of the molecules not only to gold but also to ZnO. All samples showed high response to ammonium nitrate (NH_4NO_3). The conductance of all the samples decreased irreversibly upon exposure to NH_4NO_3. The exception was 6-mercaptohexanol, which recovered and responded to multiple exposures. It also responded to additional compounds, including 2,4-dinitrotoluene (DNT), toluene, acetone, and ethanol. 4-mercaptobenzoic acid and 6-mercaptohexanol responses show that the analytes that are liquid (solid) at room temperature have positive (negative) change in conductance. A decrease in the conductance of the sample upon exposure to vapors of solid analytes indicates binding of vapors to the functional groups. For the liquid analytes, diffusion of the vapor molecules into the pores of the film increases the average permittivity, which in turn increases

the conductance because the activation energy and height of the potential well barriers are expected to decrease.[6] For 6-mercaptohexanol, changes in the conductance clearly reflect the adsorption of vapors of analytes followed by their desorption.The response to NH_4NO_3 is plotted in Fig. 12 as function of the position of the VBM.

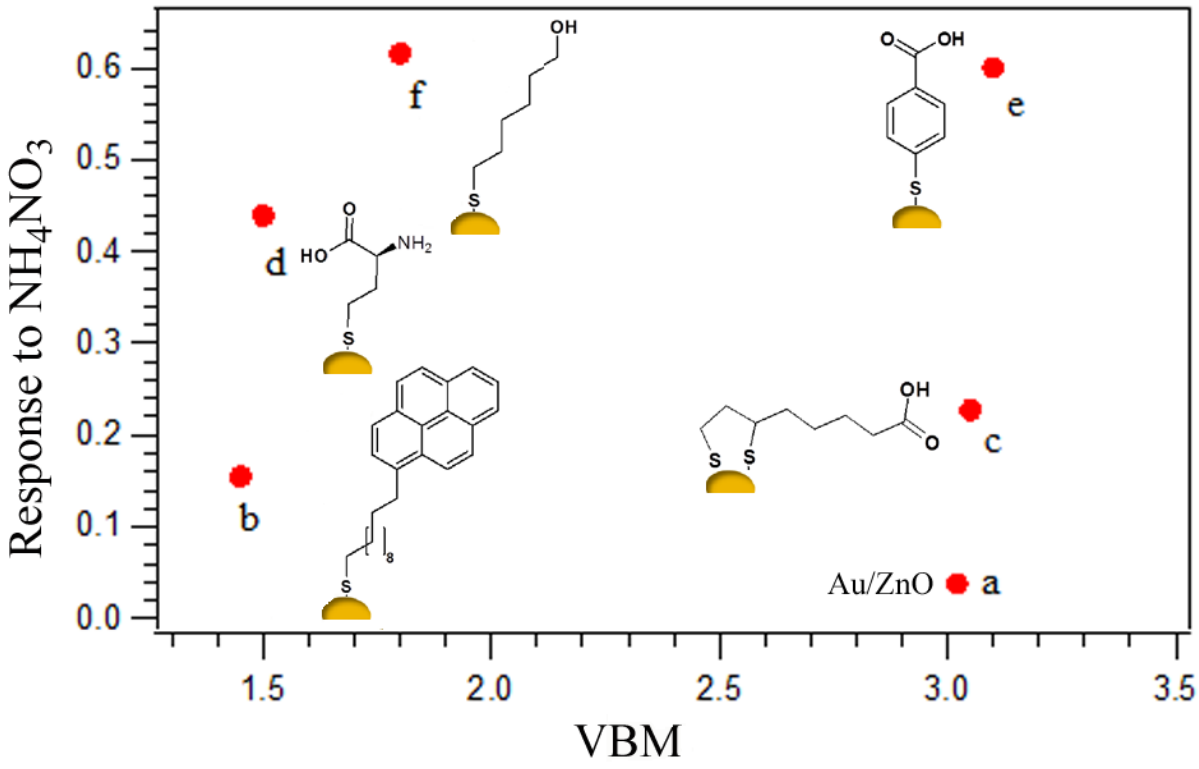

Figure 12. Samples response to ammonium nitrate exposure as a function of the position of the VBM. (a) Untreated Au/ZnO nanospring-mat and samples treated with (b) 11-(1-pyrenyl)-1-undecathiol, (c) DL-thioctic acid, (d) L-cysteine, (e) 4-mercaptobenzoic acid, and (f) 6-mercaptohexanol.

6-mercaptohexanol and 4-mercaptobenzoic acid exhibited the strongest responses, while 11-(1-pyrenyl)-1-undecathiol and the untreated sample were the least responsive. One would expect that the closer the VBM to the Fermi level, the better the sensor but Fig. 12 suggests that the

position of the VBM has little to no influence in the response to vapors of ammonium nitrate. On the contrary, the responses seem to reflect the packing density and/or ordering of thiols as determined in the XPS section. Moreover, given the dissimilarity of the five thiols, chemical interactions might also be playing an important role in sensing.

Chemical interaction between receptors and Au/ZnO surface:

All receptors, with the exception of 4-mercaptobenzoic acid, are expected to have high electron density on the sulfur atom. In the case of 4-mercaptobenzoic acid, the lone pair electrons on the sulfur are delocalized within the aromatic benzene ring, which may result in different interactions with Au/ZnO relative to the other thiols.

Chemical interaction between functional groups on receptors and explosive vapor:

Heated solid ammonium nitrate (NH_4NO_3) produces ammonia (NH_3) and oxidizing nitric acid (HNO_3) as the two main gaseous species, along with gaseous degradation products (N_2, H_2O, O_2, OH, HNO and NO_3) and ammonium nitrate.[43] Receptors with carboxylic acid groups (L-cysteine, 4-mercaptobenzoic acid, DL-thioctic acid) may interact with ammonium (NH_4^+) through electrostatic interactions and with ammonia via hydrogen bonding. On the other hand, receptors with alcohol or amino groups (6-mercaptohexanol, L-cysteine) will only interact via hydrogen bonds. The polarized nitro group ($R\text{-}NO_2$), found in many commonly used military explosives is known to interact strongly with polar groups, such as -COOH and –OH via ionic and hydrogen bond interactions. Thus, all of the receptors, except for 11-(1-pyrenyl)-1-undecathiol, may interact strongly with nitrate ions (NO_3^-). The sensor data (Fig. 12), with the exception of DL-thioctic acid, are in good agreement with the above description of chemical interactions between functional groups on receptors and vapors of ammonium nitrate. In fact, 4-mercaptobenzoic acid, 6-mercaptohexanol and L-cysteine respond better, while the response

is low for 11-(1-pyrenyl)-1-undecathiol. The former have polar linker headgroups of the form -COOH, -OH, and -NH_2 that interact with components from ammonium nitrate, while the latter does not. However, DL-thioctic acid, which has the polar linker -COOH headgroup, exhibits a relatively lower response. The characterization data already showed that the surface energy barrier is relatively high for DL-thioctic acid treated samples. From the chemical standpoint, the low response is attributable to poor long range order of the DL-thioctic acid films, where it has been reported that well-ordered films are obtained if one uses ethanol-acetic acid as solvent.[44]

4. Conclusions

In this paper, we have investigated the chemisorption of alkyl thiols on Au/ZnO nanosprings by XPS and UPS and correlated the data with the response of sensors constructed with these materials to ammonium nitrate, a signature of explosives. These thiols used in the study are L-cysteine, 6-mercaptohexanol, 11-(1-pyrenyl)-1-undecathiol, 4-mercaptobenzoic acid, and DL-thioctic acid. Our results show that the adsorption involves not only S-Au bonds, but also S-Zn bonds. XPS analysis revealed that thiols headgroups are located at the monolayer-air interface and are resistant to oxidation. The weakness of the sulfur signals from 4-mercaptobenzoic acid and 11-(1-pyrenyl)-1-undecathiol treated sample suggests that steric screening effects may play an important role in the scattering of the photoelectrons. The C/S ratios are in good agreement with the stoichiometry of the molecules, confirming the quality of the monolayers. The UPS analysis of valence bands shows that the spectra of the thiolated samples show contributions from the molecular orbitals of the thiols, S-Au and S-Zn bonding, the Au/ZnO nanospring substrate, and attenuation of some substrate bands due to thiol induced scattering. The attenuation of the Au d bands as demonstrated by UPS difference curves reflects the

conformation of each linker molecule and their orientation with respect to the surface normal. UPS difference spectra also revealed bands associated with carbon 2p and nitrogen 2p states, and more importantly with S-Au bonding and antibonding orbitals of both π- and σ-type. The formation of hybrid orbitals of both bonding and antibonding type, below and above the metal d bands, is characteristic of molecular chemisorptions on metal surfaces.

Vapor-sensing tests show that the molecules are more thermally stable on Au/ZnO nanosprings than on Au thin films. It is hypothesized that chemisorption to the ZnO surface is responsible for this enhanced stability. Regardless, the Au nanoparticles are necessary to create that depletion layer critical to sensing. The samples are highly responsive to vaporized ammonium nitrate. Au/ZnO nanosprings with SAMs of 6-mercaptohexanol or 4-mercaptobenzoic acid showed the strongest responses. The packing density and ordering of the SAMS layers appear to be the critical factor for obtaining a strong response to analytes. Therefore, protocols should be developed that maximize long range order. Only then will it be possible to effectively compare thiol functionalization to one another. In order to optimize the response of these thiols, future experiments will focus on increasing the testing temperature to find the desorption point as well as monitoring the vapor dose.

Associated Content

Supporting Information

Electron flood gun parameters during irradiation of the samples

Thermal stability of thiols on Au/ZnO nanosprings

Synthesis of 11-(1-pyrenyl)-1-undecathiol scheme and corresponding NMR spectra. These materials are available free of charge via internet at http://pubs.acs.org.

Author information

Corresponding Author

*+E-mail: dmcilroy@uidaho.edu, foue3398@vandals.uidaho.edu

Notes

The authors declare no competing financial interest

Acknowledgements

The authors would like to express their sincere appreciation to Dr T. Williams for his kind assistance with FESEM, TEM and XRD. This research was financially supported by The Office of Naval Research (Research Opportunity Number ONR BAA 09-022). DMc would like to acknowledge the support of the College of Science's Dyess Faculty Fellowship.

References.

(1) Scott, A. & Janes, D. B. Characterization of electrochemically grafted molecular layers on silicon for electronic device applications. *J. Appl. Phys.* **105,** 073512 (2009).

(2) Kronik, L. & Koch, N. Electronic Properties of Organic-Based Interfaces. *MRS Bull.* **35,** 417–419 (2010).

(3) Alloway, D. M. *et al.* Interface Dipoles Arising from Self-Assembled Monolayers on Gold: UV-Photoemission Studies of Alkanethiols and Partially Fluorinated Alkanethiols. *J. Phys. Chem. B* **107,** 11690–11699 (2003august).

(4) Bain, C. D. *et al.* Formation of monolayer films by the spontaneous assembly of organic thiols from solution onto gold. *J. Am. Chem. Soc.* **111,** 321–335 (1989).

(5) Porter, M. D., Bright, T. B., Allara, D. L. & Chidsey, C. E. D. Spontaneously organized molecular assemblies. 4. Structural characterization of n-alkyl thiol monolayers on gold by optical ellipsometry, infrared spectroscopy, and electrochemistry. *J. Am. Chem. Soc.* **109,** 3559–3568 (1987).

(6) Joseph, Y. *et al.* Self-Assembled Gold Nanoparticle/Alkanedithiol Films: Preparation, Electron Microscopy, XPS-Analysis, Charge Transport, and Vapor-Sensing Properties †. *J. Phys. Chem. B* **107,** 7406–7413 (2003).

(7) Duwez, A.-S., Pfister-Guillouzo, G., Delhalle, J. & Riga, J. Probing Organization and Structural Characteristics of Alkanethiols Adsorbed on Gold and of Model Alkane Compounds through Their Valence Electronic Structure: An Ultraviolet Photoelectron Spectroscopy Study. *J. Phys. Chem. B* **104,** 9029–9037 (2000).

(8) Dobrokhotov, V. *et al.* ZnO coated nanospring-based chemiresistors. *J. Appl. Phys.* **111,** 044311 (2012).

(9) Singh, S. Sensors—An effective approach for the detection of explosives. *J. Hazard. Mater.* **144,** 15–28 (2007).

(10) Wang, L. *et al.* High yield synthesis and lithography of silica-based nanospring mats. *Nanotechnology* **17,** S298–S303 (2006).

(11) Dasary, S. S. R., Singh, A. K., Senapati, D., Yu, H. & Ray, P. C. Gold Nanoparticle Based Label-Free SERS Probe for Ultrasensitive and Selective Detection of Trinitrotoluene. *J. Am. Chem. Soc.* **131,** 13806–13812 (2009).

(12) Goodpaster, J. V. & McGuffin, V. L. Fluorescence Quenching as an Indirect Detection Method for Nitrated Explosives. *Anal. Chem.* **73,** 2004–2011 (2001).

(13) Castner, D. G., Hinds, K. & Grainger, D. W. X-ray Photoelectron Spectroscopy Sulfur 2p Study of Organic Thiol and Disulfide Binding Interactions with Gold Surfaces. *Langmuir* **12,** 5083–5086 (1996).

(14) Watts, J. F. *An introduction to surface analysis by XPS and AES*. (J. Wiley, 2003).

(15) Libertino, S. *et al.* Layer uniformity in glucose oxidase immobilization on SiO2 surfaces. *Appl. Surf. Sci.* **253,** 9116–9123 (2007).

(16) Abdureyim, A. *et al.* Characterization of 4-mercaptohydrocynnamic acid self-assembled film on Au(111) by means of X-ray photoelectron spectroscopy. *J. Electron Spectrosc. Relat. Phenom.* **114-116,** 371–374 (2001).

(17) Moulder, J. F., Stickle, W. F., Sobol, P. E. & Bomben, K. D. *Handbook of X-ray Photoelectron Spectroscopy*. (Perkin-Elmer Corporation, Physical Electronics Division, 1995).

(18) Sadik, P. W., Pearton, S. J., Norton, D. P., Lambers, E. & Ren, F. Functionalizing Zn- and O-terminated ZnO with thiols. *J. Appl. Phys.* **101,** 104514 (2007).

(19) Kuo, F.-L., Li, Y., Solomon, M., Du, J. & Shepherd, N. D. Workfunction tuning of zinc oxide films by argon sputtering and oxygen plasma: an experimental and computational study. *J. Phys. Appl. Phys.* **45,** 065301 (2012).

(20) Heinhold, R., Williams, G. T., Cooil, S. P., Evans, D. A. & Allen, M. W. Influence of polarity and hydroxyl termination on the band bending at ZnO surfaces. *Phys. Rev. B* **88,** (2013).

(21) Islam, M. N., Ghosh, T. B., Chopra, K. L. & Acharya, H. N. XPS and X-ray diffraction studies of aluminum-doped zinc oxide transparent conducting films. *Thin Solid Films* **280,** 20–25 (1996).

(22) Powel, C. J. & Jablonski, A. *NIST Electron Inelastic-Mean -Free-Path Datbase, Version 1.2, SRD71*. (National Institute of Standards and Tectnology, 2010).

(23) Yeh, J. J. & Lindau, I. Atomic subshell photoionization cross sections and asymmetry parameters: $1 \leqslant Z \leqslant 103$. *At. Data Nucl. Data Tables* **32,** 1–155 (1985).

(24) Guglieri, C. & Chaboy, J. Characterization of the ZnO−ZnS Interface in THIOL-Capped ZnO Nanoparticles Exhibiting Anomalous Magnetic Properties. *J. Phys. Chem. C* **114,** 19629–19634 (2010).

(25) Guglieri, C. *et al.* XMCD Proof of Ferromagnetic Behavior in ZnO Nanoparticles. *J. Phys. Chem. C* **116,** 6608–6614 (2012).

(26) Guglieri, C. *et al.* Relationship between the Magnetic Properties and the Formation of a ZnS/ZnO Interface in S-Capped ZnO Nanoparticles and ZnS–ZnO Thin Films. *J. Phys. Chem. C* **117,** 12199–12209 (2013).

(27) Volkert, A. A., Subramaniam, V., Ivanov, M. R., Goodman, A. M. & Haes, A. J. Salt-Mediated Self-Assembly of Thioctic Acid on Gold Nanoparticles. *ACS Nano* **5,** 4570–4580 (2011).

(28) Schlenoff, J. B., Li, M. & Ly, H. Stability and Self-Exchange in Alkanethiol Monolayers. *J. Am. Chem. Soc.* **117,** 12528–12536 (1995).

(29) Barriet, D., Yam, C. M., Shmakova, O. E., Jamison, A. C. & Lee, T. R. 4-Mercaptophenylboronic Acid SAMs on Gold: Comparison with SAMs Derived from Thiophenol, 4-Mercaptophenol, and 4-Mercaptobenzoic Acid. *Langmuir* **23,** 8866–8875 (2007).

(30) Wells, M. *et al.* Interactions between Organized, Surface-Confined Monolayers and Vapor-Phase Probe Molecules. 9. Structure/Reactivity Relationship between Three Surface-Confined Isomers of Mercaptobenzoic Acid and Vapor-Phase Decylamine. *Langmuir* **12,** 1989–1996 (1996).

(31) Sharma, M. K. *et al.* A novel piezoelectric immunosensor for the detection of malarial Plasmodium falciparum histidine rich protein-2 antigen. *Talanta* **85,** 1812–1817 (2011).

(32) Li, Z., Niu, T., Zhang, Z., Feng, G. & Bi, S. Studies on the effect of solvents on self-assembly of thioctic acid and Mercaptohexanol on gold. *Thin Solid Films* **519,** 4225–4233 (2011).

(33) Bensebaa, F., Ellis, T. H., Badia, A. & Lennox, R. B. Thermal Treatment of *n* -Alkanethiolate Monolayers on Gold, As Observed by Infrared Spectroscopy. *Langmuir* **14,** 2361–2367 (1998).

(34) Zhang, J. *et al.* Two-Dimensional Cysteine and Cystine Cluster Networks on Au(111) Disclosed by Voltammetry and in Situ Scanning Tunneling Microscopy. *Langmuir* **16,** 7229–7237 (2000).

(35) Scudiero, L., Hipps, K. W. & Barlow, D. E. A Self-Organized Two-Dimensional Bimolecular Structure. *J. Phys. Chem. B* **107,** 2903–2909 (2003).

(36) Henrich, V. E. & Cox, P. A. *The surface science of metal oxides*. (Cambridge University Press, 1994).

(37) Göpel, W., Bauer, R. S. & Hansson, G. Ultraviolet photoemission studies of chemisorption and point defect formation on ZnO nonpolar surfaces. *Surf. Sci.* **99,** 138–156 (1980).

(38) Von Wrochem, F. Electron Structure and Charge Transport Properties of Thiols and Dithiocarbamates in Self-Assembled Monolayers. (2007).

(39) North Atlantic Treaty Organization & NATO Advanced Study Institute on Chemisorption and Reactivity on Supported Clusters and Thin Films: Towards an Understanding of Microscopic Processes in Catalysis. *Chemisorption and reactivity on supported clusters and thin films: towards an understanding of microscopic processes in catalysis*. (Kluwer Academic Publishers, 1997).

(40) Di Felice, R., Selloni, A. & Molinari, E. DFT Study of Cysteine Adsorption on Au(111). *J. Phys. Chem. B* **107,** 1151–1156 (2003).

(41) Rubloff, G. W., Lüth, H. & Grobman, W. D. Orbital energy shifts associated with chemical bonding of organic molecules on ZnO nonpolar surfaces. *Chem. Phys. Lett.* **39,** 493–496 (1976).

(42) Dobrokhotov, V. *et al.* Thermal and Optical Activation Mechanisms of Nanospring-Based Chemiresistors. *Sensors* **12,** 5608–5622 (2012).

(43) Cagnina, S., Rotureau, P., Fayet, G. & Adamo, C. The ammonium nitrate and its mechanism of decomposition in the gas phase: a theoretical study and a DFT benchmark. *Phys. Chem. Chem. Phys.* **15,** 10849 (2013).

(44) Willey, T. M. *et al.* Surface Structure and Chemical Switching of Thioctic Acid Adsorbed on Au(111) As Observed Using Near-Edge X-ray Absorption Fine Structure. *Langmuir* **20,** 4939–4944 (2004).

Appendix 2. Permission Letters

1. *Manuscript 1*: "Carbohydrate-Functionalized Locked Nucleic Acids: Oligonucleotides with Extraordinary Binding Affinity, Target Specificity, and Enzymatic Stability", Mamta Kaura, Dale C. Guenther, Patrick J. Hrdlicka.

2. *Manuscript 2*: "Synthesis, Hybridization Characteristics, and Fluorescence Properties of Oligonucleotides Modified with Nucleobase-Functionalized Locked Nucleic Acid Adenosine and Cytidine Monomers", Mamta Kaura, Pawan Kumar, Patrick J. Hrdlicka.

3. *Manuscript 3*: "Synthesis and hybridization properties of oligonucleotides modified with 5-(1-aryl-1,2,3-triazol-4-yl)-2′-deoxyuridines" , Mamta Kaura,Pawan Kumar,Patrick J. Hrdlicka

4. *Manuscript 4*. "Synthesis and Biophysical Properties of C5-Functionalized LNA (Locked Nucleic Acid)" , Pawan Kumar, Michael E. Østergaard, Bharat Baral, et al

5. *Manuscript 5*. "Self-Assembled Monolayers of Thiols Adsorbed on Au/ZnO-Functionalized Silica Nanosprings: Photoelectron Spectroscopy-Analysis and Detection of Vaporized Explosives" , Blaise-Alexis Fouetio Kengne, Saswata Karmakar, Mamta Kaura, et al

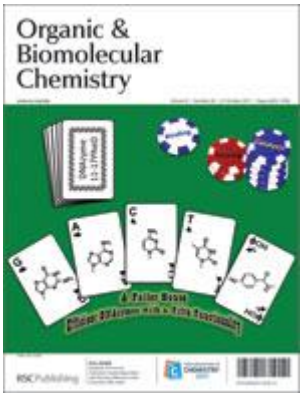

Title: Synthesis and hybridization properties of oligonucleotides modified with 5-(1-aryl-1,2,3-triazol-4-yl)-2′-deoxyuridines

Author: Mamta Kaura,Pawan Kumar,Patrick J. Hrdlicka

Publication: Organic & Biomolecular Chemistry

Publisher: Royal Society of Chemistry

Date: Oct 1, 2012